FREEZE DRYING MICROSCOPY AS A TOOL TO STUDY SUBLIMATION KINETICS

by

Purnima Raman, B.Tech, MSc.

A doctoral thesis submitted in partial fulfilment of the requirements for the award of the Degree of Doctorate of Philosophy of Loughborough University

March 2015

Dedicated to my family

ACKNOWLEDGEMENTS

I would like to express my gratitude to the Department of Chemical Engineering, Loughborough University for giving me the opportunity to carry out my PhD studies and for providing full financial support without which pursuing this research work would not have been possible.

I gratefully acknowledge my supervisors; Dr. Andrew G. F. Stapley and Prof. Chris D. Rielly for being instrumental in various aspects of initiation and progress of this research with their constant inputs and guidance, support, constructive criticism and motivation throughout the time of my PhD. Their patience and understanding helped me sail through the hard times. I consider it a great privilege for being associated with them through this thesis.

I would also like to thank the technical staffs of our department, Sean, Dave, Kim, Graham, Monika, Rob and Paul for showing kindness and patience and training me in different experimental techniques and providing technical support instrumental in the execution of this thesis.

On a personal note I would like to thank my family and friends for their love and support without which I would not have achieved what I am today. Last but not the least, I would like to give a special thanks to my husband, Joydeep, without whose motivation and support it would have been impossible to accomplish this feat.

ABSTRACT

Freeze-drying is the process of removal of water or organic solvent from a desired product by means of sublimation at a low temperature and low pressure. It is commonly employed for drying samples which are heat labile and require sensitive treatment, and is mainly used in the pharmaceutical and food industries. It is an expensive process, requiring vacuum, refrigeration and long cycle times, but does yield quality benefits due to the low temperatures involved and the porous nature of the product. Reducing drying times is important to manufacturers, and this depends on optimising rates of heat and mass transfer in the system without the sample losing its porous structure. However, freeze drying is difficult to study experimentally due to the low temperatures and pressures involved. The quality of the final product mainly depends on the sublimation rate and an optimum lyophilisation requires identification of the parameters which influence the process.

The main aim of this study is to employ freeze drying microscopy (FDM) as a useful tool to identify these process parameters and help optimise primary drying phase of the freeze drying process for two systems: lactose (relevant to pharmaceuticals) and coffee (the most widely freeze-dried food product). This equipment allows the movement of sublimation fronts to be directly visualised *in-situ* under carefully controlled (and isothermal conditions), but has scarcely been used in the literature for this purpose.

An image analysis method is developed to automatically track the movement of sublimation fronts, and the frontal data fitted to a simple mass transfer model employing surface and bulk resistances. Initial experiments with lactose solution show poor reproducibility in nucleation temperatures during the freezing step and thus primary drying rates. To improve reproducibility, a small amount of silver iodide (AgI) was added to samples which acts as a nucleating agent and increases the nucleation temperature. This addition of AgI also increases the mean ice crystal size in the samples and are easily visible under the freeze-drying microscope, and in many cases show a distinct orientation with respect to direction of sublimation front. Furthermore, the orientation greatly influences sublimation rates, being approximately factor of two faster when crystals are oriented in the direction of mass transfer. FDM experiments with coffee were less straightforward as nucleation

temperatures could not be reliably controlled, even with AgI added. Nevertheless there was a clear decrease of bulk resistance with increasing nucleation temperature.

An experimental programme was then undertaken to examine the impact of initial solid content, cooling rate, the addition of an annealing step, freeze drying temperature and aeration (for coffee samples). Frontal data were fitted to a simple mass transfer model comprising surface and bulk (per unit depth) resistances and good fits to data were obtained.

FDM experiments with lactose and coffee clearly showed the presence of a surface resistance which could also be seen as a surface layer which was devoid of ice crystals (and hence not porous when sublimed). The edge resistance first increased and then decreased with solids content. The resistance per unit depth increased exponentially with solids content, so much so that there is an optimal solids content (around 10% solids) in relation of the rate of production of dried material. Cooling rates were mainly found to affect the surface resistance rather than bulk resistance and this may be due to different levels of surface drying when the samples are being cooled for different lengths of time. Annealing substantially changed the ice crystal sizes, and had a beneficial effect on freeze drying rates and had a similar effect to adding AgI. Freeze drying rates also increased with increasing temperature approximately in line with the saturated vapour pressure (SVP) of ice which is widely held to constitute the driving force for mass transfer.

It was possible to make drying time calculations for conventional vial (lactose) and tray (coffee) drying using the frontal rate data obtained from FDM. For 10% lactose and 10% coffee (annealed) there was good agreement between the vial and tray data and predictions based on a microstructure oriented parallel to the direction of mass transfer. This was the only case where agreement was found, but also the only case where directionality was observed in FDM. The much faster drying times observed in the vial and tray experiments are thus attributed to directional solidification occurring in these systems, and this was borne out by SEM imaging. Aeration of the coffee samples was also found to substantially reduce drying times. The influence of microstructure on freeze drying rates is thus very clear.

TABLE OF CONTENTS

LIST OF FIGURES

LIST OF TABLES

LIST OF SYMBOLS

A	Area of internal dried region
a	Representative edge resistance
b	Representative resistance of dried layer
c	Final solid content of the sample required (%)
c	Actual concentration of solution
c^*	Equilibrium concentration at the point of saturation
Δc	Concentration gradient
C_g'	Concentration at glass transition
d	Fill depth in a vial
D_{eff}	Effective diffusion coefficient
dm	Change in mass of ice sublimed with time t
dt	Change in time
dw	Change in mass of ice sublimed
f	Drying factor ($0 \leq f \leq 1$)
$\Delta G^*_{critical}$	Gibb's free energy change for homogeneous nucleation
$\Delta G^*_{critical\ (het)}$	Gibb's free energy change for heterogeneous nucleation
H_s	Heat of sublimation
ΔH	Latent heat of ice sublimation
K_v	Heat transfer coefficient
M	Initial wet basis moisture content of the sample (%)
M_f	Final moisture content of (dry basis)
M_i	Initial moisture content (dry basis)
p	Saturation vapour pressure of ice at T_s
P_{sat}	Saturated vapour pressure at the stage temperature
Q_{in}	Input heat
Q_{out}	Heat released
ΔP	Difference in actual pressure applied and Saturated vapour pressure
R	Gas Constant

S	Supersaturation ratio
s	Mass of sample including initial moisture
T	Equilibrium temperature
t	Time
T_c	Condenser temperature
T_c	Collapse temperature
T_d	Dissolution temperature
T_{eu}	Eutectic temperature
T_g'	Temperature of glass transition
T_m'	End point of melting temperature line in a phase transition curve
T_p	Product temperature
t_s	Primary drying time
T_s	Temperature at the subliming ice front
T_{shelf}	Shelf temperature
ΔT	Supercooling
v	Velocity of sublimation front
w	Mass of ice sublimed
w	Mass of water to be added
w_1	Total water content
w_1'	Mass fraction of ice
w_1''	Water mass transfer
W_i	Initial weight of sample
W_f	Final weight of sample
x	Distance travelled by sublimation front

LIST OF GREEK LETTERS

α	Edge or surface resistance
β	Resistance per unit depth of internal dried region
ϕ	Factor by which Gibb's free energy change varies between homogeneous and heterogeneous nucleation

κ	Thermal conductivity of the frozen solution
ρ	Density of frozen solution (dry basis)
σ	Supersaturation
σ'	Supercooling
θ	Contact angle between ice crystal and foreign particle interface

ABBREVIATIONS

AgI	Silver iodide
Au	Gold
BCF	Burton-Cabrera-Frank
DMA	Dynamic Mechanical Analysis
DSC	Differential Scanning Calorimetry
FD	Freeze Drying
FDM	Freeze drying Microscopy
FEGSEM	Field Emission Gun Scanning Electron Microscopy
KCl	Potassium chloride
KF	Karl Fischer
LN_2	Liquid Nitrogen
mDSC	Modulated Differential Scanning Calorimetry
$MgCl_2$	Magnesium chloride
MTM	Manometric Temperature Measurement
NaCl	Sodium chloride
Non-AgI	Without AgI
P	Pressure (Pascals)
Pd	Palladium
PRT	Pressure Rise Test
PVP	Polyvinylpyrrolidone
SVP	Saturated Vapour Pressure of Ice
T	Temperature

1

INTRODUCTION

This chapter provides a basic outline of the contents of this research and provides a summarised background of the research and the necessity for a better understanding of the mass transfer phenomena that takes place during primary drying stage of a freeze-drying process. It also outlines the primary motivations that govern the purpose of this research.

1.1 Background of the research

The main rationale behind drying of materials is to improve the physical and chemical stability. The most preferred and effective way of administering pharmaceutical drugs is in the form of stable liquid formulations. However, the stability of such formulations is difficult to achieve. Physical instability in a material can be either aggregation or particle fusion while chemical instability can be hydrolysis of materials and chemical reactivity of drug compounds such as peptides, proteins and complex synthetic organic molecules, during storage (Abdelwahed *et al.,* 2006). The different chemical reactions which have been said to reduce biological activity of the various active compounds include hydrolysis, cross-linking, oxidation, aggregation and disulfide rearrangements (Franks, 1998). Apart from pharmaceutical compounds, stability of product is important even in the food industry. The main forms of food instability that occurs due to high moisture content and long-term storage include microbial spoilage, Maillard reaction and oxidation (Ubbink *et al.,* 2008). These adverse reactions and microbial contamination is highly affected by the presence of moisture in the sample, with higher water content resulting in easier spoilage of the sample. So, to improve the physical, chemical and microbiological stability of these materials and retard such chemical reactions by reducing the water activity, the most common technique is removal of water by drying and convert solutions into stable solids for long-term storage of more than 6 months. Drying of the samples results in removal of moisture or water from the sample resulting in lower microbial growth, since, micro-organisms have a necessity for a liquid substrate for their growth and metabolism (Franks, 1998 and Abdelwahed *et al.,* 2006).

Drying is one of the oldest techniques for preservation of pharmaceutical and food materials. There are a variety of drying techniques available and the type of drying technique depends on the type of material being dried and the parameters which affect the drying process such as temperature of drying, contact with air. The different types of drying techniques include vacuum drying, spray drying, fluidized bed drying, freeze-drying, spray freeze drying, hot air drying, super-heated drying, microwave vacuum drying (Lewicki, 2006 and Karimi, 2010). Drying affect various properties of the final products e.g. flowability, rehydration, wettability and dispersability. Any variation in the key operating conditions of the processes may

lead to a direct effect on the product quality and can cause clumping and stickiness which is an undesirable attribute from an industrial perspective.

The drying technique used in this research is freeze-drying, also known as lyohpilization. Freeze-drying is the process of removal of water from a desired product by means of sublimation of ice into water vapour at a low temperature and pressure. It involves three important steps – freezing, primary drying and secondary drying. It is commonly employed for drying samples which require sensitive treatment such as low temperatures, pressure and is mainly used in the pharmaceutical industry to primarily preserve the activity of the active drug compound and in food industry to maintain desired product quality with aroma and flavour retention. Freeze drying being a low temperature and pressure technique can be used to dry heat-sensitive labile products and has various advantages over common drying techniques – highly porous microstructure with good rehydration properties, very little loss of aroma and flavour compounds and maintaining product quality by prevention of adverse effects of other high temperature drying techniques such as loss of required texture, clumping of material resulting in slower rehydration and bitter taste due to too high process temperature. The main disadvantages of this process include long durations of the drying cycle due to slow drying rate and high costs incurred due to heavy usage of refrigeration and vacuum (Yeom & Song, 2010). Another limitation of the freeze-drying process is the freezing and drying-induced damages to some materials such as proteins which results in protein denaturation or loss of their biological activity and hence, must be freeze-dried in presence of protective excipients (Meister, 2009).

One of the major challenges during freeze-drying process control is detection of the endpoint of sublimation or primary drying. The process of ice sublimation during primary drying is commonly found to overlap with the diffusion or evaporation that takes place during secondary drying making it difficult to determine the precise end-point of sublimation. Switching the process parameters from primary drying to secondary drying conditions too soon can lead to residual ice melting (if primary drying is not complete till then) and structural collapse of the sample may occur (Roth *et al.,* 2001).

Hence, process optimization is a major field of research with respect to freeze drying, and focusses on factors that affect the primary drying phase of the process (which typically is the longest phase). Many researchers have made use of different techniques to understand the same and detect the end-point of sublimation such as use of mechanical samplers, real-time weighing of the samples, pressure rise tests, manometric temperature measurements (Renee *et al.,* 1993; Roth *et al.,* 2001 andGieseler *et al.,* 2007). The primary goal of all these researchers is to reduce the duration of primary drying, thereby reducing the overall operating costs of the process which currently restricts the use of freeze-drying to high value foods (such as coffee, infant formula) and pharmaceutical drug manufacture. One technique that appears to have been overlooked in freeze drying research is freeze drying microscopy. This is a popular method to determine collapse temperatures but its use in studying lyophilisation kinetics has not been explored in any great depth, despite the ability to visually track sublimation fronts.

1.2 Objectives of the study

The primary aim of this study is to improve our current knowledge of factors that govern the primary drying phase of freeze drying. The main objective of this research is to prove the use of freeze drying microscopy as a valuable tool in studying sublimation process during freeze drying *in-situ* and compare its results with those obtained from an actual freeze drying set-up. The objectives of this work are summarised below –

1. To understand the effects of initial solid content of sample solution, induced nucleation, cooling profile, freeze-drying temperature and annealing on the microstructure of the sample in the frozen state observed under the freeze drying microscope.

2. To determine kinetic parameters relating to the sublimation of the samples observed under the microscope for a model lactose system and a multi-component complex coffee system, and examine how these are affected by the frozen microstructure obtained (and thus the effects of process parameters).

3. To study the effect of different process parameters such as cooling rate – slow cooling, fast cooling and annealing and solid content on the microstructure of

freeze dried lactose in glass vials and coffee in metal trays in a lab-scale freeze-dryer.

4. To compare the predicted primary drying durations from kinetic parameters obtained from the freeze drying microscope, and actual primary drying durations obtained from equivalent experiments in a lab-scale freeze-dryer for lactose (in vials) and coffee (in trays) samples.

1.3 Organization of the thesis

This research thesis comprises of eight chapters. The contents of each chapter are summarized below -

Chapter 1 contains the introduction to this study, the objectives behind this study and a detailed outline of the thesis.

Chapter 2 provides an overview of the current available literature with regards to freeze drying kinetics. It details background study of the freeze drying process and the factors affecting the sublimation process.

Chapter 3 presents a detailed description of the experimental equipment and methodology used in this work.

Chapter 4 provides description of experimental study of freeze-drying of model lactose system under the freeze drying microscope. The experimental data are fitted to a simple mass transfer model to determine kinetic parameters (i.e. edge and bulk resistances). The effect of various parameters such as solid content, drying temperature, cooling rate and annealing on these resistances to mass transfer are investigated.

Chapter 5 discusses the freeze drying of lactose in glass vials and the effect of microstructure on the mass transfer of water vapour during primary drying is described. The effects of various process parameters such as cooling rate, annealing, induced nucleation and solid content on the sublimation kinetics are also studied. Primary drying durations of these processes are compared to the drying times predicted from the kinetic

parameters obtained from the equivalent freeze drying microscopy experiments.

Chapter 6 presents the experimental results of freeze-drying of coffee system under the freeze drying microscope. The effect of various parameters such as solid content, drying temperature, cooling rate, aeration and annealing on the sublimation kinetics of frozen coffee extract are described. The effects of these parameters on edge and bulk resistances are also discussed.

Chapter 7 discusses the freeze drying of coffee in trays and the effects of frozen microstructure on the mass transfer rates of water vapour during the primary drying stage of freeze-drying. The effects of various process parameters such as cooling rate, solid content, annealing and aeration on the primary drying durations were also studied. Primary drying durations of these processes were compared to the drying times predicted from the data obtained from freeze drying microscopy experiments.

Chapter 8 provides overall conclusions drawn from the research conducted in this study. It also provides recommendations for the future works that can be carried out in this research field.

2

LITERATURE REVIEW

This chapter of the thesis provides an overview of the current available literature with regards to the topic of this research. It supplies a detailed background study of the present scenario and helps in understanding the gaps that exist in this field of research. This chapter justifies the importance of addressing the issues raised and also helps to set the major goals and objectives for this thesis.

2.1 Introduction

Freeze drying is a process of removal of moisture by sublimation of ice into water vapour (Aguilera, 2003). Fig. 2.1 displays the phase diagram of water which is an important aspect with respect to various drying processes especially in terms of freeze drying for the current study (Santivarangkna *et al.,* 2007). Drying of materials using commonly used methods such as air drying or spray drying results in conversion of liquid to gaseous state which is highly governed by surface tension effects. However, the sublimation process involves the direct conversion of solid ice into gaseous water vapour (which forms the basis of freeze-drying) and is used to avoid effects of surface tension (Sawyer *et al.,* 2008). Freeze drying is thus mainly used with high value products especially in the pharmaceutical field, where it is possible to have both high capital investment and operating costs.

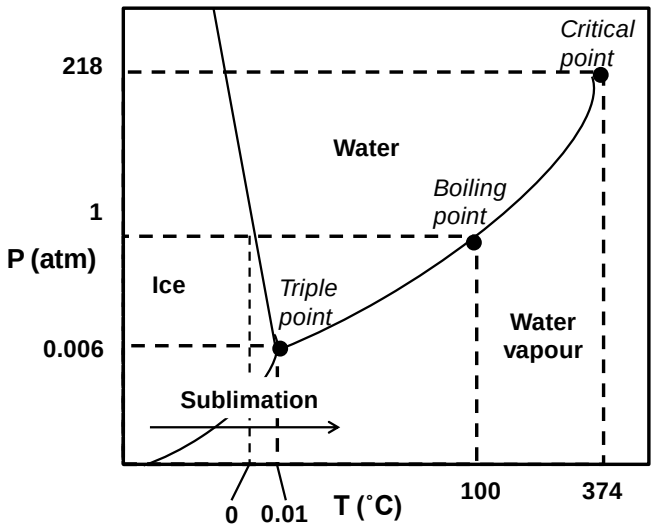

Figure 2.1: State diagram of water (not on actual scale) (P – Pressure, T – Temperature) depicting the boiling, triple and critical temperatures of water.

2.2 Freeze Drying

The main steps involved in the freeze drying process are freezing, primary drying and secondary drying (Rey *et al.,* 1975 and Passot *et al.,* 2007). The material to be freeze-dried is usually an aqueous solution placed in glass vials (in the case of pharmaceuticals) or trays (in the case of foods) that are kept on the shelf of a freeze-dryer. Cooling of the shelf causes freezing of the sample solution. Once the material is

frozen at a specific freezing rate and the temperature stabilised, the pressure is decreased, thus allowing the sublimation of the ice from the frozen material. Paradoxically, for a low temperature process, heat energy must be supplied to the sample to counteract the cooling effect of the sublimation (being an endothermic process). The heat energy is supplied through heat transfer from the supporting shelf or radiation from the chamber walls of the freeze-dryer or for some foods via dedicated radiant heaters. In the first stage of drying, known as primary drying, ice is sublimed from the sample by subjecting the frozen solution to a very low partial pressure (Krokida *et al.,* 1998 and Craig *et al.,* 1999). Primary drying is carried out at an optimal temperature so as to minimise the duration of the process but once this has been exhausted the sample enters the secondary drying phase. During this phase the temperature can be allowed to rise by raising the shelf temperature and reducing chamber pressure to promote desorption of the residual ice and also to remove the bound water present in the sample (Claussen *et al.,* 2007 and Patel & Pikal, 2011). The quality of the final product mainly depends on the sublimation rate during the primary drying: an optimum lyophilization requires the identification of the process parameters that allow a predefined sublimation profile to be performed (Carullo & Vallan, 2012). Prediction of these process parameters is important for final product morphology and lack of data required for modelling these parameters results in non-optimal cycle resulting in impaired final product structure (such as collapsed, denatured or degraded product) (Pisano *et al.,* 2011b).

The main elements of a typical freeze drier are –

- A vacuum tight chamber
- A condenser
- A vacuum pump
- Heating plates or shelves

A vacuum tight chamber consists of the heating shelves where the sample solution is placed in trays, flasks or vials. The sample receives heat from the shelves and the vacuum pump removes air and other non-condensable gases from the sample environment. The condenser removes water and maintains low partial pressure of water vapour in the chamber in order to facilitate sublimation during primary and

secondary drying process (Stapley, 2008). A schematic representation of a benchtop laboratory scale flask freeze drier is shown in Figure 2.2.

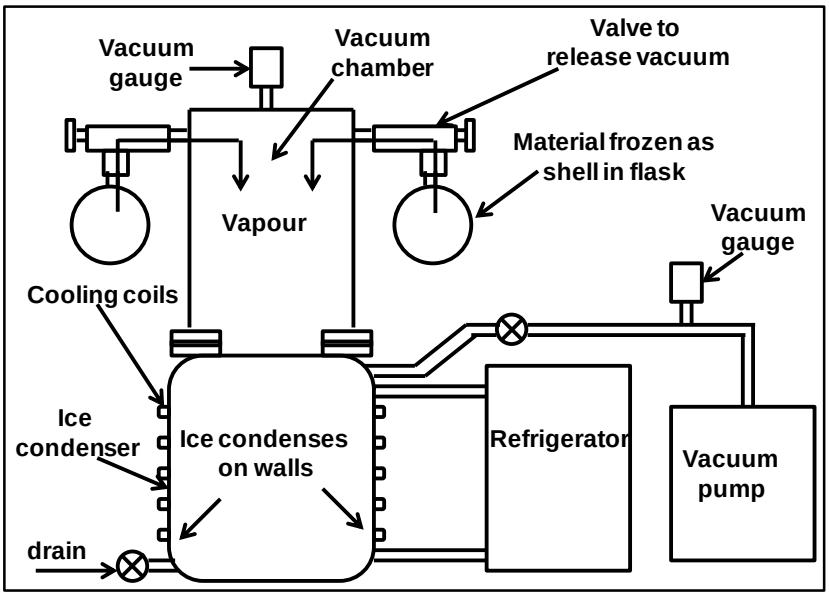

Figure 2.2: Schematic of a bench-top laboratory scale freeze drier

A freeze drier can be small-scale for laboratory research or large-scale for industrial purposes (Figure 2.3). Flask and vial-type containers are commonly used in laboratory scale set up and pharmaceutical industry while trays are used both in laboratory scale and industrial scale set ups for food freeze-drying.

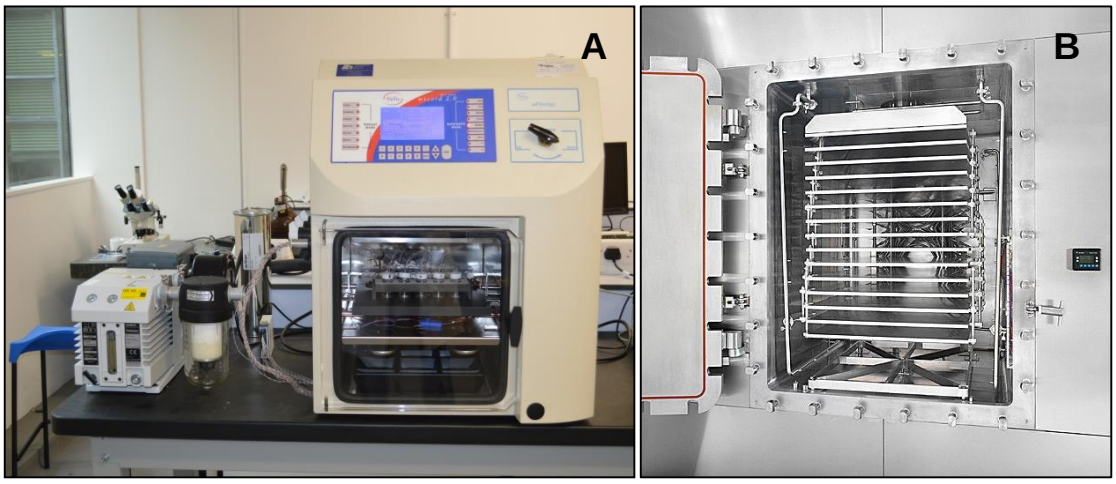

Figure 2.3: A. Laboratory scale shelf and flask freeze drier (maximum condenser capacity 3.5Kg). **B.** Industrial scale freeze drier (maximum condenser capacity can be upto 800-1000Kg) (Source: http://www.freezedryingsolutions.co.uk/lab-freeze-dryers/up-to-4kg.html)

During freeze drying, the sample temperature is controlled indirectly by controlling the shelf temperature and is a dynamic balance between the heat input from the shelf

and the chamber walls (conduction & radiation) of the freeze-dryer (Lombrana & Villarán, 1996 and Gieseler & Lee, 2008). This section (Section 2.2.4) will also discuss the various factors affecting the freeze drying process, its applications and also research carried out so far on optimization of freeze drying especially with respect to lactose and coffee as the materials to be dried.

2.2.1 Fundamentals of freezing

In general, the material to be freeze-dried (generally a solute) is dissolved in water or organic solvent prior to freeze-drying. The solute can be either amorphous or crystalline in nature. These solids vary in different properties – Amorphous solids are with short range of order in their structure (with softened range melting temperature) while crystalline solids have long order in their crystal lattice (with sharp melting point) (Meister, 2009). In solution, a crystalline solid exists in amorphous state and once dried it remains in the form of amorphous powder (Roos, 2009). However, the final product may be of crystalline form depending on the type of solvent used (some solids crystallize out of organic solvents), concentration of solid (generally in high solid contents) and cooling rate (especially very slow cooling) applied during the freezing step. Freezing is a critical step in the process of freeze drying or lyophilisation. Ice crystallization is quite similar to the solute crystallization. It involves three primary stages – supercooling, nucleation and growth of ice crystals. In supercooling, the liquid (which could be water or an organic solvent) is cooled to a sub-zero temperature. The degree of supercooling is the difference between the melting point and the actual temperature and this acts as the driving force for crystallization of ice. Once the water or the sample solution is supercooled, nucleation occurs resulting in formation of ice nuclei which grow further into large ice crystals with decreasing temperature (Franks, 2007). The rate of nucleation is generally found to increase exponentially with the degree of supercooling while the crystal growth rate is linear relative to the degree of supercooling.

For solutions, the formation of a pure ice phase in the sample results in depletion of water from solution causing it to become more concentrated in the solute and consequently more viscous. The viscosity of a concentrated amorphous solution increases with decreasing temperature and increasing solute concentration. For a

given solute, the amorphous solution has a specific viscosity-temperature relationship, which represents the effect of temperature, both directly and with changing solute concentration (Roos, 2002). As solutions become more concentrated, the melting point (T_m) falls due to freezing point depression causing the temperature required to maintain ice formation to decline steadily (see Fig 2.4). The solution eventually reaches the glass transition and due to the very high viscosity, ice crystallization stops marking the end point of freezing stage. Glass transition is the reversible state transition in amorphous materials occurring between the solid, glassy (molten or rubber-like state) and supercooled liquid states (Omar & Roos, 2007). If the glass transition is reached with very small supercooling then the concentration and temperature at this point are marked as C_g' and T_g' respectively and this point is known as the point of maximal freeze concentration (Roos, 1997 and Stapley, 2008).

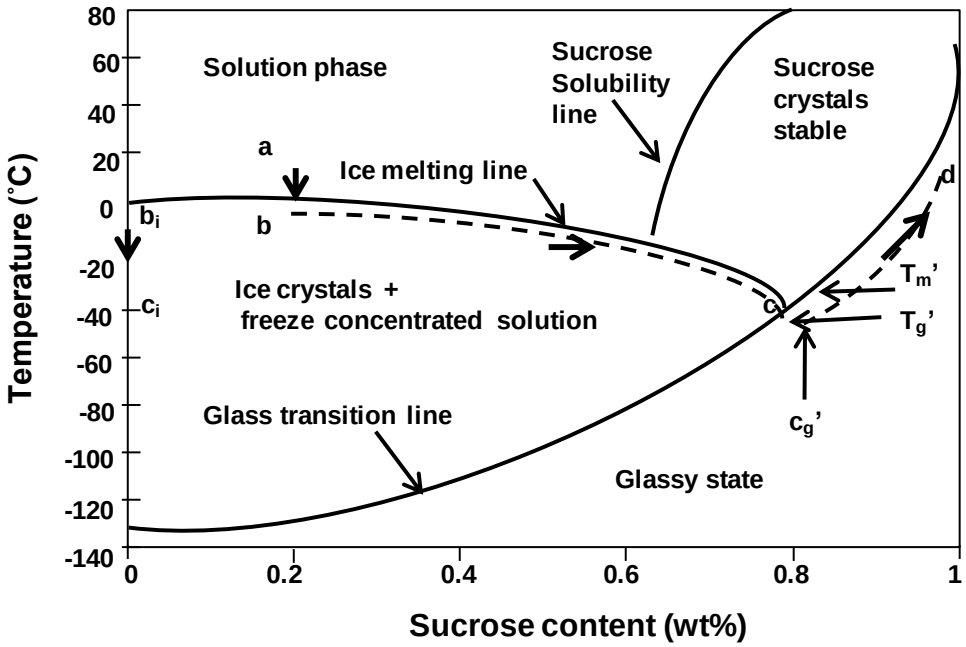

Figure 2.4: Example of a phase diagram of a common disaccharide system (sucrose in water in this case) (adapted from Stapley, 2008). The solution to be freeze-dried moves from point 'a' (solution) to 'b' (frozen) and from 'b' (frozen) to 'c' (glass transition) during the freezing phase of freeze drying.

The temperature of the solution has to be maintained between the ice melting line end point (T_m') and T_g' so as to ensure maximum freeze concentration and increasing the temperature can lead to melting of the sample. The sample solution can again be brought to optimum temperature range in order to ensure maximum freeze

concentration. This type of thermal cycle is employed in some samples and is known as annealing (Roos, 2002 and Franks, 2007). Annealing can cause 'maturation' and increases the porosity of the sample thereby increasing the primary drying rate.

The size of ice crystals formed play an important role in the morphology of the final dried product giving it its characteristic porosity and also in ensuring consistency, stability, activity (in the case of pharmaceutical ingredients), faster freeze drying process and quick reconstitution with glass transition temperature greater than the desired storage temperature (Vessot & Andrieu, 2012). It is important to maintain the storage temperature above the glass transition temperature in order to avoid glass transition in the dried product which leads to many adverse effects such as stickiness, clumping of product and further degradation of the product. The cooling rate of the sample during freezing affects the nucleation and growth process of ice crystals and hence has to be decided depending on the texture and porosity required in the final sample. A slower cooling rate leads to lower supercooling of the sample, hence favouring growth of large crystals while faster cooling rates favour nucleation leading to the formation of very small ice crystals (Woinet *et al.,* 1998b; Franks, 2007).

Ice crystallization is an important process which plays a significant role in shaping the texture and quality of the final product. With respect to food products, any crystals that form can affect the mouth-feel, texture, storage and processing of various materials like pharmaceutical drugs, coffee, ice creams, baby foods (Woinet *et al.,* 1998a and Cook & Hartel, 2011). A general schematic representation of the various steps involved in ice crystallization or freezing is displayed in Fig. 2.5 (Hiani & Sun, 2011). This section of the literature review will discuss all these steps in detail and will give special emphasis on the research carried out on ice crystallization or freezing prior to freeze drying.

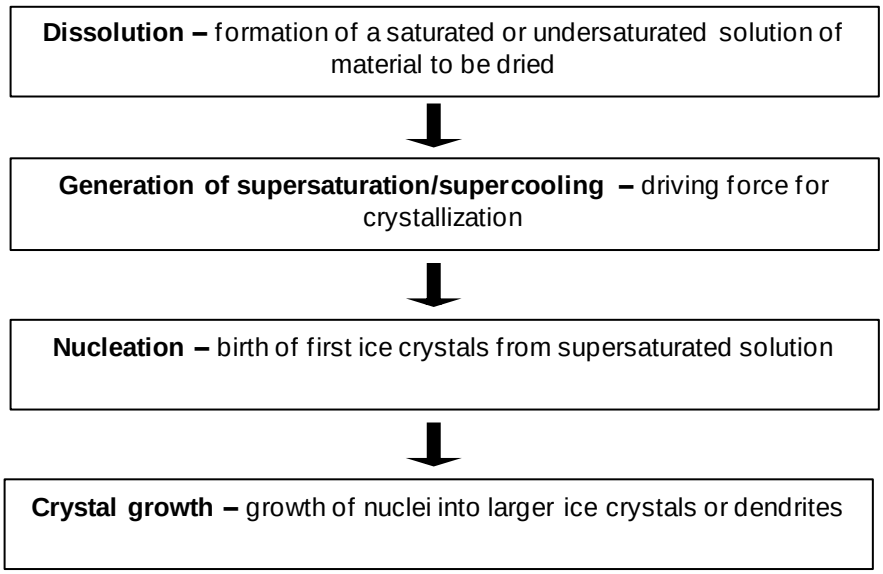

Figure 2.5: Basic steps of a crystallization process (adapted from McLeod, 2007)

Supersaturation/Supercooling: Crystallisation is liable to occur when the free energy of a molecular species is lower in the solid phase rather than the liquid phase. This can be described either in terms of either supersaturation or supercooling.

The driving force for solute crystallisation (e.g. lactose) is most usefully described in terms of supersaturation (McLeod *et al.,* 2011). This arises from a difference (Δc) between the actual concentration of solute in the solution (c) and the equilibrium concentration at the point of saturation at a given temperature (c^*) (Mullin, 2001). From this the supersaturation ratio (S) and the relative supersaturation (σ) are defined as shown below,

$$\Delta c = c - c^* \tag{2.1}$$

$$S = \frac{c}{c^*} \tag{2.2}$$

$$\sigma = \frac{\Delta c}{c^*} = S - 1 \tag{2.3}$$

Generation of supersaturation plays an important role in the crystallization behaviour of any sugar (Garnier *et al.,* 2002). Crystallization cannot take place if a solution is not supersaturated but it is not the only factor that influences the crystallization process (Garside, 1987). Supersaturation of a solution can be carried out by four different methods. The most common method is fast cooling of the

solution while solvent evaporation, drowning and chemical reactions are also used occasionally to supersaturate a solution in order to favour crystallization. Drowning is a method of introduction of another liquid medium (a non-solvent) into the system attaining thermodynamic solubility which reduces the solubility of the solute thus favouring supersaturation.

For ice crystallisation it is more convenient to refer to supercooling (ΔT). The actual driving force for crystallisation is the relative supercooling (σ') is defined as follows where T_d is the dissolution temperature, T is the actual temperature and $T_d > T$ (Mullin, 2001),

$$\Delta T = T_d - T \tag{2.4}$$

$$\sigma' = \frac{\Delta T}{T_d} \tag{2.5}$$

Nucleation: Nucleation is the process of formation of new crystals from a supersaturated or super-cooled liquid solution (McLeod *et al.,* 2011). The solid phase entities formed from the solution are known as nuclei. Nucleation marks the beginning of the process of crystallization. There are two types of nucleation – primary and secondary nucleation (Fig. 2.6). Primary nucleation involves the formation of nuclei without the influence of any external solute particles. It is classified into two types - homogeneous and heterogeneous nucleation (Garside, 1987). Homogeneous nuclei are formed in the absence of any solid interface or any external stimuli while heterogeneous nucleation comprises of effects of external influences of solid interfaces such as crystallization vessel walls, mixer blades.

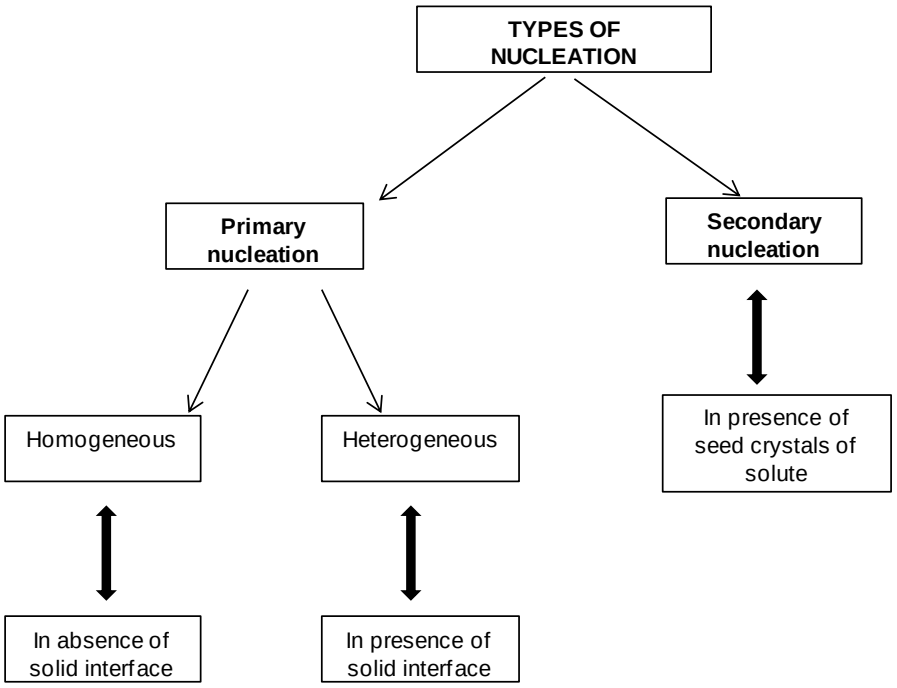

Figure 2.6: Classification of nucleation processes (adapted from Garside, 1987)

Homogeneous nucleation involves the formation of crystal nuclei spontaneously from a supersaturated solution without any external stimuli or interface. It is a difficult process as the molecules which form the nuclei have to come together resisting dissolution while orientating into a fixed lattice (Miyata & Kanno, 2005).

Heterogeneous nucleation is a process that occurs in the presence of external solid interfaces and is the most common type of primary nucleation. It can take place in solution with lower supersaturation than homogeneous nucleation and hence the width of the metastable zone in this case is smaller. Heterogeneous nucleation requires a lower Gibb's free energy change ($\Delta G^*_{critical\ (het)}$) than homogeneous nucleation ($\Delta G^*_{critical}$) and the free energy of formation is reduced by a factor of ϕ ($0<\phi<1$) and this is found to be dependent on the contact angle between the crystal and the foreign interface (Garside, 1987)-

$$\Phi = \frac{(2+\cos\theta)\,(1-\cos\theta)^2}{4} \tag{2.6}$$

$$\Delta G^*_{critical\ (het)} = \phi \Delta G^*_{critical} \tag{2.7}$$

Secondary nucleation, on the other hand, is carried out using 'seeds' of solute used for the growth of nuclei in the solution or mother liquor. These solute crystals can be

either present already in solution or are added deliberately to the solution in order to induce nucleation in a less supersaturated solution. Secondary nucleation can be further divided into two categories – shear and contact nucleation (Garside *et al.,* 2002). Another form of secondary nucleation can be seen in samples with addition of nucleating agents such as *β*-silver iodide (AgI), *Pseudomonas syringae.* The use of ice nucleating agents leads to a heterogeneous ice nucleation process that always occurs at a temperature higher than that of homogeneous ice nucleation. Nowadays, the use of nucleation agents, antifreeze proteins, ultrasound, and pressure freezing methods, also known as 'freezing assisting techniques' are constantly used to control nucleation and ice morphology before freeze drying of materials (Nagakawa *et al.,* 2006; Petzold & Aguilera, 2009; Kasper *et al.,* 2013).

Nucleation is primarily quantified by the nucleation rate, which is the number of new crystals created per unit volume and per unit time. Induction time (τ_i) is another variable that is associated with supersaturation. It is defined as the time taken for the formation of the first single nucleus of crystal and is found to be directly related to supersaturation (Nehrke, 2007). Higher level of supersaturation in a solution results in lower induction time (i. e., shorter time for the birth of crystal).

Growth of crystals: Once nucleation begins, the crystal nuclei start growing incorporating molecules into the crystal lattice. The growth of crystals also involves the movement of water molecules and other dissolved molecules away from the growing crystal. Crystal growth takes place only in the supersaturated or supercooled state until the molecules are mobile enough to be incorporated into the crystal structure. For solutions, as the growth of crystals continues, the solution becomes less supersaturated and the concentration of the liquid phase is highly reduced until phase equilibrium is reached. Various factors such as supersaturation or supercooling, viscosity, temperature, agitation and added formulation ingredients affect the growth rate of crystals in a solution (Hartel *et al.,* 2011). All these factors affect crystal growth rates in a similar fashion to how they affect nucleation rates. It has been determined that crystal growth rate generally increases with supersaturation, while crystal growth rate is found to increase to a maximum and decreases as temperature of a solution is increased. Molecular mobility in a solution is dependent on the change in temperature and solute concentration and in turn affects the growth of crystals linearly. Agitation of a solution in the presence of

growing crystals results in enhanced growth rate while presence of additives can also affect the growth of crystals. Crystal growth depends highly on the interaction between ice crystal and solution interface and there are different sites where a solute molecule can be incorporated into the crystal lattice. The different sites present on the surface of the crystal help in its growth in different ways (Garside, 1987). It has been discussed that a solute molecule attaching to the sites is likely to form more tight bonds with the growing crystal and has a reduced probability of returning to solution.

For crystal growth influenced by surface incorporation, various models have been discussed in detail in literature (Giulietti *et al.,* 2001; Mullin, 2001, Myerson, 2002 and Abu Baker, 2010). Among all these models, the most important three mechanisms are Continuous growth, Burton-Cabrera-Frank (BCF) model and Birth and spread model. Continuous growth model is found to take place in rough crystal surfaces which contain a lot of kink sites (sites on the surface of crystal) and hence the growth is continuous until all the kinks are filled. After that, layer growth model may take over the crystal growth. In case of the BCF model, also known as spiral growth, the presence of defects on the surface of crystal provides kink site for further growth layer by layer around this defect. This model generally results in a spiral growth and takes place in low supersaturation conditions (Abu Baker, 2010). Birth and spread model is a type of 2D nucleation theory model which states that a 2D nucleus is formed over the smooth crystal surface providing necessary kink site to promote crystal growth. Mononuclear model assumes that a single nucleus spreads across the surface at infinite velocity, whereas a polynuclear model assumes that nuclei are formed which do not spread instead the nuclei formed cover the surface themselves (Giulietti *et al.,* 2001). The Birth and spread model is said to be an intermediate between mononuclear and polynuclear model. This model also assumes that the nuclei can form at any location on the surface of the crystal and spread as it is formed at a constant velocity as generally seen in ice crystallization (Abu Baker, 2010).

Crystal size distribution: Crystal size distribution plays an important role in governing product quality and helps in determining efficient and low cost of drying processes and influence properties of the product like density, rehydration properties. Hence, crystal size distribution measurement is an important aspect related to such research. In the food industry, controlling the crystal size distribution is important in order to

obtain desired product characteristics. For example, in the confectionary industry, product quality generally demands very fine crystals for the desired mouthfeel. This attribute is achieved by following some basic principles – control of speed and timespan of nucleation (Hartel *et al.,* 2011); any nucleating materials added should be completely dissolved so as not to affect the growth rate of crystals and hence the size and finally addition of such agents should be properly timed so as to achieve good nucleation and required crystal size.

As well as controlling nucleation and growth of ice crystal to produce required size distributions of ice crystals in the sample, it is also possible to achieve the same using a process called annealing. Annealing is a process step in which samples are maintained at a specified sub-zero temperature for a defined period of time to partially melt and then regrow crystals and is commonly used in freeze-drying. It also dramatically influences the particle size distribution of ice crystals in the frozen samples prior to freeze-drying. If the annealing temperature is above the glass transition temperature, ice will melt following the freezing point depression curve, especially smaller ice crystals will melt completely in comparison to larger ones. Annealing is one of the most common and effective method employed to increase the ice crystal size and also enhances the primary drying rate during freeze drying (Lu & Pikal, 2004; Hottot *et al.,* 2005; Abdelwahed *et al.,* 2006a,b and Patil *et al.,* 2010). It also helps in the increase of heat transfer rate governed by heat transfer flux from shelf and surroundings towards the sublimation front inside the vial or tray and mass transfer rate controlled by water vapour mass transfer through the dried layer (Patil *et al.,* 2010).

2.2.2 Primary Drying

Primary drying is the process of removal of ice from frozen solution by the process of sublimation which can be controlled in a better way than the freezing process. At this time in the process, about 90% of water is frozen and the heat flow to ice is adjusted to balance the heat absorbed by the sublimation process at the operating temperature (Franks, 2007). This section of the report will discuss the mechanism of heat transfer from the shelf of the freeze drier to the ice front of frozen sample and mass transfer mechanism of transfer of water vapour to the condenser.

In most cases, the sample solution or feedstock in loosely stoppered vials are placed directly on freeze drier shelves and frozen below the glass transition temperature (T_g') (as discussed in the previous section) to ensure maximum freeze concentration. If cooling is carried out properly, the sample solution reaches an amorphous glassy state. The vials are then subjected to increasing temperature, but it is always maintained below T_g' so as to avoid melting of the frozen solution (Franks, 2007; Pisano *et al.,* 2011). Heat enters (Q_{in}) the product mainly from the shelf through the bottom of the vial/tray and from the surrounding chamber while sublimation of water vapour from the ice front occurs at the top resulting in heat expelled from the sample (Q_{out}) (Fig. 2.7). This results in the development of a temperature gradient in the frozen material and can lead to the formation of concentration gradient in the moving ice front. The chamber pressure is also reduced to a lower value than the saturation vapour pressure of ice at the operating temperature by applying vacuum so as to facilitate high sublimation rate (Stapley, 2008 and Pisano *et al.,* 2011).

However, the main mechanism for water removal is the use of a condenser. This provides a very cold surface (typically -60˚C) onto which water vapour condenses in the form of ice. This maintains the vapour pressure of water in the chamber at very low levels, which allows sublimation to occur. Maintaining the driving force (the temperature difference between the ice front and the condenser surface) for the removal of ice during the primary drying process is important. This temperature difference provides the water vapour pressure difference between the ice front and the condenser surface (Franks, 2007). Maintaining the condenser temperature requires a great deal of refrigeration and comprises most of the energy costs of the process.

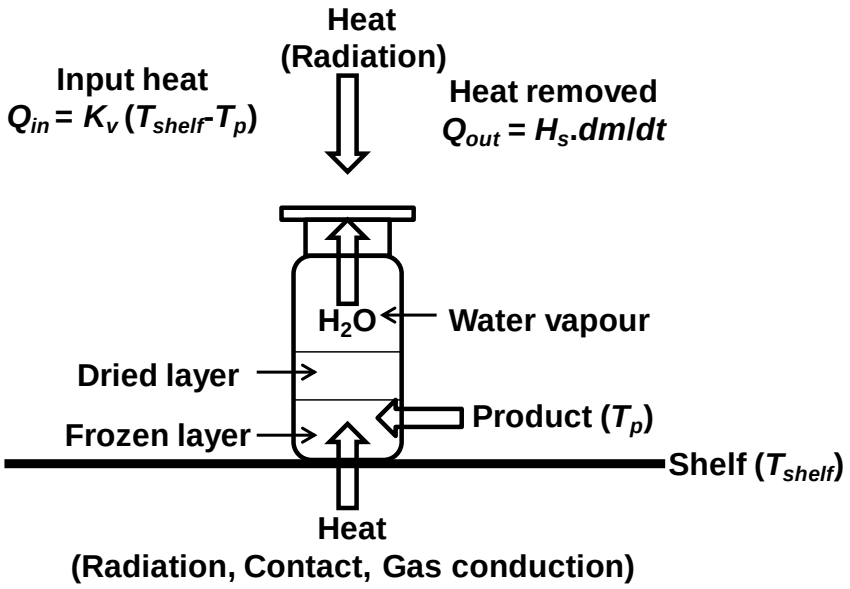

Figure 2.7: Schematic diagram of heat transfer in a freeze drier vial (adapted from Franks, 2007)

The heat and mass transfer mechanism of the primary drying step of freeze drying process can be fully understood only with the help of principles that define the supply of thermal energy to a frozen product – radiation from hot surfaces, conduction between solid surfaces such as heating plates and vials and convection or molecular collisions (Franks, 2007 and Pisano *et al.,* 2011). The phenomenon of radiation that takes place between the hot or warm surfaces is governed by Stefan's law and is particularly important near the walls and door of the freeze drier. Conduction of heat within and between the surfaces depends highly on the thermal conductivity of each material –shelves, vials, frozen solution, portion of material already dried and also on chamber pressure. Conductivity of the frozen solution and the portion of already dried material change continuously as the sublimation process proceeds. Convection within vapour phases produced by diffusion and molecular collisions affects the sublimation rate and can be described using simple kinetic theory of gases –

$$\frac{dw}{dt} = \frac{k_v}{\Delta H}\left(T_c - T_s\right) = \frac{fp}{(2\pi R T_s)^{1/2}} \tag{2.8}$$

where ΔH is the latent heat of ice sublimation, w is the mass of ice sublimed in time t, T_c is the condenser temperature, T_s is the temperature at the subliming ice front, f is the drying factor ($0 \leq f \leq 1$), p is the saturation vapour pressure of ice at T_s and k_v is the heat transfer coefficient (Franks, 2007).

The heat transfer coefficient (k_v) and total heat transfer depends on the quality of contact between the solid surfaces, e.g. the shelf or plate surface with the vial bottom, type of vial and chamber pressure (Wolff *et al.,* 1989 and Rene *et al.,* 1993). It has been described in research that major contribution to heat transfer is due to convection, i.e., molecular collisions between gas molecules and this becomes more prominent with increasing chamber pressure. This increase in chamber pressure leads to a lowering of product temperature due to increased mass transfer comparative to heat supplied. This is generally compensated by either increasing the shelf temperature or by adjusting the primary drying time (t_s) described as follows –

$$t_s = \frac{(\rho w_1 \Delta H_s w_1' d)}{\{\left(\frac{1}{k_v}\right) + \left(\frac{\kappa d}{2}\right) + \left(\Delta H_s w_1'' \frac{d}{2}\right)\}} \tag{2.9}$$

where ρ is the density of frozen solution, w_1 is total water content, w_1' is the mass fraction of ice (~0.9), d is the fill depth in the vial, κ is the thermal conductivity of the frozen solution, k_v is heat transfer coefficient and w_1'' is the water mass transfer (Franks, 2007).

This equation can be used only if the thermal conductivity of the frozen solution, mass transfer rate, sum of heat transfer and thermal conductivity between the shelf and subliming ice front are known.

2.2.3 Secondary Drying

Secondary drying is a step in the freeze drying process following primary drying where removal of unfrozen water is performed by diffusion, desorption and evaporation (Schneid *et al.,* 2011). The amount of unfrozen moisture present in samples is difficult to determine and only a few researchers have measured it using differential scanning calorimetry. In recent years, many other techniques have been developed to measure the moisture content in the sample after primary drying such as Raman Spectroscopy, Fourier Transform Near Infrared (FT-NIR) Spectroscopy, Manometric temperature measurement (MTM) and Tunable Diode Laser Absorption Spectroscopy (TDLAS) (Franks, 2007; Schneid *et al.,* 2011 and Awotwe-Otoo & Khan, 2015). It has been shown that an amorphous system has more unfrozen moisture than a crystalline system though crystalline materials sometimes have unfrozen

moisture in the form of hydrates which are water molecules embedded in their structure. These hydrates and crystalline water are difficult to remove by sublimation and primary drying.

Generally, primary drying is carried out under isothermal conditions but secondary drying follows the midpoint pathway between the glass transition curve and the collapse or softening temperature curve (Franks, 2007). The best method to carry out secondary drying efficiently to avoid collapse is by stepwise temperature-time ramping and always maintaining the temperature between the T_g' and T_s curve (Fig. 2.8).

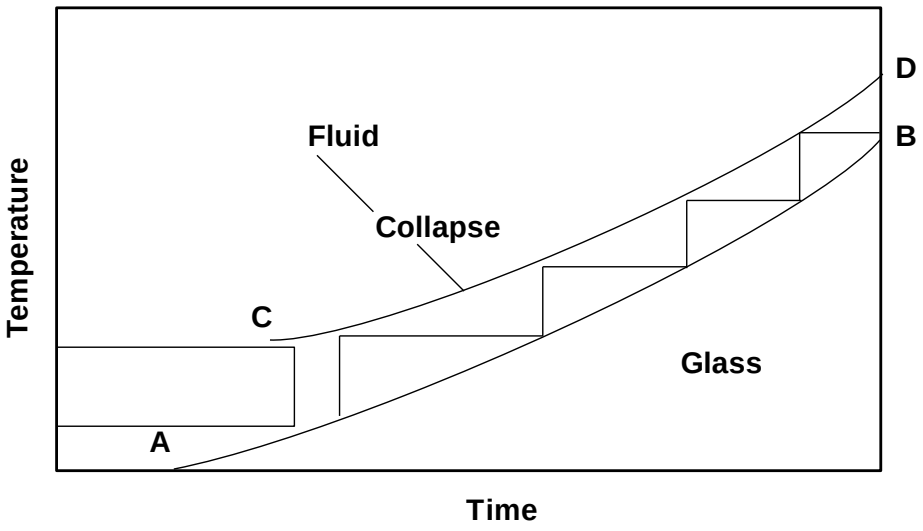

Figure 2.8: Optimal secondary drying pathway (Franks, 2007). A-B represents glass transition curve and C-D represents solubility curve.

Drying is terminated once the desired residual water content value is reached. The residual moisture content can be determined by various methods such as gravimetric method of measuring the difference in mass before and after freeze-drying, Karl-Fisher titration, thermogravimetric analysis, mass spectrometry, FT-NIR spectroscopy and alternative methods (Gas chromatography and moisture evolution analyzer) (Foster *et al.,* 2005; Vuataz *et al.,* 2010 and Bogdani *et al.,* 2011). It is important to achieve the desired residual moisture content (generally <5%, but depends on the type of product – pharmaceutical materials require quite low final moisture contents <2-3% while food products require moisture contents to be <5%) because it has a pronounced effect on the texture and shelf life of the product (reducing it by months). It causes stickiness, microbial growth and caking in the

product during storage and hence needs to be maintained below a specific value (Foster *et al.,* 2005 and Ergun *et al.,* 2010).

During secondary drying, as the sample is heated, diffusion of water molecules from the internal regions of the sample to the surface takes place, where water is converted to water vapour by evaporation (Schneid *et al.,* 2011). Diffusion is often confused with desorption in the case of freeze drying process. Diffusion of unfrozen and bound water from the sample is considered to be the rate limiting process for secondary drying and not evaporation from the surface.

After primary drying is completed, the product should be maintained at its glass transition temperature and below its collapse temperature for some time (~an hour) so as to avoid collapse of its delicate structure as the viscosity of the solid material decreases quickly if the temperature is increased above T_g' (Franks, 2007). Structural collapse affects the product quality and can also sometimes lead to protein aggregation in pharmaceutical ingredients. It is impossible to avoid a minor degree of collapse during secondary drying since the temperature of the sample has to be raised above T_g' for a given period to remove the unfrozen water.

2.2.4 Factors affecting freeze drying

Various factors play an important role in the freeze drying process on a laboratory scale or industrial scale set up. These factors can be divided into three categories – process development, process and product parameters. The product parameters are mainly the product temperature and the changes in the product during the course of the whole freeze drying process. The product temperature is the determinant of the drying rate of the sample and is controlled indirectly by adjusting the shelf temperature and chamber pressure.

The most significant process development parameters are formulation characteristics, fill volume of solution and type of container and its closure. Fill depth has also been found to exert a major influence on the primary drying time (t_s) (Tang & Pikal, 2004). The shape of the vessel plays an important role in determining fill depth and fill volume. It has been found in previous research that fill depth and resistance to further sublimation follows a linear relationship and hence, t_s varies linearly with fill depth and inversely with ΔT. Specific surface area or surface area of the material per

unit mass or volume has a direct relationship with secondary drying rate. An increase in fill volume results in lowering of cooling rate reducing the specific surface area of the product and hence reduces secondary drying rate (Franks, 2007).

High solute concentration (or low moisture content) in a formulation reduces the sublimation rate during primary drying by coating small ice crystals on the advancing ice front like a skin and a retardation factor has to be included in the estimation of t_s in order to compensate for water vapour diffusion across the amorphous layer. However, very low solid content (or high amount of water in solution) also results in weak and brittle dried material which cannot withstand rough handling of the vial during further processing and packaging (Hartel *et al.,* 2011). High solute concentration in the sample also results in decrease in secondary drying rate by reducing the specific surface area. High solid content also decreases the porosity of the dry cake and hence raises its resistance leading to lower drying rate. Apart from solid content, various other formulation characteristics influence the freeze-drying process. During freeze-drying of microbial cultures containing yeast, fungi and bacteria and protein pharmaceuticals, it is common to use protective agents or excipients such as lactose and sucrose to prevent protein denaturation and preserve the biological activity of the materials (Fonseca *et al.,* 2004 and Navarta *et al.,* 2011). Usually the excipients are chosen so that they do not affect the freeze-drying process and the final product quality in an adverse way (Wei *et al.,* 2012).

Once the process development parameters are all constant, the important process parameters that affect the freeze drying process are primary drying time, chamber pressure and shelf temperature. Condenser temperature is another process parameter that affects the freeze drying process and is generally maintained at a low value in order to ensure high sublimation rate of ice. The various factors affecting the primary drying time are ice crystal size distribution, concentration gradients within the frozen sample, density and thermal conductivity of frozen product, water content of solution, latent heat of sublimation at the operating temperature, temperature difference between ice front and shelf of freeze drier, total heat transfer coefficient from the shelf to sublimation front, mass fraction of frozen water and permeability of dried product to water vapour (porosity). In a lab-scale freeze-drying system, especially for pharmaceutical products, glass vials are used for drying of materials. The drying kinetics of the samples is found to vary between vials and reproducibility

is quite difficult to achieve. Gan *et al.,* (2005) have studied and reduced the inter-vial variance of the sublimation rate during primary drying and secondary drying stages of freeze-drying by controlling the heat input to the samples by applying temperature constraints and controlling the drying chamber wall temperature. They found that this has a more pronounced effect on inter-vial variance and reduced the primary drying duration.

In terms of shelf temperature, cooling rate affects the nucleation and growth process of ice crystal resulting in varied ice crystal size distribution. A high cooling rate leads to higher nucleation rate and leads to the formation of large number of small crystals resulting in longer sublimation time and vice versa. The different features of ice crystal growth determine the porosity and texture of the final dried product. As the ice front migrates downwards during sublimation, the dried material network offers a strong resistance to further sublimation decreasing the drying rate. This dry cake resistance is difficult to measure as it depends on the porosity of the dried material which in turn depends on the freezing process and any annealing or maturation carried out.

Product quality can be highly affected by adverse temperature changes during secondary drying due to structural collapse of the sample. Low temperature during secondary drying does not help in drying the product adequately to low water contents (Franks, 2007). Temperature has to be raised cautiously to increase the rate of water removal by diffusion to avoid collapse (Stapley, 2008). This heating process is carried out step-wise till the final drying temperature is reached and the sample can be dried at this temperature for a few hours to achieve the required final moisture content.

An increase in chamber pressure decreases the sublimation rate as heat transfer coefficient between the heat exchange fluid and subliming ice surface decreases with increase in pressure. Chamber pressure does not highly affect secondary drying rate though different products dry at different rate at same pressure (Franks, 2007). It is assumed that water content has no effect on secondary drying even though it may differ from vial to vial and product to product and depends largely on the freezing process.

2.3 Freeze Drying Microscopy

In general, microstructures of the freeze-dried materials are investigated using scanning electron microscopy and X-ray microscopic computerized tomography (Searles *et al.,* 2001, Xiao *et al.,* 2007; Voda *et al.,* 2012 and Izutsu *et al.,* 2014). Apart from these techniques, confocal laser scanning microscopy, cryo-light microscopy and electron cryomicroscopy has been used to study the ice crystal morphology of frozen materials which may be subjected to freeze-drying (Evans *et al.,* 1996; Cui *et al.,* 2006 and Acharya, 2008). All these techniques allow the visualisation of the product either in frozen state or after completion of freeze-drying. Thus in the current study, freeze drying microscopy was used as it is a technique for *in-situ* visualisation of both freezing and freeze drying processes of samples under a light microscope with the help of a controllable cryo-stage and vacuum pressure system. It helps to determine the collapse temperature of product which is considered to be an important parameter in controlling the product quality by maintaining the desired appearance and texture of the product. Freeze drying microscopes were designed in the very early days by scientists themselves. The earliest apparatus designed was published by MacKenzie, (1964) followed by Flink & Hansen,, (1978) and Pikal *et al.,* (1983). The main part of the whole apparatus is the design of the cryo-stage attached to the light microscope. Nail *et al.,* (1994) developed a stage using thermoelectric heaters (Peltiers) structured in two stages with a heat sink (of circulating fluid) on the high temperature side and the samples could be cooled to a temperature of about -47°C. Hsu *et al.,* (1995) improved the stage which could cool the sample to -60°C by using four Peltier thermoelectric heaters. Mostly the temperature of the sample is maintained constant but gradient temperature stages have also been designed and used previously (Freedman *et al.,* 1972 and Kochs *et al.,* 1989). Today freeze drying microscopes are commercially produced and widely used in pharmaceutical as well as food research. This section of the report will discuss the use of FDM to determine collapse temperatures which is the main applications of freeze drying microscopy in industry. It will also describe in detail the instrumentation, working and the use of freeze drying microscope to determine product collapse temperature and freeze drying rate of samples.

2.3.1 Principle of freeze drying microscopy

Product Collapse: For the freeze drying process to be efficient while maintaining good quality of product, the product temperature (T_p) has to be maintained below the critical formulation temperature of the product which is the eutectic temperature (T_{eu}) in case of crystalline materials and glass transition (T_g') or collapse temperature (T_c) in case of amorphous systems (Tang & Pikal, 2004 and Izutsu *et al.,* 2010). Freeze drying microscopy (FDM) is considered to be one of the best methods for the determination of this critical formulation temperature for the primary drying stage of freeze drying as product collapse can be visualised directly under similar experimental conditions as in case of the real freeze drying process (Liu, 2006). Product collapse is defined as the phenomenon of loss of porous structure of the product due to viscous flow of the amorphous phase during primary drying if the product temperature is increased above the collapse temperature. T_c is a distinctive property of the product and depends on the rate of water removal from glassy state (Pikal & Shah, 1990). Structural collapse of a product results in a variety of adverse effects such as aesthetically unsuitable collapsed cake, product shrinkage, reduced activity (in case of pharmaceutical products), poor stability, poor aroma retention, poor rehydration properties, unevenly dried product with lower solubility and a higher moisture content (Tsourouflis, 1975 and Adam & Ramsay, 1996).

In a few cases, a small amount of collapse may be introduced into sample deliberately which is known as microcollapse. Microcollapse is defined by viscous flow only in substructures or structures in a limited area of the sample (Searles, 2004). Collapse and microcollapse sometimes leads to shrinkage of the product cake causing reduction in volume of the dried cake from that of the original volume of frozen cake. Collapse also leads to reduction in sublimation rate due to clogging of pores through which water vapour was being removed leading to increased and unevenly distributed moisture content (Adams & Ramsay, 1996). It also results in undesirable appearance, loss of porosity causing reduction of specific surface area and hence slower reconstitution of the product (Chang & Patro, 2004) and hence, poses a big marketing challenge which has to be avoided. Collapse has also been found to affect protein structure in some cases leading to its degradation.

2.3.2 Application of Freeze drying microscopy

The equipment and the methodology of the use of freeze drying microscope will be discussed in Chapter 3. This section provides a background of the use of freeze drying microscopy (FDM) in various applications. FDM has been used by various researchers in order to understand and optimize the freeze drying process by increasing the freeze drying rate, while maintaining good quality of product.

Pikal & Shah, (1990) have performed very early research using FDM and have discussed the effect of experimental conditions on the product collapse temperature. According to their study, the collapse temperature is directly related to the sublimation rate, since an increase in sublimation rate causes an increase in collapse temperature. It has also been shown that collapse in vial freeze drying occurs at a slightly higher temperature than microscopic freeze drying and that collapse temperature and glass transition temperatures are two different parameters of a single product.

A study by Meister & Gieseler, (2008) investigated the effect of nucleation temperature, sublimation rate and sugar-protein mole ratio on the collapse temperature of protein-sugar mixtures. It was found that although the nucleation temperature did not have any effect on the onset of collapse temperature, sublimation rate did have a substantial effect. Another study by Meister *et al.,* (2009) discussed the effect of nucleation temperature and solute concentration on the collapse temperature of polyvinylpyrrolidone (PVP) and 2-(hydroxypropyl)-β-cyclodextrin determined by FDM. Solute concentration was found to have no effect on the nucleation temperature and had a minor effect on the onset of collapse temperature but had a significant effect on the full collapse temperature.

Freeze drying microscopy has also been used to determine the rate of the primary drying step of freeze drying by Zhai *et al.,* (2003). They have discussed a diffusion model to represent the movement of the drying front and modelled the drying rates using an effective diffusion coefficient. They have also presented a relationship between the thickness of the cake and the drying time at different drying temperatures.

Collapse temperatures of complex biological media containing *Lactobacillus bulgaricus* and important protective components like sucrose, maltodextrin were determined using FDM by Fonseca *et al.,* (2004). The structural behaviour of different components under freeze drying conditions was studied considering microcollapse temperature and collapse temperature. Addition of lactic acid bacterium (*Lactobacillus bulgaricus)* to the sample solutions was found to increase the collapse temperature and also increased the interval between microcollapse and collapse temperatures.

In another study, FDM was used by Yang *et al.,* (2010) to determine the collapse temperature of various agents used for stabilisation of living cells (NIH 3T3 Fibroblasts) during freeze drying. Bulking agents were found to affect collapse temperature of trehalose solution at low initial concentrations and ice seeding was found to affect the ice crystal morphology during the freezing stage of the freeze drying process. They have also confirmed that collapse temperature of sample (2 µl) determined from FDM can be used to prevent collapse and freeze-drying it at a slightly larger scale (vial – 1 ml).

Sacha & Nail, (2008) have studied ''glass transition-like'' multiple transitions of a series of sugars like sucrose, lactose, maltose, trehalose, fructose with the help of FDM and modulated differential scanning calorimetry (mDSC) and have investigated the significance of these thermal events on the pharmaceutical uses of the product. They have also suggested that there are two transitions – low and high temperature transitions and low temperature transitions were found to have no obvious pharmaceutical significance while the high temperature transition is associated with the collapse of the product.

Dynamic mechanical analysis (DMA) is a method used to measure phase morphology transitions such as melting, crystallization, alpha and beta transitions of samples by vibrating the sample at a constant frequency and low amplitude sinusoidally and the stiffness and damping with respect to temperature is monitored. Gearing *et al.,* (2010) have used DMA for determination of critical formulation temperature (glass transition temperature and collapse temperature) of various excipients like trehalose, dextran and lactose and compared it with the values obtained by FDM and modulated differential scanning calorimetry (mDSC). The critical product temperature

determined by DMA was found to be close to the collapse temperatures determined by FDM, but showed a difference of about 10˚C when compared to T_g' values obtained from mDSC. Application of FDM has mostly been observed in the pharmaceutical industry and very few researchers have used it with respect to the food applications and this research aims to bring forth the advantages of this technique with respect to the food industry.

2.4 Optimization of freeze-drying

Control of the freeze drying process is difficult as the direct measurement of product humidity is difficult and the heat and mass-transfer phenomena and thus the primary drying kinetics are poorly-defined and difficult to determine (Pisano *et al.,* 2011). The biggest drawback of the present set-up is the difficulty in obtaining a direct measure of the process parameters mentioned without disturbing the process or affecting the sterile conditions required for some materials being freeze-dried. The available data of the above are scarcely discussed in the literature published till date. Detection of the end point of sublimation plays an important role in the optimization and control of the process.

The sublimation front movement can be tracked in two ways – indirect and direct methods of analysis. Indirect measurements of factors such as product temperature, partial pressure of water vapour, the product's electrical resistance is a way of determining the endpoint of sublimation (Sadikoglu *et al.,* 2006; De Beer *et al.,* 2009a,b; Ganguly *et al.,* 2013). However, these methods are still being developed by various research groups as they are still in their early stages of inception. The most commonly used method to monitor the process and detect the end point of sublimation is the use of a thermocouple inserted into the sample containing vial. However, this method is said to affect the freezing process by influencing the nucleation and ice crystal growth and also affects the heat transfer to the product (Barressi *et al.,* 2009). The use of the temperature-measuring thermocouple also results in faster drying of the samples in monitored vials. Apart from temperature measurement, the use of moisture sensors, thermal conductivity gauges and mass spectrometry have been used by researchers to detect the end of primary drying stage (Brulls *et al.,* 2003). Also, non-invasive techniques for monitoring the whole

system have been currently proposed instead of using thermocouples; the most common ones being the pressure rise test (PRT), manometric temperature measurement (MTM) (Tang *et al.,* 2005; Gieseler *et al.,* 2007; Fissore *et al.,* 2013). Manometric temperature measurements (MTM) is a method to measure product temperature at the sublimation front as quickly as possible (almost less than a second) when the chamber has been isolated from the condenser for a few seconds (~25 s). This isolation results in pressure rise in the chamber (PRT) which is then analyzed using an algorithm to directly measure both pressure at the sublimation front and mass transfer resistance. Based on pressure and resistance determined, data for the product temperature, heat transfer, ice thickness, temperature at the bottom of the vial, heat transfer coefficient and sublimation rate are calculated (Gieseler *et al.,* 2007). Recently a new method for freeze-drying process control and cycle development has been proposed by Smith *et al.,* (2013), which uses a through-vial impedance measurement (LyoDEA). The method was used to characterise different process parameters such as ice nucleation onset time, complete ice solidification, glass transition, primary drying end point and sublimation rate using dielectric measurements from vials for freezing and freeze-drying of mannitol, maltodextrin, lactose (Arshad *et al.,* 2014 and Smith *et al.,* 2014). Another method is direct analysis of the product during freeze-drying using mechanical samplers which helps in collection of products from the drying chamber without disturbing the experimental conditions. Similarly, weighing the sample continuously during freeze-drying inside the chamber also provides an insight into the drying kinetics of the product. This information can also be determined by weighing the amount of ice frozen on to the condenser.

Monitoring the freeze-drying process may also be achieved by modelling of the dehydration kinetics. Different models have been proposed in literature to predict the behaviour of the product throughout the course of the process with respect to operating parameters (Segura & Oyarzún, 2012). Simulation has been often used by researchers as a very helpful tool to achieve optimal process design for freeze drying (Giordano *et al.,* 2011; Fissore *et al.,* 2011a; Pisano *et al.,* 2013). Many of the works presented in literature focus on simulation of the freezing process, however, a few were devoted to primary and secondary drying stages simulation (Mascarenhas *et al.,* 1997; Boss *et al.,* 2004; Song *et al.,* 2005 and Nam & Song, 2007). The importance of

freezing stage in freeze-drying process has been widely recognized and the effects of freezing step on the subsequent stages, the final product structure and rehydration properties have been discussed in detail in literature. Among these works, Patapoff & Overcashier (2002) studied the effect of the different freezing conditions on mass transfer resistance of the freeze-dried samples. A variation of resistance between the dried cake and the lower frozen layer has been discussed. This variation has been interpreted with respect to the structural difference between the layers (vertically) due to the freezing method. Also, Cannon & Trappler (2000) have discussed the effects of the freezing rate on the final product morphology and in turn, affect the primary drying rates.

Simulation has also been seen to give information on freezing in vials and due to the change in temperature throughout the vial, simulation can also provide information regarding heat transfer (Nakagawa *et al.,* 2007; Nakagawa *et al.,* 2009). Apart from this, effects of factors such as chamber pressure, sample fill volume on heat transfer during freezing stage of the freeze drying process has also been covered by Brulls & Rasmuson (2002) using theoretical modelling as well as experimental studies. The dynamic axisymmetric model obtained by means of a finite difference method provides good agreement between simulated and experimental value for heat transfer in the vial. Another simulation study by Nakagawa *et al.,* (2007) proposes a two-dimensional axisymmetric model that estimates temperature profiles and average ice crystal sizes from the simulated results. Other researchers have also used models to describe the heat transfer in the onset of nucleation with respect to factors such as physical properties of the sample solution, degree of supercooling (Qin *et al.,* 2003). The aim of the study by Muzzio & Dini, (2011) was to develop a finite-element analysis model to simulate the freezing stage of the freeze drying process, taking into account the vial shape; apparent heat capacity and temperature gradients as fitting parameters.

A number of other freeze-drying models have been developed by various researchers to predict freeze-drying cycles to control the product quality and minimise operating cost. There have been one-dimensional or pseudo-steady state models, two-dimensional axisymmetric unsteady state models as well as spatially multi-dimensional, unsteady state models (Pikal *et al.,* 1983, 1984; Kuu *et al.,* 1995; Schoen *et al.,* 1995; Mascarenhas *et al.* 1997; Sheehan & Liapis, 1998). The multidimensional

model described by Sheehan & Liapis, (1998) highlights the dynamic behaviour of the primary and secondary drying stages of the freeze drying process. However, in the Sheehan and Liapis model the effect of the bottom curvature of the vial was approximated by employing a constant heat transfer coefficient introducing errors into the simulated results as the pocket of air under the curve would have different conductivity at low pressures.

Zhai *et al.,* (2005) have also conducted studies in order to achieve process optimization by investigating the basic heat and mass transfer mechanisms during the primary drying stage of vial freeze-drying of pure ice by observing the sublimation front movement directly. The theoretical model developed by the authors takes into account the curvature of vial bottom, the heat transferred from the glass vial sidewalls and the heat accumulation in the glass vials. Good predictions of the rate and geometry of ice sublimation front movement, the sublimation time, temperature profile and the influence of the total chamber pressure were achieved in comparison to experimental from the simulations. However, the scarce availability of heat and mass-transfer resistance data and limited knowledge of product properties restricts the use of these models to only a limited range of operating conditions.

2.5 Materials

2.5.1 Lactose

Lactose is an important carbohydrate or disaccharide found in milk of mammals, typically there is 4-6% in cow's milk and 5-8% in human milk. When lactose is hydrolysed it yields one unit of the monosaccharide glucose and one unit of the monosaccharide galactose due to the breakage of the β1→4 glycosidic linkage (Fig. 2.9) (Garnier *et al.,* 2002). Lactose is comparatively cheaper, non-toxic and found to be less sweet in taste than its monomeric units – galactose and glucose.

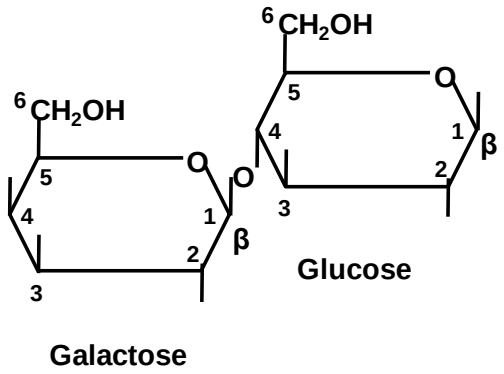

Figure 2.9: Structure of Lactose molecule.

Dry lactose is commonly found as amorphous and crystalline lactose. Crystalline lactose exists in two different isomeric forms as anomers and they are referred to as *α*-lactose and *β*-lactose. The two different types of lactose have different effects on various properties like crystal morphology and solubility. *α*-lactose and *β*-lactose interconvert between each other and display the phenomenon known as mutarotation (Dincer *et al.,* 1999). The rate of conversion of one form into another is dependent on a number of conditions such as the lactose concentration, the temperature and pH of the solution. At room temperature, the ratio of the two anomers is around 40% *α*-lactose to 60% *β*-lactose. *α*-lactose generally exists as a monohydrate due to the presence of a water molecule in its crystal structure. The *β*-form is anhydrous and crystallizes out of solution only at temperatures above 93.5°C while below that temperature *α*-lactose crystals are formed (Johnson & Conforti, 2003).

Solubility of lactose is highly temperature-dependent and also depends on its mutarotation. It has been found that *β*-lactose is more soluble than the *α*-form of lactose. The mutarotation plays an important role in the temperature-dependent solubility of lactose. As lactose is dissolved in water, the solubility is found to increase proportionately due to the conversion of *α*-form to *β*-form (Johnson & Conforti, 2003). Due to its higher solubility, *β*-lactose is perceived to be sweeter in taste than *α*-lactose. The phase diagram of lactose similar to that of sucrose shown in Fig. 2.2, has been discussed in literature by Ubbink *et al.,* (2008) which describes not only the solubility curve, but also the freezing and glass transition curves of lactose with respect to its whole milk.

Industrial production of Lactose: Production of lactose is mainly carried out from whey permeate left after the production of cheese and whey. The use of the ultrafiltration process in the dairy industry can be made economical if the permeate produced as waste is used as a means of production of lactose. The main steps involved in the production of lactose include concentration of permeate, removal of whey, crystallization and centrifugation for collection of crystals (Schuck & Dolivet, 2002 and Roelfsema *et al.,* 2010). Commercially α-lactose has more applications when compared to *β*-lactose. Pharmaceutical grade lactose involves a few additional steps in the production process. Refining with activated carbon to remove peptones, recrystallization, centrifugation, drying and milling of the dried lactose is performed to meet the high pharmaceutical standards.

Applications of Lactose: Lactose is one of the most commonly used excipients in the pharmaceutical industry (Varshosaz *et al.,* 2012). It is used as an excipient and filler in tablets and capsules. Lactose is also being used in nasal drug delivery as a carrier (Steckel & Bolzen, 2004). Derivatives of lactose like lactilol, lactobionic acid, lactulose are also used for the treatment of various diseases (Johnson & Conforti, 2003; Gutiérrez *et al.,* 2012). Lactulose is used as a laxative while lactobionic acid is used as a carrier for various antibiotics. Lactose is also used as a low calorie sweetener, in products for diabetics and also in slimming products. In the food industry, there are a number of applications of lactose. The major use of lactose is in baby and infant foods (Nasirpour *et al.,* 2007), in skimmed milk and condensed milk products (Roos, 2009). It is also used in various frozen desserts like ice creams, baked products and coffee creamers (Roelfsema *et al.,* 2010).

Freeze drying of Lactose: Freeze drying of lactose has been studied mainly in the food and pharmaceutical industries due to its wide application as a pharmaceutical excipient and as a constituent in various milk products – milk powders, whey powders, desserts and confectionaries. Very few researchers have focussed on the freeze drying of lactose. Some of those studies will be discussed in this section. Tsourouflis, (1975) has determined the collapse temperatures of different carbohydrate solutions namely lactose, maltose and sucrose with respect to their use in fruit juice powders. He has also studied the effect of moisture content, rate of freezing and initial concentration on the collapse temperature of single carbohydrate solutions and multicomponent systems (e.g. lactose and sucrose). Collapse in the

samples was observed visually by the change in appearance, where the sample appeared to be a highly viscous material rather than a dry solid. In context of lactose solution, collapse temperature was found to be higher than all three sugars tested. Rate of moisture absorption during humidification and collapse temperature was higher in the case of fast frozen samples than in slow frozen samples.

Chen *et al.,* (2008) have compared the freeze drying rates of sucrose and lactose solutions by photographic recording, using heat flux sensors, temperature and manometric measurements. They have discovered that the use of heat flux sensors is a good non-invasive technique to monitor the sublimation process of freeze drying in vials. Measurement of product temperature alone is not an efficient technique to monitor the sublimation process and determine sublimation rate. Manometric measurement was also used with a number of vials in the lyophilizer chamber in order to give a noticeable pressure rise, and the method therefore measures an average sublimation rate for the collection of vials. Comparison of sublimation rates lead to the conclusion that initial sublimation rate of lactose solutions is slower compared to that of sucrose solutions. The major portion of the sublimation cycle has similar rates in both cases and decreases towards the end of the primary drying cycle.

Usually, freeze drying of lactose is carried out to understand the crystallization process of lactose and hence very few researchers have focussed specifically on its freeze drying kinetics. Hence, this research project aims to bring forth both the freeze drying kinetics as well as the crystallization kinetics of lactose and the dependence of both processes on each other.

2.5.2 Coffee

Coffee is an important beverage consumed in great quantity throughout the world. Coffee bean, and in turn, the final freeze-dried instant coffee, is a multi-component complex system of water, carbohydrates, lipids, amino acids, aliphatic acids, caffeine, and minerals (Rivera *et al.,* 2011). These components also include alkaloids, phenolic compounds, polyphoenols and diterepenes summarised in Table 2.1 (Brezova *et al.,* 2009 and Frost-Meyer & Logomarsino, 2012). Some of these components are volatile in nature (higher volatility than water, i.e., evaporates quicker in comparison to water) and contribute to the flavours and aroma associated with coffee. The retention of these compounds is an important aspect of freeze-drying of coffee during

manufacture. During freezing, these various components are trapped between the ice crystals forming the unfrozen boundaries of ice crystals and thus govern the process of sublimation - higher the concentration of these compounds, slower the sublimation process as it makes removal of ice and volatiles difficult (Sagara *et al.,* 2005 and Khwanpruk, 2009). Apart from sublimation these compounds may also influence the freezing process itself, by either acting as seeds for ice crystals (heterogenous nucleation), delaying or inhibiting ice crystal formation. However, the effect of individual component on freezing has not been investigated in detail in literature and is an avenue worthy of exploration in future.

Table 2.1: The various important components present in green coffee beans and their amount in 150ml coffee solution adapted from Frost-Meyer & Logomarsino, 2012.

Compound	Molecular Formula	Amount in Coffee (150ml)
Caffeine	$C_8H_{10}N_4O_2$	Varies with brewing method ~45-80mg
Cafestol	$C_{20}H_{28}O_3$	Varies with brewing method ~0.15mg or 0.75-12mg
Kahweol	$C_{20}H_{26}O_3$	Varies with brewing method ~0.15mg or 1-15mg
Chlorogenic acid (CGA) & Caffeic acid	$C_{16}H_{18}O_9$	~50-250mg CGA & 25-130mg Caffeic acid
Trigonelline	$C_7H_7NO_2$	~2mg

All these components are directly and/or indirectly affected by harvesting methods as well as the industrial processing steps especially the roasting process. The characteristic flavour and aroma of coffee produced during roasting affect the quality and stability of the final product.

Production of Instant Coffee: The production of coffee involves a pathway generally described by the phrase 'seed to cup' which include a varied number of steps (Huang & Zhang, 2013). The coffee production starts with the initial phase of planting of the bean (seed), harvesting of the coffee cherries and processing of the cherries either by wet or by dry method. If the wet method is used for processing, the beans are dried and milled by hulling followed by polishing, grading and sorting (Corrêa *et al.,* 2010).

Once, the beans, known as 'green coffee' are selected, they are transported to the production unit. Here, the coffee beans are roasted to develop aroma, flavour and soluble solids of the coffee. This step is followed by grinding to achieve specific particle size so as to facilitate the next step in the process, that is, the extraction of the soluble solids (Mateus *et al.,* 2007). The soluble and insoluble solids are, thus, separated by centrifugation and concentrated by reducing the water content of the slurry. The concentrated coffee slurry is then subjected to foaming or aeration so as to increase the size and facilitate the final freeze drying process. Once the foaming process is completed, the material is subjected to freezing resulting in a mass of ice and coffee which is then granulated to achieve the size of the final product. These frozen granules are finally, vacuum freeze-dried to remove all the water present by the process of sublimation resulting in the final dried product known as instant coffee.

Freeze drying of coffee: Freeze drying is an important step in the production of instant coffee. Spray drying has also been used extensively to produce instant coffee, however, freeze drying is said to produce better quality of product. Although, freeze drying is an expensive and energy intensive process, it preserves the flavour and aroma of coffee during the process due to the low-temperature conditions used during drying compared to spray drying (MacLeod *et al.,* 2006). One of the manufacturers' main areas of concern is reducing drying times, whilst still maintaining the final residual moisture content and the product quality.

Many researchers have focussed on the study of sublimation kinetics during freeze drying of coffee solutions. Ferguson *et al.,* (1993) have presented a numerical model with respect to heater temperature, ambient moisture content and chamber pressure and their effect on drying time has been studied. The model employs finite-element analysis and also makes use of temperature gradients to track the movement of the sublimation front through the coffee sample during freeze drying and was found to display good co-relation with experimental results. Sagara & Ichiba, (1994) developed a mathematical model to determine the thermal conductivity and permeability for the dried layer of coffee sample undergoing freeze-drying. Thermal conductivity was found to decrease proportionally to the porosity and temperature of dried layer. Permeability was seen to increase with increasing the porosity, pressure and temperature of the dried layer. They also point out that solid content of the

sample is a critical factor which governs the structure of the final product by influencing the freezing process and the water vapour transport properties mainly depend upon the nature of this structure during drying.

Sagara, (2001) have displayed the effect of thermal conductivity on porosity of coffee during freeze drying. They discussed that lower thermal conductivity resulted in higher porosity of coffee cake (29-45% w/w). Pardo *et al.,* (2002) have studied the effect of ice crystal sizes in frozen coffee, determined by image analysis, on the freezing rates described by Neumann's model. According to this model, in unidirectional freezing process, movement of the freezing front is directly proportional to time and is based on the assumption of isothermal phase change from liquid to solid. It is said to be based on the unsteady state conduction between the frozen and unfrozen layers of the sample and is commonly applicable to most cases studying freezing kinetics (Pardo & Niranjan, 2011). While in the research work presented by Boss *et al.,* (2004), a suitable mathematical model for the freeze drying process was developed and validated with experimental data obtained for the process for skim milk and soluble coffee in order to optimize the method. Apart from optimization of the process, effect of freeze drying process parameters such as freezing and drying temperatures on the aroma characteristics of soluble coffee have also been elucidated by Sagara *et al.,* (2005). The optimal design of the method takes into account the distinguishing changes in aroma affected by freeze-drying conditions.

2.6 Conclusion

Freeze drying is a drying technique commonly used these days for the production of heat-sensitive products high value especially in the pharmaceutical industry, although it is used for the drying some niche food products such as coffee, infant-formula due to the low temperature operating conditions. The main drawback of the system is the high refrigeration costs incurred due to the long durations of freezing conditions in which the samples are maintained for drying. Thus, optimization of the freeze-drying process can be achieved by reducing the primary drying time for the products being dried. To achieve this control of the process, it is important to have greater understanding of the heat and mass transfer phenomena that takes place during freeze-drying.

Many researchers have focussed on gaining knowledge of the heat and transfer processes and the effects of various process and product parameters on drying kinetics of products as discussed in this chapter. However, most of the literature focussed on the use of modelling and simulation in order to predict and determine the various process parameters that influence the primary drying stage of freeze-drying. It would be beneficial to have a better understanding of the influence of the product properties such as solid content and experimental conditions such as cooling rate on the microstructure of the frozen material thereby indirectly understanding their effects on the sublimation kinetics.

Moreover, the lack of use of equipment such as the freeze drying microscope to achieve this understanding of the effect of microstructure on freeze-drying kinetics is an avenue that has been scarcely explored by researchers of this field. Hence, the main objective of this thesis is to overcome this gap in this field of research and to gain a better understanding of the effect of various operating parameters on frozen microstructure using freeze drying microscopy. These parameters include solid content, induced nucleation, cooling rate, drying temperature, annealing and aeration. The aim of this research is also to correlate this information obtained from the freeze drying microscopy with the freeze drying kinetics of products in a lab-scale freeze dryer similar to a real freeze-drying system.

3

EXPERIMENTAL METHODOLOGY

This chapter gives an overview of the investigative techniques used in this research. Initially, the basic principles of the techniques are discussed followed by their applications and finally the different experimental procedures for each technique is outlined. This chapter focuses on the methodology for the analysis of images obtained from freeze drying microscopy and measurement of the sublimation front velocity using MATLAB. It also outlines the basic twin-resistance model for the fitting of the data thus obtained from MATLAB. This is used to determine the edge resistance and resistance of the dried matrix from the experimental data.

3.1 Introduction

This chapter demonstrates the various materials and experimental methodologies used in this research. Firstly, the different materials are described followed by details of moisture content determination and sample preparation methods. The basic principles of the experiments conducted on freeze drying microscopy (FDM) and shelf Freeze Dryer (FD) are thoroughly discussed. This section of the thesis also discusses in detail the methodology for the FDM image analysis of the freeze-drying of lactose and coffee samples. This is followed by descriptions of various analytical techniques including Field Emission Gun Scanning Electron Microscopy (FEGSEM) and Differential Scanning Calorimetry (DSC). The above mentioned techniques are explained and their operation and application to this study are illustrated followed by its experimental protocol.

Previously, only few researchers have used freeze-drying microscopy as a tool to understand the freeze-drying process (Zhai *et al*., 2003 and Borgognoni *et al*., 2012), but these have used mainly manual methods of data extraction. The main aim of this study was to develop an image analysis method and which would enable large amounts of images to be analysed. This chapter also describes the proposed twin-resistance model adapted from Quast & Karel, (1968) which describes how the frontal position varies with time during sublimation observed under FDM, and can therefore be used to fit to the data obtained. This will allow a systematic study of different factors that affect freeze drying kinetics in this system. This will hopefully provide insights that can be applied more widely to conventional freeze drying systems.

3.2 Materials

Materials, such as α-lactose monohydrate, Sodium chloride (NaCl), Potassium chloride (KCl), Magnesium chloride ($MgCl_2$) and Silver iodide (AgI) were purchased from Fisher Scientific (Loughborough, UK). Lactose was stored in an air-tight bottle to prevent any moisture absorption. Spray-dried Nescafe coffee was purchased from the local supermarket and stored in a cool and dry place with little exposure to

atmosphere. Lactose and coffee were selected as the basic starting materials as they are commonly freeze-dried in the pharmaceutical and food industries respectively. Lactose is a single component system while coffee is a more complex multi-component system. Sodium chloride, magnesium chloride and potassium chloride were used as eutectic mixtures for the temperature calibration of the microscope.

3.3 Determination of Moisture Content

Moisture content of a material can be expressed using either a wet basis or dry basis. The dry basis moisture content is defined as the ratio of the weight of water to the dried weight of the sample while wet basis moisture content is defined as the ratio of the weight of water to the initial total weight of the sample. The methods to determine moisture content can be divided into two: primary methods and secondary methods (Grabe, 1989). Primary methods or direct methods are those in which the water content in the sample is removed totally and moisture content is calculated from the difference of weight. Secondary methods are indirect methods in which some physical or chemical characteristics of the sample are measured that are affected by the moisture content of the sample. The most common indirect methods are electrical capacitance or conductance methods (Chen, 2003).

3.3.1 Hot-air oven drying method

Oven drying methods are the simplest moisture content determination methods compared to other techniques. Two kinds of drying ovens are commonly used: hot air ovens and vacuum ovens. Air ovens are more convenient and less expensive than vacuum ovens and can be easily used for materials which are not drastically affected by high temperature. To determine the moisture content of the purchased spray-dried Nescafe coffee, 5 g of sample was weighed and dried at 105˚C in the high-temperature oven overnight (~24hrs) until the weight of the sample was almost constant (Navaratne, 2013). The moisture content of the coffee sample was determined on a wet basis by the formula -

$$M = \frac{W_i - W_f}{W_i} x100 \qquad (3.1)$$

where M is the moisture content, W_i is initial weight of the sample and W_f is final weight of the sample.The moisture content of the coffee sample was calculated to be 5.5 ± 0.2% (an average of three sample sets).

3.3.2 Karl Fischer titration

One of the most commonly used methods to determine total water/moisture content of samples is Karl-Fischer (KF) titration. KF titration is a bipotentiometric method for determination of total moisture content of materials which may contain water in the 'bound' as well as 'free' state (Tavcar *et al.,* 2012). It is based on the oxidation of sulphur dioxide by iodine with the consumption of water molecules. In KF titration, the endpoint of a titration can be determined by visual observation of color or by electrometry (coulometry or volumetry). The volume of the titrant needed for the reaction represents the total amount of water present in the sample (Rückold *et al.,* 2000).

KF coulometric titration was used to determine the moisture content of the as received α-lactose monohydrate. The oven drying or high temperature drying method was not used in this case, as it does not take into account the moisture or water molecules present as a hydrate (bound water) in *α*-lactose monohydrate. KF titration of lactose was carried out on a CA-21 Mitsubishi water meter, Japan. Initially, a water standard is run on the meter to determine the calibration factor followed by the actual lactose sample solution. The analyte solvent and cathode used in this case was chloroform and methanol mixture and sulphur dioxide and iodine compound respectively. The moisture content of the as received α-lactose monohydrate was determined on a wet basis to be 5.8 ± 0.3%.

3.4 Sample preparation

3.4.1 Solutions with varying solid content

Five different solid concentrations of α-lactose monohydrate (5%, 10%, 20%, 30% and 40%) were prepared by dissolving specific masses of lactose powder into a glass sample beaker containing a weighed amount of hot distilled water (70˚C). The amount of water to be added to each sample was determined as follows:

$$w=s\left\{\left(\frac{100}{c}\right)-\left(\frac{m}{c}\right)-1\right\} \quad (3.2)$$

where, w is the mass of water to be added (g), s is the mass of sample including initial moisture (g), c is the final percentage solid content of the sample required and m is the initial wet basis moisture content of the sample (%) determined according to Section 3.3.

3.4.2 Aeration of Coffee extract

Aeration of coffee extract prior to freeze drying is a commonly used commercial technique to induce faster freeze drying and also subsequent rehydration and create the microstructure necessary to create the foaming properties found in instant coffee. In an industrial set-up, generally carbon dioxide is commonly pumped through the coffee extract and followed by depressurizing the coffee solution in order to create the air-bubbles of the required size.

For the purpose of this study, a 50% (w/w) coffee solution was aerated using a commercially available cream whipper (Mosa Professional 0.5 L, Mosa Industrial Corp., Huwei, Taiwan) with nitrous oxide capsules to pressurize the vessel (Fig. 3.1).

Figure 3.1: Cream whipper used for aeration of 50% coffee extract before freeze drying.

Nitrous oxide capsules are safe to be used in food preparations and are usually used for making whipped cream using the cream whippers.

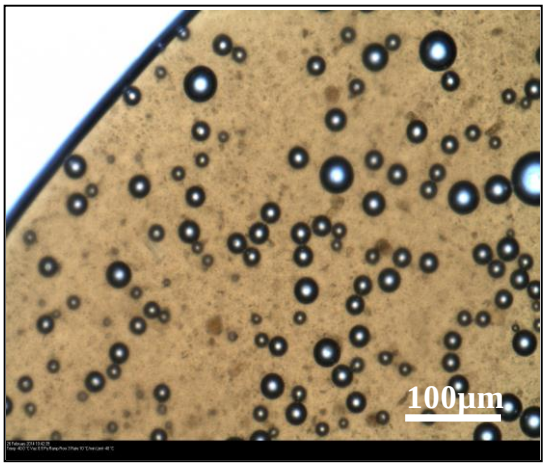

Figure 3.2: Air bubbles incorporated into 50% Coffee solution observed under the freeze drying microscope after freezing

50% coffee extract was used in order to have a thick consistency like cream so as to achieve successful aeration. Aeration using this method resulted in thick coffee foam with required microsized bubbles varying in an average size of less than 50 µm as shown in Fig. 3.2.

3.5 Freeze-drying microscopy

Freeze drying microscopy (FDM) is a technique which allows the direct visualization of the freeze drying process on a small scale. It permits the observation of freezing of samples, followed by sublimation, which is viewed in the form of sublimation front movement. The sublimation front is observed as the dividing line between the dark freeze-dried layer and the light frozen layer, which increases in depth with time as the front proceeds further into the sample. Fig. 3.3 shows the basic principle behind this phenomenon observed under freeze drying microscopy. The dark and light layers are observed due to the differences in scattering behaviour between the dried layer and frozen layer. The dried layer does not allow the light to pass through in a straight direction due to the presence of air voids in the matrix while the frozen layer consists of ice crystals which readily allow the light rays to pass through directly. This

behaviour occurs because of the difference in refractive indices of ice (1.3) and air (1.0) (present in voids) present in the two different layers.

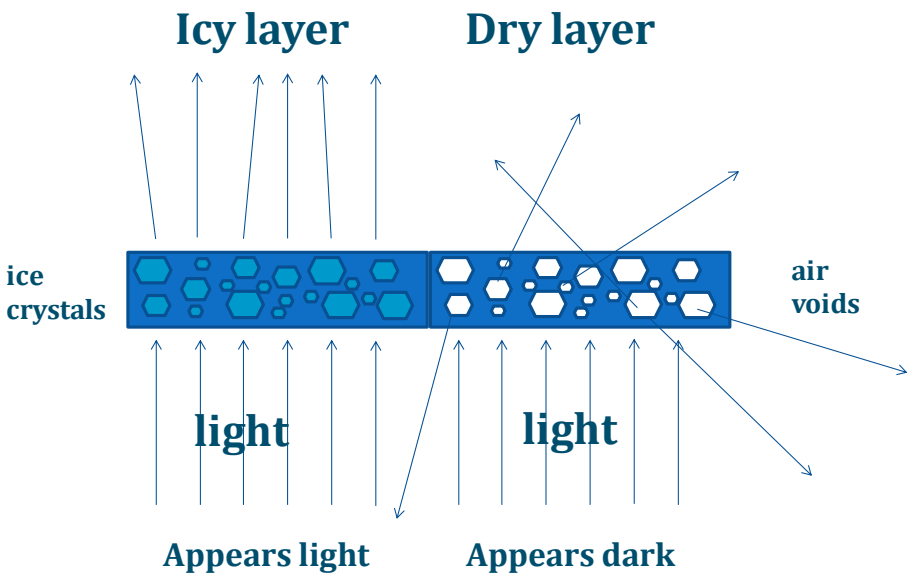

Figure 3.3: Basic principle of sublimation process as observed under freeze drying microscope.

Usually, FDM is used to determine the critical formulation temperature (also known as the collapse temperature) of the material to be freeze-dried. However, in this study, it has been used as a tool not only to determine the factors which affect the collapse temperatures but also to observe the sublimation rates of different materials.

3.5.1 Instrumentation

An Olympus BX43 polarised light microscope (Olympus Microscopy, Essex, UK) with a Linkam FDCS196 variable temperature control stage (Linkam Instruments, Tadworth, UK) coupled to a Q-Imaging Retiga-2000R camera (Surrey, Canada) (Fig. 3.4) was used to perform all the experiments.

The stage pressure, temperature and image capture were controlled using the Linksys 32 software data capture system (Linkam Instruments, Tadworth, UK). The stage was sealed so that a vacuum could be drawn using a vacuum pump. The pressure was measured using a Pirani gauge and controlled using an automatic valve over a range of 1 Pa to 100000 Pa. Liquid nitrogen was used as the coolant and was passed through the silver block of the stage upon which the sample glass slides were mounted (see Fig. 3.4 inset). Images of the samples of 1600x1260 pixels (which

correspond to 399x314 microns) were recorded at intervals of 10 seconds throughout the experiment.

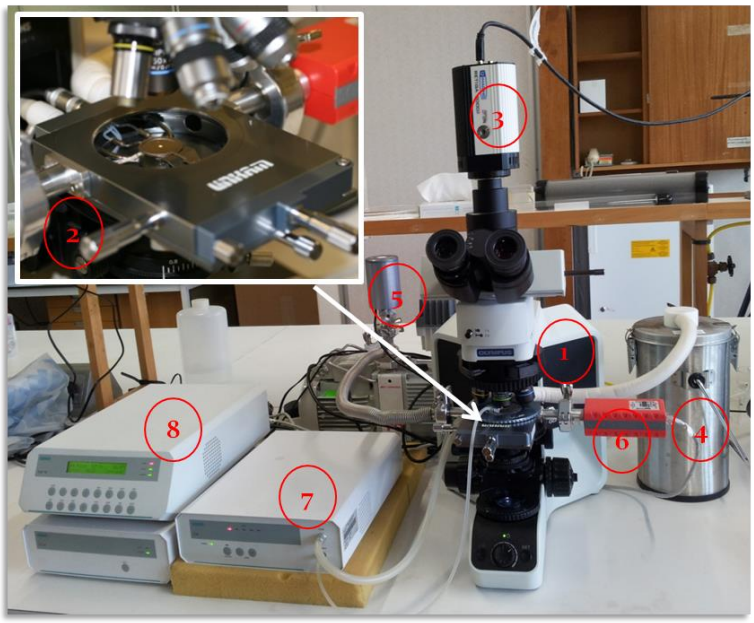

Figure 3.4: A freeze drying microscope used in this research with illustration of all its components -1. An Olympus BX2 microscope. 2. A Linkam FDCS196 variable temperature control stage. 3. A Retiga 2000R digital camera. 4. Liquid nitrogen carrier. 5. A Vacuum pump. 6. A Pirani gauge. 7. Liquid nitrogen pump. 8. Temperature controller.

3.5.2 Sample preparation

To perform the experiments, 2 µl of sample was loaded on to a circular glass slide (16 mm diameter), with two thin strips of adhesive tape as spacers to achieve a uniform thickness (30 µm) and covered with another glass coverslip (13 mm diameter) which was loaded on to the stage assembly under ambient conditions. Apart from this, a few more sample thickness were investigated – 50 µm, 70 µm and 0 µm (no spacer). The absence of spacers leads to variation in the thickness of the sample solution thereby further causing potential variations in sublimation front velocity between repeat runs. The use of spacers thicker than 30 µm resulted in a dense sample which resulted in difficulty to observe the ice crystals formed and the movement of sublimation front through all the samples. Hence, spacer thickness of 30 µm was used for all the experiments. A drop of silicone oil was used to attain good thermal contact between the silver block and the bottom of the lower coverslip (Fig. 3.5).

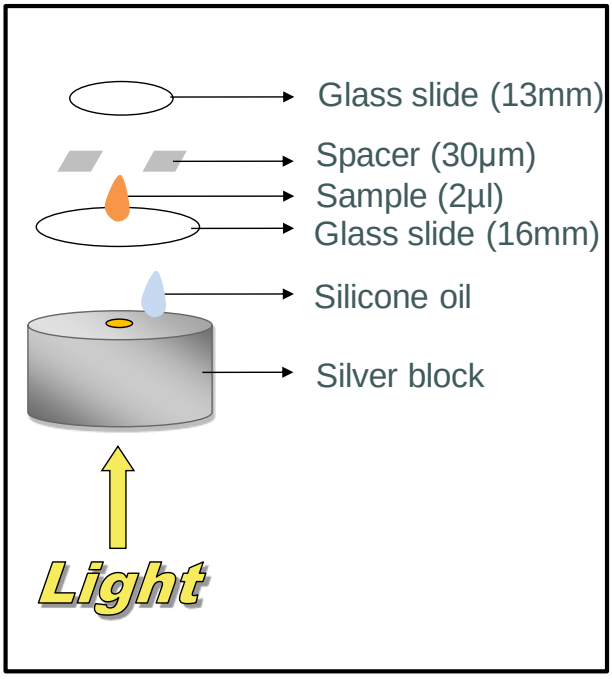

Figure 3.5: Illustration of the sample loading on to a Freeze drying microscope stage

3.5.3 Stage temperature calibration

Calibration of the stage temperature sensor was carried out using 10% solution (w/w) each of NaCl, KCl and $MgCl_2$ (Fonseca *et al.,* 2004; Meister *et al.,* 2009). 2 µl of the salt solution was placed between the microscope slides and loaded on to the stage. The sample was cooled at 10 $K.min^{-1}$ and the melting temperature of the eutectic crystal (ice and salt crystal) was noted from the images obtained (see Appendix A). The deviation in measured temperatures for these transitions were within ±0.3˚C of the values published in literature for NaCl (-21.1˚C), KCl (-10.7˚C) and $MgCl_2$ (-33.6˚C) (Meister *et al.,* 2009).

3.5.4 Experimental conditions

Lactose: A sample volume of 2 µl of sample solution was prepared and loaded on to the microscope stage for the collapse temperature and frontal velocity determination. Initially, three different cooling profiles were investigated with lactose solution as summarised in Table 3.1. Once the sample solution was frozen to the final temperature of drying, a reduction of the vacuum pressure to 1 Pa (below the equilibrium vapour pressure of ice at -40˚C of 12.8 Pa) was carried out to facilitate sublimation. This process resulted in the sublimation of ice into water vapour from the sample and movement of the sublimation front was generally observed for about

1000 s. For some experiments, a miniscule amount of AgI (<10μg) was placed on the bottom glass slide before loading of the sample. The purpose of the AgI, which is a nucleating agent for ice, was to induce nucleation at a higher temperature in the samples. The different cooling profiles, final freeze-drying temperatures and lactose solid contents considered for these experiments of lactose are summarised in Table 3.1. In some cases, the sublimation front was also observed for a much longer duration (~ 1 hr) for improved study of the effect of the dried region thickness (from the sample edge) on frontal velocity.

Table 3.1 Various cooling profiles, solid contents and final temperatures of drying used under FDM for lactose solutions.

Lactose Solid Content (% w/w)	Cooling profile ($K.min^{-1}$)		Final drying temperature (°C)	
	Non AgI	AgI	Non AgI	AgI
5		10	-40	-40
10	1	2	-40	-40
10	10	10	-40	-30, -40, -50
10	40	50	-40	-40
20		10	-40	-40
30		10	-40	-40
40	1	2	-40	-40
40	10	10	-40	-30, -40, -50
40	40	50	-40	-40

Coffee: Different solid contents of coffee solutions were also subjected to various cooling profiles and final temperatures of drying as described in Table 3.2.

Table 3.2 Various solid contents of coffee solutions and the cooling profile and final temperatures of drying followed under FDM.

Coffee Solid Content (% w/w)	Cooling profile ($K.min^{-1}$)	Final drying temperature (°C)	
	Non-AgI & AgI	Non-AgI	AgI
2	10	-40	-40
5	10	-40	-40
10	2	-40	-40
10	10	-40	-30, -40, -50
10	50	-40	-40
20	10	-40	-40
30	10	-40	-40
40	10	-40	-40
50	2	-40	-40
50	10	-40	-30, -40, -50
50	50	-40	-40

Similar cooling profiles, drying temperatures and solid contents to lactose were followed in case coffee solutions, both with and without AgI. Additional experiments with solid contents 2% and 50% (w/w) were also conducted in case of coffee and the drying temperatures and cooling profiles were investigated in 50% instead of 40% Coffee.

Annealing: The effect of the process of annealing on ice crystal size and, in turn, on the sublimation kinetics was also studied in case of 10% and 40% lactose and 10% and 50% coffee samples. The sample solutions were subjected to a process of freezing, heating and subsequent cooling in order to increase the size and number of ice crystals formed. The different cooling/heating profiles followed for the annealing process are summarized as follows -

Profile I - Cooling at 10 $K.min^{-1}$ to -40˚C followed by slow warming at 2 $K.min^{-1}$ to -20˚C and isothermal hold for 10 mins followed by final cooling at 10 $K.min^{-1}$ to an isothermal hold at -40˚C.

Profile II - Cooling at 10 $K.min^{-1}$ to -40˚C followed by slow warming at 2 $K.min^{-1}$ to -10˚C and isothermal hold for 10 mins followed by final cooling at 10 $K.min^{-1}$ to an isothermal hold at -40˚C.

Profile III - Cooling at 10 $K.min^{-1}$ to -40˚C followed by slow warming at 2 $K.min^{-1}$ to -20˚C and isothermal hold for 60 mins followed by final cooling at 2 $K.min^{-1}$ to an isothermal hold at -40˚C.

Profile IV - Cooling at 10 $K.min^{-1}$ to -40˚C followed by slow warming at 2 $K.min^{-1}$ to -10˚C and isothermal hold for 60 mins followed by final cooling at 2 $K.min^{-1}$ to an isothermal hold at -40˚C.

Ice crystal/pore size: 10% and 40% lactose solutions and 10% and 50% coffee solutions were also freeze-dried under the microscope overnight (with and without AgI) in order to obtain completely dried samples without any structural collapse. These samples were used to determine the ice crystal size using scanning electron microscope under higher magnifications which were not possible using FDM. ImageJ software was used to measure the size of the pores left behind from the ice crystals formed from the images obtained from both FDM and FEGSEM.

Collapse temperature: To measure the collapse temperature, the sample lactose solutions (10% and 40%) were subjected to various cooling and heating profiles summarised in Table 3.3. This was carried out in order to determine the effect of cooling rates on the collapse temperature of sample. The Liquid nitrogen quenching (LN_2) cooling rate was achieved by bringing the glass slide containing the sample solution into direct contact with liquid nitrogen in a tray and placing it on a pre-cooled FDM stage maintained at -50˚C.

Table 3.3 Various cooling and heating rates followed to determine effect on collapse temperature of lactose sample.

Lactose Solid content (%w/w)	Cooling rate (K.min^{-1})	Heating Rate (K.min^{-1})
10	2	1
		10
	50	1
		10
	LN_2 quenching	1
		10
40	2	1
		10
	50	1
		10
	LN_2 quenching	1
		10

Once the specified final temperature of drying was reached, the frozen sample was held at the temperature for 5 mins and subjected to a vacuum pressure of 1 Pa to facilitate sublimation. The process of sublimation was observed for 5 mins and the sample was heated at a specific rate (shown in Table 3.3) in order to observe the onset of collapse. The starting point or onset of structural collapse was designated as the collapse temperature (T_c) of the sample. The onset of collapse is identified with the appearance of a light band next to the moving dark sublimation front. This temperature is defined as the collapse temperature of the sample.

The different profiles for determining collapse temperature was followed only for 10% and 40% lactose solution as lactose is a single component system and the effects of cooling profile could be seen much more significantly as compared to the complex-multicomponent coffee system. Collapse temperature determination of 10% and 50% coffee solutions were also carried out but only following a single cooling profile of 10 K.min^{-1} and heating profile of 1 K.min^{-1}.

3.5.5 Image analysis of the sublimation front movement

Linksys32 software was used to capture images from the freeze drying microscope of the sublimation process carried out for lactose and coffee solutions. The camera software captured images at a rate of 1 per 10 seconds. Figs. 3.6 A & 3.6 B show images of 10% lactose solution before freezing and after freezing respectively observed under the freeze drying microscope.

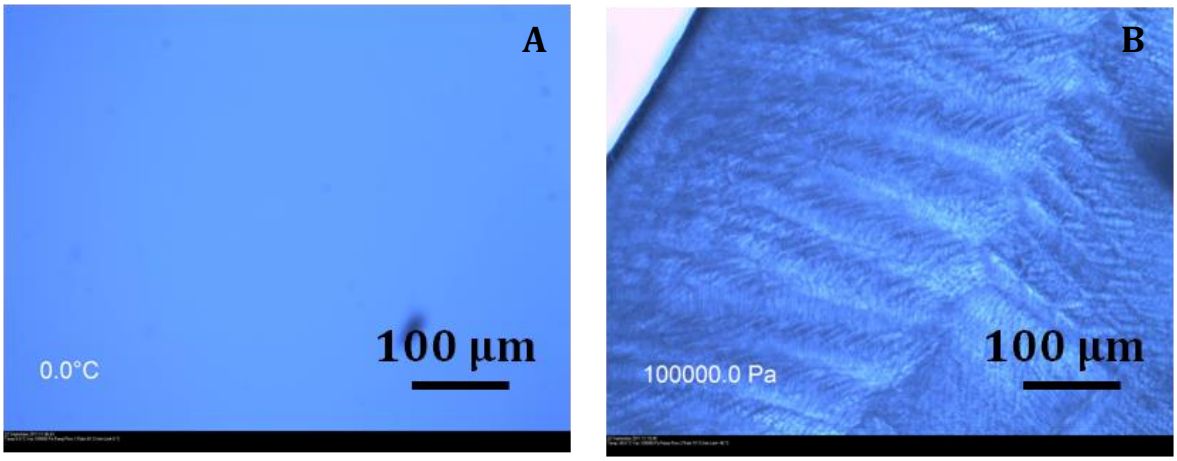

Figure 3.6: A.10% lactose solution image before freezing and **B.** 10% lactose solution after freezing, under the freeze-drying microscope

These images were then analysed using an in-house image analysis program developed by Dr. Andrew Stapley in MATLAB within the department of Chemical Engineering, Loughborough University.

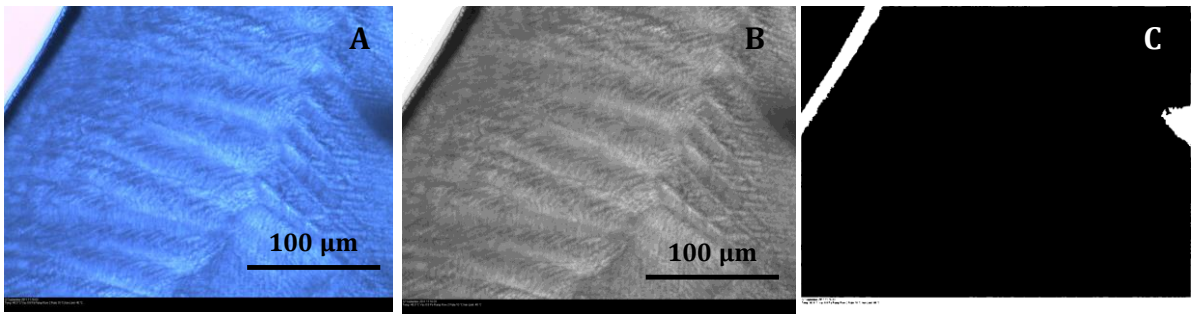

Figure 3.7: A. 10% Lactose frozen under freeze drying microscopy, **B.** Image shown in A converted to grayscale followed by **C.** Thresholded into binary image with white sublimation front

The images obtained were first calibrated into grayscale and then thresholded to a set value in the program to produce a binary image, with the sublimation front seen as a white band on a black background (Fig. 3.7). The threshold value set was only

sensitive to the various solid content of the sample and was not required to be changed for different repeat runs of a single solid content. The user would then define a line parallel to the edge of the sample by defining two pixel points on the first image (Fig. 3.8).

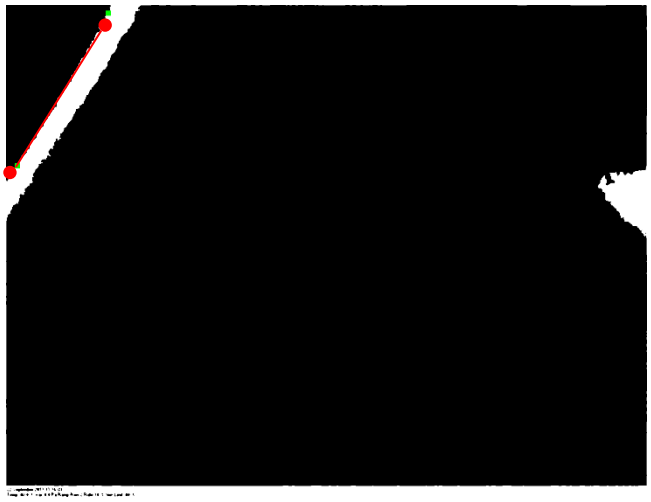

Figure 3.8: The two pixel points and the line parallel to edge of sample defined in MATLAB

A single line or multiple lines perpendicular to the sublimation front would be constructed by the program. The location of these perpendiculars can be defined by the user in the program. The movement of the sublimation front was then tracked along each line (as the transition from white to black pixels) on each successive image (Fig. 3.9). These pixel points were recorded and converted to frontal distance (μm) which was then plotted as a function of time (s).

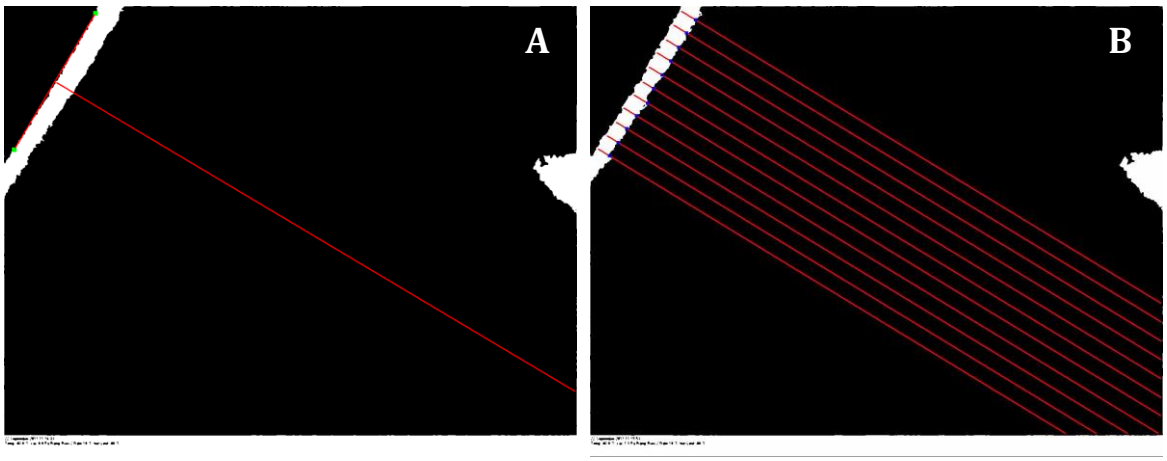

Figure 3.9: A. Single line analysis and **B.** Multiple line analysis carried out in MATLAB

Multiple line analysis was performed to ascertain how uniform the measured frontal positions were at different positions throughout the front line. Typically, eleven lines equally spaced were used and the number of lines to be used for each analysis was defined by the user (Fig. 3.9).

3.5.6 Parameterised Modelling to describe the sublimation front movement

A simple mass transfer model was developed to fit the data for movement of the sublimation front through the sample. The sample solution was very thinly spread between two impermeable glass slides in good thermal contact with a temperature-controlled microscope stage. Hence, heat transfer resistances were not considered as limiting factors affecting the progress of the front, as the sample was effectively under isothermal conditions at the programmed temperature. Fig. 3.10 shows the factors taken into account for the model, namely, the edge of the sample as a dense non-porous layer and the internal porous non-uniform microstructure. The model uses the concept of a sublimation front moving through the sample and movement of mass of water vapour through the sample. This is well established in the literature and a distinct sublimation front could be seen on all freeze drying runs performed.

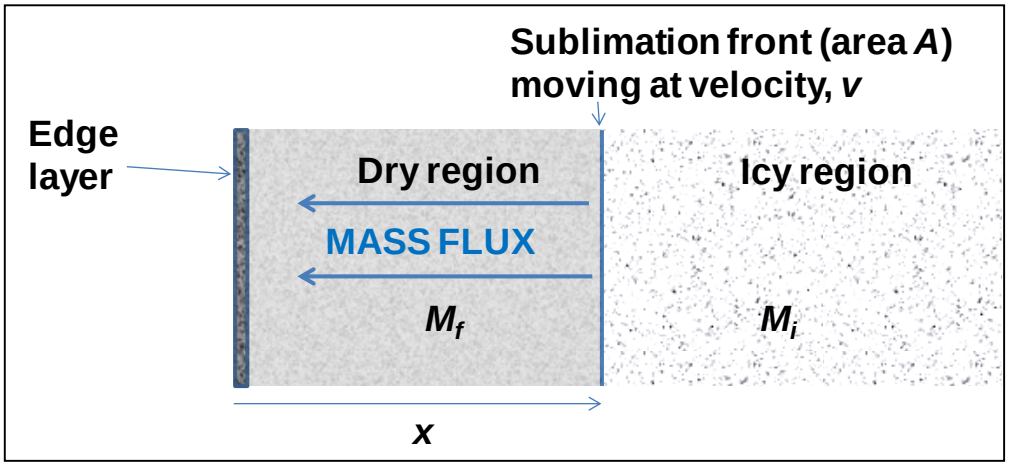

Figure 3.10: The proposed model defining the behaviour of the sublimation front movement through the frozen sample under freeze-drying microscopy

The primary drying rate was controlled by mass transfer from the sublimation front where the water vapour flows through the internal dried region of area *A* and then through the edge layer of the sample. The driving force is the difference in water vapour pressure between the front and the edge of the sample. The vapour pressure

at the front is taken to be equal to the saturated vapour pressure P_{sat} at the stage temperature, (this assumes that water vapour was the only gas in the vapour phase around the sample if all the other gases were withdrawn by the vacuum pump). The frozen matrix was initially at a uniform moisture content of M_i (dry basis), solid frozen density (dry basis) of ρ and dried by sublimation to a final moisture content of M_f (dry basis). The water content of edge layer of the sample was assumed to be negligible. The frozen solid density of the samples were measured by pouring a defined amount of sample solution (5 ml) in metal beakers and then weighed after freezing. The density of the samples (ρ) was calculated on dry basis from the change in the volume of the sample after freezing. The method was similar to the one published in literature by McDonald & Turcotte, (1948).

The mass transfer model described in the current study is a modification of the model proposed by Quast & Karel, (1968) which demonstrates the presence of a surface layer with low permeability followed by higher permeability in the rest of the frozen layer. The frontal data obtained were fitted to the model based on two resistance terms – a constant edge layer resistance (α) and resistance per unit depth of internal dried region (β) that increases proportionally with distance (x) of sublimation front from the edge of the sample. The importance of edge layer in the mass transfer of water vapour has been discussed in detail by many researchers. It is said to be formed by the highly concentrated solution and the transport of water vapour through this layer is either due to the presence of cracks on the surface and in the absence of cracks, it is said to be through diffusion (Kochs *et al.,* 1993).

The mass flux of water vapour perpendicular to the drying front (driving force/resistance) is thus given by,

$$\text{Mass flux} = \frac{P_{sat} - P}{\alpha + \beta x} \tag{3.3}$$

where P is pressure applied to the system and P_{sat} is saturated vapour pressure at a specific operating temperature.

The mass flux can also be related to the velocity of the front as follows:

$$\text{Velocity of the front, } v = \frac{dx}{dt} \tag{3.4}$$

Amount of dry solid swept out per unit time = $\frac{\rho A dx}{dt}$ (3.5)

Moisture removed per unit time = $\frac{\rho(M_i - M_f)Adx}{dt}$ (3.6)

Hence, Mass flux = $\frac{\rho(M_i - M_f)dx}{dt}$ (3.7)

Combining equation 3.3 and equation 3.7,

$$\frac{\rho(M_i - M_f)dx}{dt} = \frac{P_{sat} - P}{\alpha + \beta x} = \frac{\Delta P}{\alpha + \beta x} \quad (3.8)$$

This can be more simply expressed as

Velocity of the front, $v = \frac{dx}{dt} = \frac{1}{a + bx}$ (3.9)

Where,

$$a = \frac{\alpha\rho(M_i - M_f)}{\Delta P} \text{ and } b = \frac{\beta\rho(M_i - M_f)}{\Delta P} \quad (3.10)$$

Integration of equation 3.9 yields

$$t = ax + \frac{bx^2}{2} \quad (3.11)$$

Equation 3.11 can therefore be fitted to experimental data for t as a function of x *(t=f(x))*. Data fitting using least square regression for parameter estimation, to determine goodness of fit and confidence intervals were incorporated into the MATLAB program based on the model described above, in order to obtain the representative edge resistance (a) and resistance per unit depth from the dried region (b). The value of a governs the initial (at x=0) frontal velocity (they are inversely related, as can be seen from equation 3.9). The value of b influences the curvature of the t vs x plot. To obtain accurate values for b sufficient time is required for significant curvature to have emerged on the plots. The calculations for α and β values were performed using the various parameters detailed in Appendix C and

rearranging equation 3.10 to obtain the actual edge resistance and resistance of dried layer.

3.6 Conventional Freeze drying

Conventional freeze drying of sample solutions were carried out in glass vials (for lactose) and metal trays (for coffee) in a VirTis AdVantage Plus Benchtop shelf based Freeze Dryer (Fig. 3.11) (SP Industries, Warminster, PA).

Glass vials: The glass vials used for freeze drying were filled with about 4 mL of lactose solution to ~13 mm height in the vial. The vials were kept in good thermal contact with the shelf using thermal grease. The glass vial used was of 10 ml capacity with an inner neck diameter to be 12.6 mm, outer neck diameter of 24.0 mm and a height of 45.3 mm.

Metallic trays: Circular metallic trays with about 13 mm height of sample (~90 ml) were used for freeze drying coffee solution keeping in line with the methods used in an industrial freeze drying plant of coffee.

Temperature measurement: Temperature measuring T-type thermocouples, to be placed inside the glass vials containing samples to be freeze dried at three different depths – one near the bottom (11 mm), the second in the middle (7 mm) and the third one near the surface (3 mm from surface), were set up inside the chamber of freeze dryer.

These thermocouples were placed in such a way so as to track the movement of the sublimation front through the sample during the drying sample and finally determine the end point of drying. An additional thermocouple was attached to the surface of the shelf to measure the shelf temperature. The temperature data were recorded onto a computer using the Labview-Signal express program developed by Jim Muddimer within the department of Chemical Engineering, Loughborough University.

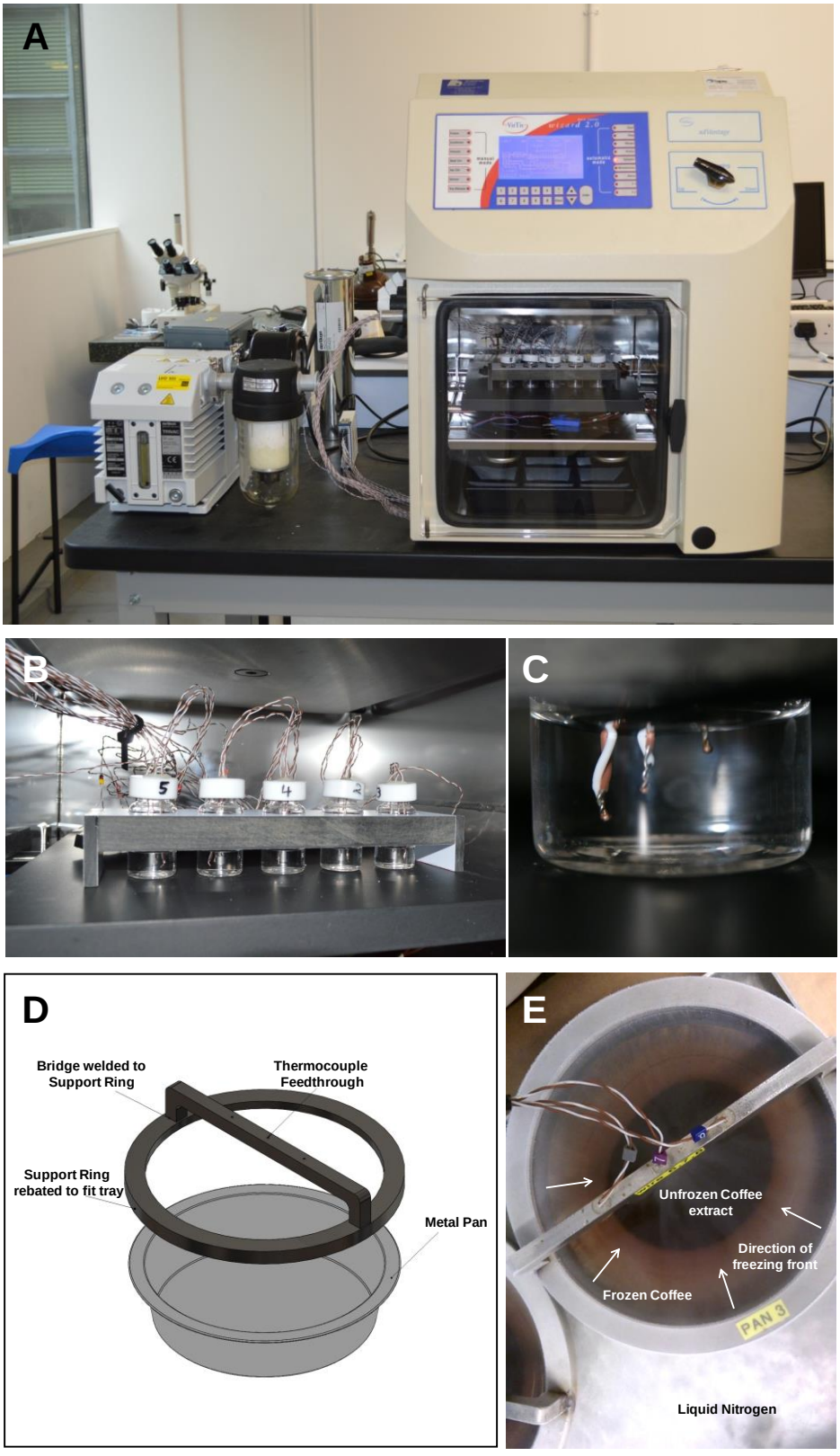

Figure 3.11: A. Virtis AdVantage Plus Shelf freeze dryer. **B.** Vials with thermocouple set up **C.** Magnified image of three thermocouples inside vial. **D.** Schematic representation of metal tray and support ring constructed for placement of thermocouples. **E.** 50% Coffee placed in metal tray frozen by LN_2 quenching.

Profiles: The samples in the vials/trays were loaded onto the freeze-dryer shelf and the door to the chamber was vacuum sealed. The vials are cooled to a temperature of about -40˚C by maintaining the shelf at -43˚C at a rate specified in Table 3.4 and maintained for 60mins to freeze the samples. The condenser was then switched on inside the freeze drying chamber and maintained at -60˚C. The vacuum pump is switched on and the frozen samples are then freeze dried at 10 Pa. The various cooling profiles and solid contents investigated for both lactose and coffee solutions are summarized in Table 3.4. The shelf temperature and chamber pressure profiles investigated are displayed in Fig. 3.12.

Table 3.4 Different cooling profiles carried out for shelf freeze-drying of lactose solution and coffee solution in vials and trays.

Solid Content (%w/w)	Cooling profile ($K.min^{-1}$)
10% Lactose	1. Cooled to -43˚C at 1 $K.min^{-1}$ 2. Cooled with immersing in LN_2 and placed on precooled shelf at -43˚C
40% Lactose	1. Cooled to -43˚C at 1 $K.min^{-1}$ 2. Cooled with immersing in LN_2 and placed on precooled shelf at -43˚C
10% Coffee	1. Cooled to -43˚C at 1 $K.min^{-1}$ 2. Cooled with immersing in LN_2 and placed on precooled shelf at -43˚C
50% Coffee	1. Cooled to -43˚C at 1 $K.min^{-1}$ 2. Cooled with immersing in LN_2 and placed on precooled shelf at -43˚C

Apart from these cooling profiles, 10% lactose and 50% coffee solution was also subjected to an annealing process (see Fig. 3.13). The samples were cooled to -40˚C and maintained for 30 mins and then heated to -10˚C and held at that temperature isothermally for 120 mins before cooling it back again to -40˚C (maintained for 30 mins) before sublimation was commenced.

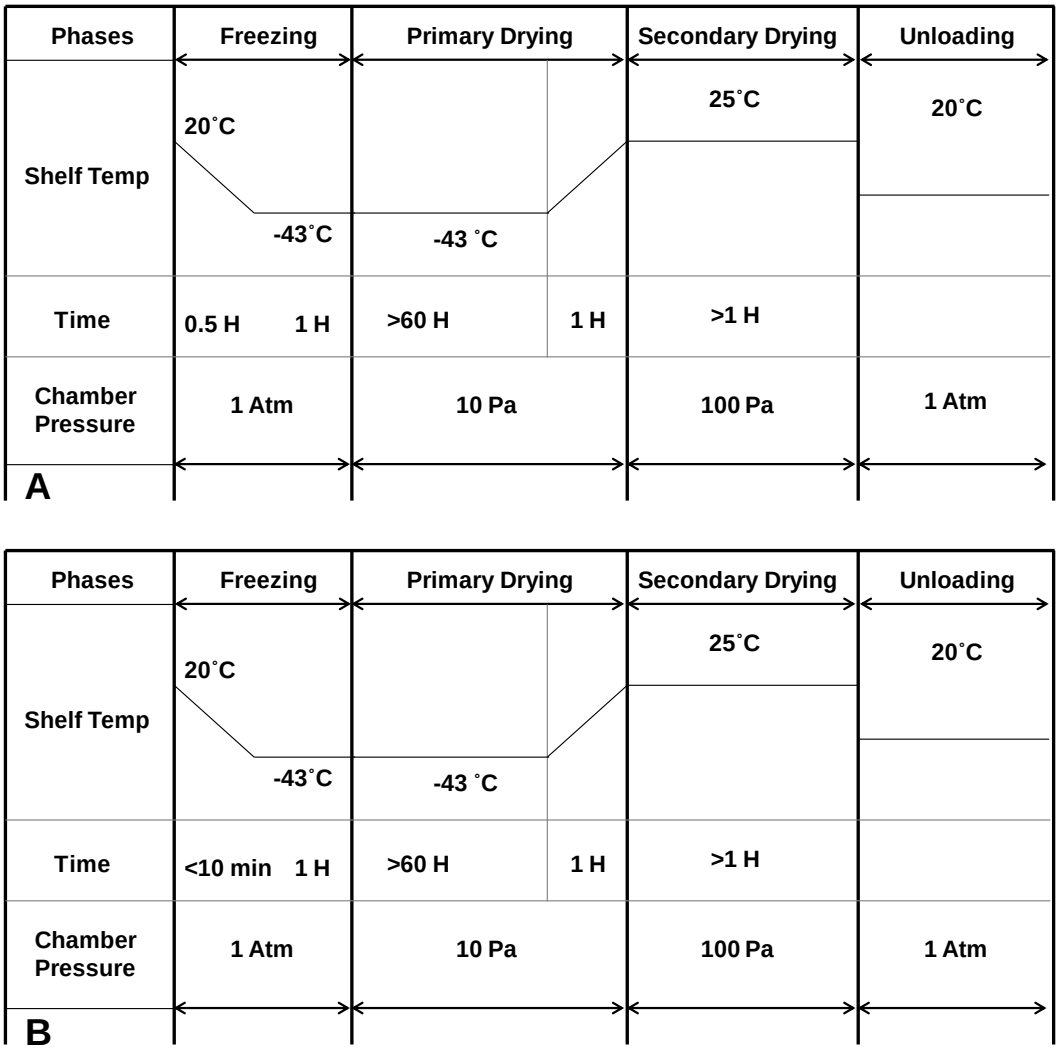

Figure 3.12: Temperature-Pressure and time profiles investigated in case of vial and tray freeze-drying of lactose and coffee respectively. **A.** Cooling rate of 1K.min^{-1}. **B.** Cooling of samples using liquid nitrogen quenching.

The samples were freeze dried until the temperatures of the thermocouples inside the samples had risen to a steady higher value (~-25˚C) above the shelf temperature (~-40˚C). These vials were then subjected to a secondary drying cycle by rising the shelf temperature to 25˚C and increasing the chamber vacuum pressure to 100 Pa for 4 hrs before removing the vials from the freeze-dryer. The dried samples were stored in a nitrogen glove bag and also prepared for scanning electron microscopy for comparison with the freeze-dried samples obtained from freeze drying microscopy.

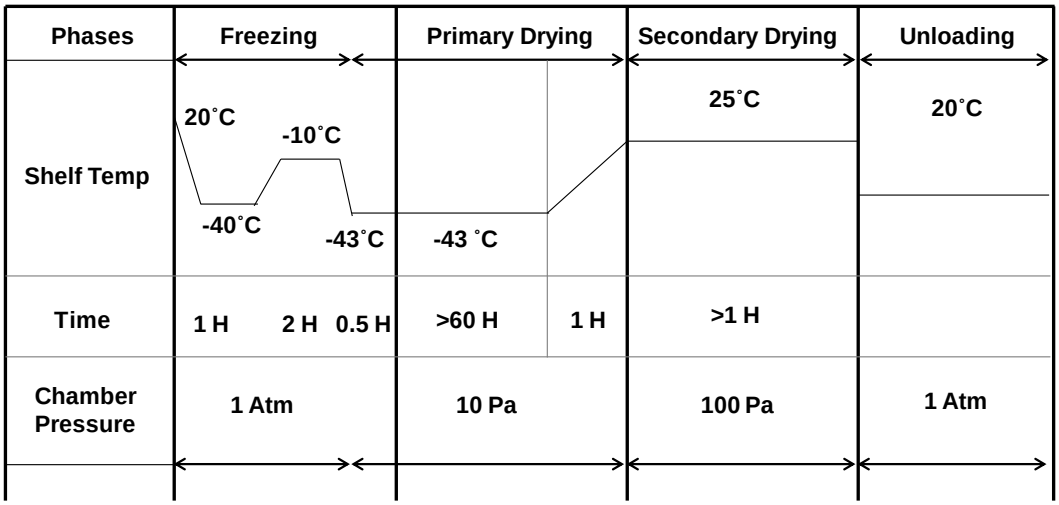

Figure 3.13: Temperature-Pressure and time profiles investigating the annealing profile in case of vial and tray freeze-drying of lactose and coffee respectively.

3.7 Field Emission Gun Scanning Electron Microscopy (FEGSEM)

Scanning Electron Microscopy is a commonly used technique to study the microstructure and surface properties of various materials. It provides a very high-magnification high-resolution images of the said materials. The basic principle involves sputter coating of the sample with a very thin layer (10-20 nm) of gold followed by bombardment of electrons on to the surface of the material. This results in the release of secondary electrons from the surface of the material which is detected and the image of the material is formed. The Field Emission Gun is an electron gun which gives a concentrated primary electron beam which is incident upon the sample and results in higher resolution images than normal scanning electron microscope (Crewe *et al.,* 1968).

To study the ice crystal structure of the freeze-dried samples, a Leo 1530VP high resolution field emission gun scanning electron microscope (FEGSEM) (Leo Elektronenskopie GmbH, Oberkochen, Germany) shown in Fig. 3.14 was used at a range of magnifications (about 100X to 20KX).

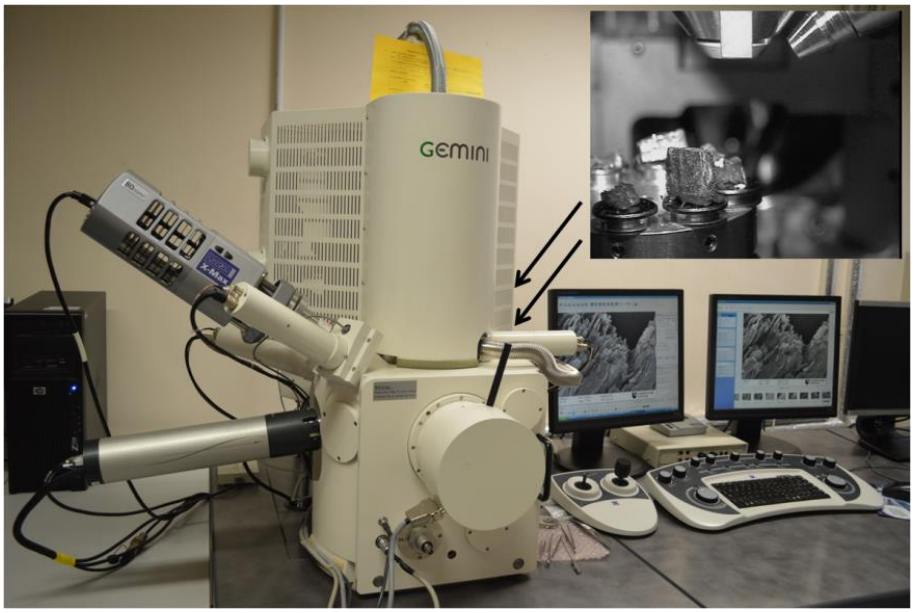

Figure 3.14: Field emission gun scanning electron microscope used in this study. Inset: stage of the FEGSEM with freeze-dried coffee samples.

Figure 3.15: Gold/Palladium (Au/Pd) sputter coater used for gold coating of freeze dried samples before conducting FEGSEM

The glass slides, vials and trays containing the freeze-dried sample were transferred to a small box containing silica gel or to a nitrogen purged glove bag (See Appendix B) in order to minimize contact with room air to avoid moisture sorption and immediately taken for the sample preparation process. The freeze-dried samples were prepared for SEM inside the nitrogen glove box so as to minimise contact with air. Samples were cut at a specific position – top, middle and bottom of the sample,

using a cork borer and scalpel as accurately as possible. Initially, a thin layer of Au/Pd coating was sputtered onto the samples via an EMITECH SC7640 Au/Pd sputter coater (Quorum Technologies Ltd, East Grinstead, UK) (Fig. 3.15 & Appendix B) to provide conduction paths for releasing the excessive surface charges generated during imaging. The sputtering time for Au/Pd coating was 80 s.

The imaging of the internal structures was achieved using secondary electrons released from the top surfaces of the samples, which were generated by an incident electron beam with 5 kV accelerating voltage within a working distance of ~15 mm.

3.8 Differential Scanning Calorimetry

Differential Scanning Calorimetry is commonly used to analyse the thermal behaviour of various sugar solutions. It can be used to determine crystallization and melting behaviour and also glass transition phenomenon that takes place in various food solutions. The basis of the technique is based on the difference in the amount of heat required to increase the temperature of a sample pan in comparison to that required for an empty reference pan and is measured as a function of temperature. This method is highly sensitive to the various changes that a sample undergoes with phase transitions, such as crystallisation or melting. The heat energy absorbed or released (endothermic and exothermic reaction respectively) during such transitions is measured and the difference in the amount of energy required heating the sample and reference at the same rate is plotted as a function of temperature. The DSC program thus generates a curve of this energy measured with change in temperature which is known as a DSC thermogram. Step changes in the DSC correspond to changes in the sample heat capacity which occurs at the glass transition (Omar & Roos, 2007). In the current study, DSC was used to determine the glass transition temperatures of the different samples and compare them to collapse temperatures determined from FDM. The values determined were analysed to determine, which of these techniques is more suitable to set the primary drying temperature in the real freeze-drying cycle performed in the bench-top freeze-dryer.

DSC experimental procedure: A heat flux DSC (model DSC Q10, TA Instruments, Crawley, UK) equipped with a thermal analysis data station was used (Fig. 3.16). Nitrogen (99.999% purity) was used as a purge gas which flowed at approximately 50 mL/min. The DSC instrument was calibrated for temperature and enthalpy using an indium standard.

Figure 3.16: The TA Q10 DSC instrument used in this research

Usually the DSC set up consists of two sealed aluminium DSC pans mounted on top of elevated constantan platforms which are heated with the same furnace. One of the pans contains about 10-15 mg of sample and the other one is empty acting as a reference. The temperature difference between the two pans is measured and the enthalpy change in the pan is calculated using a calibration factor.

15±1 mg of sample was weighed and hermetically sealed in an aluminium pan, with an empty pan as a reference. A small amount of AgI (~1 mg) is added to some of the pans to study the effect of AgI on the glass transition temperature of the samples. The main purpose of using DSC in this research was to determine the glass transition temperature of the freeze-concentrated phase of frozen samples. This is closely related to the sample collapse temperature. This glass transition temperature (onset) is calculated from the DSC thermogram obtained. The samples placed in the pans are subjected to a cooling rate of 10 $K.min^{-1}$ to -40˚C to observe the freezing of the sample

and held at the defined temperature for 5 mins followed by heating of the sample at 5 $K.min^{-1}$ to observe the glass transition as well as the melting phenomenon.

3.9 Conclusions

The main aim of this chapter was to provide a detailed description of the different materials and methodology used in the course of this study. It highlighted the temperature profiles and various experimental conditions used to investigate the effects of different parameters on the sublimation process. It also includes the image analysis method followed using MATLAB to track the sublimation front movement. The twin-resistance parameterized model has also been outlined which will be used to determine the actual resistance the material being freeze-dried poses to the movement of the water vapour through the frozen matrix undergoing sublimation.

The effect of various parameters such as cooling profiles, annealing, final temperature of drying and solid content on these resistances will also be described in detail in the subsequent chapters. The knowledge of these resistances will provide a pathway to optimize the process of freeze drying as it will help in devising ways to decrease these resistances thereby reducing the duration of the sublimation process.

4

FREEZE DRYING MICROSCOPY OF A MODEL LACTOSE SYSTEM

Freeze drying microscopy is applied to study the effect of various parameters (initial solids content, presence of silver iodide, freezing rate, annealing and drying temperature) on the kinetics of freeze drying of a model lactose system. The effects of these parameters on edge resistance and resistance of dried layer are studied and also related to microstructure.

4.1 Introduction

Many different methods and devices have been developed over the years to study and improve freezing and freeze-drying processes (Rosenthal & Rall, 1984 and Nail *et al.,* 1994). One such development is the FDM stage. This allows the direct visualisation of the sublimation front, as the dried region appears much darker than the un-dried icy region. This is due to greater light scattering in the dried region than the icy region. Light is able to transmit through the icy region with minimal scatter as the two phases (ice and the freeze concentrated matrix) have similar refractive indices. However, when the ice sublimes to leave voids, the large differences in refractive index between the air and the solid matrix causes significant scatter. Thus the boundary between the two regions is obvious.

The most common current use of FDM is the determination of collapse temperatures (T_c) of products to be freeze-dried. Here, the temperature is allowed to rise as freeze drying progresses. Since such a substantial increase in temperature can directly increase the productivity by reducing the sublimation time, it can safely be said that T_c is of critical importance for a sublimation process (Pikal & Shah, 1990). Product collapse occurs due to the occurrence of a glass transition near the ice vapour interface, resulting in a decrease in the viscosity of the solute phase and a loss of the porous structure created during the sublimation of ice (Pikal and Shah, 1990).

There are many reports in the literature regarding the use of FDM to determine the T_c of various products (Adams & Ramsay, 1996; Zhai *et al.,* 2003; Meister *et al.*, 2009; Meister & Giesler, 2009 and Yang *et al.,* 2010). Meister *et al.,* (2009) investigated the effect of solids content and nucleation temperature on collapse temperature. They found a large degree of scatter in ice nucleation temperatures, which could therefore not be controlled from experiment to experiment, and consequently found it difficult to see any correlation with T_c data. However, solids content was found to correlate positively with collapse temperature.

Very few researchers have used FDM to determine frontal velocity or to link it to sublimation rate; potentially this information could be used to better understand the freeze drying process and improve its efficiency, thereby decreasing its overall cost. Zhai *et al.,* (2003) have been among the few researchers who have tried to measure

primary drying rates using FDM. They characterised the drying rate by determining an effective diffusion coefficient, D_{eff} and suggested that sublimation rate increase near the collapse temperature was due to increase in channelling of water vapour through the dried layers. They also showed that the sublimation times calculated using these D_{eff} values were in practical agreement with the sublimation times in a conventional laboratory freeze-dryer (Zhai *et al.*, 2003).

The core objective of this study is to use FDM as a tool to gain a better understanding of the sublimation process. To accomplish this goal, FDM is first performed on a simple system, namely a model lactose system with varying solid contents. The effect of various cooling profiles, annealing and temperatures of drying on the edge resistance and resistance of the dried layer are investigated in detail. Sample microstructures are also examined using FEGSEM to assess the effects of process parameters on microstructure and how this might affect freeze drying rates. Collapse temperature of various solid contents of lactose were also investigated and compared to the glass transition temperatures obtained using DSC. The effect of cooling profiles and heating profiles on collapse temperatures is also determined using FDM.

4.2 Materials and methods

4.2.1 Materials

α-lactose monohydrate and silver iodide were purchased from Fischer Scientific (Loughborough, UK) for the purpose of this research as described in Section 3.1.

4.2.2 Moisture content determination

Moisture content of the α-lactose monohydrate bought was determined using KF titration as discussed in Section 3.3.2.

4.2.3 Sample preparation

Sample preparation of varying lactose solid contents was carried out as explained in Section 3.4.1.

4.2.4 Freeze drying microscopy

The sample preparation for FDM was carried out as described in Section 3.5.2 and the experimental protocol to be followed was discussed in Section 3.5.4. For sublimation kinetics the following factors were investigated:

- The presence of an ice nucleating agent AgI
- Initial solid content (5-40%)
- Cooling rate during freezing (2, 10, 50 $K.min^{-1}$)
- Sublimation temperature (-30˚C, -40˚C, -50˚C)
- Annealing (4 different profiles)

Not all combinations of variables were tested. Most experiments were variations on a couple of base cases which had either 10% or 40% solids content, a cooling rate of 10 $K.min^{-1}$, a freeze drying temperature of -40˚C, and with silver iodide present (for reasons that will become apparent). A system pressure of 1 Pa was used for all experiments.

Collapse temperatures were also studied (in the presence of AgI) with the following factors examined:

- Initial solid content
- Cooling rate during freezing
- Heating rate during collapse temperature determination

Glass transition temperatures of frozen samples were also determined by DSC for comparison (see Section 3.8).

4.2.5 Field Emission Gun Scanning Electron Microscopy

FEGSEM was carried out on the freeze dried samples obtained from FDM to assess the internal microstructure, as described in Section 3.7.

4.3 Results and discussion

4.3.1 Experiments performed without silver iodide (AgI)

Fig. 4.1 inset shows the icy and dry regions of a 10% (w/w) lactose solution (without AgI) frozen at -40˚C undergoing sublimation under the freeze-drying microscope (20X). The microstructure in the image is evident as there are variations in colour across the sample, although the ice crystals formed are too small to be individually observed, even under magnifications as high as 100X. The sublimation front progression, however, was quite uniform along the length of the front.

Frontal distances versus time plots for 10% lactose solution are also shown in Fig 4.1. These show the expected curvature of the plots as the front progresses into the sample, but repeat runs of these experiments were found to show poor reproducibility (see e.g. Fig. 4.1), and this was found across all the solid concentrations.

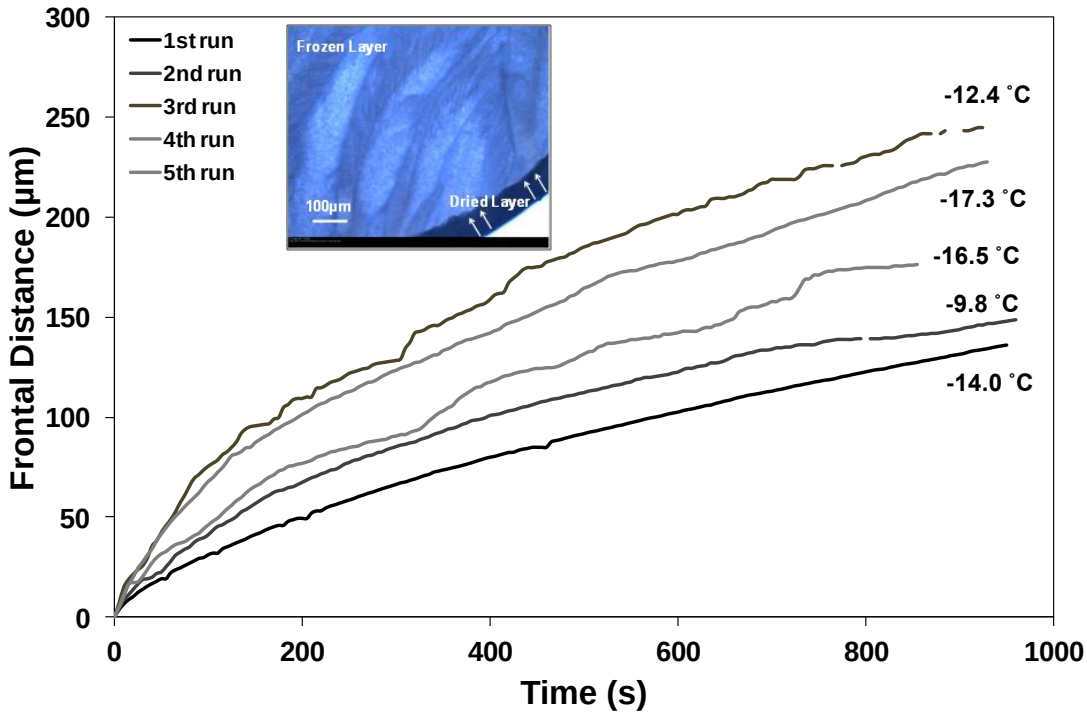

Figure 4.1: Frontal distance versus time plot of five repeat runs for 10% lactose solution (inset) frozen at -40˚C at a rate of 10K min^{-1} and freeze dried at 1 Pa. The values presented with each curve is the nucleation temperature of that run.

Furthermore, nucleation temperatures were also found to vary over a wide temperature range (between -17.3˚C and -9.8˚C). Thus the nucleation process is inherently random in this system. This stochastic behaviour of the nucleation temperature of various materials has been widely reported in literature (Vessot & Andrieu, 2012). A further observation is that when nucleation does occur in the experiments it produces a very rapid and immediate solidification of the sample. This occurs so quickly that it is almost impossible to catch an image of the solidification process in progress.

It has been widely reported that the freezing profile and the nucleation temperature have a direct effect on the sublimation rate in a freeze drying process (Searles *et al.,* 2001; Patel *et al.*, 2009 and Konstantinidis *et al.,* 2011). The differences in nucleation temperature result in a difference in supercooling when solidification occurs, and this may affect the samples as it is said to have a significant effect on the ice crystal formation (Franks, 2008) by affecting the nucleation rate. Increasing the amount of supercooling in the sample increases the nucleation rate more than the growth rate which results in a larger number of small crystals. The sublimation rate has been found to be slower in samples where nucleation temperature is lower due to smaller ice crystals (Sane & Hsu, 2010). The effects of other process variables, such as solid content, temperature profile and final drying temperature, on the primary drying rate may be obscured by such run-to-run variability produced by variations in the nucleation temperature.

In order to overcome this inconsistency in reproducibility of the nucleation temperature, various methods were investigated. Different cooling profiles were explored – fast (50 $K.min^{-1}$), very fast (130 $K.min^{-1}$), slow (1 $K.min^{-1}$), combination rate (10 $K.min^{-1}$ to -10˚C followed by 1 $K.min^{-1}$ to -40˚C) to try to achieve a more consistent nucleation behaviour. The varying cooling rates were applied in order to vary the rate of increase of supercooling, which might affect the nucleation temperature.

Another method tried was to scratch the slides using a metal file in order to create sites for nucleation to occur. Fig. 4.2 shows the repeat runs performed on scratched slides but the method did not yet again result in reproducible nucleation temperatures or frontal velocities as evident from the plot.

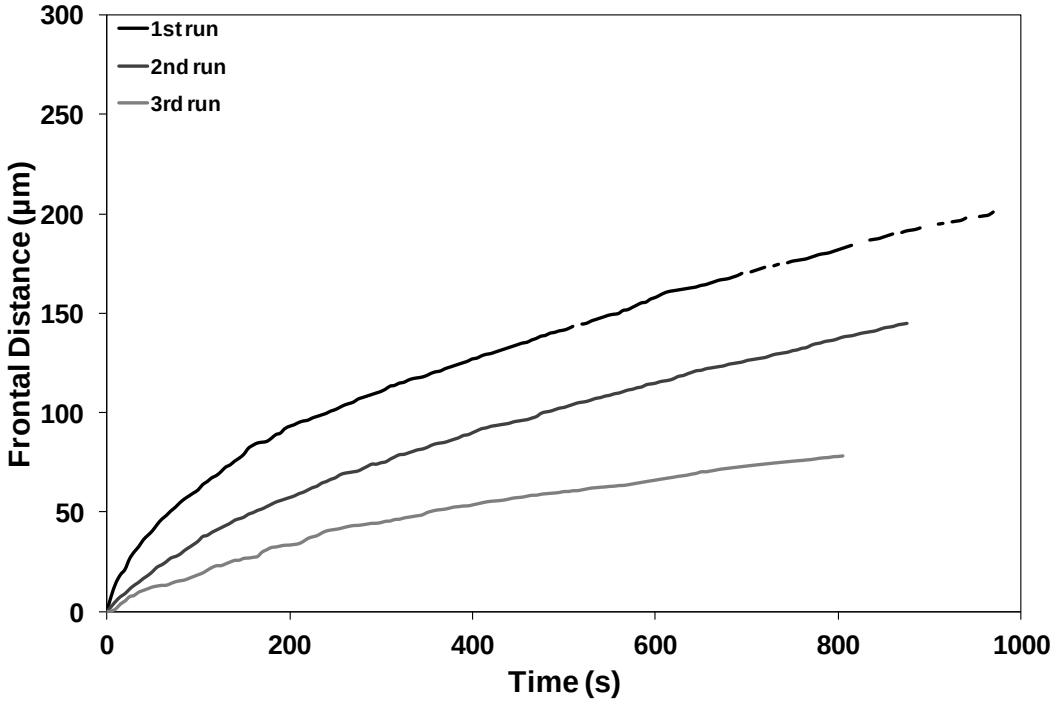

Figure 4.2: Frontal distance versus time plot of three repeat runs of 10% lactose frozen at -40˚C and freeze dried at 1 Pa using scratched glass slides to create sites for nucleation.

4.3.2 Effect of addition of AgI

Various methods have been reported in the literature for controlling ice nucleation, such as the ice fog technique, or the addition of *Pseudomonas syringae* or silver iodide (AgI) (Cochet & Widehem, 2000; Searles *et al.,* 2001; Widehem & Cochet, 2003 andPatel *et al.*, 2009). Forced ice nucleation has been carried out for decades to cause artificial rain and snowfall in various countries. The fog technique involves the introduction of microscopic ice crystals into the freezing chamber in the form of fog under high pressure and these crystals act as nuclei to induce ice crystal formation. However, this would be difficult to achieve under a microscope slide. *Pseudomonas syringae* produces proteins through ice nucleation active genes which act as nuclei for ice crystal formation. This was considered as a possible method, but was not preferred due to its biological effects as a pathogen and the extra experimental complexity that using a bacterium entails.

AgI has a hexagonal crystal structure similar to that of ice and is quite stable at low temperatures; hence it is able to act as a seed and can cause ice crystal formation (Edwards & Evans, 1960; Edwards *et al.*, 1962; Clausse *et al.,* 1991; Searles *et al.,*

2001 and Petzold & Aguilera, 2009). The effect of the surface charge of silver iodide on ice nucleation has also been investigated previously and it has been observed that nucleation was least affected when AgI was highly charged, as the electric field causes the water molecules to order and become difficult to nucleate (Edwards & Evans, 1961). Silver iodide was thus tried as it has a very low solubility (3×10^{-7} g per 100 mL of water) and could be easily added to the samples. Obviously, AgI cannot be used in a real food or pharmaceutical freeze drying process due to contamination issues, but is used here to allow this avenue of research to be undertaken.

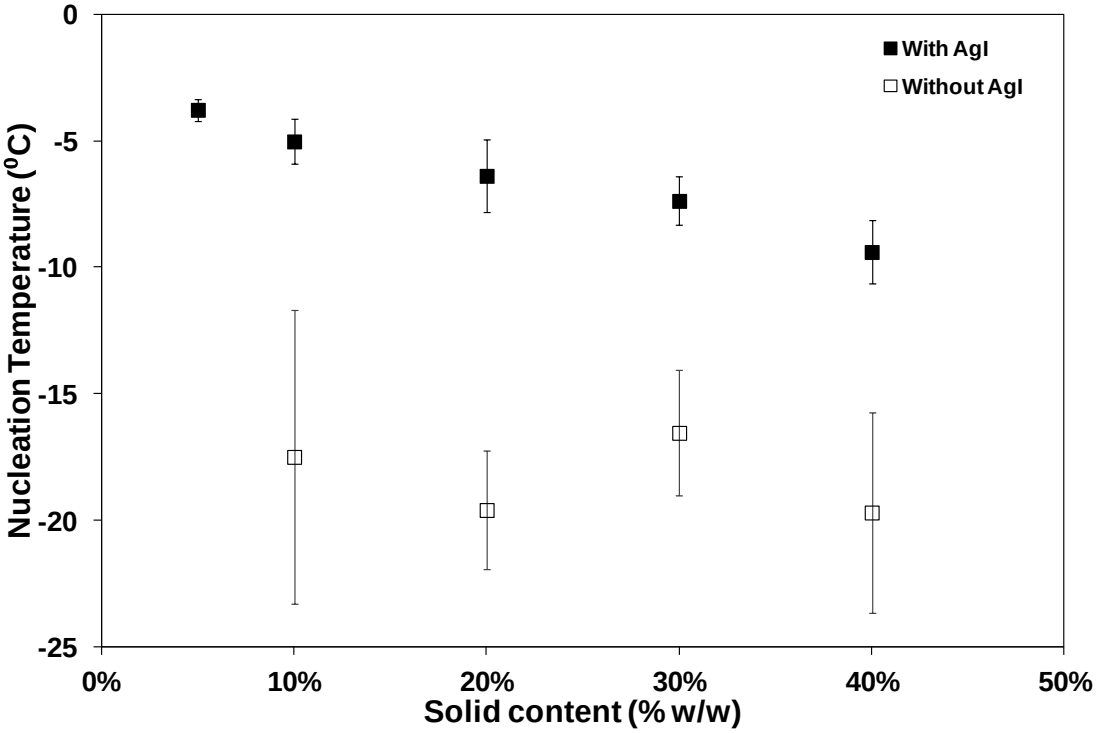

Figure 4.3: Average nucleation temperatures (at least four repeats) of different solid contents of lactose with and without AgI. Samples were frozen using a cooling rate of 10 K.min^{-1} and freeze dried at -40˚C and 1 Pa. Error bars represent standard deviation calculated from atleast four repeats in each case.

The addition of AgI was found to raise and also bring reproducibility to the nucleation temperature (Fig. 4.3), and so AgI is clearly acting as a nucleation agent. A steady decrease of nucleation temperature with increasing lactose solid content was also observed which mirrors the freezing point depression. All solutions exhibit freezing point depression with increasing solid content and nucleation takes place just below the freezing point temperature thus reached. Previous studies (Whittier, 1933) have reported a freezing point depression of about 2˚C in lactose solutions for 40% (w/w)

lactose. This is slightly less than the variation of nucleation temperature seen here between 5% and 40% (w/w) of approximately 4˚C (Fig. 4.3).

4.3.3 Microstructure

One consequence of the rise in nucleation temperature from the addition of AgI was that it was possible to discern individual ice crystals. This is a result of the decrease in the relative rate of nucleation compared to growth during solidification at the higher temperatures. Long thin ice crystal structures were observed which had various different orientations.

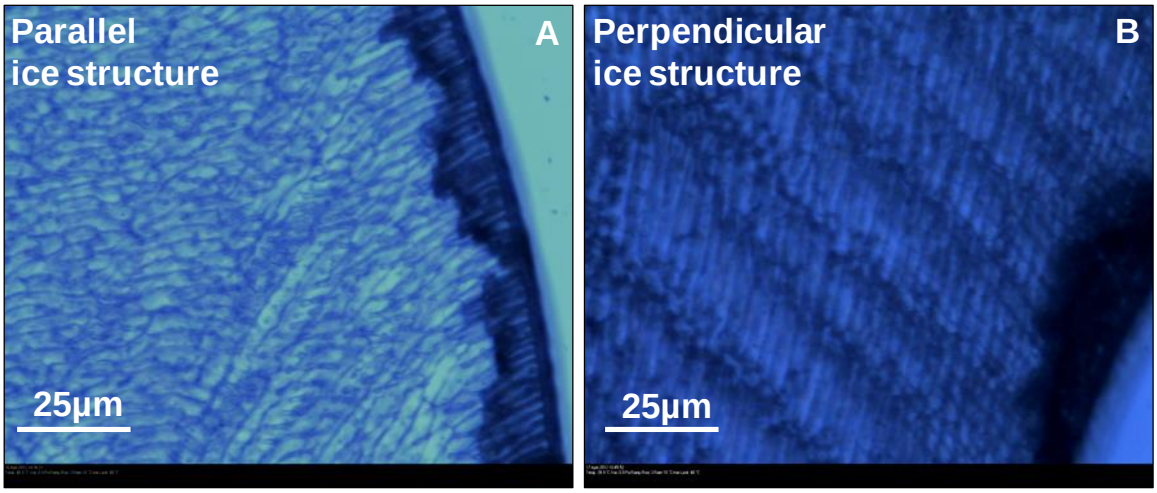

Figure 4.4: A. Parallel orientation, and **B.** Perpendicular orientation, observed under higher magnification (100X) in 10% lactose frozen with AgI at a cooling rate of 10 K min^{-1} and freeze dried at -40˚C and 1 Pa. Images are representative of at least four runs in each case.

Figs. 4.4 A & 4.4 B show ice crystal orientations that are parallel and perpendicular to the direction of movement of the sublimation front respectively. These crystal orientations were visible only in the case of 5% and 10% (w/w) lactose solutions (Figs. 4.5 A & 4.5 B). As the concentration increased, the crystals became smaller and the orientations became less distinct (Figs. 4.5 C-E). This effect may be attributed to the fact that the amount of sub-cooling at nucleation increases with increasing lactose solid content. The freezing point does not drop as quickly as the nucleation temperature resulting in finer and smaller ice crystals between high concentrations of lactose. Another factor may be the increased viscosity at the higher lactose contents that will favour growth less.

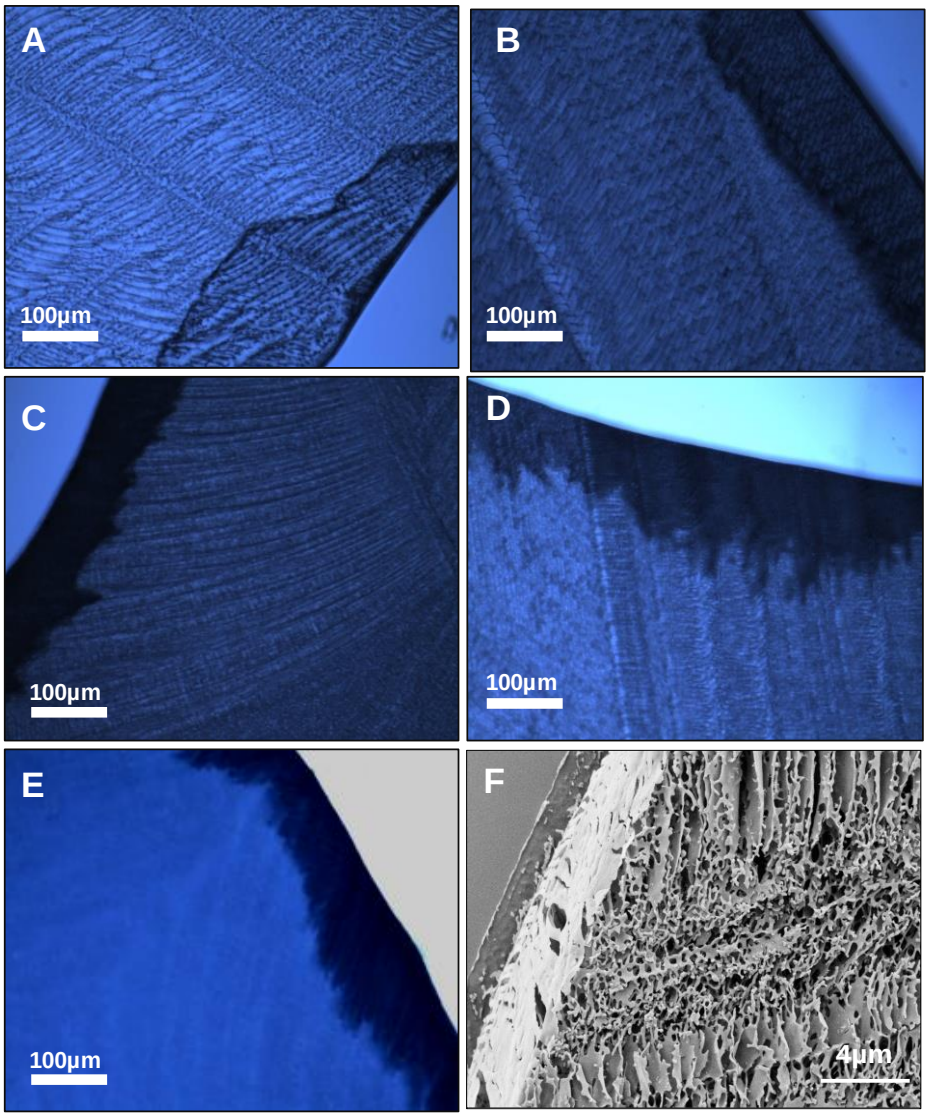

Figure 4.5: Microscope images of lactose frozen and freeze-dried under FDM at -40˚C and 1 Pa pressure. **A.** 5% lactose. **B.** 10% lactose. **C.** 20% lactose. **D.** 30% lactose. **E.** 40% lactose. **F.** FEGSEM image of the edge of 10% lactose freeze dried under FDM. Images are representative of at least four runs in each case.

To further examine the sample microstructures, SEM images were taken of freeze dried samples. Fig. 4.5 F shows an SEM image of the edge of freeze dried 10% lactose (under FDM). The pore structure seen in the image shows evidence of directionality observed in the previous crystal structure, which confirms this finding from the microscope images. The porous microstructure did not continue to the edge of the sample which appears to be relatively non-porous, and provides support for the concept of the edge resistance used in the model. A thin layer at the edge can also be seen in Fig. 4.5 A. The thickness of this edge was seen to vary between different runs investigated and is likely to result in different edge resistances.

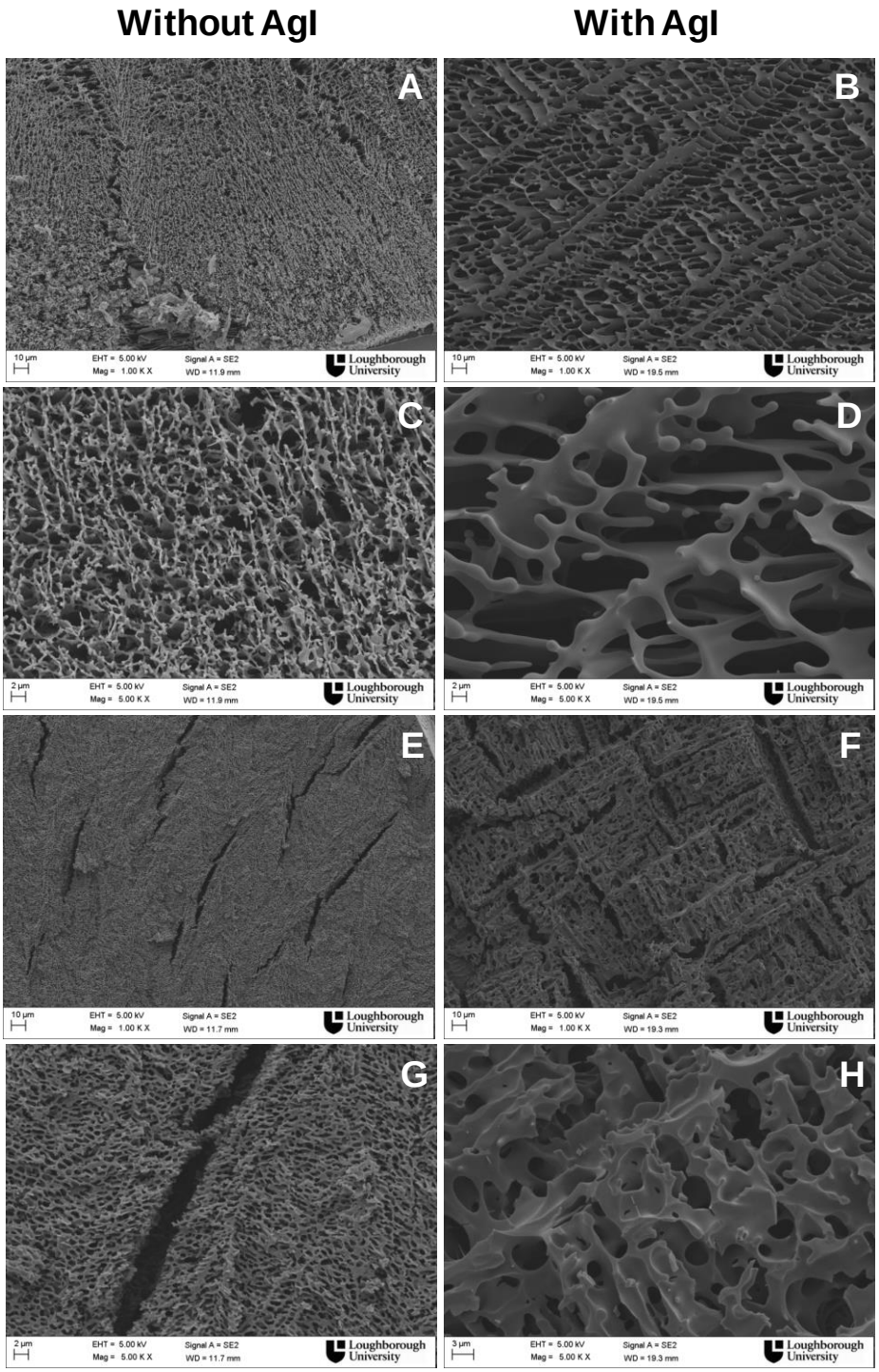

Figure 4.6: Field emission gun scanning electron microscope images of freeze dried (under FDM) lactose with and without AgI. **A** & **C.** SEM images 10% lactose freeze dried without AgI (1KX and 5KX magnification). **B** & **D.** SEM images 10% lactose freeze dried with AgI (1KX and 5KX magnification). **E** & **G.** SEM images 40% lactose freeze dried without AgI (1KX and 5KX magnification). **F** & **H.** SEM images 40% lactose freeze dried with AgI (1KX and 5KX magnification). Images are representative of at least four runs in each case.

Fig. 4.6 shows scanning electron microscopy (SEM) images obtained at two different magnifications (1KX and 5KX) from 10% and 40% lactose solutions (w/w), with and without AgI. For most of these samples, the microstructure is too small to be visible under the microscope, and so SEM is the only way to examine these samples' microstructures. The addition of AgI was found to affect the size and order of ice crystal formation significantly as absence of AgI resulted in much finer and randomly shaped crystals in 10% lactose (Figs. 4.6 A-D). This orderliness and difference in size of ice crystal was also observed in freeze dried samples obtained from 40% lactose although the size of ice crystal was much smaller due to the presence of higher amount of lactose in the sample (Figs. 4.6 E-H). This further proves the effect of concentration on the freezing point depression and, in turn, on the nucleation temperature which results in smaller ice crystals with less directionality (Figs. 4.5 C-E). The cracks observed in Figs. 4.6 E and 4.6 G was thought to be due to the removal of the upper coverslip before conducting SEM since no cracks were visible in microscope images of the FDM samples.

4.3.4 Effect of crystal orientation on sublimation kinetics

The MATLAB analysis was used in order to determine the frontal position at different points on the same drying front and to ascertain the degree of uniformity of movement along the front. There were variations in frontal velocity due to variations in structure orientations in the same frozen sample; however for a given orientation, highly reproducible results were obtained (Fig. 4.7 A). The sublimation front movement was observed to move faster through regions with ice crystals orientated parallel to the front, compared to perpendicular orientations. This difference in front velocity can be attributed to the larger number of mass transfer barriers encountered per unit distance when in the perpendicular compared to the parallel orientation. This does not explain the variations in initial front velocity which is not governed by the bulk microstructure. However, it can be observed that in the parallel configuration some ice crystals are able to penetrate the surface layer to some extent, and reduce the effective resistance to mass transfer. It is therefore highly plausible that the problems in reproducibility encountered in the non-AgI experiments (Fig. 4.1) are the consequence of differences in the orientation of the crystal microstructure. There was much less variation between runs when experiments were

performed using 40% lactose solutions (Fig. 4.7 B). However, these samples showed less directionality in microstructure when observed by SEM (Fig. 4.6).

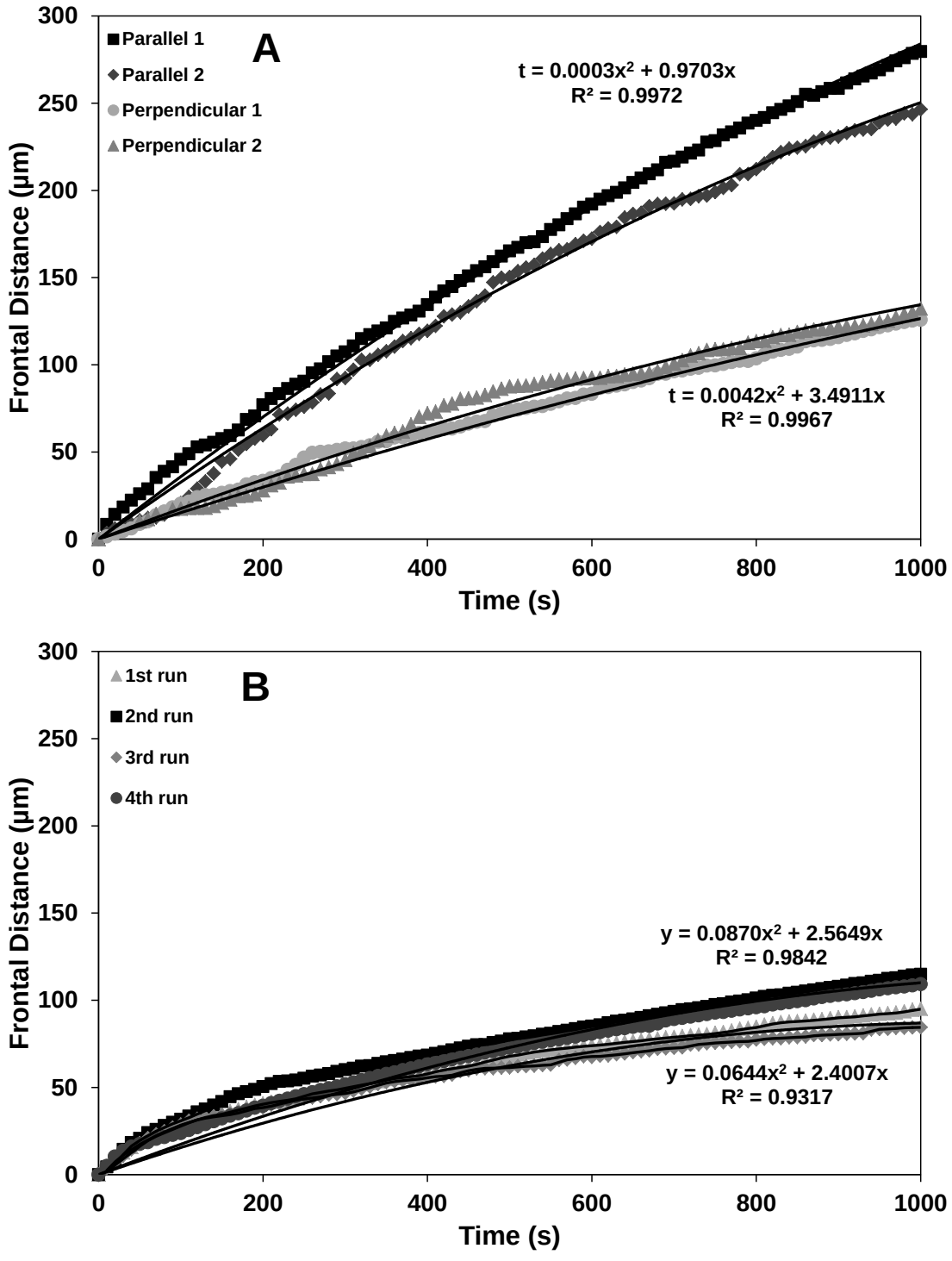

Figure 4.7: Frontal distance versus time plot of repeat runs. **A.** 10% lactose and **B.** 40% lactose solutions (both with AgI) freeze dried under FDM at -40˚C and under a vacuum pressure of 1 Pa after previously freezing at a cooling rate of 10 K.min^{-1}. The repeat runs are representative of at least four runs in each case. The equation represents the fitted curve for *t* vs *x*.

4.3.5 Effect of concentration on sublimation kinetics

The representative edge resistance, a and representative resistance of dried layer, b values from all the freeze drying experiments performed with AgI at -40˚C are shown in Figs. 4.8 A & 4.8 B respectively while Figs. 4.9 A & 4.9 B show the corresponding values of actual edge resistance, α and actual resistance of dried layer, β, using equation 3.10. The a and b values were determined by fitting t as a function of x, (see equation 3.11) while the calculations for α and β values were performed using the various parameters detailed in Appendix C and equation 3.10. This transformation includes dividing a or b by $\rho(M_i-M_f)$ to produce α and β respectively but this does not greatly affect the trends in the data.

The a values were seen to increase for initial solid contents from 5 to 20% (w/w) while decreasing again from 20 to 40% (w/w). The α values showed a similar trend but did not decrease as much at the higher solids contents. Higher α values were found for the case when the crystal orientation was perpendicular to the direction of frontal movement than parallel. It is believed that the "parallel" crystals may penetrate the outer layer more than when "perpendicular" thereby giving a smaller resistance to mass transfer.

Both b and β values were found to dramatically increase with increasing solid content from 5 to 40% (w/w). This effect is due to the larger quantity of solid in the dry region that the water is required to diffuse through which manifests as thicker walls, more walls or a combination of the two. The b and β values were found to be higher for perpendicular ice crystal orientations than parallel orientations, and this can be attributed to the higher number of lactose boundaries per unit distance into the sample with the perpendicular orientation.

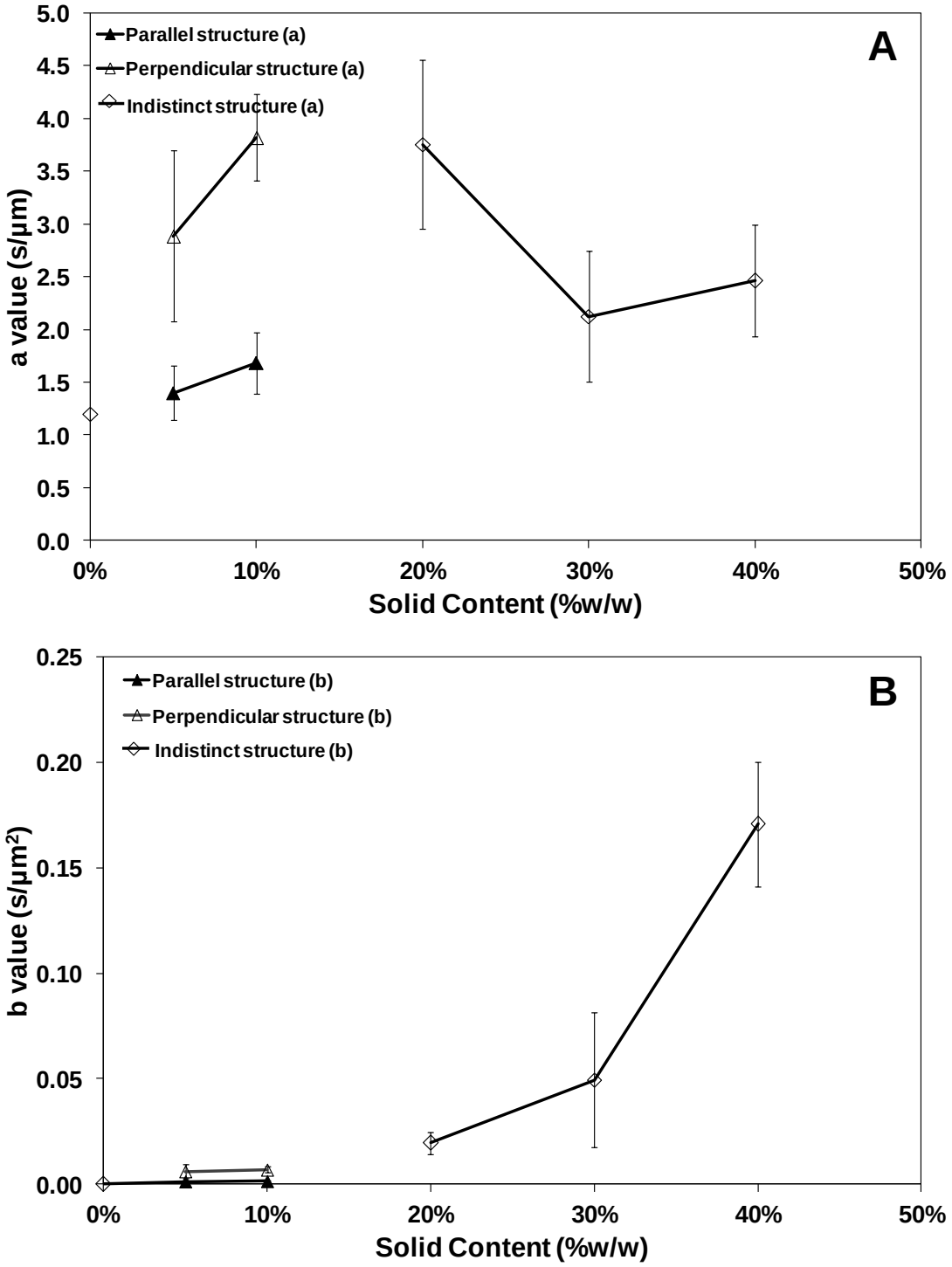

Figure 4.8: Effect of initial lactose solid content (5 to 40%) **A.** *a* values, representative edge resistance. **B.** *b* values, dried layer resistance, obtained from FDM after freeze-drying at cooling rate of 10 K.min^{-1} to -40˚C and at vacuum pressure of 1 Pa. Values are average of at least four runs with standard deviation as the error in each case.

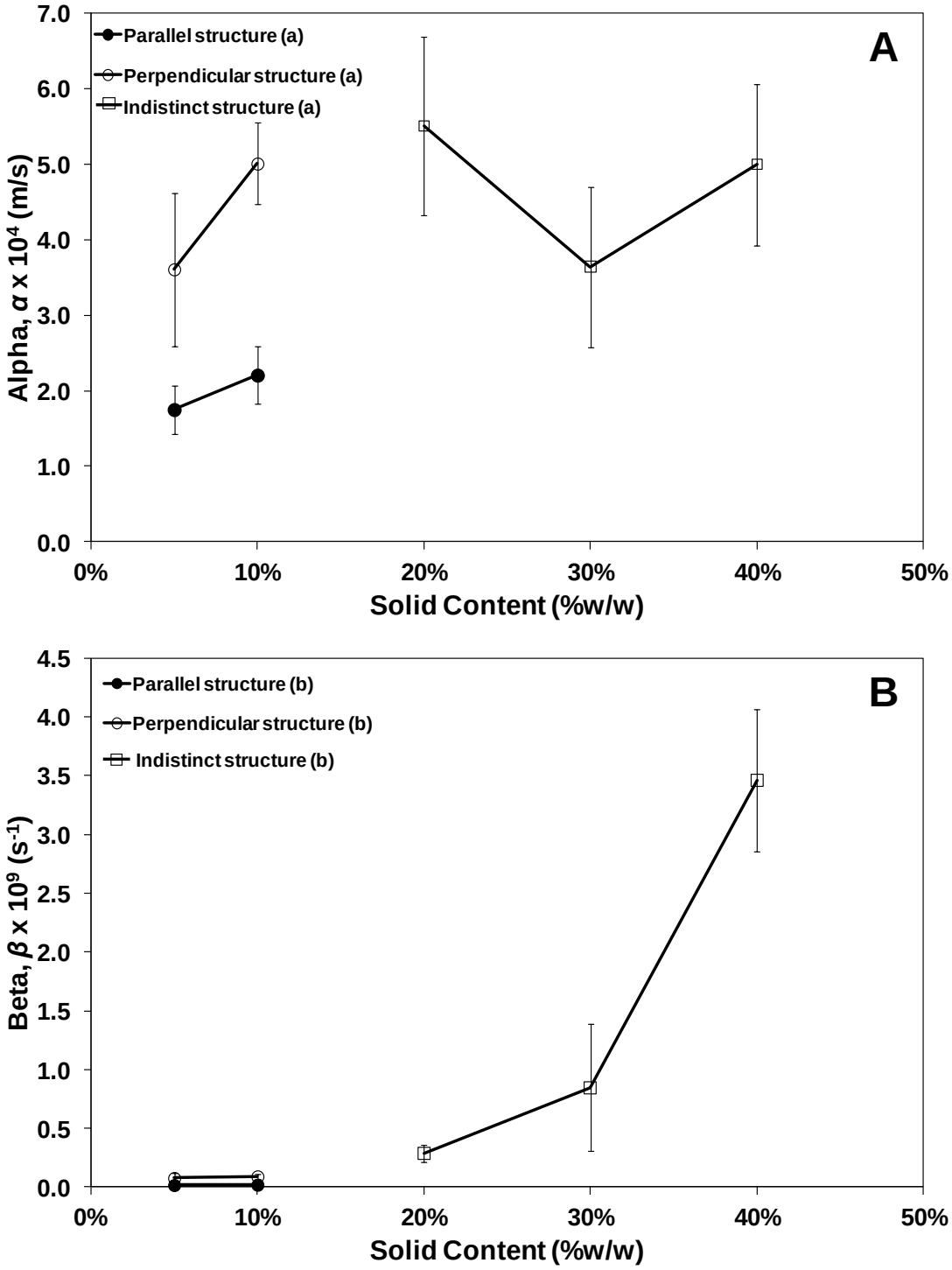

Figure 4.9: Effect of initial lactose solid content (5 to 40%) on **A.** α values, actual edge resistance. **B.** and β values, actual dried layer resistance, obtained from FDM after freeze-drying at cooling rate of 10 K.min^{-1} to -40˚C and at vacuum pressure of 1 Pa. Values are average of at least four runs with standard deviation as the error in each case.

Table 4.1 Depth into the sample where $a=bx$ and the frozen solid density (dry basis) of the lactose for different solid contents.

Solid Content (% w/w)	Depth (mm)		Frozen solid density ($kg.m^{-3}$)
	Parallel orientation	Perpendicular Orientation	
5	3.32	1.10	50.3
10	1.15	0.32	102.9
20	0.19		214.6
30	0.07		331.0
40	0.02		465.3

Fig. 4.10 A shows the amount of dry solid produced for different solid contents with time, calculated by multiplying the frontal distance (x) by the frozen solid density (ρ) (see Table 4.1). The depth into the sample, where the contribution of edge resistance is equal to that of resistance from the dried layer, that is $a=bx$, is also displayed in Table 4.1. The 40% lactose content shows the fastest production of solid produced and 5% lactose producing lowest amount of dry solid with time. However, at short times frontal distances are most influenced by the surface resistance term. This is evidenced by Table 4.1 which shows the depths at which the two resistances are equal to each other.

In conventional freeze drying systems, the times and distances are much longer than shown in Fig. 4.10 B, and so predicted values of ρx have been extrapolated for longer times using the previously fitted values of a and b (Fig. 4.10 B). These show that the best production rate would be achieved with 10% solutions and with the crystals oriented parallel to the direction of frontal movement. Good rates were also achieved with 20% and 30% solids contents but less so with 40% and 5% contents. Hence there is clear evidence that intermediate concentrations are optimal.

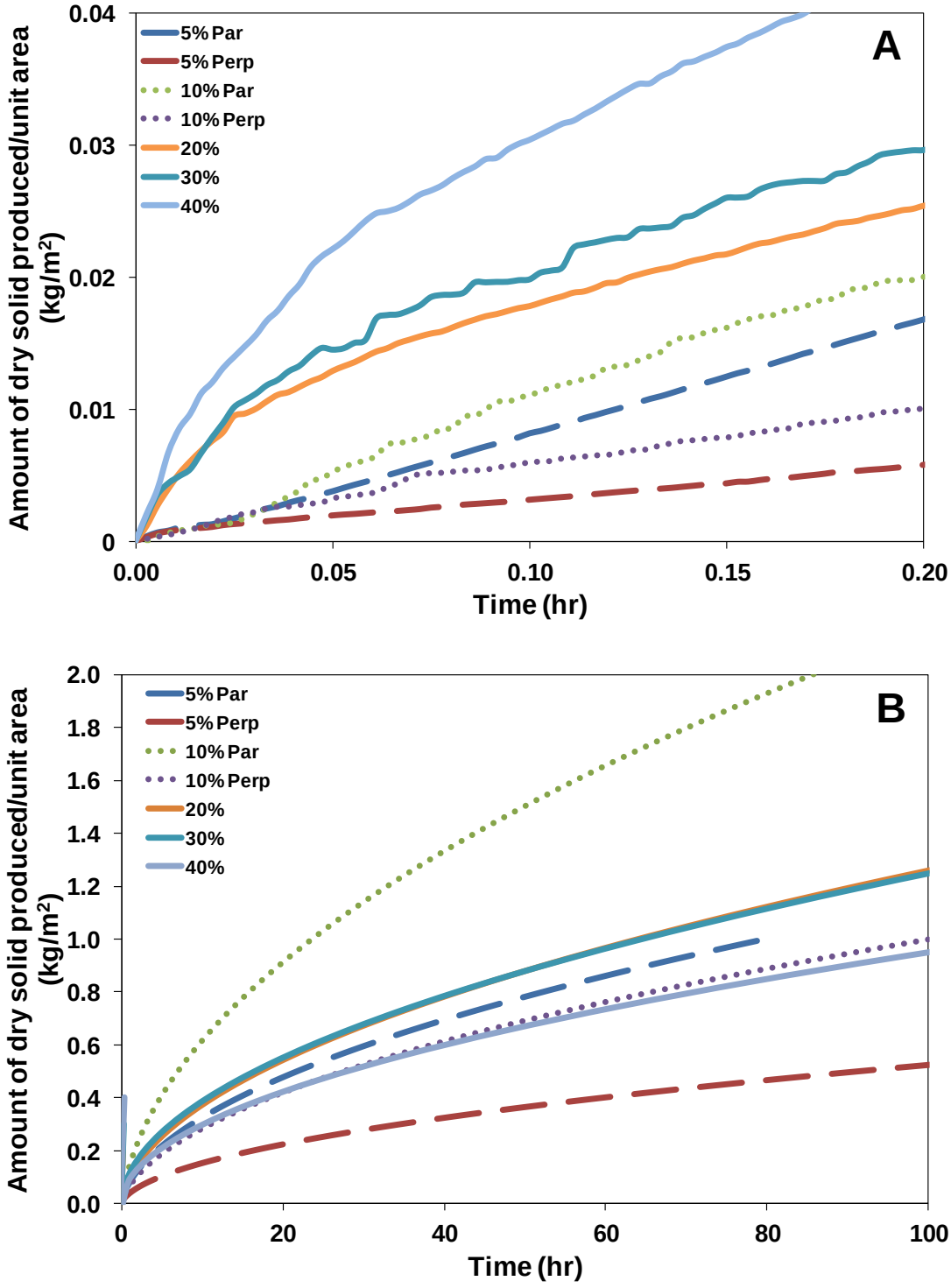

Figure 4.10: A. Amount of dry solids produced per unit area for different solid contents based on FDM data obtained**. B.** Predicted extrapolated amount of dry solids produced per unit area for different solid contents based on FDM *a* & *b* values. Par – Parallel orientation, Perp – Perpendicular orientation. Values are average of at least four runs in each case.

A direct comparison of 10% with 20 and 30% solid contents is difficult due to the lack of an orientation effect with the latter samples, which could practically be induced via

directional solidification in conventional freeze drying. Of course, in large scale commercial freeze drying, consideration might also need to be taken of the energy costs (which are favoured by starting with higher solids contents) as well as production rates.

4.3.6 Effect of cooling rate

Various cooling rates (2 $K.min^{-1}$, 10 $K.min^{-1}$ and 50 $K.min^{-1}$) during freezing were investigated in order to study their effect on freezing and in turn on the subsequent sublimation process via possible changes in the microstructure.

Fig. 4.11 A shows the effect of cooling rate on the nucleation temperatures of 10% and 40% lactose frozen with AgI at -40˚C. The nucleation temperatures were seen to decrease with increasing cooling rate. This is because as the cooling rate is increased the sample solutions tend to take longer to nucleate ice crystals due to the lesser degree of supercooling achieved at a faster rate. Also, the initial solid content of sample solution also shows a trend similar to seen in Fig. 4.3 for all cooling rates; higher solid contents result in lowered nucleation temperatures.

Fig. 4.11 B displays the effect of cooling rate on the α values for 10% and 40% (w/w) lactose solutions while Figs. 4.11 C & 4.11 D show the effect of cooling rate on the β values for 10% and 40% (w/w) lactose solutions respectively. The α values were found to decrease with increases in cooling rate at both lactose contents. This is presumably due to an increase in dried edge thickness and resistance when the cooling rate is lower. There are two possible mechanisms for this variation. Firstly, surface evaporation may occur during cooling which will increase the thickness of the surface layer. This will then be thicker if the cooling rate is slower as more time is taken to cool the sample. Secondly, the surface layer may be caused by freeze concentrated liquid becoming expelled from main body of the sample as ice is formed. There may be more time for liquid to be expelled if cooling rates are lower. The β values were found to be quite unaffected by the cooling rate as it was still quite high to allow any variation between nucleation and growth process of the ice crystals between the freeze-concentrated lactose. Hence, the ice crystals were not able to grow to larger sizes even with a slow cooling rate of 2 $K.min^{-1}$ compared to 50 $K.min^{-1}$.

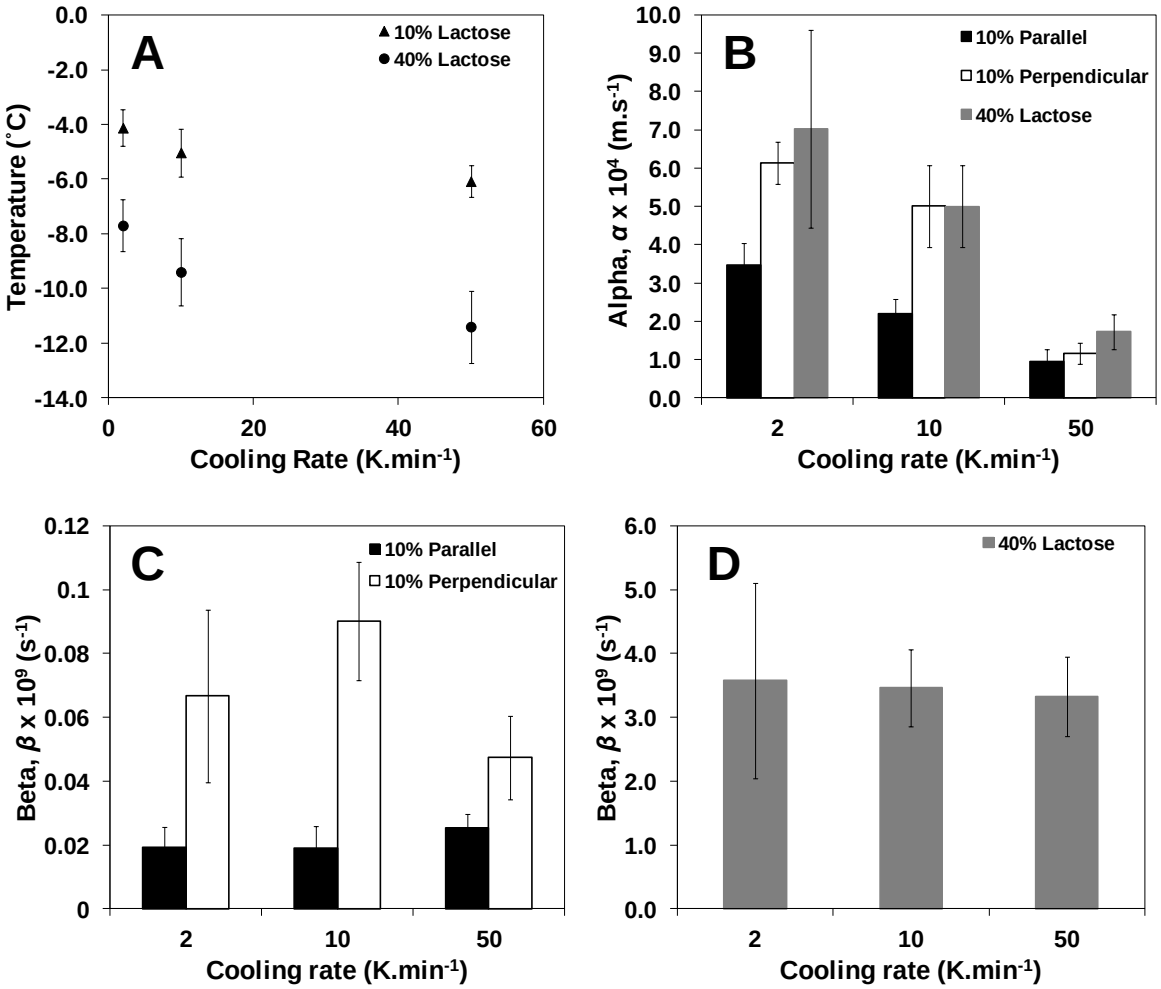

Figure 4.11: A. Effect of cooling rate (2 K.min^{-1}, 10 K.min^{-1} and 50 K.min^{-1}) on nucleation temperatures of 10% and 40% lactose frozen at -40˚C with AgI. **B.** Effect of cooling rate (2 K.min^{-1}, 10 K.min^{-1} and 50 K.min^{-1}) on α values of 10% and 40% lactose calculated from a & b values when freeze-dried under FDM at -40˚C and vacuum pressure of 1 Pa. **C.** Effect of cooling rate (2 K.min^{-1}, 10 K.min^{-1} and 50 K.min^{-1}) on β values of 10% lactose calculated from a & b values when freeze-dried under FDM at -40˚C and vacuum pressure of 1 Pa. **D.** Effect of cooling rate (2 K.min^{-1}, 10 K.min^{-1} and 50 K.min^{-1}) on β values of 10% lactose calculated from a & b values when freeze-dried under FDM at -40˚C and vacuum pressure of 1 Pa. Values are average of at least four runs with standard deviation as the error in each case.

4.3.7 Effect of freeze drying temperature

Three different final freeze drying temperatures were investigated (-30˚C, -40˚C and -50˚C) for both 10 and 40% (w/w) lactose solutions. Fig. 4.12 shows initial frontal velocities for 10% and 40% lactose solutions at the three different final drying temperatures and shows an increase with increasing drying temperature. The frontal velocity of 10% lactose was found to vary with ice crystal orientation. The variation with temperature is broadly similar to that of the equilibrium vapour pressure of ice

(also shown in Fig. 4.12). This supports the widely held view that vapour pressure is the driving force for mass transfer in freeze drying.

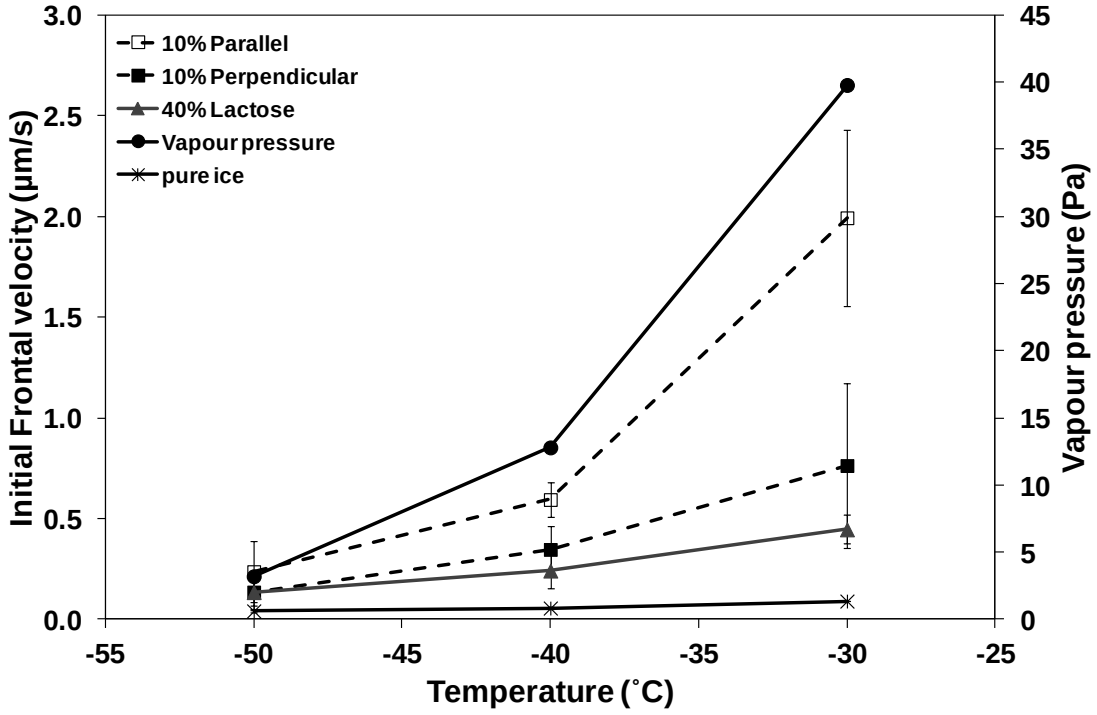

Figure 4.12: Initial frontal velocity of pure ice, 10% (two orientations of ice crystals – parallel and perpendicular) and 40% lactose calculated from α values and equilibrium vapour pressure for varying final temperatures of drying (-30, -40 and -50˚C) determined by freeze drying under FDM at 1 Pa. Values are average of at least four runs with standard deviation as the error in each case.

Figs. 4.13 A & 4.13 B show the variation of calculated α and β values respectively with drying temperature. For the case of 10% lactose solutions these were subdivided according to the orientation of the crystals.

In contrast, a single value of α and β was presented for 40% lactose solutions as the microstructures were too small to be distinguishable. α values of parallel orientation of lactose were found to be quite low and constant for all three final temperatures of drying investigated whereas they were found to increase significantly with increasing temperatures of drying for both 10% perpendicular orientation and 40% lactose. This seems to be the opposite of initial frontal velocity shown in Fig. 4.12. The frontal velocities do not seem to be increasing in line with the saturated vapour pressure for all samples except 10% lactose- parallel orientation. This behaviour was thought to

be due to the resistance in the linkam stage itself which was confirmed from the frontal velocities pure ice at -30˚C & -40˚C shown in Fig. 4.12.

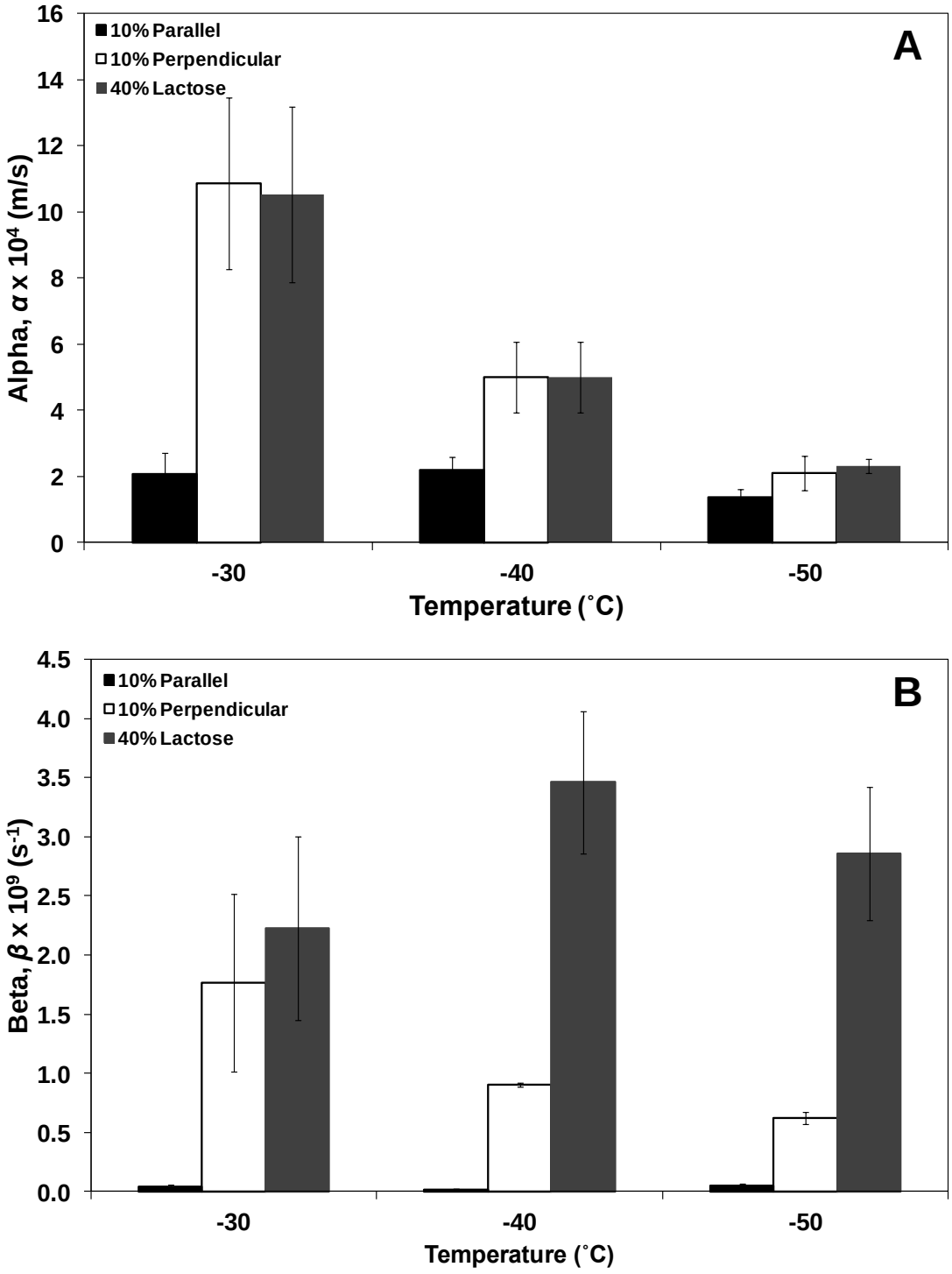

Figure 4.13: A. Effect of temperatures of drying (-30, -40 and -50˚C) on alpha values of 10% and 40% lactose calculated from *a* and *b* values. **B.** Effect of temperatures of drying (-30, -40 and -50˚C) on beta values of 10% and 40% lactose calculated from *a* and *b* values. Values are average of at least four runs with standard deviation as the error in each case.

The *a* values of pure ice (from which the velocities are calculated) were found to effectively correspond to the representative resistance of the freeze drying microscope stage as they displayed very low frontal velocities at all three temperatures even though pure ice does not offer any specific resistance to sublimation with respect to the edge of the sample.

β values shown in Fig 4.13 B were found to be very low with drying temperature in case of 10% parallel orientation and consistent for all three temperatures investigated. However, for 10% perpendicular orientation, β values were found to increase with increasing temperature of drying. This behaviour was again credited to the variation in pressure difference as discussed above in case of α values.

In the case of 40% lactose, the β values were found to be quite variable and were not seen to show any pattern with increasing temperature of drying. It was thought the resistance of the dried layer was not significantly affected by the pressure driving force with high lactose concentrations. The removal of water vapour was observed to be difficult at all three temperatures of drying with increasing depth of the sample due to higher concentration of lactose around the ice crystals.

4.3.8 Effect of Annealing

Annealing of 10% and 40% lactose solutions was carried out using four different cooling/heating profiles. The different cooling/heating profiles followed are - Profile I Profile II, Profile III and Profile IV (discussed in detail Section 3.5.4). Figs. 4.14 A & 4.14 B shows the edge resistance (α values) and resistance of dried layer (β values) respectively of 10% lactose solution for non-annealed as well as annealed samples (all four profiles), both with and without AgI.

Annealing did not substantially lower α values with the exception of profile I. In most cases these values rose during annealing, particularly profile III. The reason for the higher α value was thought to be due to evaporative drying which in the case of profile III took place over 60 mins at -20˚C. In Profile IV, α values were lower than profile III. These had the same hold time but were held at a higher temperature of -10˚C which would have caused some partial melting of ice crystals which may have then liberated water to re-dissolve some of the outer layer.

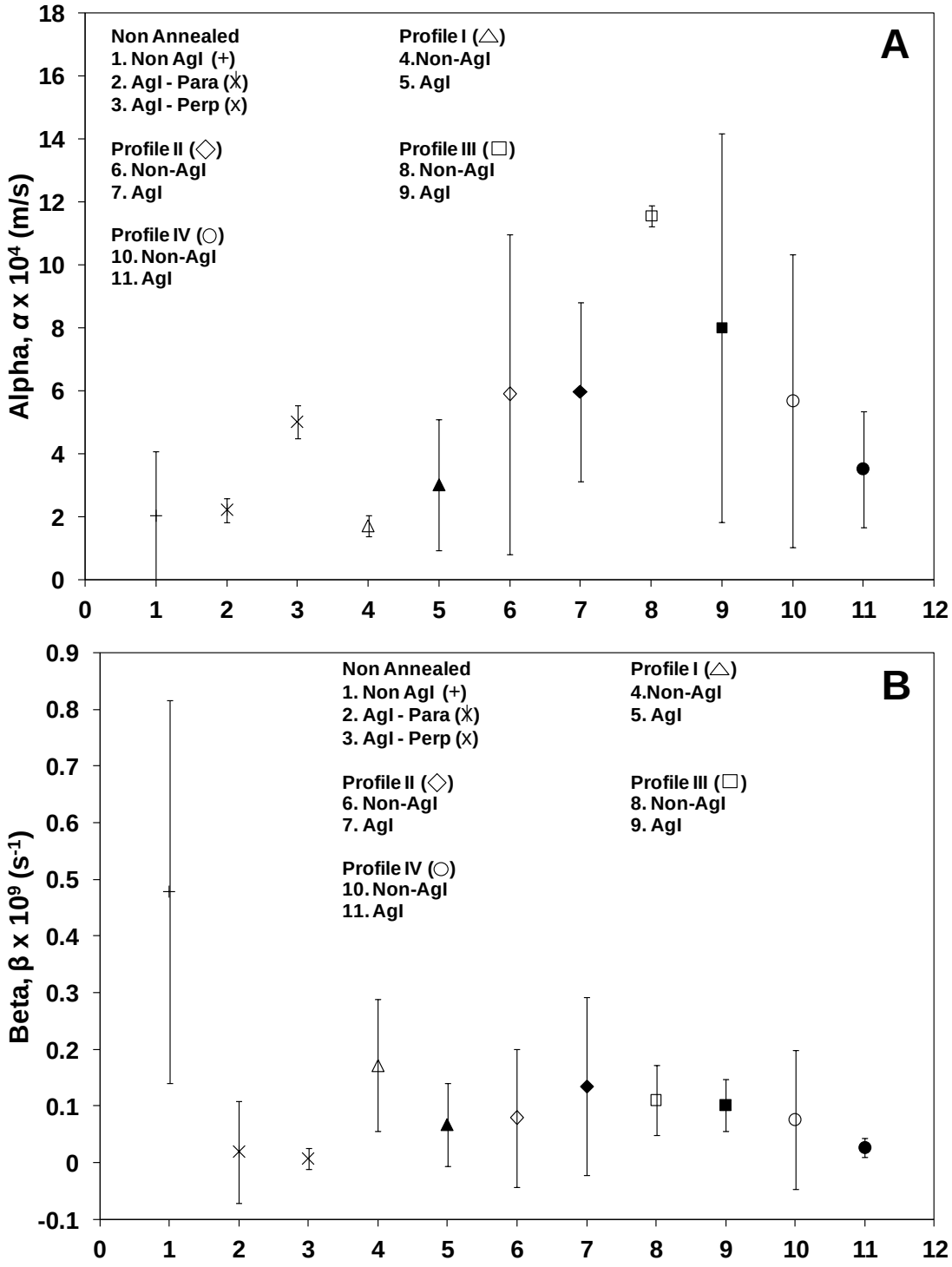

Figure 4.14: A. α values of 10% lactose varying with different annealing profiles compared with non-annealed samples with and without AgI. **B.** β values of 10% lactose varying with different annealing profiles compared with non-annealed samples with and without AgI. Values are average of at least four runs with standard deviation as the error in each case.

For non-AgI samples, annealing showed reductions in β values across all profiles, particularly Profiles II and IV. AgI samples showed higher b values after annealing and so annealing does not improve mass transfer in these cases.

Figs. 4.15 A & 4.15 B show the difference in microstructure before and after annealing with profile IV in 10% lactose frozen without AgI. It is clear from the microstructure that the process of annealing dramatically increases the size of the ice crystals formed and the effect of these large ice crystals was evident in the decreased resistance of dried layer, β values thus observed in Fig. 4.14 B.

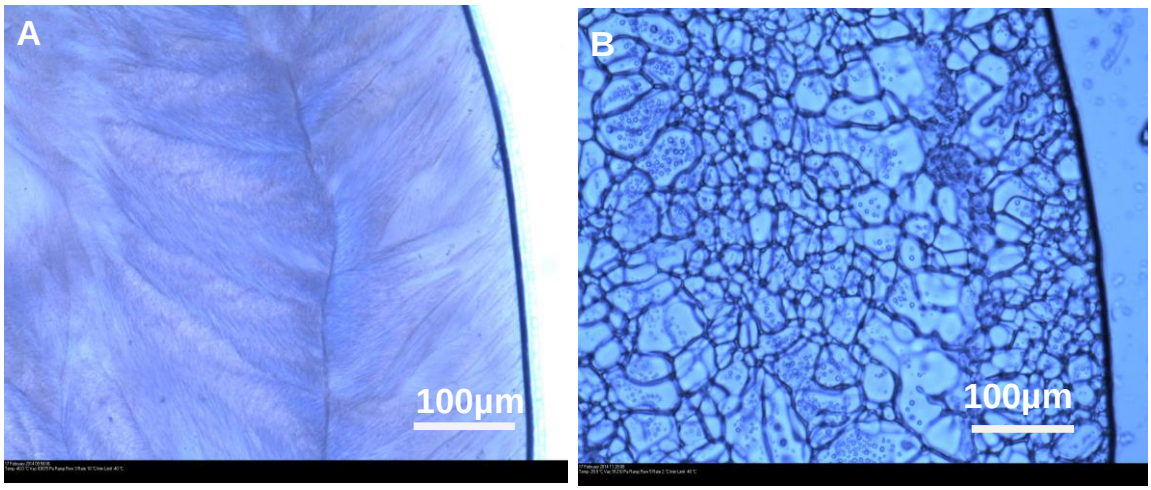

Figure 4.15: Microscope images of 10% lactose under FDM **A.** 10% Lactose frozen at 10 K.min^{-1}. **B.** Annealed at -10˚C and cooled to -40˚C (profile IV). Images are representative of at least four runs in each case.

However, these microstructural effects were visible only in the case of 10% lactose and not in case of 40% lactose. In 40% lactose samples, during the heating and holding period at -10˚C, crystallization of lactose out of the freeze concentrated solution was observed (Fig. 4.16 C). However, the solution was found to re-freeze when cooled again to -40˚C and was also observed to freeze-dry quite quickly (Fig 4.16 D). The acceleration of sublimation rate may be attributed to the change in amount of freeze concentrated lactose and amount of ice crystals trapped between lactose compared to non-annealed 40% lactose. The final moisture content of the frozen matrix was difficult to calculate due to lack of knowledge about the amount of lactose crystallization in the sample and also, the movement of the sublimation front during freeze drying was found to be rather non-uniform and hence a and b values were calculated for 40% lactose.

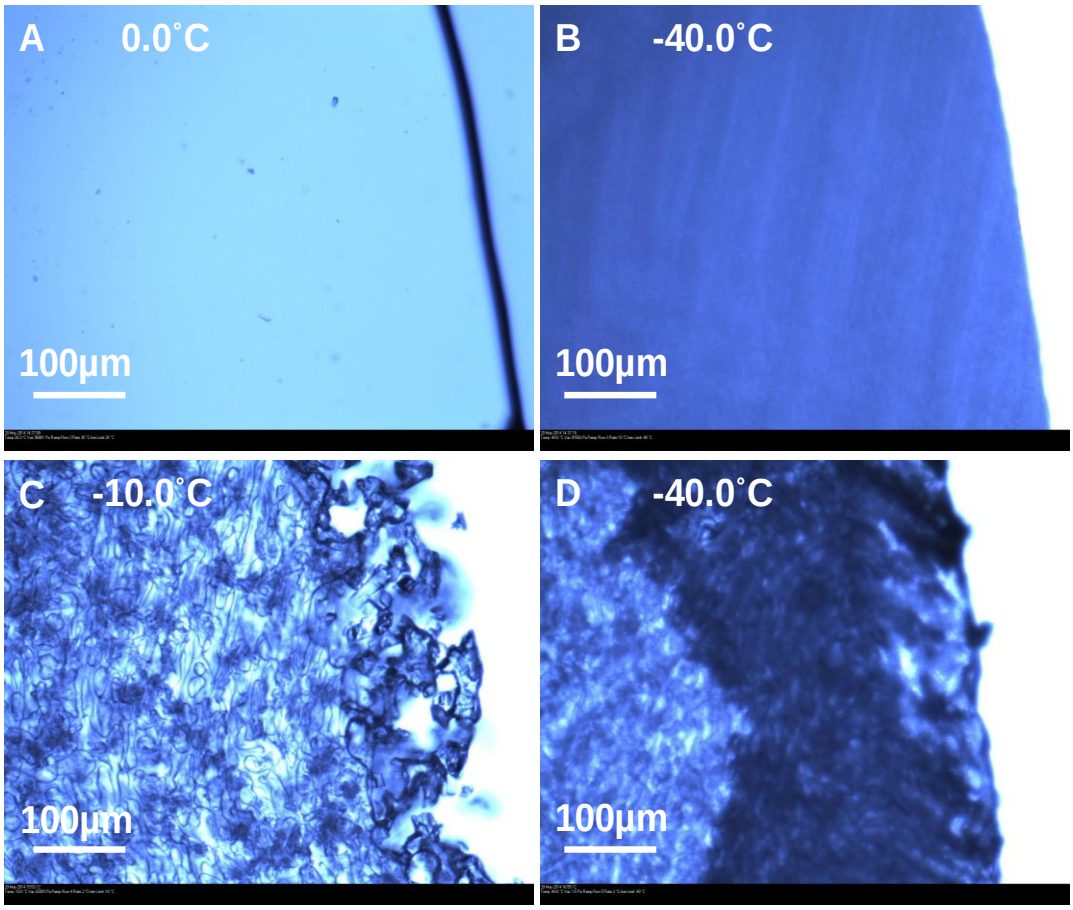

Figure 4.16: A.40% lactose at 0˚C before being frozen at 10 K.min^{-1}. **B.** Frozen 40% lactose at -40˚C. **C.** Annealed 40% lactose at -10˚C. **D.** Sublimation process in annealed 40% lactose. Images are representative of at least four runs.

4.3.9 Collapse temperatures

Effect of concentration: The effect of solid content of lactose solutions on the collapse temperature was also investigated. The collapse temperature is determined by the point where the lactose sample starts to lose its structure due to viscous flow as the temperature is increased. Collapse first occurs at the front as this corresponds to the highest moisture content in the lactose matrix, before secondary drying has had a chance to occur. The collapsed region appears lighter due to the reduction in light scatter as a result of loss of frozen structure, compared to the uncollapsed dried region (darker region) which was dried below the collapse temperature and has remained intact. Fig. 4.17 (inset) shows the process of structural collapse as seen under FDM; the onset of collapse was measured by observing the light band formation in FDM images obtained while heating the sample.

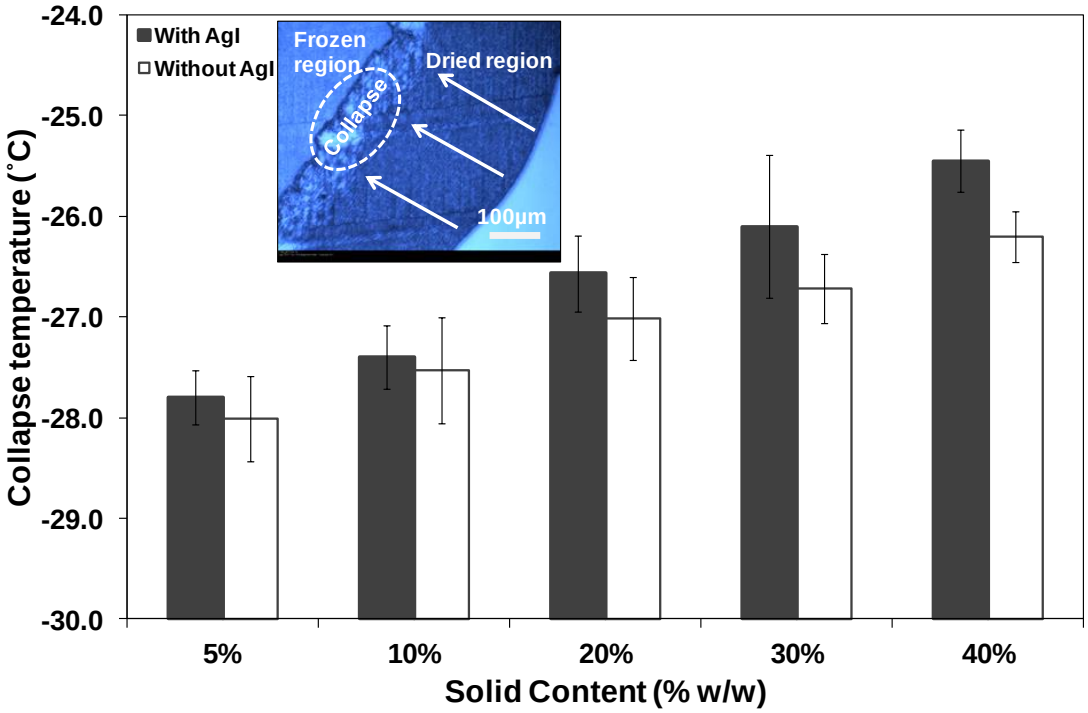

Figure 4.17: Effect of lactose solid content on the collapse temperature (T_c). **Inset:** shows the process of collapse observed in 10% lactose freeze dried under FDM at -40˚C at 1 Pa vacuum pressure and collapsed by heating at 1 K.min^{-1}. Values are average of at least four runs with standard deviation as the error in each case.

For samples containing AgI it was found that collapse temperatures showed an increasing trend with increasing solid content (Fig. 4.17). Higher solid content samples were found to be more tolerant of higher temperatures than lower solid contents as they were able to more closely approach the maximally freeze concentrated state.

Experiments with solid contents 10% and 30% solid content were also conducted without AgI for comparison. The 10% lactose solutions were found to have similar collapse temperatures both with and without AgI. The 30% lactose solutions showed a small variation however the difference was within ±1˚C between AgI and non-AgI samples. Even though the range of value seems small but is quite significant when considering temperatures for freeze-drying in an actual system. Thus the nucleation temperature does not noticeably affect the collapse temperature. This increasing trend of collapse with increasing solid content is in agreement with values that have been shown for different materials such as Polyvinylpyrrolidone (PVP), Trehalose, previously by various researchers (Meister *et al.,* 2009 and Yang *et al.*, 2010).

Glass transition temperatures: Glass transition temperature (T_g') is another measure of the critical formulation temperature of the sample to be freeze dried.

The detection of onset glass transition temperature was carried out using DSC (Fig. 4.18) with the protocol described by Omar & Roos, (2007) (see Section 3.8).

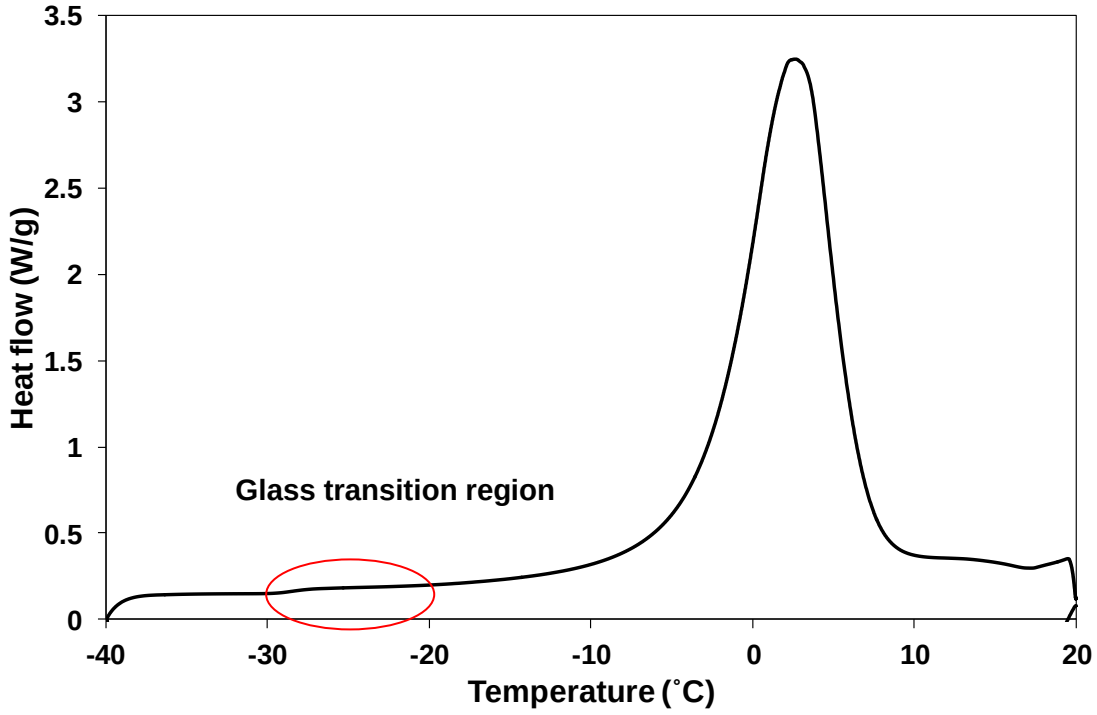

Figure 4.18: DSC thermogram of 10% lactose with AgI cooled at 10 K.min^{-1} and heated at 5 K.min^{-1}. Values are average of at least three repeat runs with standard deviation as the error.

The step change in heat flow due to the change in heat capacity at the glass transition is quite small (see e.g. Fig. 4.18) compared to the overall melting thermogram obtained from DSC (enhanced image of step shown in Fig. 4.19). This is the biggest disadvantage of using DSC to determine the T_g' which will be used to determine the operating temperature of primary drying during an actual large scale freeze-drying process. In some cases this could be confused with instrument noise and so is not the most robust or reliable method of detection of critical formulation temperature.

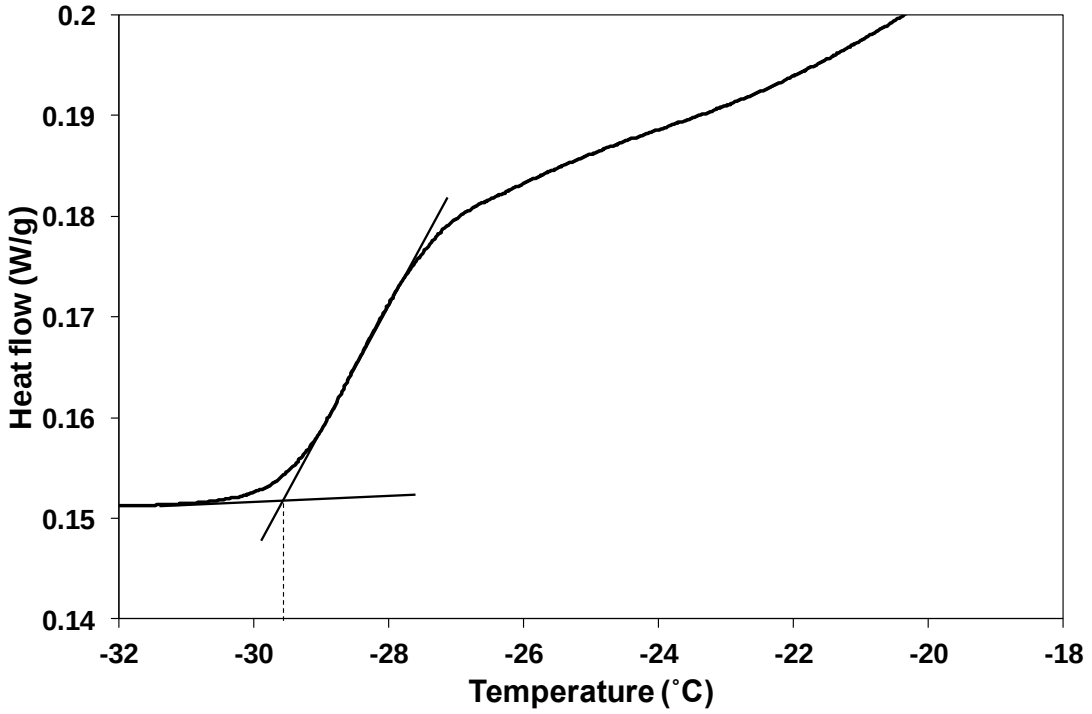

Figure 4.19: DSC thermogram of 10% lactose with AgI cooled at 10 K.min^{-1} and heated at 5 K.min^{-1} highlighting the glass transition temperature. Values are average of at least three repeat runs with standard deviation as the error.

The glass transition temperatures of 10% and 40% lactose with and without AgI are summarized in Table 4.2. AgI containing samples were found to have slightly higher T_g' values compared to samples without AgI for both 10% and 40% lactose solutions.

Table 4.2 Onset glass transition temperatures (T_g') and collapse temperature of 10% and 40% lactose determined using DSC with and without AgI calculated from average of atleast three repeats.

Glass transition temperature (˚C)			
10% Lactose		40% Lactose	
AgI	Non-AgI	AgI	Non-AgI
-29.4±0.1	-29.9±0.2	-29.1±0.2	-29.2±0.2
Collapse temperature (˚C)			
10% Lactose		40% Lactose	
AgI	Non-AgI	AgI	Non-AgI
-27.4±0.3	-27.5±0.5	-25.5±0.3	-26.2±0.2

Comparing these T_g' values to the collapse temperatures in Fig. 4.17, it is clear that these values are lower by about 2˚C for both 10% lactose and about 4˚C for 40% lactose. The T_c and T_g' values were quite close to those published in literature by various researchers (Fureby *et al.,* 1999; Wang, 2000 and Sablani *et al.,* 2010). This comparison of the temperatures is in agreement with the trends suggested in the

literature that collapse temperatures for aqueous solutions are generally 1-2˚C above the glass transition temperatures, although in some cases, in complex bacterium preservation media, it can be as high as 10˚C above T_g' (Fonseca *et al.,* 2004 and Yang *et al.,* 2010).

Effect of cooling rate: Effect of cooling rate on collapse temperature was investigated for both 10% and 40% lactose with and without AgI. Fig. 4.20 shows the variation of collapse temperature with different cooling rates – 2 K.min^{-1}, 50 K.min^{-1} and sample slide dipped in liquid nitrogen for fastest freezing, all with a heating rate of 10 K.min^{-1}. Similar trends were seen with heating rate of 1 K.min^{-1} as well (see Appendix). It can be clearly seen that both 10% and 40% lactose display different behaviours with different cooling rates. While 10% lactose with AgI was found to have increased collapse temperature with increasing rate of cooling, 40% lactose with AgI was found to show a decreased T_c with increased cooling rate.

Effect of heating rates: The effect of changing the heating rate from 10 K.min^{-1} to 1 K.min^{-1} on the collapse temperature of 10% and 40% lactose, both with and without AgI was also investigated (Fig. 4.21). It was clearly observed that increasing the heating rate led to an increase in the observed collapse temperatures of all the samples. A similar behaviour has been reported by Meister, (2009), with onset collapse temperature of sucrose. It was reported that increasing the heating rate from 1 K.min^{-1} to 10K.min^{-1}, increased the onset collapse temperature of 5% w/w sucrose by 2˚C. 10% lactose displayed similar behaviour (increase by ~2˚C) with the change in heating rate, while 50% lactose displayed an increase of about 5˚C for AgI containing samples. This behaviour may have two causes. Firstly, there is probably a thermal lag effect in the system. Secondly, collapse takes time to occur with faster cooling rate (as it is a flow process) and so this introduces an additional lag. Similar trends were seen in samples freezing with other cooling rates - 50 K.min^{-1} and frozen with liquid nitrogen (see Appendix D).

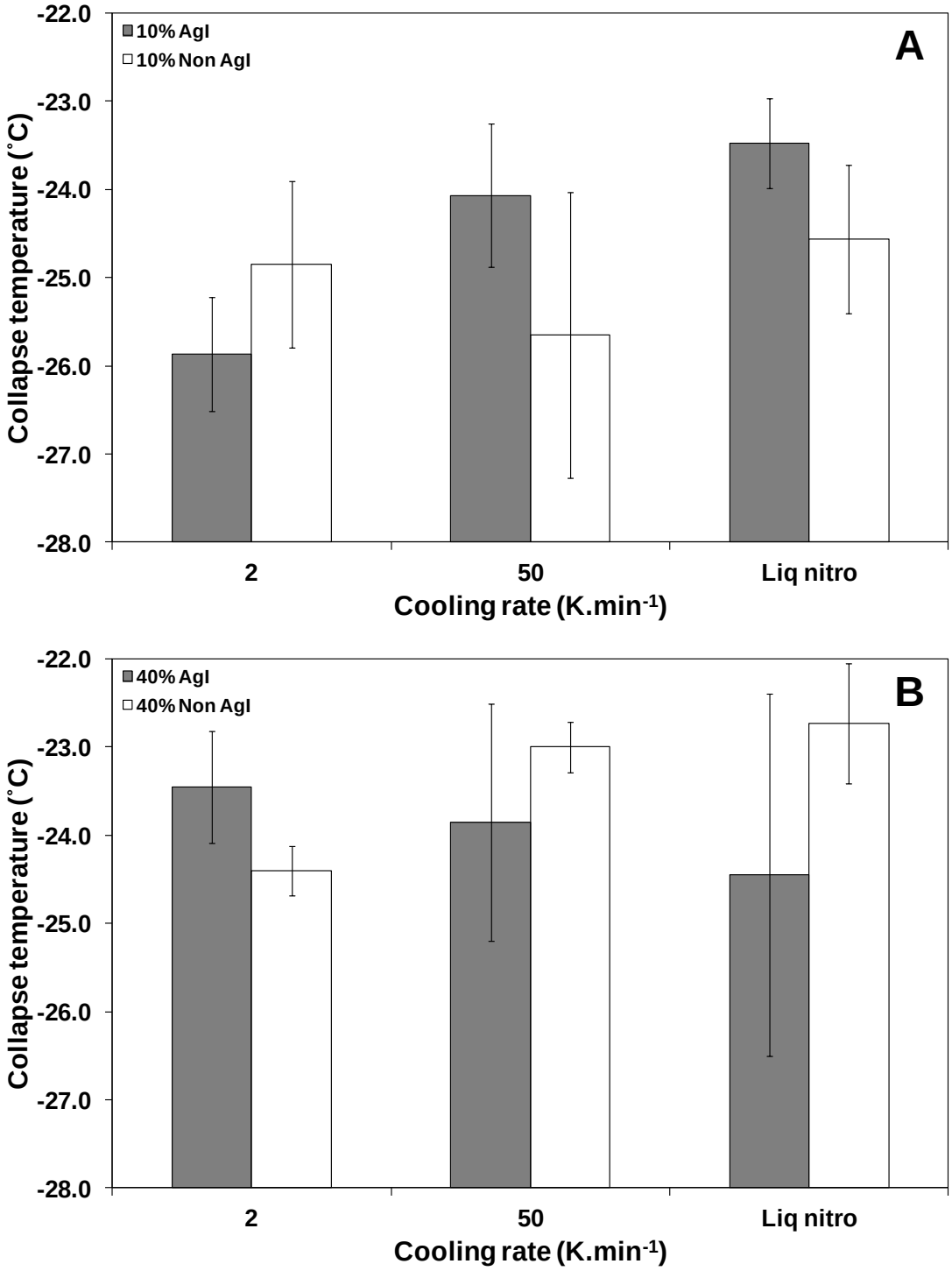

Figure 4.20: Effect of cooling rates on collapse temperature. **A.** 10% with and without AgI, freeze dried at 1 Pa and heated at 10 K.min^{-1} **B.** 40% with and without AgI, freeze dried at 1 Pa and heated at 10 K.min^{-1}. Values are average of at least three repeat runs with standard deviation as the error in each case.

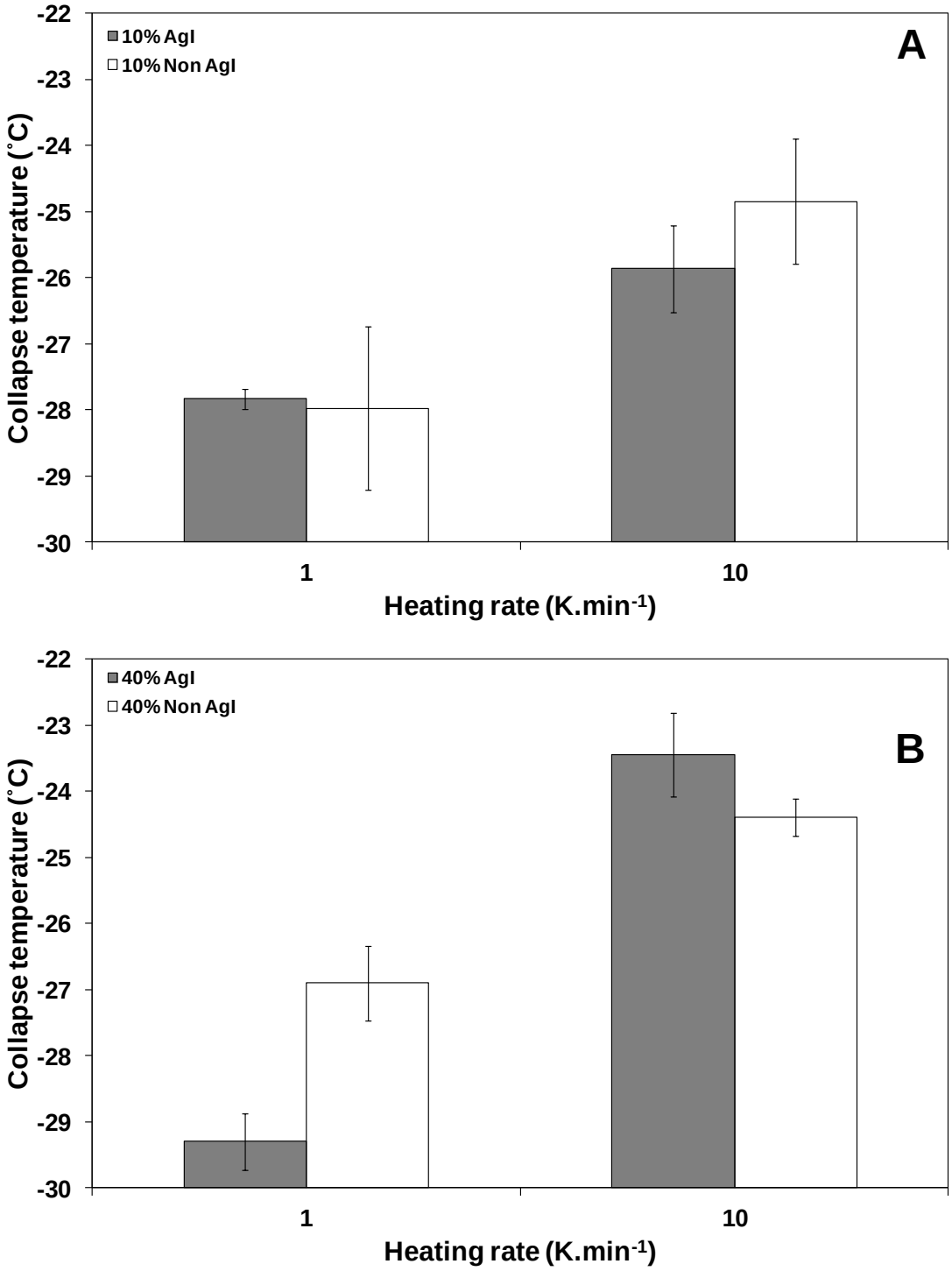

Figure 4.21: Effect of heating rates on collapse temperature. **A.** 10% with and without AgI with a cooling rate of 2 K.min^{-1}. **B.** 40% with and without AgI with a cooling rate of 2 K.min^{-1}. Values are average of at least three repeat runs with standard deviation as the error in each case.

4.4 Conclusions

The purpose of this study was to use FDM to gain a better insight into the various factors such as initial lactose content, freezing rate, and lyophilisation temperature that affect the primary drying phase of the freeze-drying process. Silver iodide was used to induce ice nucleation and was found to bring a consistent pattern to nucleation temperatures when compared to non-silver iodide experiments. By also reducing the degree of supercooling on nucleation, the addition of a nucleation agent also meant that crystal sizes were large enough to be observed for dilute (≤10% solids) systems. Silver iodide was used in order to gain a better understanding of behaviour of frozen structure on the freeze-drying process, although it would not be able to be used in food or pharmaceutical industry applications. However, it does show that controlling nucleation (which can be achieved via a variety of other means) may improve freeze-drying rates.

The ice crystal size and orientation were found to directly influence the frontal velocity. The observed kinetics was also consistent with the presence of an edge layer resistance along with an increasing resistance per unit depth into the porous region. These two regions could also be clearly discerned on microscope and SEM images.

The effects of solid content (5 to 40% w/w), cooling profile (2 $K.min^{-1}$, 10 $K.min^{-1}$ & 50 $K.min^{-1}$) and final temperature of drying (-30˚C, -40˚C & -50˚C) on the representative edge resistance (α) and representative resistance of the dried region (β) were also investigated. The representative edge resistance α was found to increase initially with lactose solid content (5, 10 and 20% w/w) followed by a decrease at higher solid contents (30 and 40% w/w) while β values were found to increase dramatically with increasing solid content. The rate of production of dried solid lactose was found to be higher with an initial lactose content of 40% than 5% lactose over the first few minutes of an experiment, but extrapolated data over the timescales commonly encountered in commercial freeze-drying show the existence of an optimal lactose content of around 10%.

Cooling rates (2 $K.min^{-1}$, 10 $K.min^{-1}$ and 50 $K.min^{-1}$) were mainly found to affect the surface resistance and this may be due to different levels of surface drying when the samples are being cooled for different lengths of time. Freeze drying rates also

increased with increasing temperature approximately in line with the vapour pressure of water which is widely held to constitute the main driving force for mass transfer. However, there was some effect of sample drying temperature (-30˚C, -40˚C and -50˚C) on α and β values.

The effect of annealing on the ice crystal morphology and thus, on the sublimation kinetics were also investigated using four different annealing profiles. 10% lactose solutions (without AgI) were found to be greatly affected by the annealing process (lower β values) but did not improve samples that did have AgI. The microscope images showed large scale changes in microstructure as a result of annealing with much larger and more circular crystals forming. 40% lactose samples were seen to result in crystallization of lactose from the freeze-concentrated matrix and hence, the sublimation kinetics was not investigated in great detail.

Collapse temperatures (T_c) were also determined as a function of solid content of lactose solutions which was found to increase with increase in solid content from about -28˚C to -25˚C for 5 to 40% w/w solid content and was compared to the glass transition temperatures (T_g'). T_c was found to be 1-2˚C higher than T_g', in good agreement with previously published literature.

A greater understanding of the effect of the structure of the frozen matrix on the freeze-drying process has thus been achieved in this chapter. It can be said that edge of the sample, size and orientation of ice crystals around it plays a significant role in determining sublimation front velocities. Ice crystals parallel to the direction of sublimation were found to have faster front velocity and the larger ice crystals in AgI containing samples facilitated faster front movement.

5

VIAL FREEZE-DRYING OF LACTOSE

Freeze drying of lactose in glass vials and the effect of microstructure on the mass transfer of water vapour was investigated. The effects of freezing method and initial solids content on the primary drying were also studied. Primary drying durations of these processes were compared to the drying times estimated from the equivalent freeze drying microscopy experiments.

5.1 Introduction

Freeze drying of materials in vials is well established in the pharmaceutical industries. In the food industry, the use of freeze-drying is restricted to high-value goods such as baby food formula and coffee (Wolff *et al.,* 1989 and Zhai *et al.,* 2004). However, freeze-drying is much more prevalent in the pharmaceutical industry as the higher margins offset the high investment and operating costs (Rene *et al.,* 1993 and Baressi *et al.,* 2009).

As has been described in previous chapters, a typical freeze-drying cycle consists of three important stages: freezing, primary drying and secondary drying. After the initial freezing stage, the frozen sample is subjected to the primary drying stage, during which water vapour is sublimated from the frozen material by reducing the chamber pressure (thus decreasing vapour pressure) while the freeze-dryer shelf temperature is maintained at a constant sub-zero temperature (Franks, 1998).

The shelf temperature, and in turn, the temperature of the product at which it is freeze-dried is maintained below its collapse temperature during primary drying in order to achieve desired structural integrity of the product (Franks, 1998). As the secondary drying stage commences, the shelf temperature (and hence the product temperature) is increased and the chamber pressure further decreased so that unfrozen water bound to the semidried material can be removed to achieve the desired residual water content in the final product (Zhai *et al.,* 2005).

In order to reduce the operating costs of the freeze-drying, it is important to optimise and improve the existing vacuum freeze-drying process. This requires a better understanding of the heat and mass transfer phenomena which significantly limit and control the sublimation kinetics (Wolff *et al.,* 1989). Over the years quite a few researchers have focussed on optimising the freeze-drying temperature and pressure, thus reducing freeze-drying times (Rene *et al.,* 1993; Tang & Pikal, 2004; Gan *et al.,* 2005 and Tang *et al.,* 2005).

To improve the heat and mass transfer rates in a freeze drying process, the fundamentals of the effect of ice crystallization on microstructure and thus, the movement of the sublimation front through the sample needs to be understood in detail and which at this current situation seems to be ill-defined. In the present

scenario in freeze-drying operations, the biggest limitation is the difficulty and complexity in directly measuring the important process parameters without affecting the process itself and/or damaging the sterile process conditions (especially in pharmaceutical industry).

A number of researchers have focussed on several possibilities for detecting the movement of the sublimation front and also, the end of the sublimation phase. While some researchers have focussed on methods that involve indirect measurement of different process parameters such as product temperature, the electrical resistance of the product and the partial pressure of water vapour (Rene *et al.,* 1993), others use methods to analyse the product directly during the process.

In the indirect methods of monitoring primary drying, the most widespread (though invasive) is the measure of product temperature using a thin thermocouple inserted into the sample in a vial. This method, however, may directly affect the nucleation and ice crystal growth, especially in a large scale operation (Roy & Pikal, 1989). Apart from temperature measurements, moisture sensors and mass spectrometry have been suggested by some researchers to detect the end of sublimation phase (Oetjen, 2004). Recently, non-invasive techniques, such as the pressure rise test, which involves in-line measure of the pressure rise that occurs when the valve between the drying chamber and condenser is shut-off (for a very short duration), have been also proposed to monitor the whole system (Barresi *et al.,* 2009).

Monitoring of freeze drying processes has also conducted in conjunction with the use of various mathematical models of the dehydration kinetics. Different models have been described in the literature to predict the freezing, primary drying and secondary drying phases of the process with respect to various operating parameters (Zhai *et al.,* 2004). However, the lack of understanding of the heat and mass-transfer resistances, different product properties and effects of process parameters (such as cooling profile, temperature of freeze-drying) limits the applicability of these models to only a confined range of process conditions (Rene *et al.,* 1993).

The objective of this chapter is to investigate the freeze-drying of lactose in glass vials so as to gain a better understanding of the mass transfer phenomenon that takes place during the sublimation process and how it is affected by microstructure. To

achieve this, freeze-drying was performed on a model lactose system, using thermocouples to monitor the movement of the sublimation front. Various experimental conditions were varied to generate different microstructures: the use of AgI as a nucleating agent, and freezing profile, (slow cooling, inclusion of an annealing step, or cooling in LN_2). SEM was then used to visualise the microstructures of the final freeze dried products. The sublimation kinetics were also then compared for the different microstructures and also compared to the data extrapolated from the FDM of lactose. Experiments were performed for both 10% and 40% initial lactose contents, which are considered in turn.

5.2 Materials and methods

5.2.1 Materials

α-lactose monohydrate and silver iodide was purchased from Fisher Scientific (Loughborough, UK) for the purpose of this research as described in Section 3.1.

5.2.2 Moisture content determination

Moisture content of the lactose bought was determined using the KF titration as discussed in Section 3.3.2.

5.2.3 Sample preparation

Sample preparation of varying lactose solid contents was carried out as explained in Section 3.4.1.

5.2.4 Vial Freeze-drying

Conventional freeze drying of sample solutions was carried out in glass vials for lactose solutions in a VirTis AdVantage Plus Benchtop shelf based Freeze Dryer (SP Industries, Warminster, PA) as described in Section 3.7.

5.2.5 Field Emission Gun Scanning Electron Microscopy

FEGSEM was carried out on the freeze dried samples obtained from FDM as described in Section 3.7.

5.3 Results and discussion

In most research papers studying the freeze drying of lactose, the main focus has been the crystallization of lactose and hence very few researchers have focussed specifically on the freeze drying kinetics. Hence, this research project aims to bring forth the freeze drying kinetics of lactose and in turn, understand better the effect of ice nucleation and ice crystal morphology on the primary drying rates.

Freeze drying of lactose (initial concentrations – 10% and 40% w/w) was carried out in glass vials with and without the use of the nucleating agent, silver iodide (AgI). Each run involved the use of 5 vials, each containing 4 ml (about 14 mm in depth) of lactose solution and each with three T-type thermocouples at three different depths (3 mm, 7 mm, 11 mm) from the top of the sample.

Fig. 5.1 shows typical temperature measurement curves from the three thermocouples inside a vial during a freeze drying run of lactose where samples were cooled slowly. It also displays the measure of shelf temperature from a separate thermocouple attached to the freeze dryer shelf in direct contact with the vials. The plot displays good correlation with a typical temperature change profile presented in literature displaying the change in temperature with the movement of the sublimation front (Elia & Barresi, 1998). It is evident from the plot that there are significant differences between shelf temperature and the temperatures of the vials before the start of primary drying. The vials have a concave rather than flat base and the resulting cavity acts as a resistance to heat transfer between the shelf and glass vial. To overcome this resistance in later experiments, thermal grease was applied to the vials in order to improve thermal conduction.

The temperature vs time plot of a single vial (Fig. 5.1) also displays the increase in temperature at the three different sample depths with the end point of sublimation. It is clear that the sample undergoes sublimation at different times at the three sample depths investigated with the highest thermocouple increasing in temperature first, followed by the middle thermocouple and then the lowest thermocouple. This shows that the sublimation front moves through the sample as expected from the top towards the bottom of the sample.

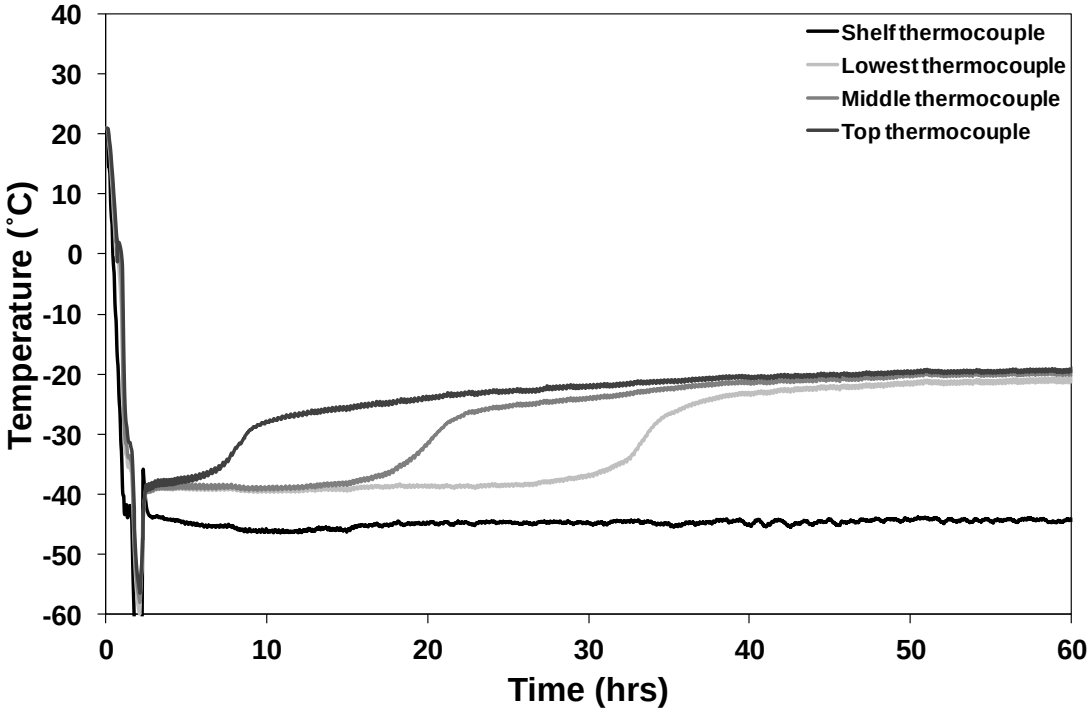

Figure 5.1: Vial (without thermal grease) freeze-drying data plot of 10% lactose freeze dried at -40˚C and 10 Pa indicating the shelf temperature and temperature change with time as the sublimation front moves through the vial passing the three thermocouples at different vial depths. Curves are representative of at least five repeat runs.

Many researchers have studied the effects of freeze-dryer wall temperatures on the primary drying rates of various samples (Gan *et al.,* 2005 and Yeom & Song, 2010). It has been observed that it significantly affects the sublimation rate in vials due to radiation from the walls (Gan *et al.,* 2005). It is said to be helpful, to be able to control the temperature of the walls so as to have better control of the sublimation process. However, in our current set-up it was not possible to control the wall temperature due to lack of such a system in the freeze dryer used. Hence, the vials were deliberately kept away from the walls of the chamber to minimise the radiation effects on the sample. This also facilitated operating conditions of the vials to be near-identical. Vials were also kept in direct contact with the shelf without using a holding tray to gain better thermal contact with the shelf.

Another noteworthy point observed from the plot is the temperature difference between the shelf and the product after completion of primary drying. The product temperature was found to be quite high (~15˚C) compared to the shelf temperature. This was thought to be an unusual behaviour as the product temperature was

expected to be quite closer to the shelf temperature. This difference was thought to be due to a dynamic balance between the heat input from the environment (temperature of chamber ~-20˚C & temperature of walls ~+20˚C), the shelf temperature and the heat removed from the system during sublimation (endothermic). This hypothesis was supported by similar results observed by Zhai *et al.,* 2003 & Zhai *et al.,* 2005 which displayed similar differences (~15˚C) between product and shelf temperature while freeze drying of glass bead slurries and pure water respectively.

5.3.1 Vial vs vial Comparison

The end point of sublimation was determined by drawing a tangent on the curve and calculating the difference from the end point of freezing to the time determined from the tangent.

Figs. 5.2 A & 5.2 B show temperature measurements from thermocouples of vials containing 10% lactose without AgI and with AgI respectively (slow cooling profile). Each figure shows data from two repeats. The reproducibility between the vials was quite close. It can also be seen that the differences between the shelf temperature and the initial freeze drying temperatures are now much closer. The difference between the shelf and the vial thermocouples has thus effectively been eliminated by applying the thermal grease, and the closeness of all three vial temperatures to the shelf can also be attributed to the fact that the sample is initially icy with a high thermal conductivity (akin to that of ice). As the sublimation front passes through the material the thermal conductivity of the freeze dried material it leaves behind is much lower (akin to insulating material) which allows a temperature gradient to occur, and allows thermocouples in the dried layer to rise. Thus the point of passing of the sublimation front can be approximately identified as the point when the temperature of a thermocouple starts to rise. In practice, a tangent to the rising curve was constructed and the point where this intercepts the initial freeze drying temperature was taken as the time point when the front is passing. To minimise experimental error, quoted drying times for each condition in the rest of this thesis were averaged for at least five vials.

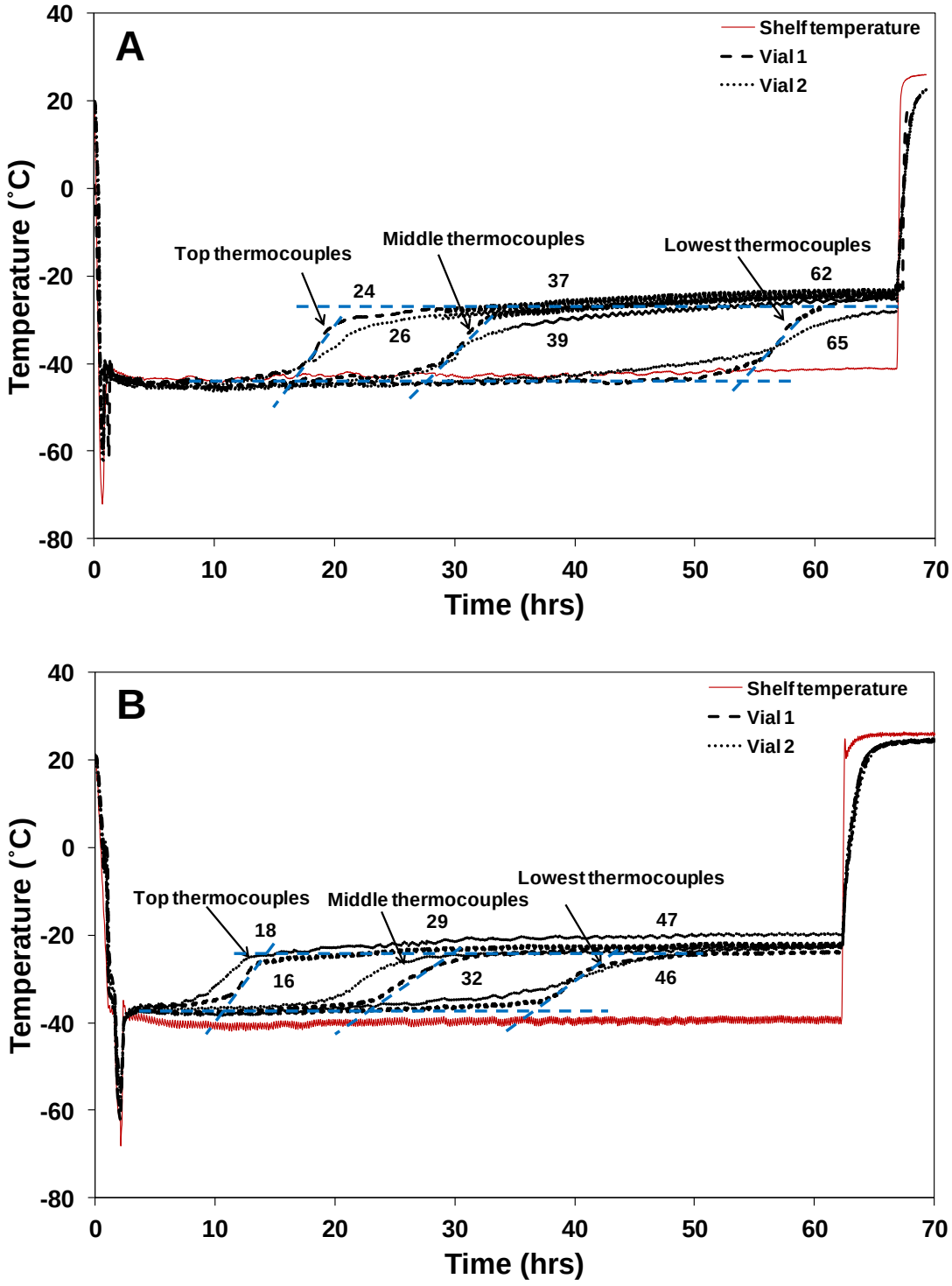

Figure 5.2: Vial (with thermal grease) freeze-drying data plot of 10% lactose freeze dried at -40˚C and 10 Pa. Each figure shows a comparison of temperature (at three depths) vs time plot between two vials **A.** without AgI. **B.** with AgI. Curves are representative of at least five repeat runs.

The plots also show similar trends as discussed in previous chapter, that is, AgI containing samples were found to dry faster in comparison to frozen lactose samples

dried without AgI, and the sublimation rate appears to slow with time. This will be further discussed in detail in the next section of this chapter.

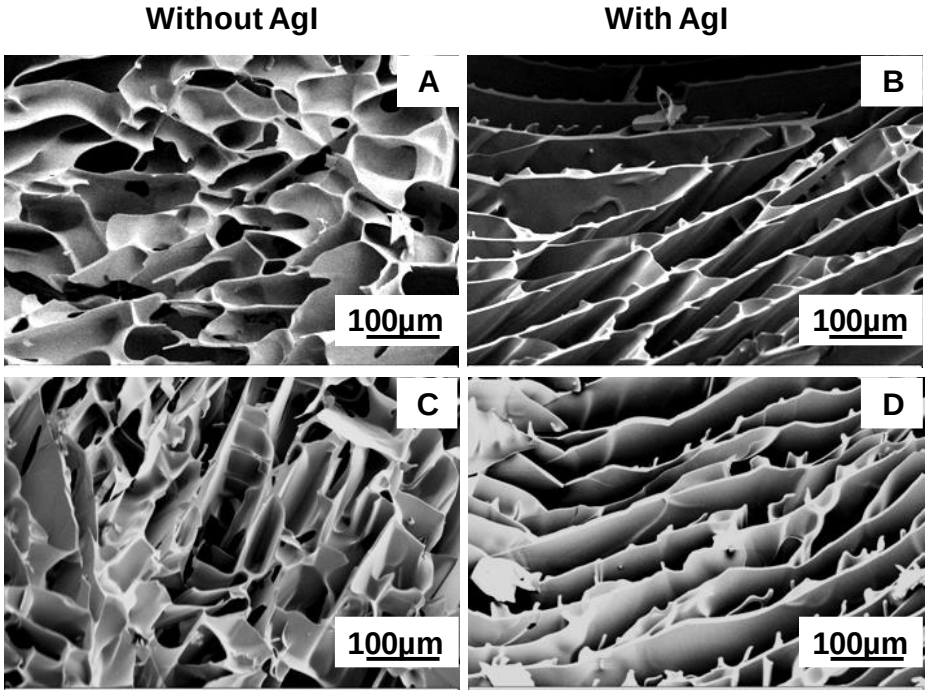

Figure 5.3: FEGSEM images of the internal microstructure of 10% lactose freeze dried at -40˚C and 10 Pa, without AgI (A & C) and with AgI (B & D) (just below the top surface of the sample). Images are representative of at least five repeat runs.

SEM images of the microstructure of freeze-dried samples (10% lactose) are shown in Fig. 5.3. Figs. 5.3 A & 5.3 C show the internal structures from two different vials without AgI while Figs. 5.3 B & 5.3 D show the internal structure from two different vials with AgI. It is evident from the figure, that the microstructure of vials freeze-dried under similar conditions is quite similar in size and shape of ice crystal voids. Lactose samples without AgI though, were found to have a more random internal microstructure, while samples with AgI were seen to have a more oriented structure clearly indicating the effect of AgI on nucleation process of the lactose solution. This directionality very likely explains the fact, discussed from Fig. 5.2 that the AgI containing samples dried faster than samples without AgI (compared to Fig. 5.3 A & 5.3 C) facilitating easier water vapour removal.

5.3.2 Effect of freezing profiles (10% lactose samples)

The effects of freezing profile and the presence of AgI on the microstructure and primary drying behaviour are investigated in this section on 10% lactose samples.

Slow cooling: Fig. 5.4 shows the internal microstructures of 10% lactose, freeze dried in vials previously frozen at a slow cooling rate (1 $K.min^{-1}$), both without AgI (left side images) and with AgI (right side images). Figs. 5.4 A & 5.4 B show the difference in surface of the samples without and with AgI after freeze drying respectively. The surface of AgI containing samples seems more porous in comparison to samples without AgI (both in terms of size and number of pores). This could be another contributing factor to the faster drying of frozen lactose samples with AgI. The cracks also seem to appear where the ice crystals beneath the surface have come in contact with the top layer and forged their way through creating the surface breaks.

Figs. 5.4 C & 5.4 D display the vertical cross section of the freeze dried lactose while Figs. 5.4 E-H show the internal microstructure of cross-section of the sample from the top (just below the surface layer) and bottom of the vials of both cases respectively. In terms of vertical cross section, the samples do not look different as the microstructure is not that apparent; however, the horizontal cross sections of ice crystal morphologies are very variable in shape and size. Another observation was that microstructure also seems to vary with height within the vial with larger crystals towards the top of the vial and smaller crystals towards the bottom of the vial. This feature was observed in both cases and was thought to be due to the directional solidification observed in the vials wherein the lactose solution starts to freeze from the bottom of the vial and moves towards the top of the vial. This behaviour was seen since the vial is in contact with the shelf at the bottom providing the required cooling rate resulting in the ice nucleation from the bottom (thus, smaller crystals) which grows into larger ice crystals towards the top of the sample surface.

Lactose samples freeze dried with AgI were found to have larger and much more uniform ice crystal pores (left behind after drying) in comparison to samples without AgI, especially at the bottom of the vial resulting in faster and easier water vapour removal and thus, faster primary drying rates as also seen in Fig. 5.2. Fig. 5.4 G & 5.4 H also shows the bottom layer of the samples without and with AgI respectively.

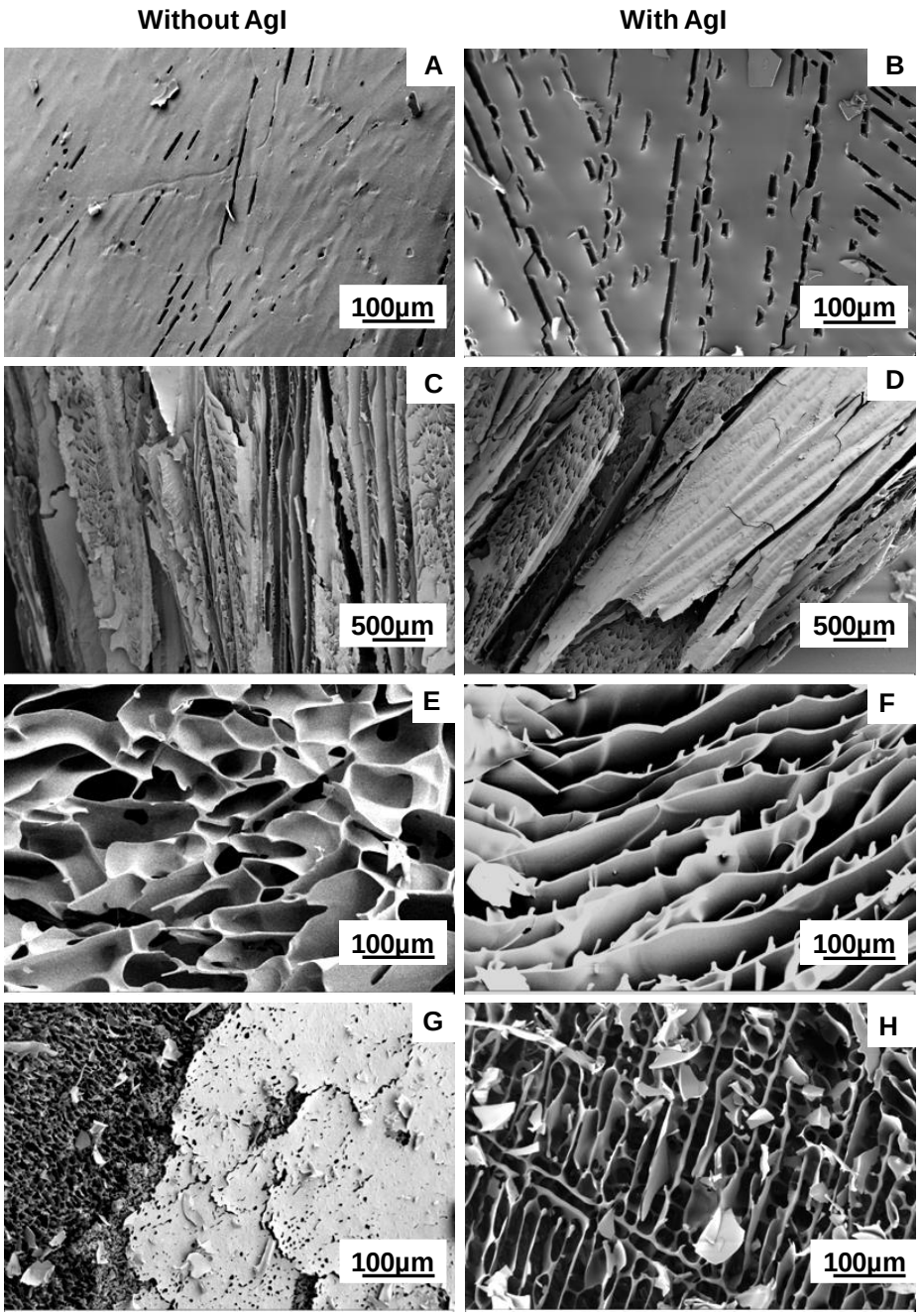

Figure 5.4: FEGSEM images of **10% lactose** frozen at a cooling rate of **1 K.min^{-1}** and freeze dried at -40˚C and 10 Pa without AgI (left) and with AgI (right). **A** & **B.** Surface microstructure without and with AgI. **C** & **D.** Vertical cross-sectional microstructure without and with AgI. **E** & **F.** Cross-sectional internal microstructure without and with AgI, where samples have been collected from the top layer of the samples. **G** & **H.** Cross-sectional internal microstructure without and with AgI, where samples have been collected near the bottom of the vials. Images are representative of at least five repeat runs.

The smooth layer at the bottom of the sample seen in Fig. 5.4 G was visible only in sample without AgI and not in samples containing AgI. The debris seen in Fig. 5.4 H are the remains of the smooth layer at the bottom of the samples with AgI because

AgI containing samples were found to be more fragile in comparison to samples without AgI due to increased porous nature of the sample (due to higher nucleation point and more ice crystals).

Table 5.1 Freeze drying times obtained for 10% lactose with and without AgI for the different cooling rates experimentally from freeze dryer (1 K.min^{-1} and LN_2 quenching) and estimated from freeze drying microscopy (2 K.min^{-1}, 10 K.min^{-1} and 50 K.min^{-1}). Values are average of at least five repeat runs for experimental time and four repeat runs for estimated time with standard deviation as error in each case.

Freeze drying time			Sample depth (mm) / Cooling rate (K.min^{-1})	3	7	11
Experimental (hrs)	Without AgI		1	11.5±2.9	24.5±2.9	44.1±6.6
			LN_2 quenching	22.7±2.0	50.7±2.8	76.1±2.1
	With AgI		1	9.8±1.1	17.4±3.3	27.2±6.7
			LN_2 quenching	19.0±0.7	39.5±5.4	59.7±8.4
Estimated (hrs)	Without AgI		2	8.1±3.9	29.5±9.5	52.9±9.4
			10	6.5±1.5	33.7±7.3	68.5±17.4
			50	5.2±1.0	20.5±5.0	59.2±11.8
	With AgI	Parallel orientation	2	4.1±1.0	15.2±4.1	32.9±9.4
			10	3.2±0.9	13.2±4.1	29.7±9.6
			50	3.0±0.6	14.6±2.7	34.8±6.2
		Perpendicular orientation	2	10.3±2.9	43.7±14.8	99.8±35.9
			10	11.8±2.1	54.2±10.5	127.2±25.1
			50	5.3±1.4	26.4±7.2	63.5±17.4

Times taken for sublimation fronts to reach 3 mm, 7 mm and 11 mm depth are shown in Fig 5.5 A, and in Table 5.1. Data are also shown for annealed data which will be discussed in the next subsection, but it is clear that AgI samples (filled symbols) dry faster than the corresponding non-AgI samples. This reflects the more open structures seen on the SEMs.

The freeze-dryer primary drying times in Fig 5.5 A are calculated from the actual freeze drying temperature vs time plots (as shown in Figs. 5.1 & 5.2), while Fig 5.5 B shows drying times estimated from the *a* & *b* values (apparent edge resistance and resistance of dried layer) determined from the freeze drying microscope frontal distance vs time data.

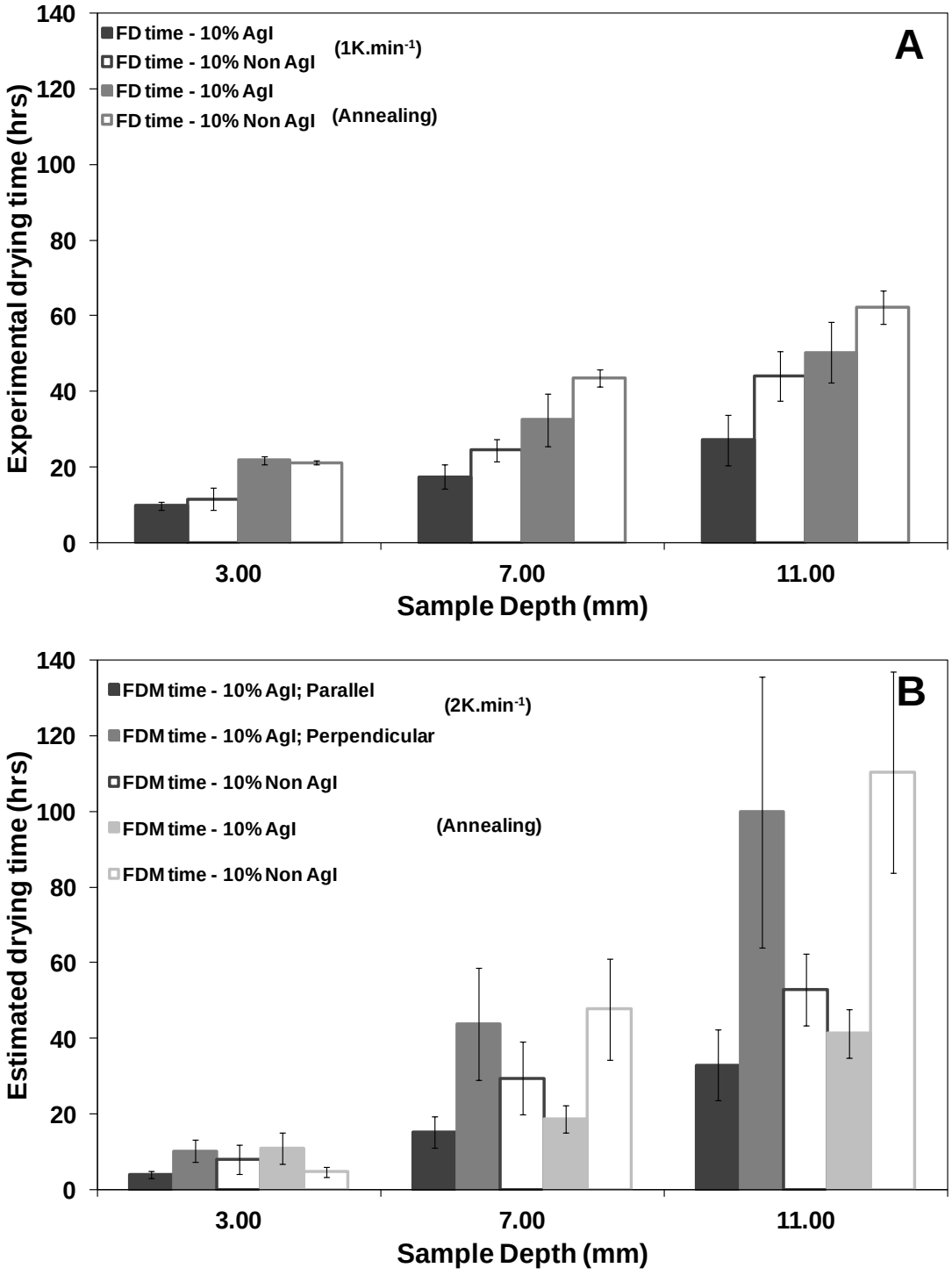

Figure 5.5: A. Experimental vial drying times at -40˚C and 10 Pa obtained for **10% lactose** that had either been slow cooled at a rate of **1 K.min^{-1}** or subjected to an additional **annealing step**, either with or without AgI **B.** Drying times for the same distances estimated from *a* and *b* values from equivalent FDM data at -40˚C at 1 Pa **for 10% lactose** samples (with or without AgI) frozen previously either at a cooling rate of 2 K.min^{-1}, or via an annealing profile at -10˚C and then frozen at a cooling rate of **1 K.min^{-1}**. Values are average of at least five repeat runs for experimental time and four repeat runs for estimated time with standard deviation as error in each case.

Comparison of these times indicate that apart from estimated drying times of 10% lactose with AgI (with perpendicular ice crystal orientation) especially at 11 mm sample depth, all other drying times were quite close to each other at all sample depths– estimated and experimental. This difference was attributed to the difference in ice-crystal orientation in vial (which is parallel to sublimation front due to directional solidification) in comparison with 10% lactose with perpendicular orientation to the sublimation front. The relative closeness of the parallel data matches the SEM observation that the main crystal orientations within the samples were vertical, which is parallel to the direction of mass transfer.

Annealing: Annealing is the process of cooling a sample to initially freeze it, then heating (and holding at that temperature) and followed by re-cooling of the sample. This method is generally employed to overcome the variation in nucleation temperature between samples which results in different ice crystal morphologies and thus, different primary drying rates.

Table 5.2 Freeze drying times obtained experimentally and from freeze drying microscopy for 10% lactose with and without lactose for annealing profiles studied. Values are average of at least five repeat runs for experimental time and four repeat runs for estimated time with standard deviation as error in each case.

Freeze drying time	Cooling profile / Sample depth (mm)		3	7	11
Experimental (hrs)	Annealing (at -10˚C)	Without AgI	21.2±0.5	43.5±2.2	62.2±4.5
		With AgI	21.8±1.2	32.5±7.0	50.3±8.0
Estimated (hrs)	Annealing (Profile IV on FDM)	Without AgI	4.7±1.3	47.7±13.3	110.3±26.6
		With AgI	10.1±4.1	18.6±3.6	41.3±6.4

It can be seen in Fig 5.5 A and Table 5.1 & 5.2 that annealed samples take longer to dry than non-annealed samples, both for AgI and non-AgI samples. This seems counter-intuitive as annealing is often used as a methodology to improve freeze drying rates.

Fig. 5.6 shows the FEGSEM images of 10% lactose without and with AgI annealed at -10˚C in vials. Figs. 5.6 A & 5.6 B show the surfaces of the annealed samples with and without AgI. This surface microstructure is quite similar to the surface morphology of freeze-dried PVP subjected to annealing at -10˚C presented in literature by Abdelwahed *et al.,* (2006b).

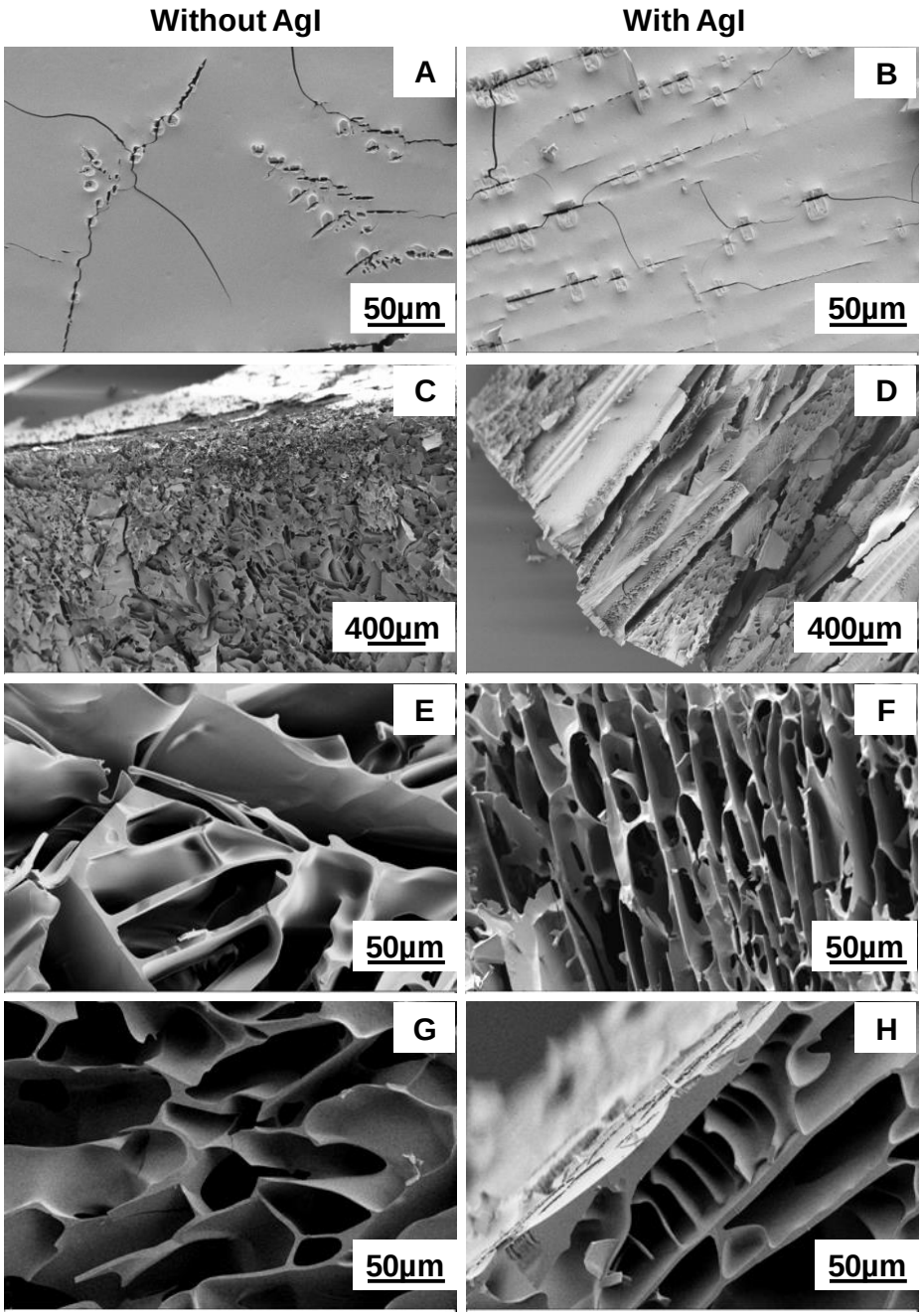

Figure 5.6: FEGSEM images of **10% lactose** frozen at a cooling rate of 1 K.min^{-1}**, annealed at -10˚C** and again cooled at 1 K.min^{-1} and freeze dried at -40˚C and 10 Pa without AgI (left) and with AgI (right). **A** & **B.** Surface microstructure. **C** & **D.** Vertical cross-sectional microstructure. **E** & **F.** Cross-sectional internal microstructure where samples have been collected from the top layer of the samples. **G** & **H.** Cross-sectional internal microstructure where samples have been collected from the bottom layer of the samples. Images are representative of at least five repeat runs.

The samples without annealing seem to have much more porous surface layer (larger pores or cracks in Fig. 5.4 A & 5.4 B). This difference could be because the surface layer becomes thicker with the longer duration of freezing process in an annealing

experiment in comparison to the other cooling rate causing the surface to be much more intact and difficult for the ice crystal below to forge their way through to the top. The rate of increase of thickness has also been discussed in the case of freeze-dried PVP, with thicker surface layer observed for samples annealed at -10˚C. However, the thickness of the surface layer does not seem to affect the sublimation rate of PVP as faster sublimation was observed for samples annealed at -10˚C than other annealing profiles (Abdelwahed *et al.,* 2006b). Figs. 5.6 C & 5.6 D show the vertical cross-sections of annealed sample without and with AgI after freeze drying and Figs. 5.6 E-F and 5.6 G-H show the internal microstructure of the annealed samples without and with AgI at the top and bottom of the vial respectively. Both the vertical cross section and internal microstructure seem quite different when compared between AgI and non-AgI samples. The use of AgI seems to affect the ice crystal re-formation and hence the morphology is more directional in AgI containing samples while being completely random in non-AgI samples. The size of the ice crystal voids is also smaller in comparison to Figs. 5.4 E-F but larger than ice crystal voids of Figs. 5.4 G-H. Also, the comparison between the microstructure of the top and bottom of the vial shows that the ice crystal sizes to be quite similar throughout the vial (in both AgI & non-AgI samples). This indicates that annealed samples do not show the effects of directional solidification as was the case in slow cooling rate samples. The ice crystal voids seem randomly formed thus showing to the fact that during annealing, the ice crystals are reformed from previously melted ice crystals. This could be another contributing factor to the longer duration of primary drying seen in Fig. 5.5 A.

Liquid nitrogen quenching: Apart from slow cooling rate and annealing, the effect of a fast cooling rate on the ice crystal morphology and hence on the primary drying behaviour was also investigated. To achieve this, the 10% lactose solution containing vials were subjected to liquid nitrogen quenching (dipping the vials into liquid nitrogen).

Fig. 5.7 shows the FEGSEM images of 10% lactose with and without AgI frozen by liquid nitrogen quenching and freeze dried on a pre-cooled shelf at -40˚C and 10 Pa pressure. Figs. 5.7 A & 5.7 B show the surface morphology of the samples without and with AgI after freeze drying.

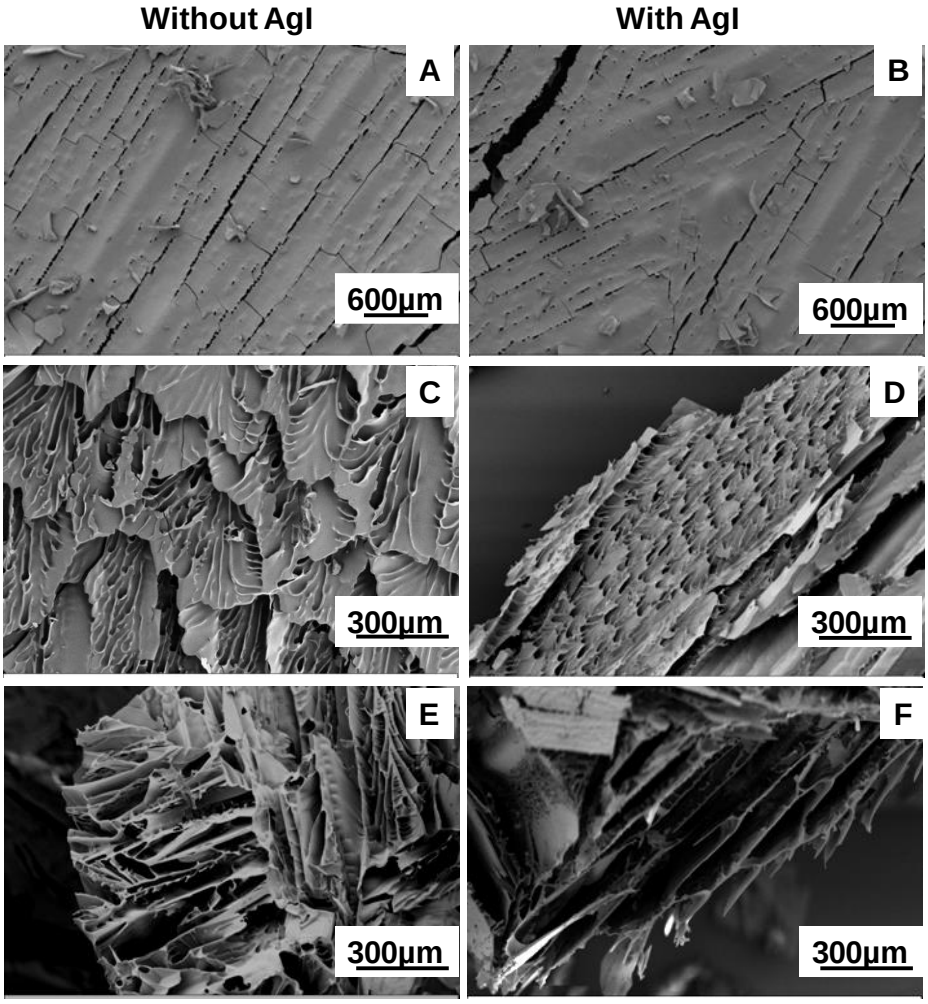

Figure 5.7: FEGSEM images of **10% lactose** frozen at a fast cooling rate by **liquid nitrogen quenching** and freeze dried at -40˚C and 10 Pa without AgI (left) and with AgI (right). **A** & **B.** Surface microstructure. **C** & **D.** Vertical cross-sectional microstructure. **E** & **F.** Cross-sectional internal microstructure where samples have been collected from the top layer of the samples. Images are representative of at least five repeat runs.

The bigger cracks seen in the AgI containing samples are due to the preparation process for performing FEGSEM and not due to the freeze-drying process (as these were not visible to the normal eye after freeze-drying was completed but were visibl when the samples were cut for preparation of sample for SEM). In comparison to the other cooling rates the surface morphology of this set of samples is quite different and seems to be quite fragile, although the pores or cracks on the surface are not as large as Fig. 5.4 A & 5.4 B (1 $K.min^{-1}$ cooling rate).

Figs. 5.7 C & 5.7 D display the vertical cross-section, while Figs. 5.7 E & 5.7 F show the internal microstructure of the samples frozen with liquid nitrogen without and with

AgI. The microstructure of vertical cross-section shows differences between samples without and with AgI, however, the internal ice crystal void morphology is quite similar between the two samples. This internal microstructure is same throughout the vial and the size of these voids was found to be much smaller than the ice crystal sizes of the other slower cooling rates. The use of AgI did not seem to affect the freezing process in this case as the crystals seem randomly formed since the cooling rate was too fast and from all sides of the vial instead of just at the bottom of the vial (as in other cases studied). Similarly, due to the use of liquid nitrogen for freezing the samples from all sides of the vial (obviously except top), there is less pronounced directional solidification and thus the crystals do not have the opportunity to grow into bigger crystals towards the top and hence are random and of almost similar sizes throughout the sample (from top to the bottom).

In terms of internal microstructure, though, AgI containing samples do not seem different from samples without AgI, however, when comparing the primary drying times (see Fig. 5.8), it shows that the latter is slower than the former. It is difficult to pin point the exact reason for this behaviour. The plot in Fig. 5.8 A also shows that in both cases the drying times are slightly higher than the range (20-80 hrs) when compared to Fig. 5.5 A for the other slow cooling rates in all the sample depths investigated. This is an expected trend as the ice crystal void sizes are smaller than those seen in other cooling rates.

Apart from comparison with drying times of other cooling rates, Figs. 5.8 A & 5.8 B also compare the primary drying times determined from the freeze dryer data and the drying times obtained from extrapolating from *a* and *b* values obtained from the freeze drying microscopy data for the cooling rates – 10 $K.min^{-1}$ and 50 $K.min^{-1}$. A 10 $K.min^{-1}$ cooling rate showed lower primary drying times as it allows the crystals grow in size in comparison to 50 $K.min^{-1}$ rate and liquid nitrogen quenching, resulting in faster water vapour removal. The drying times of 10 $K.min^{-1}$ cooling rate samples are faster than those obtained from the freeze dryer for faster cooling rate but the times obtained from 50 $K.min^{-1}$ (especially perpendicular orientation & Non-AgI samples) are quite close to those from the freeze dryer.

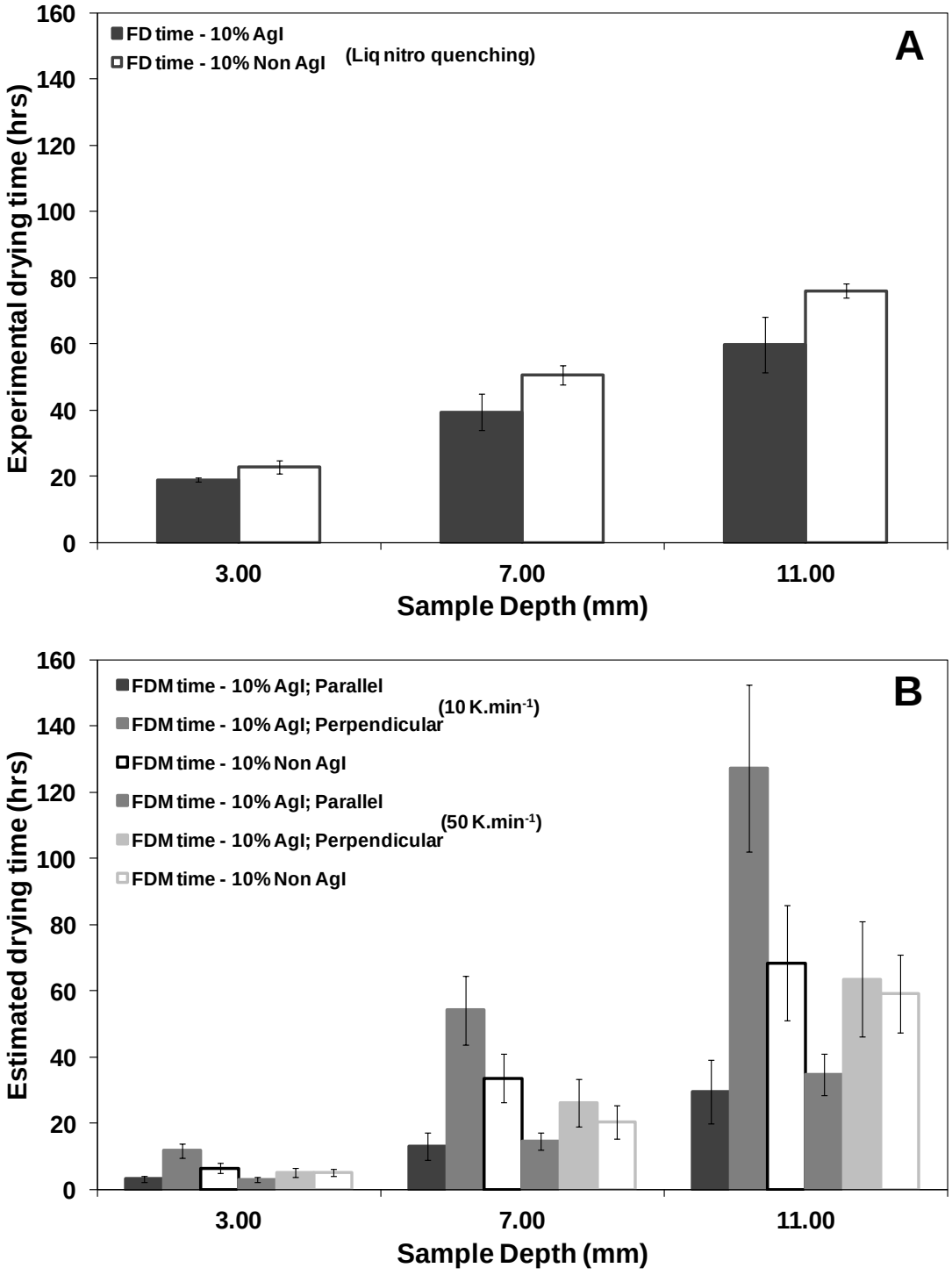

Figure 5.8: A. Experimental vial drying times at -40˚C and 10 Pa obtained for **10% lactose** that had previously been frozen using **liquid nitrogen quenching** of vials, either with or without AgI **B.** Drying times for the same distances estimated from *a* and *b* values from equivalent FDM data at -40˚C at 1 Pa for **10% lactose** samples (with or without AgI) that had been previously frozen either at a cooling rate of **10 K.min^{-1}**, or **50 K.min^{-1}**. Values are average of at least five repeat runs for experimental time and four repeat runs for estimated time with standard deviation as error in each case.

This behaviour could be due to the freezing of the samples from sides of the vial when dipped in liquid nitrogen, resulting in ice crystal structure similar to perpendicular orientation (with respect to direction of sublimation front), though it could not be confirmed from the FEGSEM images of the microstructure (Fig. 5.7 E & 5.7 F).

5.3.3 Effect of freezing profiles (40% lactose samples)

Slow cooling: In case of 40% lactose solution frozen in vials at 1 K.min^{-1} and freeze-dried at -40˚C and 10 Pa, it was observed from Fig. 5.9 A & 5.9 B, lactose crystals were seen instead of a uniform ice crystal void lattice in the SEM microstructure.

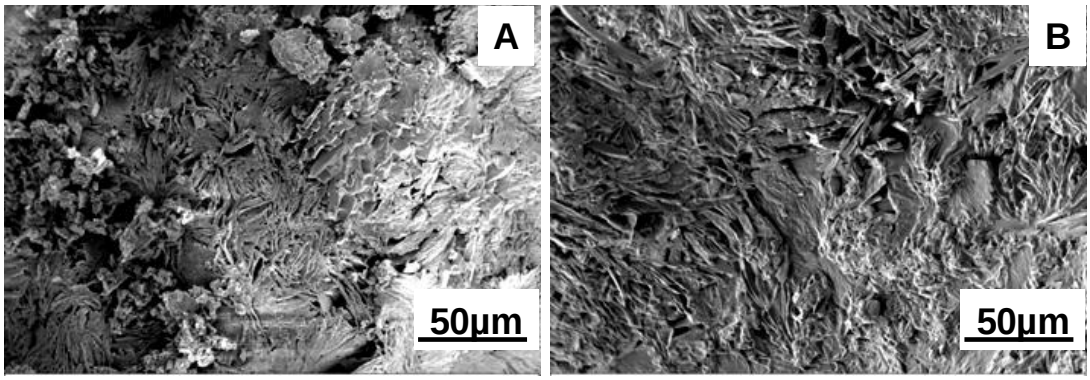

Figure 5.9: Cross-sectional internal microstructure images of **40% lactose** frozen at a cooling rate of **1 K.min^{-1}** and freeze dried at -40˚C and 10 Pa. **A.** Without AgI. **B.** With AgI. The samples have been collected from the top layer of the samples after annealing and freeze-drying. Images are representative of at least four repeat runs.

This behaviour was seen for both samples with AgI and without AgI. It is evident that due to the high concentration, slow cooling rate and the hold period before start of the sublimation process, lactose crystals crystallized out of the supersaturated solution. This was confirmed to be crystallized lactose from results published in literature on crystallization of lactose by Islam & Langrish, (2015). The percentage crystallinity of lactose was not determined in this case although the ratio of crystalline to amorphous lactose could be easily determined using DSC, DVS or XRD as has been described in literature (Roos & Karel, 1992; Kedward *et al.,* 1998; Kedward *et al.,* 2000 and Vollenbroek *et al.,* 2010).

Annealing: This crystallization of lactose from solution was also observed in vials with 40% lactose solution which were subjected to the process of annealing. As before, this involved cooling the vials at 1 K.min^{-1} to -40˚C and heating of the samples to -10˚C

followed by a hold period of 2 hrs and cooling again at 1 K.min^{-1} to -40˚C before commencing sublimation.

Due to the long duration of this process at a low temperature, lactose was again found to crystallize out of solution (see Fig. 5.10 A & 5.10 B) for both AgI and non-AgI solutions and similar to the previous cooling rate investigated (1 K.min^{-1}) as seen in Fig. 5.9. In the current case, the crystals were seen to be larger in size and significantly more prominent as annealing also appeared to occur with the lactose crystals (i.e. dissolution of smaller crystals and growth of those remaining), as a result of the temperature profile used.

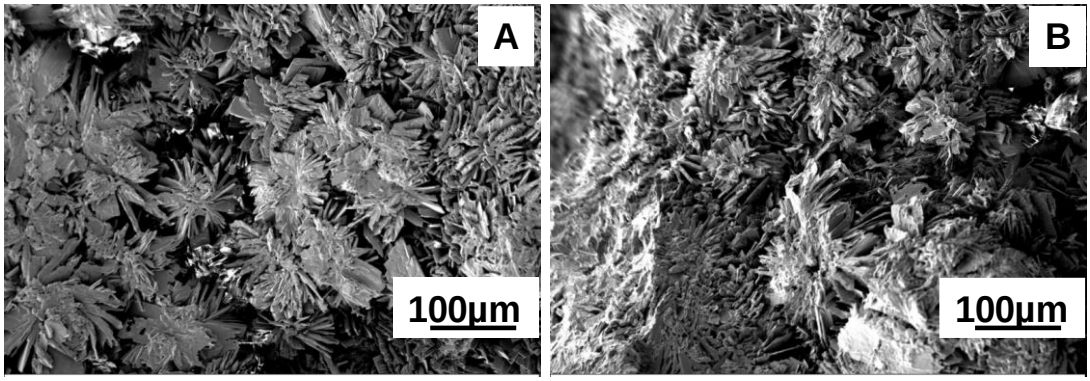

Figure 5.10: Cross-sectional internal microstructure images of **40% lactose** frozen at a cooling rate of 1 K.min^{-1} and **annealed at -10˚C** and again cooled at 1 K.min^{-1} and freeze dried at -40˚C and 10 Pa. **A.** Without AgI. **B.** With AgI. The samples have been collected from the top layer of the samples after annealing and freeze-drying. Images are representative of at least four repeat runs.

Liquid nitrogen quenching: To further probe this issue of lactose crystallization and also to investigate the effect of a fast cooling rate, 40% lactose solutions (with and without AgI) in vials were subjected to liquid nitrogen quenching by dipping the vials in a container of liquid nitrogen. The samples were then transferred to a pre-cooled freeze dryer shelf (at -40˚C) and subjected to sublimation at 10 Pa vacuum pressure. Fig. 5.11 shows the FEGSEM images of lactose (with and without AgI) frozen by liquid nitrogen quenching and freeze dried in vials. Fig. 5.11 A & 5.11 B shows the surface of 40% lactose (initial concentration) without and with AgI – frozen at fast cooling rate, freeze dried at 10 Pa. The surface of the AgI containing sample is quite porous in comparison to the sample without AgI which seems to be a dense layer at the surface and lacks the pores or cracks clearly visible in Fig. 5.11 B.

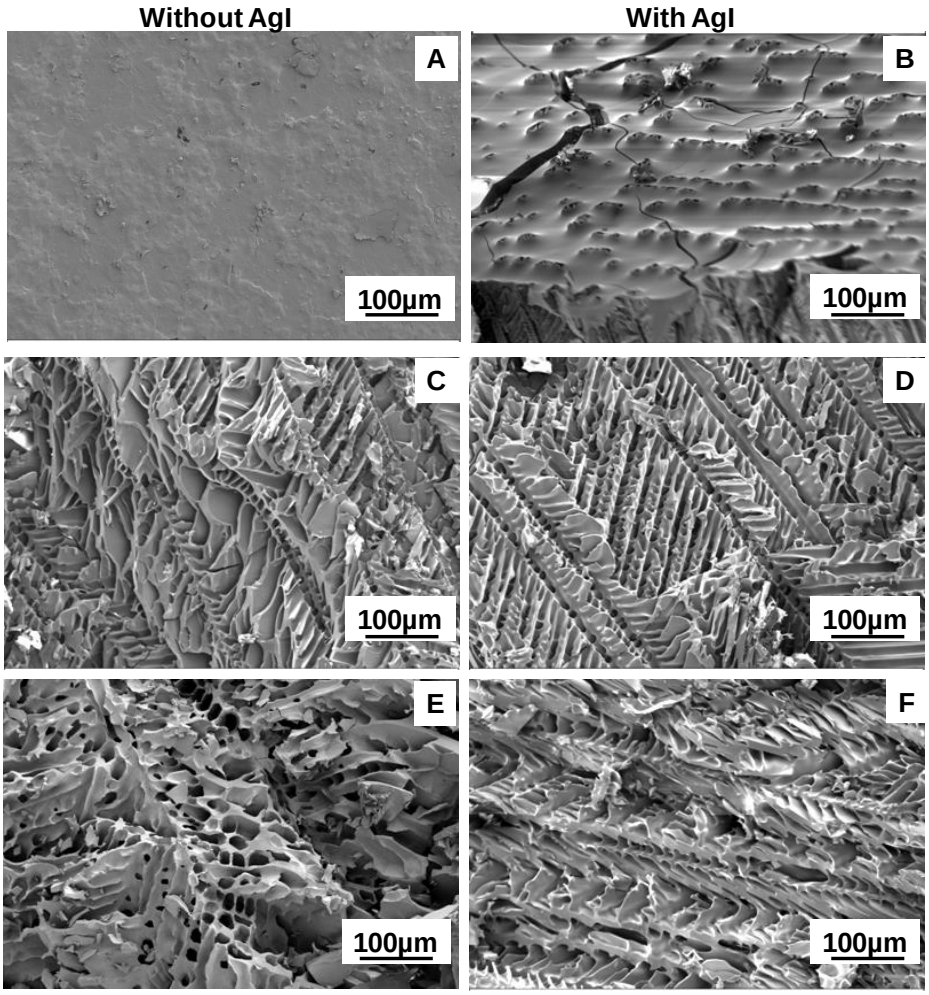

Figure 5.11: FEGSEM images of **40% lactose** frozen at a fast cooling rate by **liquid nitrogen quenching** and freeze dried at -40˚C and 10 Pa without AgI (left) and with AgI (right). **A** & **B.** Surface microstructure. **C** & **D.** Vertical cross-sectional microstructure. **E** & **F.** Cross-sectional internal microstructure where samples have been collected from the top layer of the samples. Images are representative of at least five repeat runs.

The vertical cross section and the internal microstructure of the samples without and with AgI are shown in Fig. 5.11 C-F. The most noticeable feature is that no significant lactose crystallisation appears to have occurred, presumably due to the much faster cooling rate, which has enabled the sample to reach the glassy state before lactose crystals were able to nucleate. When this microstructure is compared to that of 10% lactose (Fig. 5.4, 5.6 & 5.7), it is evident that due to higher initial concentration, the morphology of 40% lactose is denser and has smaller ice crystal voids.

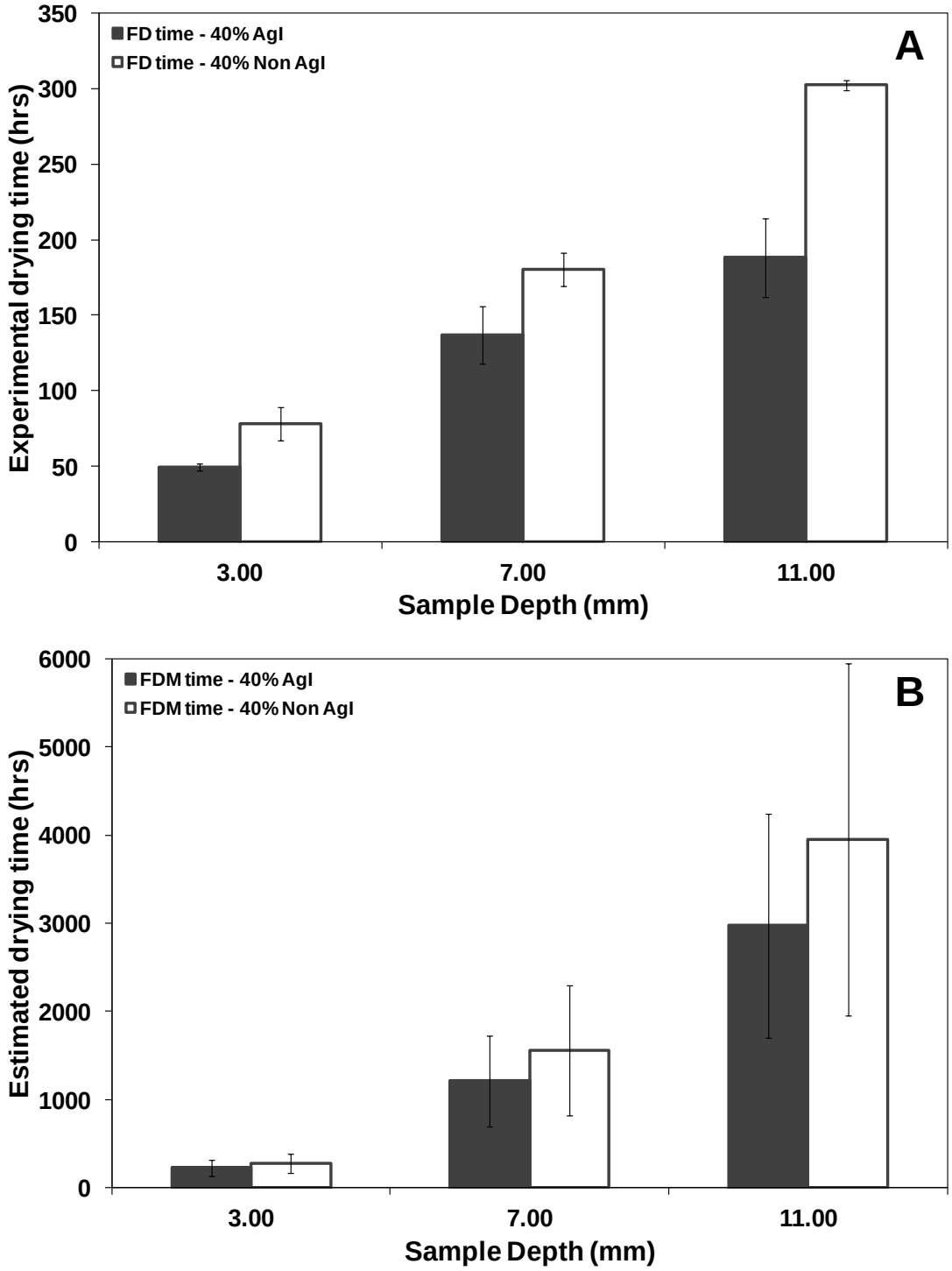

Figure 5.12: A. Experimental vial drying times at -40˚C and 10 Pa obtained for **40% lactose** that had been slow cooled at a rate of **1 K.min^{-1}**, either with or without AgI **B.** Drying times for the same distances estimated from *a* and *b* values from equivalent FDM data at -40˚C at 1 Pa for **40% lactose** samples (with or without AgI) frozen previously either at a cooling rate of **2 K.min^{-1}.** Values are average of at least five repeat runs for experimental time and four repeat runs for estimated time with standard deviation as error in each case.

Samples containing AgI were found to have a more directional ice crystal void lattice while samples freeze dried without AgI were found to have a random morphology throughout the vials. The effect of these microstructural features will be discussed with respect to primary drying times calculated from the freeze dryer.

The primary drying times from the freeze-dryer are shown in Fig. 5.12 A & Table 5.3 for 40% lactose with and without AgI freeze dried after freezing at the slow cooling rate of 1 $K.min^{-1}$. As with 10% lactose samples, it again displays that AgI does affect the microstructure and also the surface morphology of the sample, thereby resulting in lower sublimation durations compared to samples without AgI.

Table 5.3 Freeze drying times obtained for 40% lactose with and without AgI for the different cooling rates experimentally from freeze dryer (1 $K.min^{-1}$ and LN_2 quenching) and estimated from freeze drying microscopy (2 $K.min^{-1}$, 10 $K.min^{-1}$ and 50 $K.min^{-1}$). Values are average of at least five repeat runs for experimental time and four repeat runs for estimated time with standard deviation as error in each case.

Freeze drying time		Sample depth (mm) / Cooling rate ($K.min^{-1}$)	3	7	11
Experimental (hrs)	Without AgI	1	78.1±11.3	180.3±11.2	302.2±3.5
		LN_2 quenching	75.7±9.4	143.9±14.3	201.6±9.5
	With AgI	1	49.4±2.2	137.0±18.9	188.1±25.9
		LN_2 quenching	88.9±20.0	186.9±13.1	216.8±2.6
Estimated (hrs)	Without AgI	2	273.1±105.9	1558.3±736.1	3953.8±200.0
		10	260.8±53.1	1406.9±421.5	3522.2±790.7
		50	245.4±74.3	1394.6±409.0	3322.2±705.8
	With AgI	2	223.4±95.4	1207.2±516.1	2975.1±1272.2
		10	215.3±37.6	1166.0±203.1	2875.0±500.7
		50	205.8±38.5	1118.0±209.0	2759.2±515.8

However, it was observed that there is a significant difference between the actual primary drying times and the estimated ones from FDM (Fig 5.12 B). Initially, it was thought that the drastic difference was due to the crystallization of lactose observed (Fig. 5.9) which results in altering of the initial concentration of solution subjected to freeze drying in vials. This could be the reason for the low primary drying duration in the actual freeze drying times obtained.

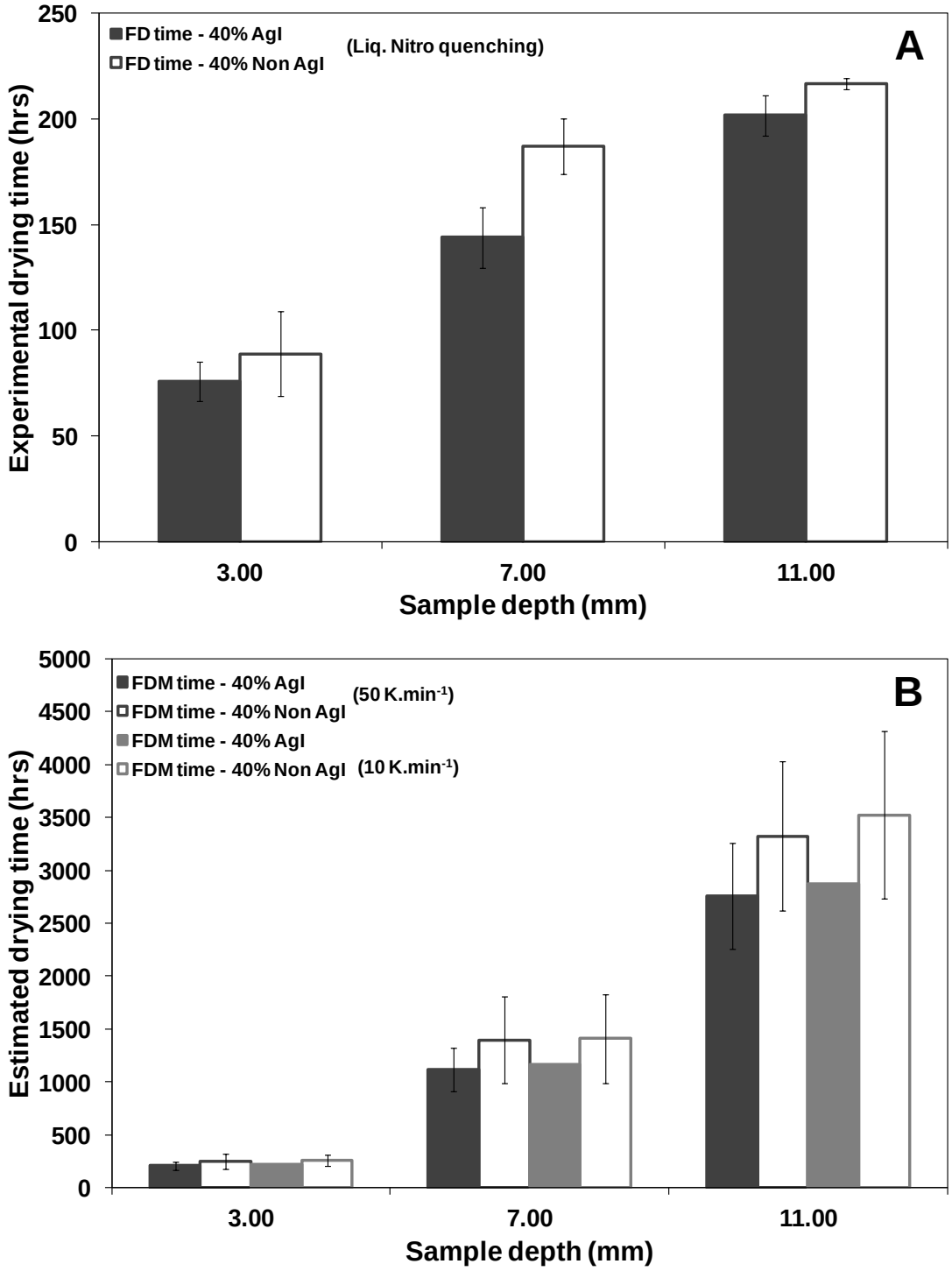

Figure 5.13: A. Experimental vial drying times at -40˚C and 10 Pa obtained for **40% lactose** that had previously been frozen using **liquid nitrogen quenching** of vials, either with or without AgI **B.** Drying times for the same distances estimated from *a* and *b* values from equivalent FDM data at -40˚C at 1 Pa for **40% lactose** samples (with or without AgI) that had been previously frozen either at a cooling rate of **10 K.min^{-1}**, or **50 K.min^{-1}**. Values are average of at least five repeat runs for experimental time and four repeat runs for estimated time with standard deviation as error in each case.

However, when the drying times of 40% lactose freeze dried with and without AgI subjected to a fast cooling rate (by LN_2 quenching), seen in Fig. 5.13 A, 5.13 B & Table 5.3 were compared with that of the slow cooling rate (Fig. 5.12 A), it was observed that even in this case, the experimental and estimated drying times were vastly different. The experimental drying times were found to be much faster than the estimated times. They are still, however, much slower than vial drying of 10% lactose samples, and slow cooling rate samples dry faster when compared to samples frozen with a faster cooling rate. This behaviour was also seen in the case of 10% lactose, and the reason for this behaviour was thought to be due the difference in morphology seen for the two cooling rates – larger crystal voids in slow cooling and smaller crystal voids in fast cooling.

The discrepancy between drying times from vial experiments and FDM predictions is thus presumably due to morphological differences. In FDM no directionality was seen on the microscope images for 40% samples, but directionality was seen on vial drying with liquid nitrogen quenching, so this could explain the faster drying rates (than expected) in the vial. For the slow cooled and annealed samples, some directionality is also likely to have been created but this may have been eclipsed by the lactose crystallisation. It can be seen that crystals do not form a completely solid matrix as there are voids between individual crystals, whereas a glassy matrix is more likely to be a continuous solid. Therefore mass transfer through a crystalline network is likely to be faster.

Apart from comparisons with the drying times estimated using FDM and experimental drying times obtained from the freeze dryer, the experimental data was also analysed based on the cooling profiles investigated – slow, fast cooling and annealing for both 10% & 40% lactose at the three different sample depths -3 mm, 7 mm and 11 mm. Fig. 5.14 shows the drying time comparison of 10% and 40% samples subjected to the different cooling profiles with and without AgI. 40% lactose was subjected to only slow ($1K.min^{-1}$) and fast cooling (LN_2 quenching) profiles and not annealing because of the long duration of annealing profile, i.e., freezing, heating followed by further cooling, prior to primary drying resulted in crystallization of lactose from the highly concentrated solution. AgI containing samples of 10% lactose displayed quicker freeze-drying than samples without AgI for all cooling rates and

sample depths and re-affirmed the results observed in FDM that AgI does result in larger ice crystals thus facilitating quicker water vapour removal. However, in case of 40% lactose, presence of AgI did not result in consistent behaviour with change in cooling rate and sample depth. This was thought to be due to the high solute concentration present in solution, causing difficulty for AgI to act as an effective nucleating agent, as AgI acts a seed for ice crystallization as it has molecular structure similar to that of ice.

When studying the effect of cooling rates – slow, fast cooling and annealing on sublimation duration of 10% lactose at three sample depths, it can be observed from Fig. 5.14 A, 5.14 B & 5.14C, the fast cooling rate displays slower drying at all depths due to smaller ice crystals formed. Slow cooling results in fast drying as ice crystals have enough time to grow in size and thus allow faster water vapour removal. Annealing experiments displayed slower drying (almost two times) than slow cooling rate but faster drying than fast cooling rate. This behaviour was thought to be unusual since annealing is expected to increase the amount of ice crystals present in the sample due to the melting and recrystallization step in the method. However, the main reason for this phenomenon was hypothesized to be due to the thick surface microstructure displayed by annealed sample in comparison to slow cooled samples thus resulting in drying time to be two times slower in initiation and thus carrying over to the rest of the depth of sample.

In the case of 40% lactose, the samples cooled at two different cooling rates did not display any evident difference in sublimation rates (Fig. 5.14 D, 5.14 E & 5.14 F). This behaviour was thought to be due to the high solute concentration resulting in lack of difference in ice of crystal microstructure between the two cooling rates. However, it could also be due to the lactose crystallization that takes place in slow cooling rate as seen Fig. 5.9. However, in case of fast cooling rate, the movement of the sublimation front was found to be similar at deeper depths as ice crystal size was seen to be uniform throughout the sample as there was not much scope for crystals to grow in size (Fig. 5.11).

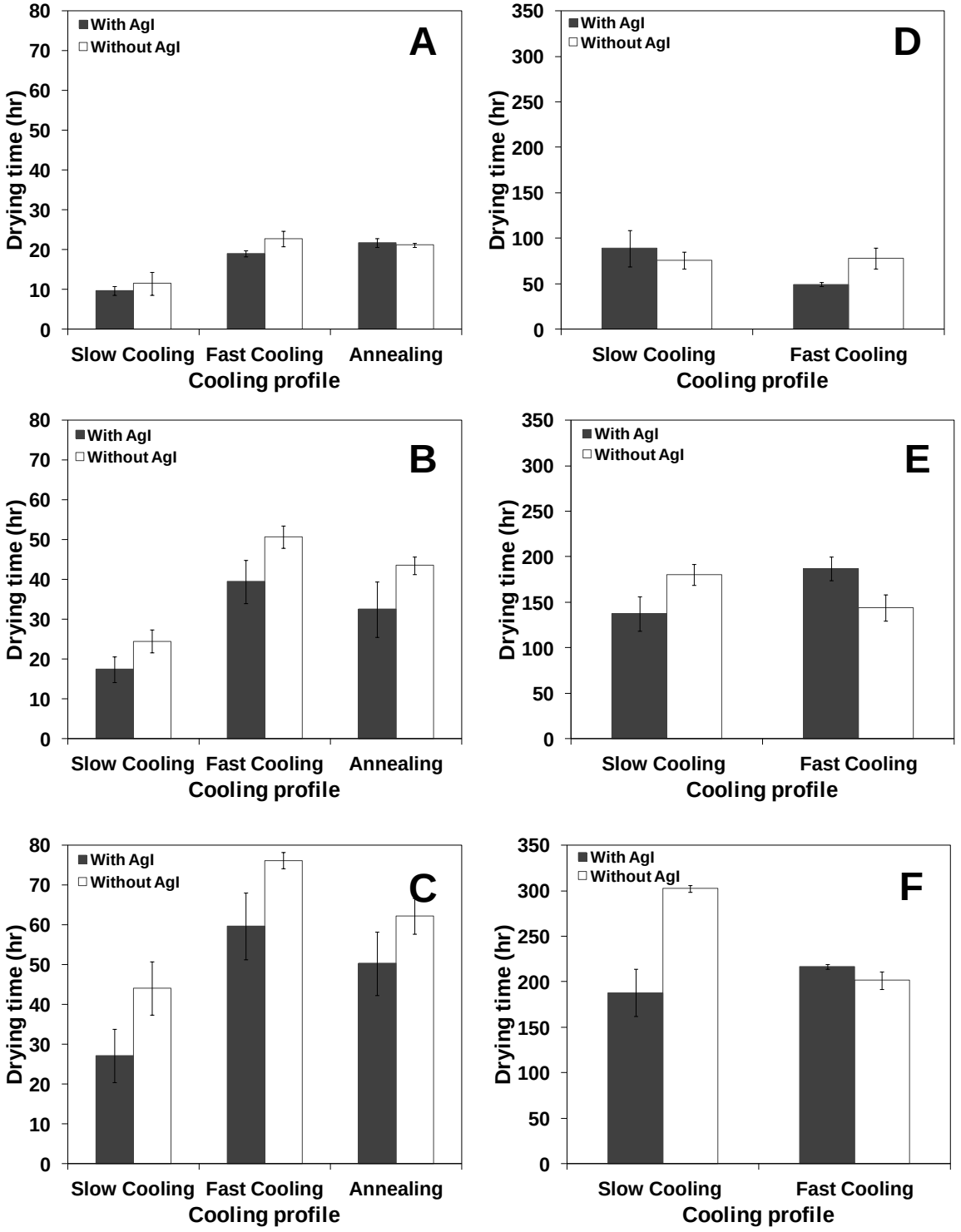

Figure 5.14: Effect of cooling profiles – slow, fast cooling and annealing on the drying times at different depth of the sample. **A. & D.** 3 mm. **B. & E.** 7mm. **C. & F.** 11mm for 10% Lactose and 40% Lactose respectively. Values are average of at least five repeat runs for experimental time and four repeat runs for estimated time with standard deviation as error in each case.

5.4 Conclusions

Freeze drying of lactose with two different solid contents (10% and 40% w/w) was accomplished successfully with and without the presence of AgI. The effect of different cooling rates on the freezing phase and thus on ice crystal morphology was investigated. The ice crystal void microstructure after freeze drying was analysed using scanning electron microscopy and its effect on the primary drying kinetics of lactose was also described in detail in this chapter.

Freeze drying of any sample is governed by two most important phenomena – heat transfer and mass transfer. This chapter focussed mainly on the effect of cooling rates and solid contents on the mass transfer phenomenon in the primary drying phase of the process. Heat transfer does play a role in freeze drying, but as the frontal temperatures are close to -40˚C in all situations (due to the close thermal contact between the front and the shelf through the icy layer and the thermal grease), the saturated vapour pressure at the front will not vary significantly. Sublimation rates are therefore influence predominantly by mass transfer factors.

Glass vials containing lactose solutions for both solid contents and with and without nucleating agent were subjected to three different cooling profiles – slow cooling (1 $K.min^{-1}$), fast cooling (liquid nitrogen quenching) and annealing. The average primary drying times were calculated from a minimum five vials. Good reproducibility was achieved between the temperature measurements of different vials (both with and without AgI) by keeping the vials away from the walls of the freeze drying chamber (to minimise radiation effects).

Cooling rates were found to significantly affect the ice crystal morphology of 10% lactose. In the slow cooling rate investigated, the samples dried in the vial displayed different morphologies within the vial. The samples were found to show signs of directional solidification with freezing from bottom towards the top of the sample. The ice crystal voids were seen to grow from smaller size to larger size towards the top of the sample displaying directional solidification. The ice crystal voids display similar morphology of hexagonal solid concentrated sugar matrix surrounding the void (similar to a honey-comb structure) (Aguilera, 2005 and Reyes *et al.,* 2008). However, the faster cooling rate displayed smaller ice crystal voids throughout the

vial as the crystals could not grow due to the fast cooling rate throughout the sample. The surface layer of the samples also displayed different morphologies with respect to cooling rates. Thicker surfaces were seen in annealed samples while samples with slow and fast cooling showed thinner surface layer. The ice crystal voids were seen to penetrate through the surface layer only in the slow and faster cooling rates except the annealed samples. The trends displayed by ice crystal voids, in these cases, was found to be quite similar to the effect of freezing rate on the microstructure of spray-frozen sucrose (20% w/w) studied by Hindmarsh *et al.,* (2007). The research displayed that plunging droplets into liquid nitrogen resulted in smaller random ice crystals while slow cooling of droplets resulted in nucleation and growth of ice crystals (from centre to outwards) which is a similar behaviour to the directional solidification seen in the current research of vial freeze drying of lactose. In addition the effect of cooling rate on microstructure and in turn, vial freeze-drying behaviour of trehalose, studied by Gieseler, (2004), showed a similarity in microstructure with this current research. It has been observed that the effect of cooling rate on the ice crystal void morphology and surface microstructure was similar in both cases. The surfaces of slow cooled and LN_2 quenched samples were found to show similar features and the surfaces seem to be pierced at the top by the ice crystals growing from beneath the surface. The internal morphology of the LN_2 cooled samples was found to display similar freezing patterns of smaller and random ice crystals. However, slower cooling of trehalose seems to have a more fragile void structure than that of lactose observed in the current study. This research also focuses on freeze drying of sucrose and Bovine Serum Albumin and these materials display similar surface microstructure to that of lactose.

Average primary drying times obtained from the freeze dryer data were compared with the drying times obtained from the extrapolation of *a* and *b* values from FDM (based on mass transfer) for both solid contents and cooling profiles. It was observed that for 10% lactose the predicted and experimental drying times were in quite close agreement over all the cooling rates investigated including the annealing process, when compared with FDM data where the microstructure is aligned parallel to the direction of mass transfer. This fits in with the finding that directional solidification in the vials also produces a microstructure aligned to the direction of mass transfer. However, for the higher solids content (40%) samples, the experimental drying times

were far less than the predicted drying times. In these higher concentration samples, lactose was observed to have crystallised (in SEM images), which may be causing a more porous matrix. However, in liquid nitrogen quenched samples lactose did not crystallise and vial drying times were still shorter than predicted by FDM. It seems likely that the discrepancy is due to directional solidification occurring in the vial samples which did not occur in the FDM experiments. This hypothesis can be confirmed if directional solidification could be achieved in FDM samples either on the FDM stage or outside the set-up and immediately freeze-dried under FDM. The drying times thus estimated could be compared to these experimental drying times. Vial freeze drying times were still shorter for 10% lactose content samples compared to 40% samples, and this is easily explained by the larger resistance that will be presented at the higher solids content.

The main conclusions that were drawn from this research were that ice crystal morphology, cooling rate and solid content play an important role in governing the primary drying phase of the freeze-drying process. Cooling rate results in governing the surface layer and ice crystal morphology which in turn causes faster or slower drying rates. Slower cooling rates and annealing process result in larger ice crystals which increase the rate of water vapour removal from the sample while faster cooling results in comparatively smaller crystals and thus slightly longer durations of drying. However, annealing did not produce the expected increases in sublimation rates, and this is probably due to the fact that the directionality of the microstructure in the direction of mass transfer is partially destroyed by annealing. The addition of AgI was found to reduce sublimation times. The AgI crystals would have settled to the bottom of the vials and acted as nucleation agents from the bottom of the vial. FDM evidence would suggest that they would allow a lower degree of subcooling on ice crystallization that would cause larger crystals which would still grow upwards from the base of the vial and still produce a directional microstructure, even in the case of 40% lactose solutions. AgI cannot be used in pharmaceutical formulations for regulatory reasons, however it does suggest that promoting nucleation at the base of a vial by other means could produce tangible reductions in freeze drying times. Another important conclusion that was drawn from these results was that though FDM did display good predictions of drying times in case of 10% lactose, however, the model needs to be improved in order to incorporate the effect of the larger volume of

sample, larger size and orientation of ice crystals (due to directional solidification). This may lead to an effective use of FDM as a valuable tool to optimise the freeze-drying in a real system.

6

FREEZE DRYING MICROSCOPY OF COFFEE SYSTEM

Freeze drying microscopy was applied to study the effect of various process parameters (initial solids content, presence of silver iodide, freezing rate, annealing steps and drying temperature) on the kinetics of on the freeze drying of a multi-component coffee system. The effects of these parameters on edge resistance and resistance of dried layer were investigated in detail.

6.1 Introduction

Freeze drying is considered a favorable method for drying of coffee as it is one of the few methods which successfully retain various volatile components and aroma compounds present in coffee (Sagara *et al.,* 2005 and Galilea *et al.,* 2008). Coffee has a diverse composition which consists of a variety of components from proteins to oils and insoluble solids which makes its behaviour more complex than a binary system such as lactose/water.

FDM is a potential tool to study the effect of this microstructure on the sublimation kinetics of coffee. The most common use of FDM is to determine the collapse temperature of a product which is to be freeze-dried, but it also allows visualisation of the ice-crystal morphology and hence can be used to study its effect on the process of sublimation (Nail *et al.,* 1994 and Meister *et al.,* 2009).

However, very few researchers have focussed on using FDM to determine frontal velocities or to link it to sublimation rates. Potentially this information could be used to better understand the freeze drying process and improve its efficiency, thereby decreasing its overall cost. Zhai *et al.*, (2003) and Borgognoni *et al.,* (2012) have been among the few researchers who have tried to measure primary drying rates using FDM. While the former research group used freeze-drying microscopy as an exploratory tool to determine coefficient of diffusion of water vapour (D_{eff}) for freeze drying of different types of buffer solutions such as Tris-HCl and citrate, the latter used it to develop a model to predict the estimated primary drying times for freeze-drying bovine pericardium. Borgogononi *et al.,* (2012) also found that chamber pressure did have a significant effect on the drying times with lower pressure resulted in faster drying and higher pressure resulted in slower drying time.

The aim of this study was to use freeze drying microscopy to study the kinetics of freeze drying of coffee solutions at various concentrations. The effects of nucleation temperature, temperature of drying and annealing on sublimation kinetics were also investigated. As aeration prior to freeze-drying is a process commonly used in the coffee industry to enhance the rehydration properties of coffee, it was also decided to study the effects of aeration on the freeze drying kinetics of coffee.

6.2 Materials and methods

6.2.1 Materials

Nescafe coffee (Spray-dried) was purchased from the local supermarket and silver iodide was purchased from Fisher Scientific (Loughborough, UK) as described in Section 3.1.

6.2.2 Moisture content determination

The initial moisture content of the as-received coffee was determined using the hot-air oven drying method as discussed in Section 3.3.2.

6.2.3 Sample preparation

Sample preparation of varying coffee solid contents was carried out as explained in Section 3.4.1.

6.2.4 Freeze drying microscopy

The sample preparation for FDM was carried out as described in Section 3.5.2 and the experimental protocol to be followed was discussed in Section 3.5.4. For sublimation kinetics the following factors were investigated:

- The presence of an ice nucleating agent AgI
- Initial solid content (2-40%)
- Cooling rate during freezing (2, 10, 50 $K.min^{-1}$)
- Freeze drying temperature (-30˚C, -40˚C, -50˚C)
- Annealing (Profile IV – see section 3.5.4)
- Aeration (see section 3.4.2)

Not all combinations of variables were tested. Most experiments were variations on a couple of base cases which had either 10% or 50% solids content, a cooling rate of 10 $K.min^{-1}$, a freeze drying temperature of -40˚C, and with silver iodide present (for reasons that will become apparent). A system pressure of 1 Pa was used for all experiments.

Collapse temperature determination of 2 to 50% coffee solutions were also carried out but only following a single cooling profile of 10 $K.min^{-1}$ and heating profile of 1 $K.min^{-1}$.

Glass transition temperatures of frozen samples were also determined by DSC for comparison (see Section 3.8).

6.2.5 Field Emission Gun Scanning Electron Microscopy

FEGSEM was carried out on the freeze dried samples obtained from FDM as described in Section 3.7.

6.3 Results and discussion

6.3.1 Effect of nucleation temperature

Nucleation temperatures of different solid contents of coffee cooled at 10 $K.min^{-1}$, without AgI and with AgI, are shown in Fig. 6.1 A. These were found to be quite variable, although there was a trend of decreasing nucleation temperature with increasing solids content. This variation is thought to be the reason for the variation in frontal distance vs time plot between repeat runs observed in Fig. 6.1 B. This trend was attributed to the freezing point depression due to increased solid content.

Fig 6.1 B shows the results of frontal analyses made using MATLAB for seven repeat runs freeze drying a 10% coffee solution. It can be seen that these results are also relatively variable similar to those observed in the case of lactose in Fig. 4.1

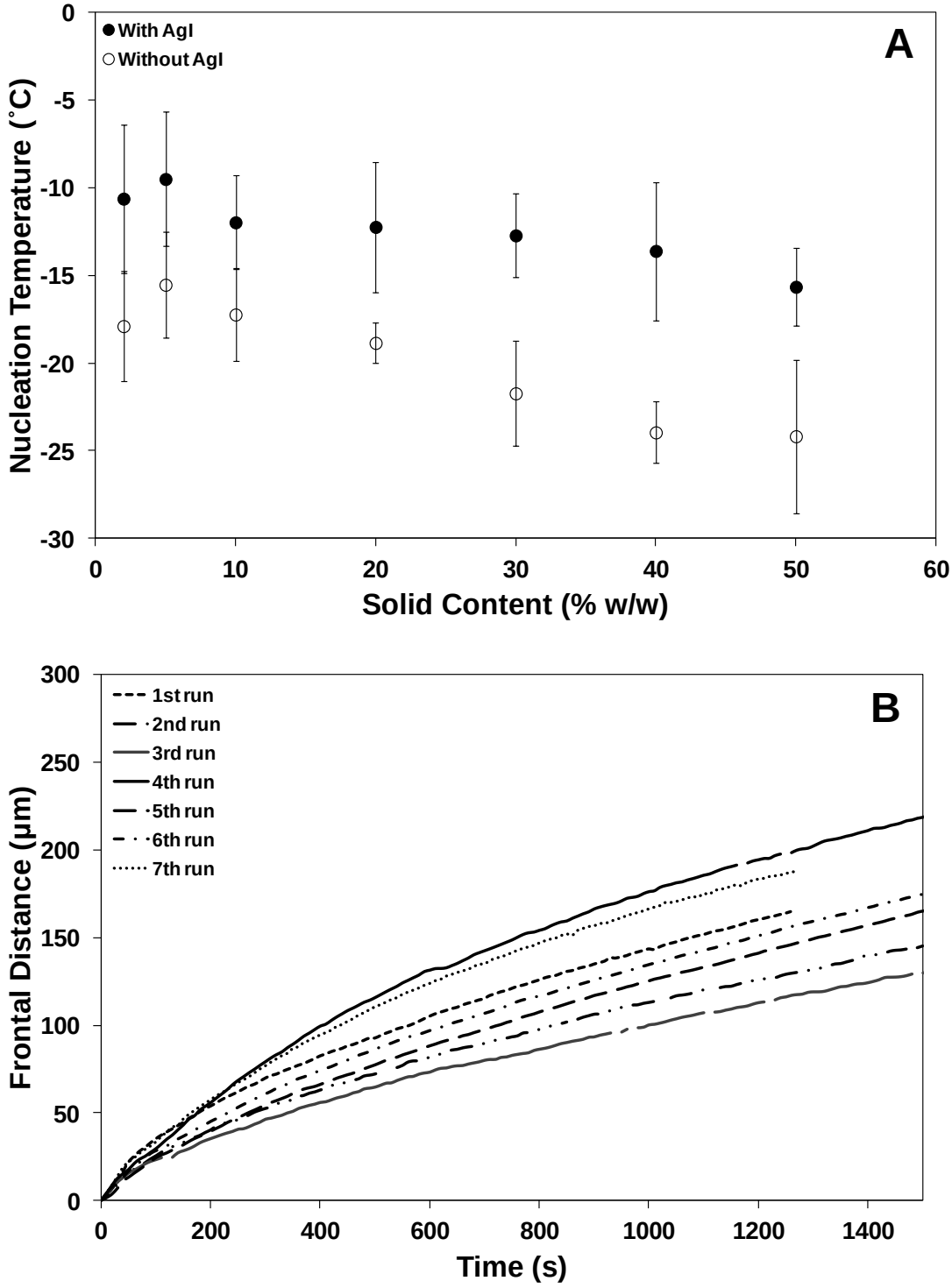

Figure 6.1: A. Nucleation temperature with solid content (2, 5, 10, 20, 30, 40 & 50% w/w) of coffee samples cooled to -40˚C at a rate of 10 K.min^{-1} with and without AgI. Values are average of at least six repeat runs for with standard deviation as error in each case. **B.** Sublimation front movement in 10% coffee solution frozen at -40˚C at a cooling rate of 10 K.min^{-1} and freeze dried at 1 Pa under FDM for seven repeat runs.

In the experiments with lactose in the previous chapter it was found that differences in sample microstructure between runs caused a lack of reproducibility of freeze drying kinetics. This variability in microstructure is caused during the freezing step, and the lack of reproducibility in nucleation temperature indicates that the freezing is an uncontrolled process. This variability in nucleation temperature would likely affect the microstructure of the frozen coffee samples thus in turn influencing the frontal velocity. Higher nucleation temperature may result in lower supercooling causing lesser amount of nucleation followed by growth of large ice crystals while lower nucleation temperature results in higher degree of nucleation with lesser growth. This variation in ice crystal sizes results in variation of sublimation front velocity seen in Fig. 6.1 B.

To overcome the reproducibility problem of nucleation temperatures and frontal progression rates, silver iodide (AgI) was added to the samples before freezing. AgI has been used as an ice nucleating agent with lactose freeze drying experiments, and was able to significantly improve the reproducibility in this system as discussed in Chapter 4.

However, with coffee samples, although the addition of AgI is able to raise nucleation temperatures while freezing compared to non-AgI experiments (Fig. 6.1 A), they are still very variable. Due to coffee being a multi-component material consisting of proteins, oils and insoluble solids, and this could interfere with the way AgI acts as an ice nucleating agent resulting in different temperatures of nucleation.

Fig. 6.2 shows microscope images of frozen 10% coffee samples both without and with AgI. As with lactose samples, the addition of AgI did lead to an increase in the size of the ice crystals but the orientation of the crystals was not consistent throughout the sample. No specific ice crystal orientation patterns were observed as were seen in case of lactose samples. Again, this was thought to be due to the multi-component nature of the coffee samples which could interfere and cause randomness in the way ice crystals were formed during the freezing process.

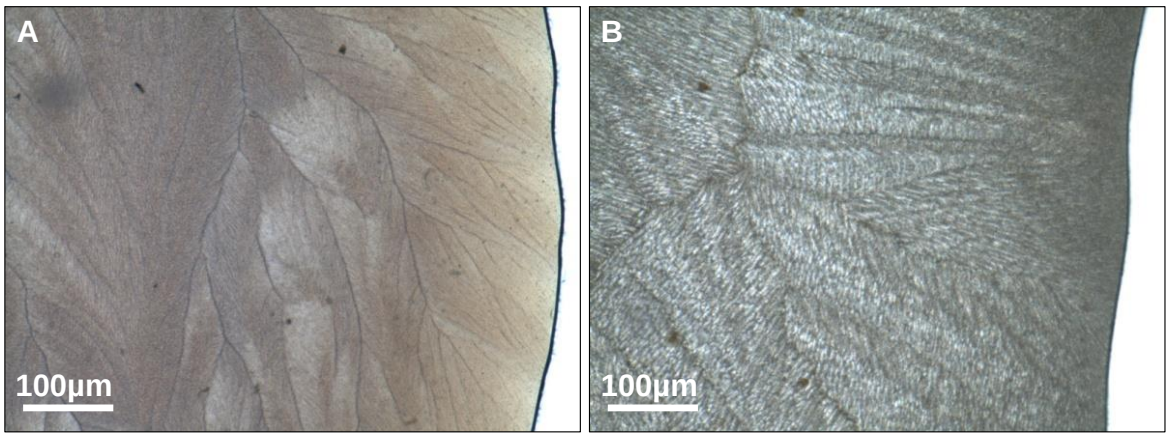

Figure 6.2: A. 10% coffee samples frozen without AgI at a cooling rate of 10 K.min^{-1} to -40˚C under FDM. **B.** 10% coffee samples frozen with AgI at a cooling rate of 10 K.min^{-1} to -40˚C under FDM. Images are representative of at least four repeat runs.

The variation in nucleation temperature also resulted in different sublimation velocities between repeat runs. The frontal distance versus time plot was fitted into the twin-resistance model and the a and b values thus determined were used to calculate the edge resistance, α and resistance of dried layer, β as described in Chapter 3. These results of fitting the frontal movement data to the model are shown plotted against nucleation temperature (from the previous freezing step) for 2% initial solid content of coffee in Fig 6.3.

The α values were not seen to show any trend with respect to nucleation temperature in both with and without AgI experiments, since the edge thickness, and hence edge resistance, was not affected by the nucleation temperature. β values were, however, found to show a significant trend, decreasing with increasing nucleation temperature especially for experiments conducted with AgI. This was presumed to be a result of changes in ice crystal size, with higher nucleation temperatures resulting in larger ice crystals and thus, lower resistance to the transfer of water vapour while lower nucleation temperatures resulting in a higher resistance due to smaller ice crystals. These trends were observed in all the initial solid contents (2 to 50% w/w) investigated.

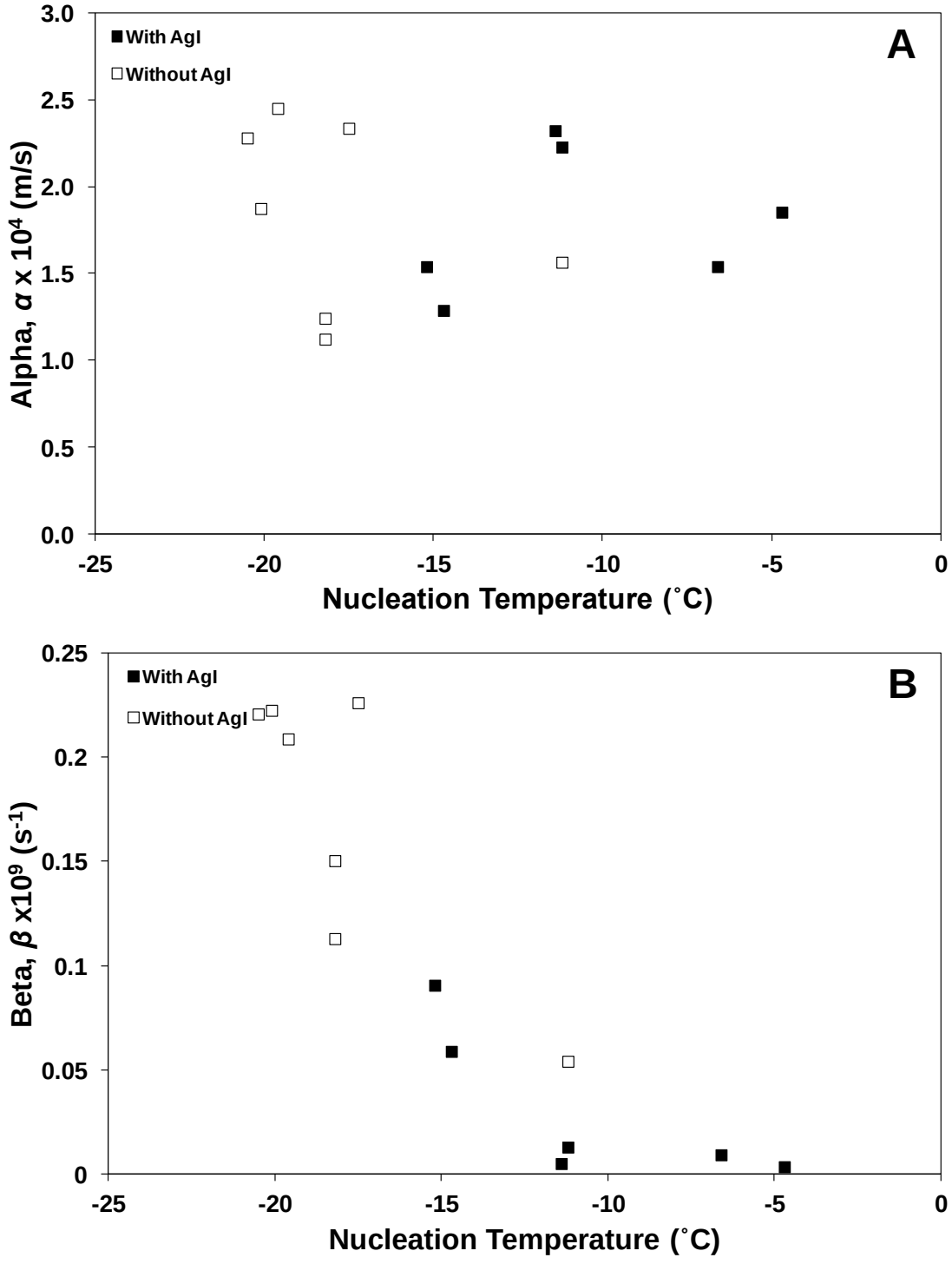

Figure 6.3: A. Fitted edge resistance, α values of 2% coffee solutions cooled at 10 K.min^{-1} to -40˚C and freeze dried at 1 Pa vacuum pressure under FDM plotted against previous nucleation temperature of at least six repeat runs. **B.** Fitted resistance of dried layer, β values of 2% coffee solutions cooled at 10 K.min^{-1} to -40˚C and freeze dried at 1 Pa vacuum pressure under FDM plotted against previous nucleation temperature of at least six repeat runs.

6.3.2 Effect of solid content

The effect of initial solid content of coffee solutions (2, 5, 10, 20, 30, 40 and 50% w/w) on the sublimation rates was also investigated. As microstructure is a key factor in understanding the kinetics of freeze drying, this is considered first.

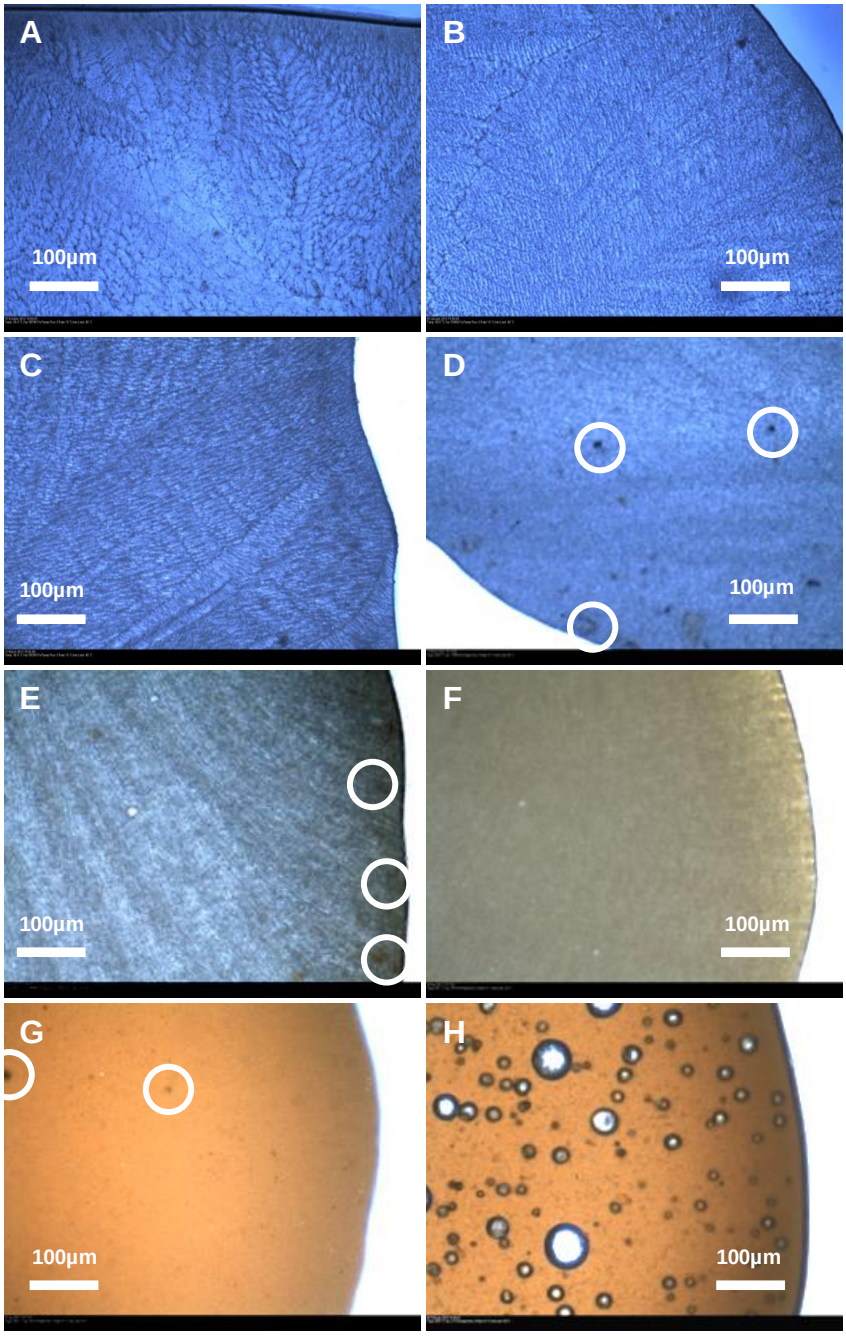

Figure 6.4: Freeze-drying microscope images of coffee (with AgI) frozen at a cooling rate of 10 K.min^{-1} to -40˚C. **A**. 2%. **B.** 5%. **C.** 10%. **D.** 20%. **E.** 30%. **F.** 40%. **G.** 50% and **H.** 50% (aerated). Circles in the figures represent insoluble materials & oils in coffee. Images are representative of atleast four repeat runs.

The microstructures of frozen coffee solutions, with different initial solid contents (containing AgI), under the microscope are displayed in Fig. 6.4. Even with the use of AgI, the ice crystal sizes were found to be small (<10 μm) for lower solid contents namely, 2, 5 and 10% (Figs. 6.4 A-C) while the microstructure was indistinct for higher solid contents (Figs. 6.4 D-F) including aerated coffee samples (Fig. 6.4 H). The images also displayed the presence of insoluble materials (particularly noticeable in higher solid contents) which could be the cause of the variability in nucleation temperatures as they might interfere with the way in which AgI acts as a nucleating agent.

Most of these samples have microstructures too small to be clearly visible under the microscope, as shown in Fig. 6.4, so SEM was used to examine these samples' microstructures. Fig. 6.5 displays field emission gun scanning electron microscope (FEGSEM) images obtained at two different magnifications (1KX and 5KX) from 10% and 50% coffee solutions (w/w), with and without AgI. AgI-containing samples were found to have relatively large size ice crystals while the absence of AgI resulted in much finer crystals in 10% coffee (Figs. 6.5 A-D). This difference in size of ice crystals was also observed in 50% coffee freeze-dried samples (under FDM) although much smaller due to the presence of higher amount of coffee in the sample (Figs. 6.5 E-H). A similar effect was also seen with lactose in Chapter 4. The variation in ice crystal sizes further confirms the effect of initial coffee concentrations on the freezing point depression and, hence on the nucleation temperature resulting in smaller ice crystals as the concentration increases (Figs. 6.4 D-G). The cracks observed in Figs. 6.5 E-G are believed to have been formed during the removal of the upper coverslip before conducting SEM since no cracks were visible in 10% coffee samples (where the coverslip was easily removed) and microscope images of the FDM samples (for both 10 and 50% coffee). However, compared to SEM images of lactose samples shown in Fig. 4.6 (Chapter 4), coffee samples were not seen to show any type of orientation or order of ice crystal morphology even for 10% initial concentration. This reinforces the results discussed in Section 6.3.1, that the addition of AgI did not improve reproducibility of sublimation front velocities, as it did not result in any definite ice crystal orientations in coffee samples due to the multi-component nature of a coffee system.

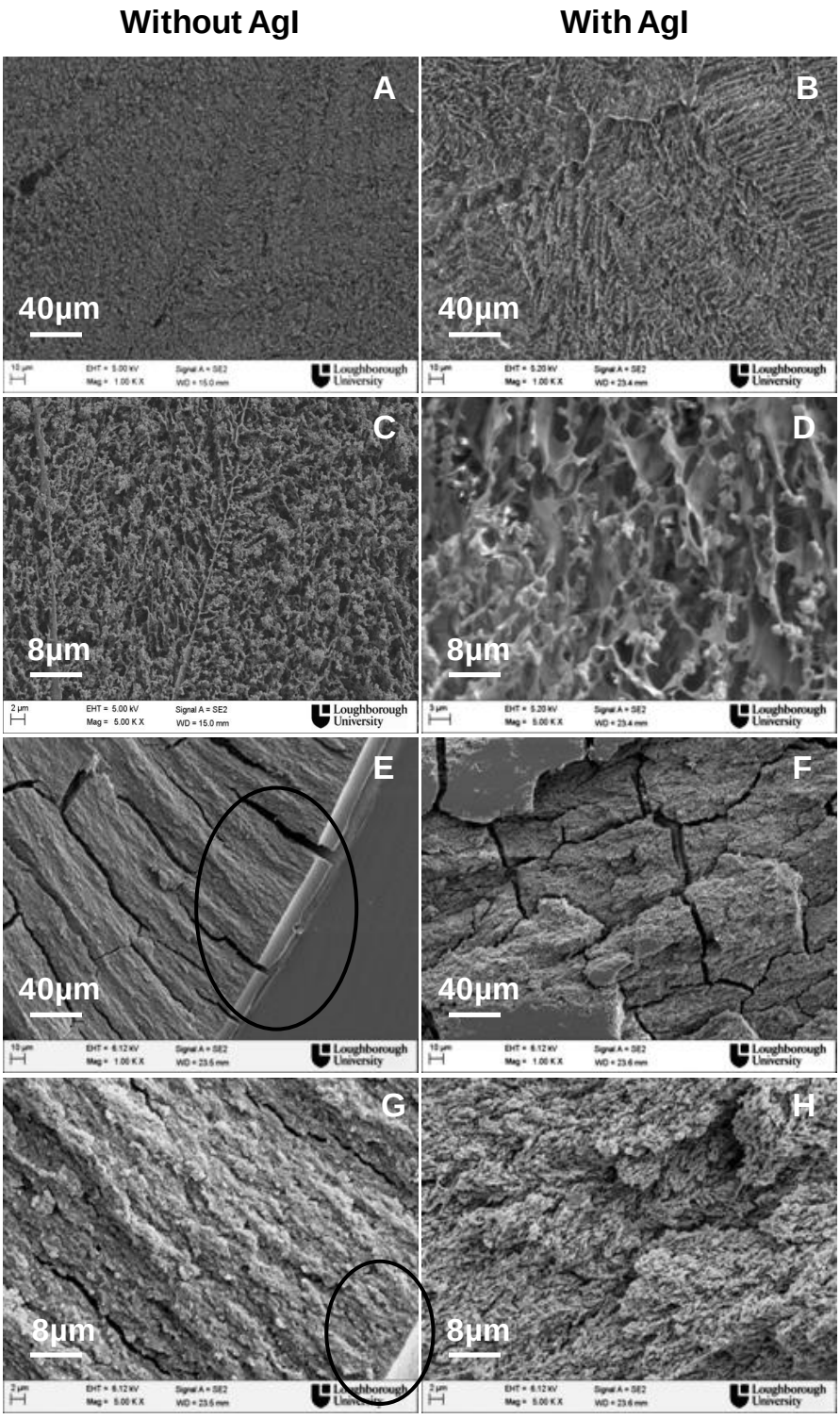

Figure 6.5: Field emission gun scanning electron microscope images of freeze dried (under FDM) coffee with and without AgI frozen at a cooling rate of 10 K.min^{-1} to -40˚C and then freeze-dried at 1Pa vacuum pressure. **A & C. SEM** images 10% coffee freeze dried without AgI (1KX and 5KX magnification). **B & D.** SEM images 10% coffee freeze dried with AgI (1KX and 5KX magnification). **E & G.** SEM images 50% coffee freeze dried without AgI (1KX and 5KX magnification). **F & H.** SEM images 50% coffee freeze dried with AgI (1KX and 5KX magnification). Circles in figures displays the sample edge. Images are representative of at least four repeat runs.

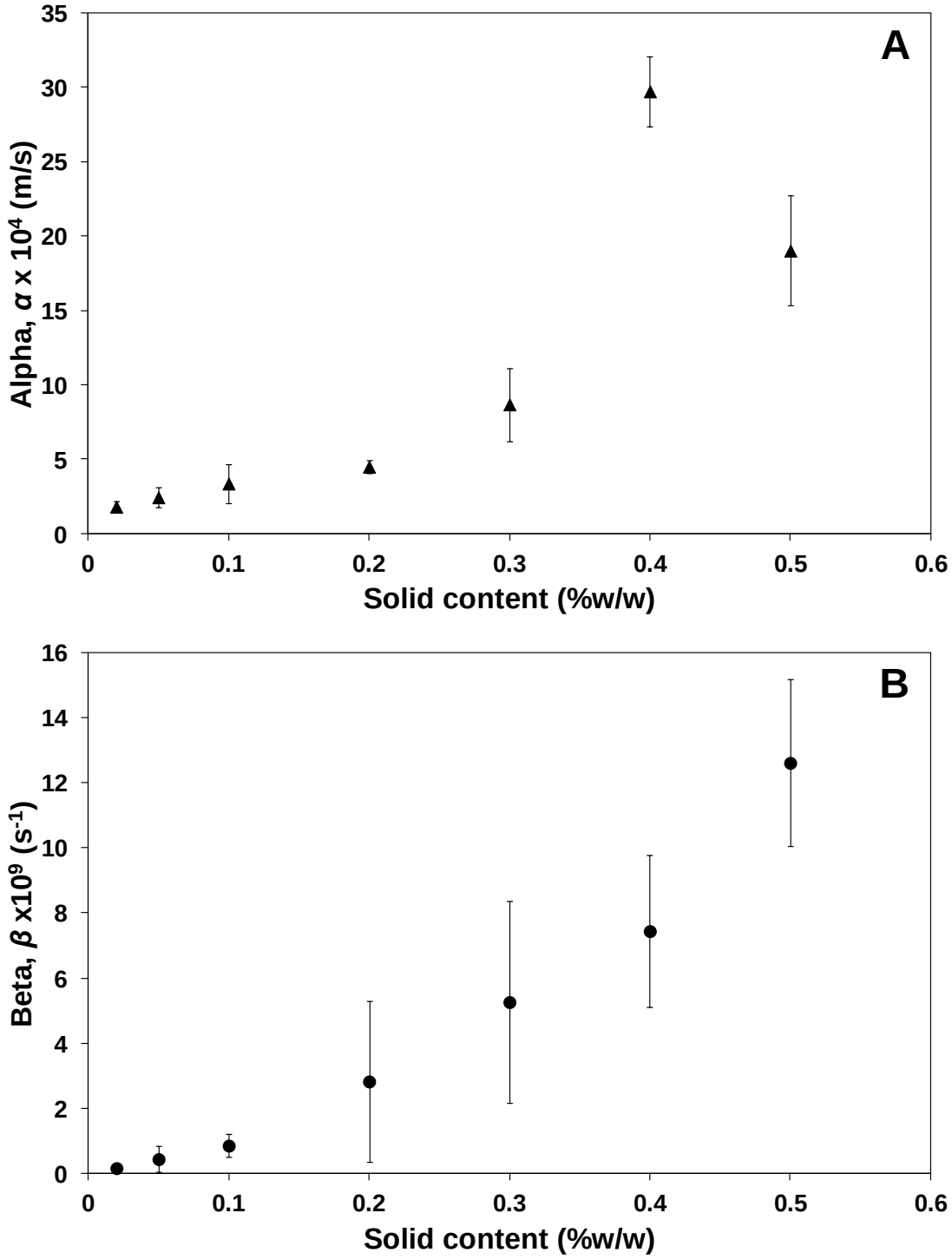

Figure 6.6: A. Effect of initial solid content of coffee (with AgI) on α values, actual edge resistance. **B.** Effect of solid content on β values, resistance of dried layer, cooled to -40˚C at 10 K.min^{-1} and freeze dried at 1 Pa**.** Values are average of at least four repeat runs with standard deviation as error in each case.

Since nucleation temperatures between repeat runs were not reproducible (Fig. 6.1 A), a large number of experiments were performed from which runs were selected

from a particular range (-15±5˚C for all solid contents) of nucleation temperatures. Nucleation temperatures that were outside this range were not used. The experiments thus selected were used to determine *a* and *b* values, which in turn were used to calculate α and β values. The *a* and *b* values were determined by fitting *t* as a function of *x*, (see section 3.5.6) while the calculations for α and β values were performed using the various parameters detailed in Appendix C. Figs. 6.6 A & 6.6 B shows α and β values respectively, thus determined from the experimental runs. α values were seen to increase gradually until a maximum at 40% solid content, but did decrease again at 50%. It was assumed to be due to gradual increase in the thickness of the edge of the sample (as seen in Fig. 6.6 E & 6.6 G). The value was found to decrease for 50% coffee and this could be due to the presence of cracks in the edge of the sample as is apparent from the figure.

However, β values are observed to increase continuously with increasing solid content. This increase of β was clearly due to the increasing quantity of solids in the dry region that water needs to diffuse through in order to escape the sample. This effect is also due to the dried layer appearing in the form of thicker and/or greater frequency of walls, i.e., void ice crystal boundaries surrounded by dried coffee material.

Table 6.1 Depth into the sample where $a=bx$ and the frozen solid density (dry basis) of the lactose for different solid contents.

Solid Content (% w/w)	Depth (mm)	Frozen solid density ($kg.m^{-3}$)
2	0.12	19.87
5	0.06	50.31
10	0.04	103.01
20	0.02	213.72
30	0.02	332.04
40	0.04	453.03
50	0.01	581.75

Fig. 6.7 A shows the amount of dry solid coffee produced for varying solid contents with time, calculated by multiplying the frontal distance by the dry solid density (see Table 6.1). The dry solid density (also known as frozen density calculated on dry

basis) was measured according to the method given in section 3.5.6. The 30%, 40% and 50% initial coffee contents show the fastest production of solid while 2% coffee produced lowest amount of dry solid with time.

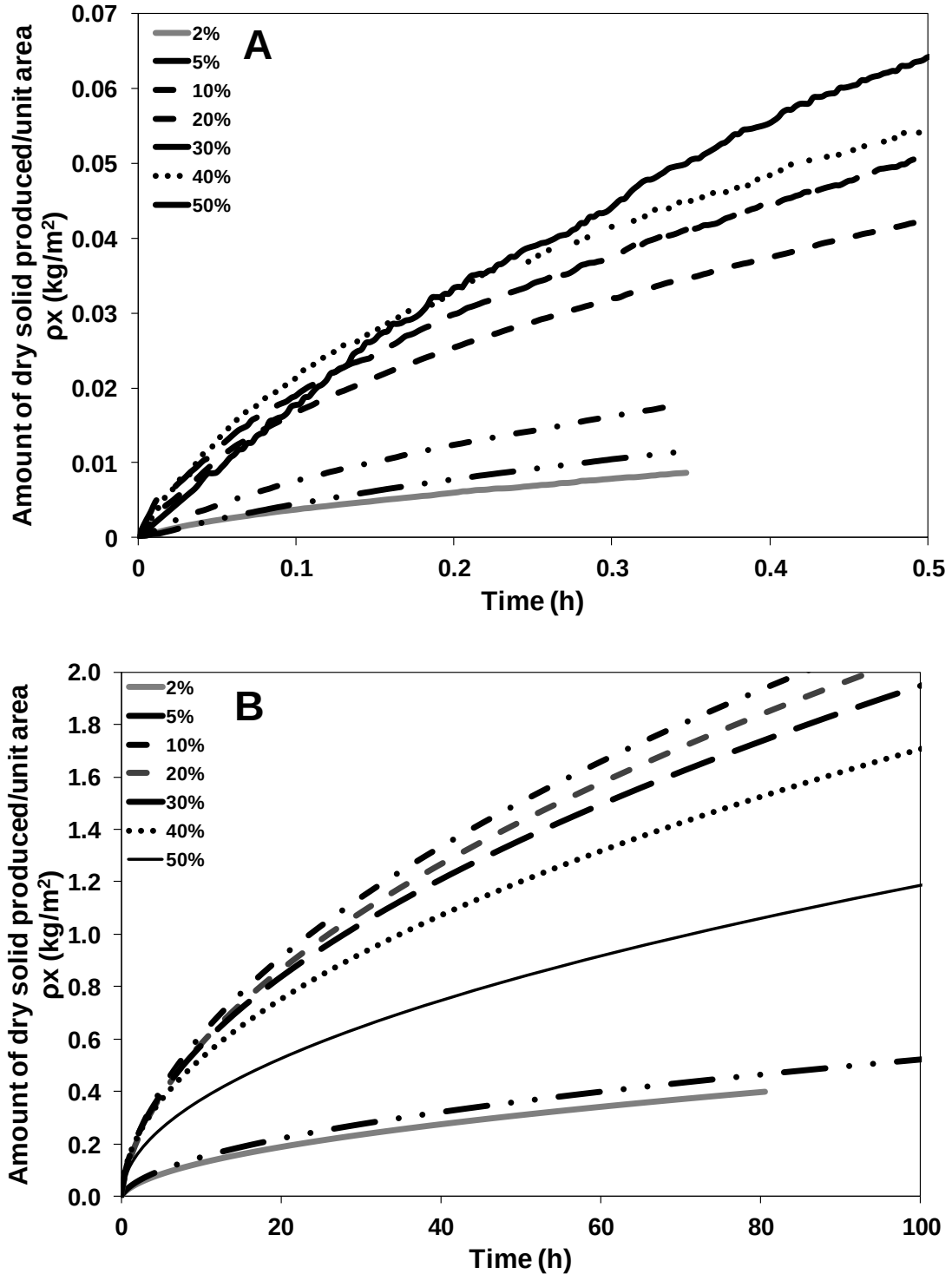

:

Figure 6.7: A. Amount of dry solids produced per unit area for different solid contents based on FDM data obtained. **B.** Predicted extrapolated amount of dry solids produced per unit area for different solid contents based on FDM *a* & *b* values. Curves represent average of at least four repeat runs.

However, when analysing for a short time period, frontal distances are most influenced by the edge resistance term. This is evidenced by Table 6.1 which shows the depths at which the two resistances are equal to each other. It shows the same trend as the effect of solid content on alpha values thereby confirming that for the initial period sublimation rate is significantly controlled by edge resistance.

As discussed in Chapter 5, in a real freeze drying system, the duration of the runs and the frontal distances are much longer than shown in Fig. 6.7 A, and so predicted values of ρx have been extrapolated for longer times using the a and b values (Fig. 6.7 B). The figure shows that the best production rate would be achieved with 10% coffee solution followed by 20%, 30%, 40% and 50% solid contents respectively but very less with 5% and 2% solid contents. Thus, it can be concluded that intermediate concentrations could be optimal for long term drying runs such as in a conventional system. This would depend on microstructural aspects also, which could be different in a conventional system.

6.3.3 Effect of cooling rate

Three cooling rates (2 K.min^{-1}, 10 K.min^{-1} and 50 K.min^{-1}) were investigated in order to study their effect on the freezing of coffee solutions (10% and 50% w/w) and in turn on the subsequent sublimation process via possible changes in the microstructure.

The nucleation temperature range used in samples with AgI in this case is shown in Fig. 6.8. The range was selected based on the maximum number of repeats obtained on the said nucleation temperature. Since the nucleation temperature also varies with cooling rate, hence the temperatures selected were different for all three cooling rates. For samples without AgI, this range was expanded from ±2˚C shown in Fig. 6.8 to ±5˚C to incorporate the difference in nucleation temperatures in samples frozen with AgI. This means, for example, if nucleation temperature considered for 10% coffee samples with AgI is -8±2˚C, for samples without AgI, the range would be -8±5˚C.

Another point of interest is the similarity in the trend (with previous lactose chapter) observed in the nucleation temperature with cooling rate. Lower cooling rate results

in quicker nucleation and faster cooling rate causes slower nucleation of ice crystals due to lesser time to achieve the requisite degree of supercooling to occur.

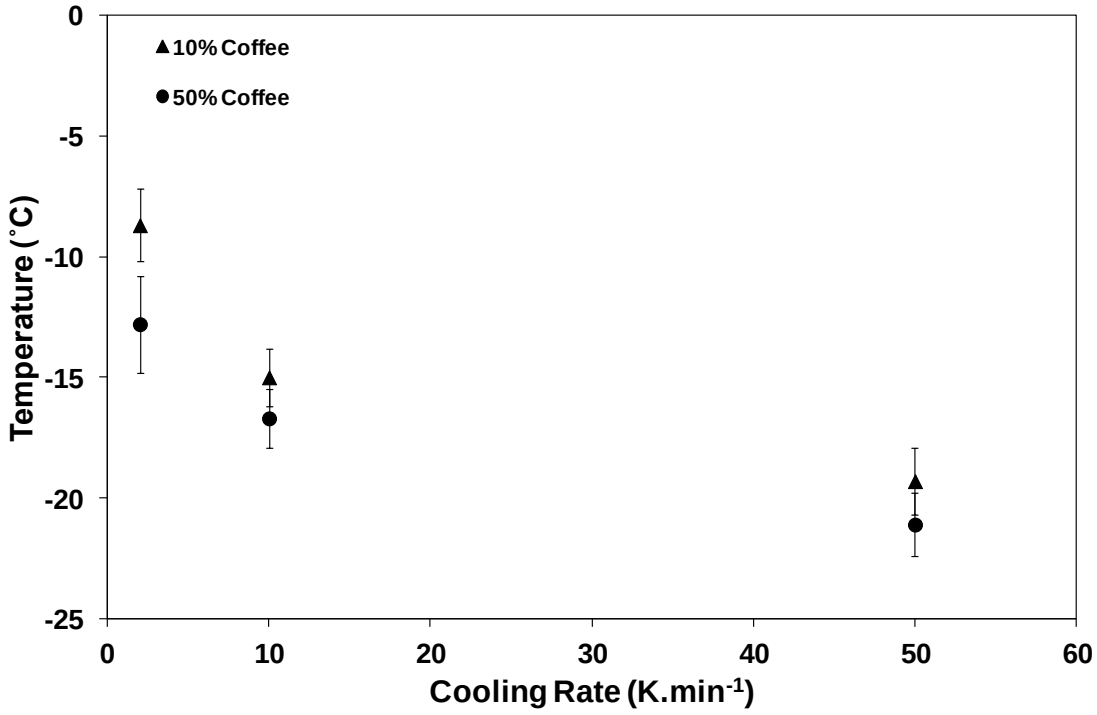

Figure 6.8: The nucleation temperature range selected for the investigation of the effect of cooling rates (2 K.min^{-1}, 10 K.min^{-1} & 50 K.min^{-1}) on the sublimation of coffee (10% & 50% w/w) frozen at -40˚C and freeze dried at 1 Pa. Values are average of at least four repeat runs with standard deviation as the error in each case.

Figs. 6.9 A & 6.9 B shows the effect of cooling rate on the α values for 10% (w/w) and 50% coffee solutions with and without AgI respectively. For a given solid content the α values were generally found not to vary significantly with cooling rate. However, with-AgI samples mostly gave lower α values than non-AgI samples. The one exception to the above was the 50% coffee sample with AgI which gave a much lower α value when cooled at 2 K.min^{-1}. This was a lot closer to the values found at lower solids contents and may indicate that sufficiently large crystals were able to grow and pierce the edge layer. However, when compared between the different solid contents investigated, 50% coffee displayed higher α values than 10% coffee. The main reason for this difference is thought to be higher evaporative drying at the edge of 50% coffee samples than 10% coffee due to lesser amount of water present in the sample which is seen in all three cooling rates for 50% coffee except samples with AgI frozen at 2 K.min^{-1} cooling rate.

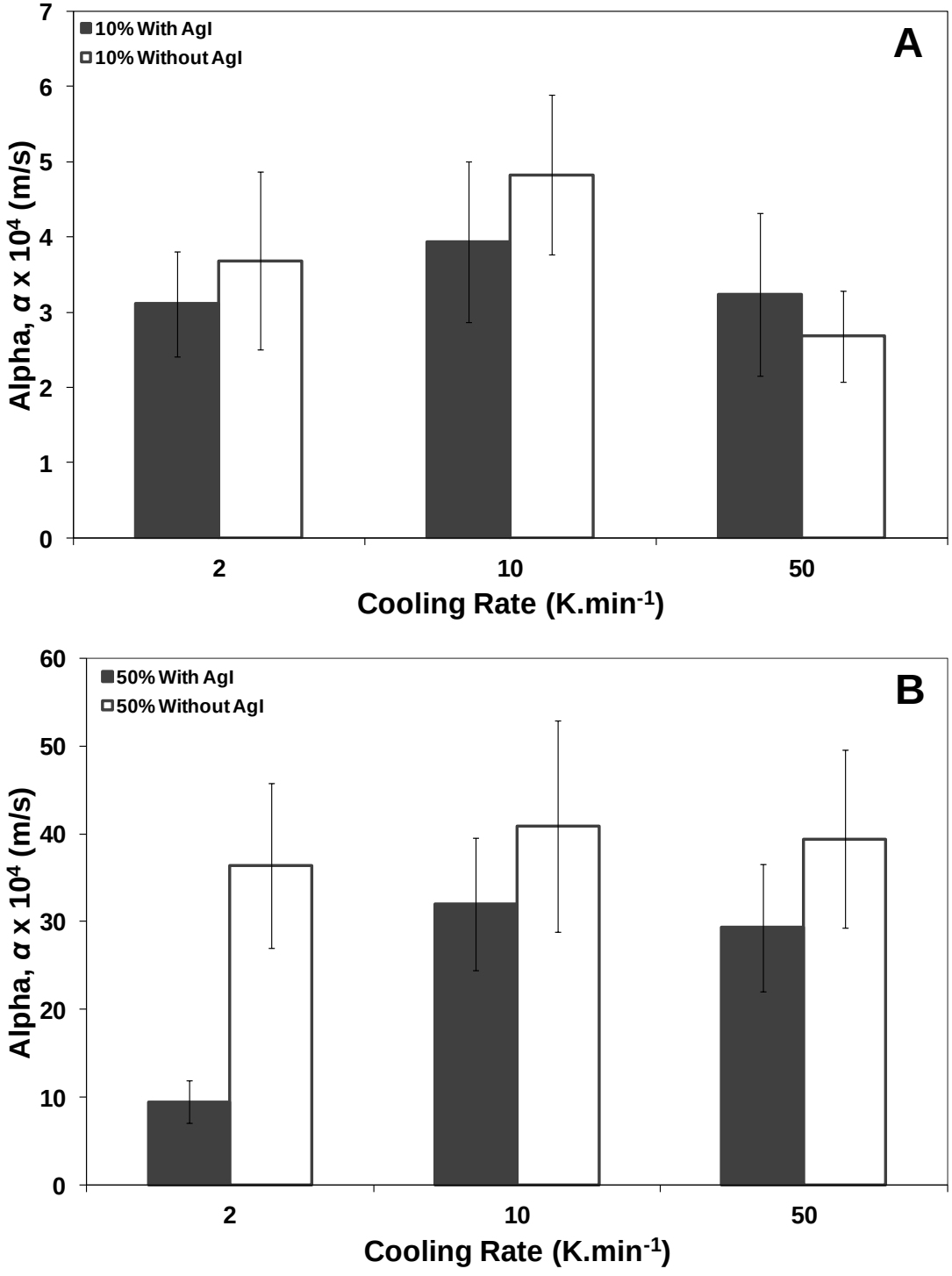

Figure 6.9: A. Effect of cooling rate (2 K.min^{-1}, 10 K.min^{-1} and 50 K.min^{-1}) on α values of 10% coffee with and without AgI calculated from a & b values when freeze-dried under FDM at -40˚C and vacuum pressure of 1 Pa. **B.** Effect of cooling rate (2 K.min^{-1}, 10 K.min^{-1} and 50 K.min^{-1}) on α values of 10% coffee with and without AgI calculated from a & b values when freeze-dried under FDM at -40˚C and vacuum pressure of 1 Pa. Values are average of at least four repeat runs with standard deviation as error in each case.

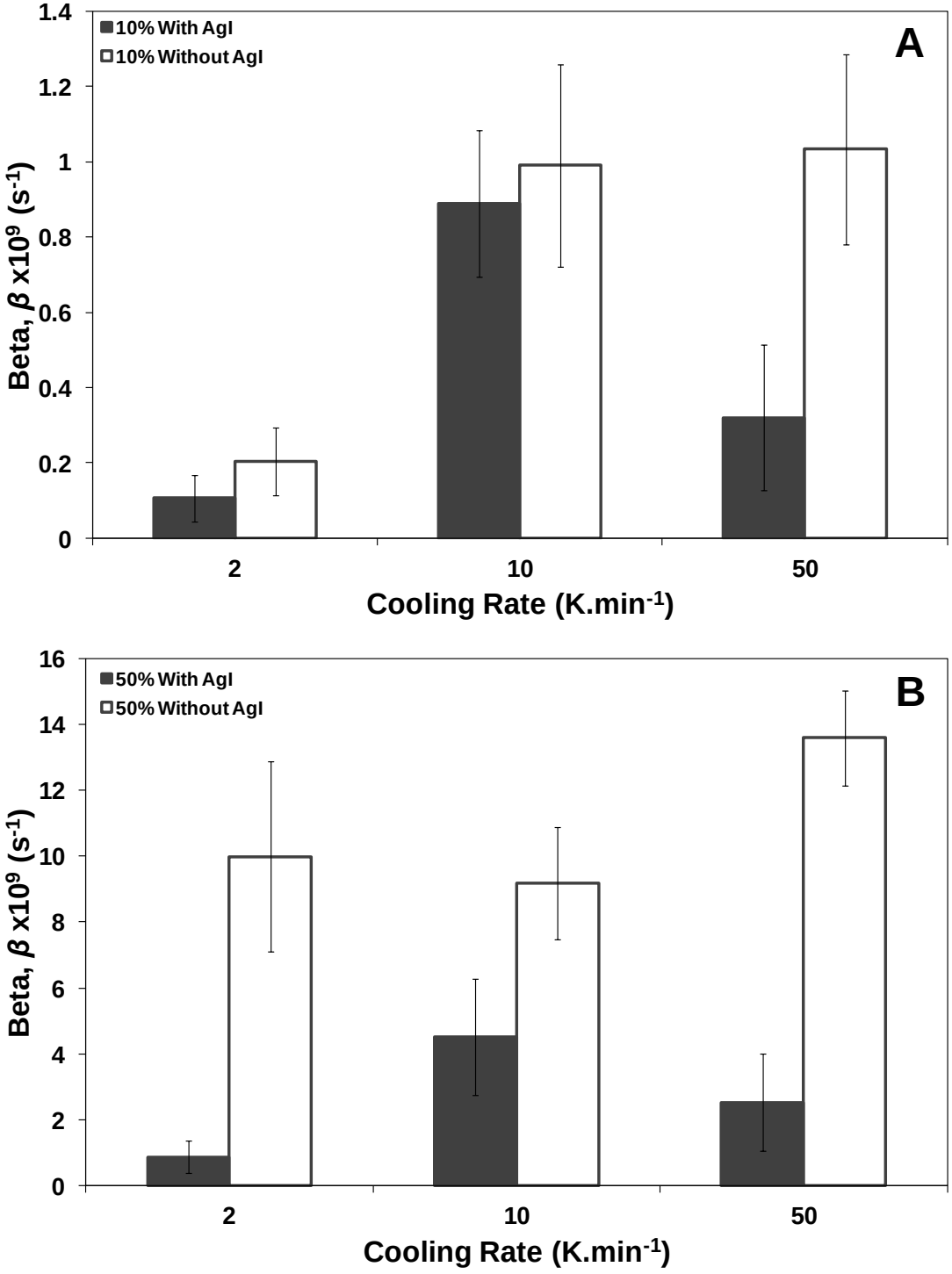

Figure 6.10: A. Effect of cooling rate (2 K.min^{-1}, 10 K.min^{-1} and 50 K.min^{-1}) on β values of 10% coffee with and without AgI calculated from *a* & *b* values when freeze-dried under FDM at -40˚C and vacuum pressure of 1 Pa. **B.** Effect of cooling rate (2 K.min^{-1}, 10 K.min^{-1} and 50 K.min^{-1}) on β values of 50% coffee with and without AgI calculated from *a* & *b* values when freeze-dried under FDM at -40˚C and vacuum pressure of 1 Pa. Values are average of at least four repeat runs with standard deviation as error in each case.

Figs. 6.10 A and 6.10 B show the effect of cooling rate on β values for 10% and 50% (w/w) coffee solutions with and without AgI respectively. The β values were seen to have the same trends as the α values in Fig. 6.9. The effect of cooling rates on behaviour of dried layer resistance was also credited to the microstructure of the samples. As is evident from the nucleation temperature trend, slower cooling resulted in quicker nucleation, thus facilitating sufficient time for the crystals to grow in size (thus displaying lower β values for cooling rate 2 K.min^{-1}), whereas at a faster cooling rate, the ice crystal remain small due to lack of time for crystals to grow before reaching the temperature of drying. Although, the samples frozen at 50 K.min^{-1} do not display larger ice crystal, they could have significant number of smaller ice crystals justifying to some extent the increase in β values of 10% coffee with increasing cooling rate of 10 K.min^{-1} but decreasing again for cooling rate 50 K.min^{-1} (See Fig. 6.10 A). However, samples frozen without AgI show a significant difference compared to samples with AgI especially in the case of 10% coffee frozen at 50 K.min^{-1} and 50 % coffee. Now, this could be attributed to the wider range of nucleation temperatures considered for samples frozen without AgI, resulting in deviating β values than the trend displayed by samples with AgI.

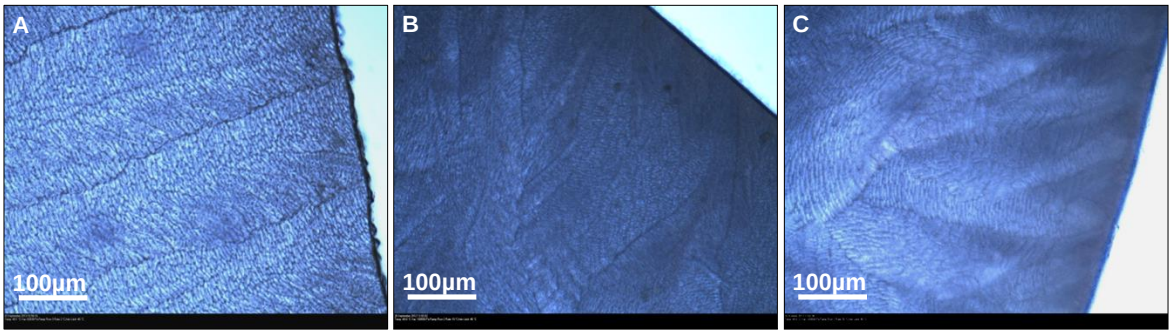

Figure 6.11: A. 10% Coffee frozen with AgI at a cooling rate of 2 K.min^{-1} under FDM at -40˚C and vacuum pressure of 1 Pa. **B.** 10% Coffee frozen with AgI at a cooling rate of 10 K.min^{-1} under FDM at -40˚C and vacuum pressure of 1 Pa. **C.** 10% Coffee frozen with AgI at a cooling rate of 50 K.min^{-1} under FDM at -40˚C and vacuum pressure of 1 Pa. Images are representative of at least four repeat runs.

Fig. 6.11 shows the difference in ice crystal morphology due to variation in cooling rates. 2 K.min^{-1} cooling rate resulted in larger, uniform and well-distributed ice crystals (due to longer duration for growth to occur) which in turn contributed to lower resistance values for both 10% and 50% coffee. However, a 10 K.min^{-1} cooling rate showed a denser microstructure (Fig. 6.11 B) with smaller ice crystals resulting

in higher resistance, while a 50 K.min^{-1} showed lower resistance resulting from smaller but higher number of ice crystals. High rate of cooling gives no time for crystals to grow, but causes higher number of ice crystal nuclei to form, thus increasing the overall amount of ice crystals present in the sample resulting in lower resistance compared to a 10 K.min^{-1} cooling rate.

6.3.4 Effect of drying temperature

Three different freeze-drying temperatures were investigated (-30˚C, -40˚C and -50˚C) for both 10% and 50% coffee solutions with and without AgI frozen at a cooling rate of 10K.min^{-1} and freeze-dried under FDM at 1 Pa. For these set of experiments, the nucleation temperature range used for 10% coffee was -9.0±2˚C for AgI containing samples while for non-AgI samples it was -9.0±5˚C and for 50% coffee the range used was -13.0±3˚C and -13.0±5˚C in both cases respectively.

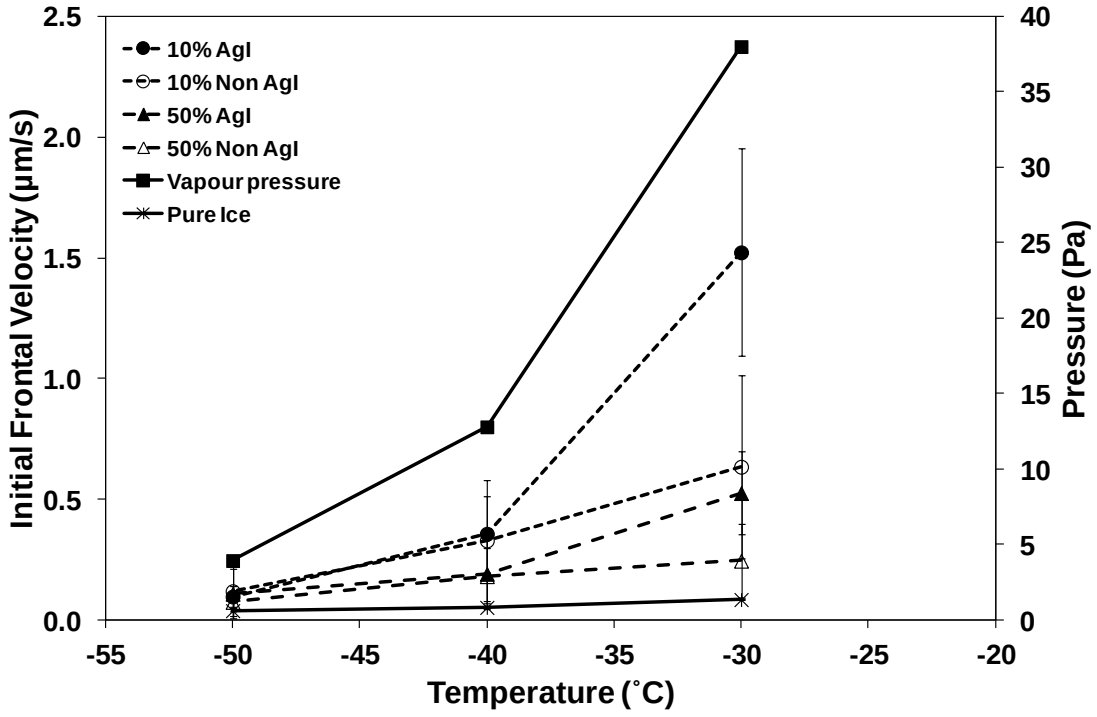

Figure 6.12: Initial frontal velocity of 10% and 50% coffee calculated from *a* values and equilibrium vapour pressure for varying final temperatures of drying (-30, -40 and -50˚C) determined by freeze drying under FDM with a cooling rate of 10 K.min^{-1} at 1 Pa. Values are average of at least four repeat runs with standard deviation as error in each case.

Fig. 6.12 shows initial frontal velocities for 10% and 50% coffee solutions with and without AgI at the three different final freeze-drying temperatures (under FDM), and

shows an increase with increasing freeze drying temperature. The variation with temperature is quite similar to that of the equilibrium vapour pressure of ice (also shown in Fig. 6.12). This behaviour further reinforces the results shown in the previous chapter that vapour pressure is the driving force for mass transfer in freeze drying.

Figs. 6.13 A & 6.13 B show the effect of drying temperature on calculated α values of 10% and 50% coffee freeze-dried under FDM with and without AgI. α values of 10% coffee were found to be quite low (~2 to $9x10^4$ $m.s^{-1}$) for all three final temperatures of drying investigated compared to 50% coffee where they were found to increase significantly with increasing temperatures of drying (~2 to $50x10^4 m.s^{-1}$). As discussed in the Chapter 4 and seen in Fig. 6.12, the frontal velocity calculated for pure ice from a values is quite low, which is not expected for pure ice (as it should not ideally have an edge resistance) and these values are in fact as a representation of resistance offered by the linkam stage itself to water vapour flow.

The saturated vapour pressure (SVP) of ice varies with operating temperatures investigated by a factor of 10. Similarly, the α & β values were found to vary in a similar trend with this change in pressure, and thus temperature. This further proves that vapour pressure is a significant driving force for sublimation. The edge resistance and resistance of the dried layer are affected by change in drying temperature (influencing pressure) and thus facilitating quicker diffusivity of water through the matrix at higher temperature. Effect of temperature on water vapour removal is pronounced in case of both edge resistance and movement through the dried layer. The diffusion rate through edge also increases with increasing SVP and temperature as pressure directly drives flow through the solid edge walls via evaporation process (lower α values).

10% coffee samples were found to be quite similar when compared with and without AgI for all three temperatures investigated, however, 50% coffee showed rather noticeable difference between AgI and non-AgI samples especially in case of -40 and -50˚C with AgI containing samples showing lower resistance most probably due to larger ice crystal sizes (due to the presence of AgI) penetrating through the edge of the sample.

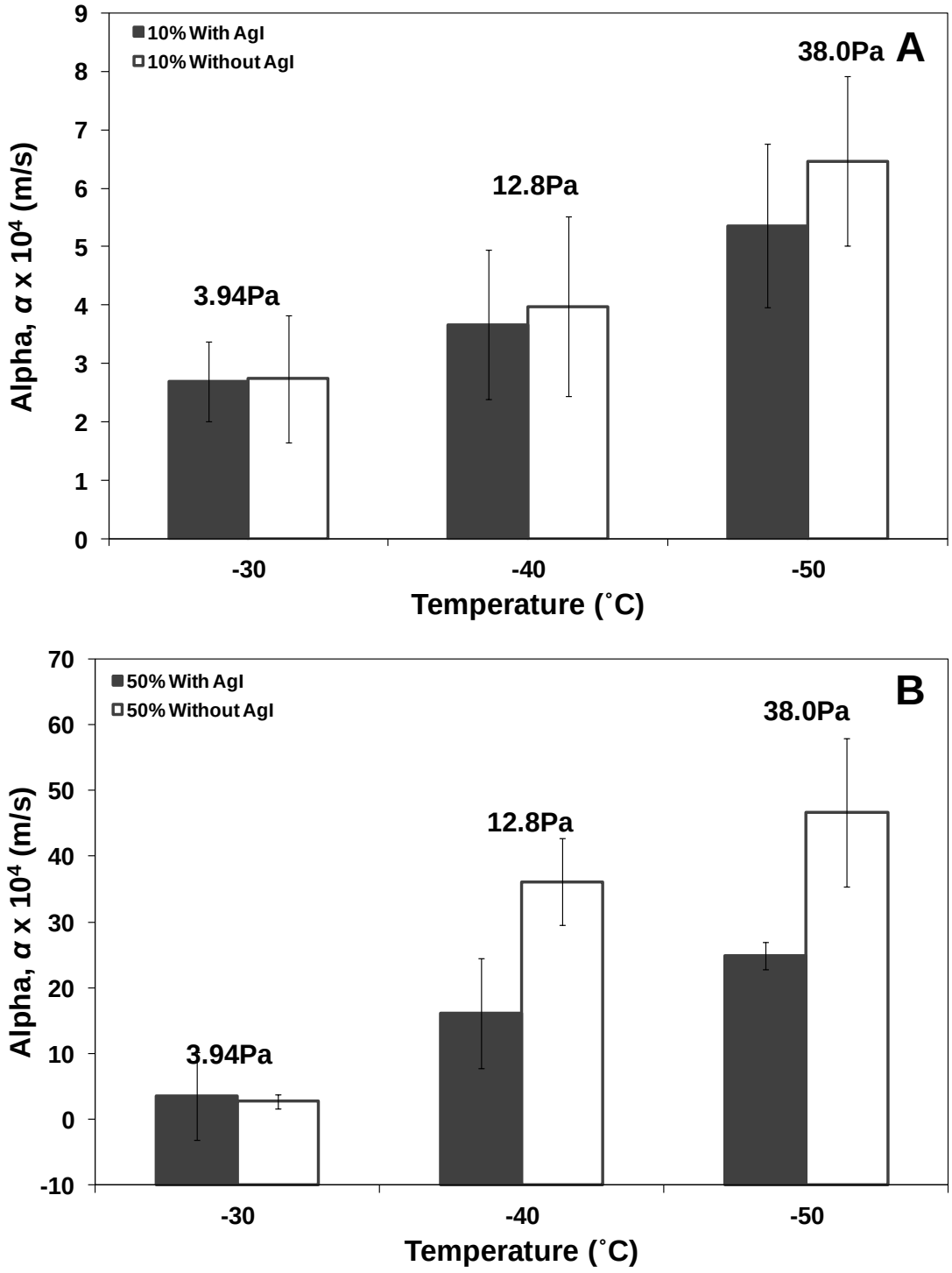

Figure 6.13: A. Effect of temperatures of drying (-30, -40 and -50˚C) on *α* values of 10% coffee calculated from *a* and *b* values obtained from FDM, with samples freeze-dried at 1 Pa. **B.** Effect of temperatures of drying (-30, -40 and -50˚C) on *α* values of 50% coffee calculated from *a* and *b* values obtained from FDM, with samples freeze-dried at 1 Pa. Values are average of at least four repeat runs with standard deviation as error in each case.

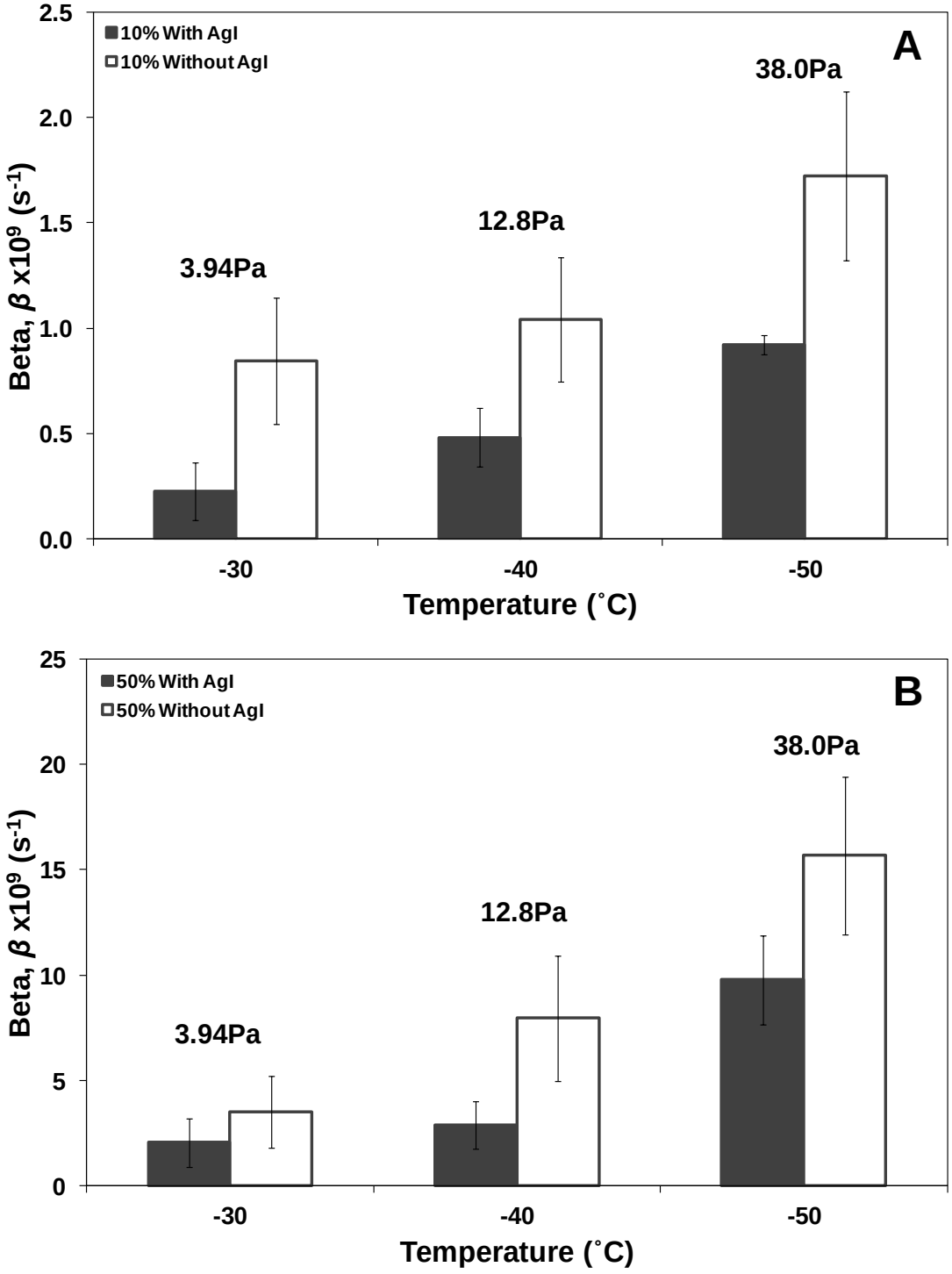

Figure 6.14: A. Effect of temperatures of drying (-30, -40 and -50˚C) on β values of 10% coffee calculated from *a* and *b* values obtained from FDM, with samples freeze-dried at 1 Pa. **B.** Effect of temperatures of drying (-30, -40 and -50˚C) on β values of 50% coffee calculated from *a* and *b* values obtained from FDM, with samples freeze-dried at 1 Pa. Values are average of at least four repeat runs with standard deviation as error in each case.

Figs. 6.14 A & 6.14 B show the effect of drying temperature on calculated β values of 10% and 50% coffee freeze-dried under FDM with and without AgI respectively. β values shown in Fig 6.14 A were found to be very low in case of 10% coffee compared to 50% coffee for all three temperatures investigated. In addition, β values were found to decrease with increasing temperature of drying for 10% coffee and especially for 50% coffee for as was anticipated as this behaviour was again credited to the variation in pressure difference as discussed in the case of lactose in Chapter 4. The resistance of the dried layer is directly affected by temperature as it can be seen that pressure directly drives flow through ice crystal matrix removing water vapour but also removes it from the solid lactose matrix through either diffusion through pores or evaporation between the solid walls. However, for 10% coffee without AgI displayed β values higher than 10% coffee with AgI reinforcing the fact that AgI increased ice crystal sizes resulting in lower resistance of the dried layer compared to samples without AgI. β values of 50% coffee also displayed similar behaviour when compared in terms of AgI and non-AgI samples as is evident from figure 6.14 B.

6.3.5 Effect of Annealing

Annealing profile IV was followed, on 10% and 50% coffee with and without AgI, which involved freezing the sample to -40˚C, heating to -10˚C, holding for 60 mins to allow melting and recrystallization of the sample and then cooling the sample to -40˚C. Figs. 6.15 & 6.17 show the difference in microstructure before and after annealing for 10% coffee and 50% coffee with AgI respectively.

Annealing profile IV was used as it was found to significantly affect the freezing and freeze drying of lactose samples (see section 4.3.8). Both α and β values were found to be low for 10% lactose frozen with AgI annealed with Profile IV compared to all the profiles investigated.

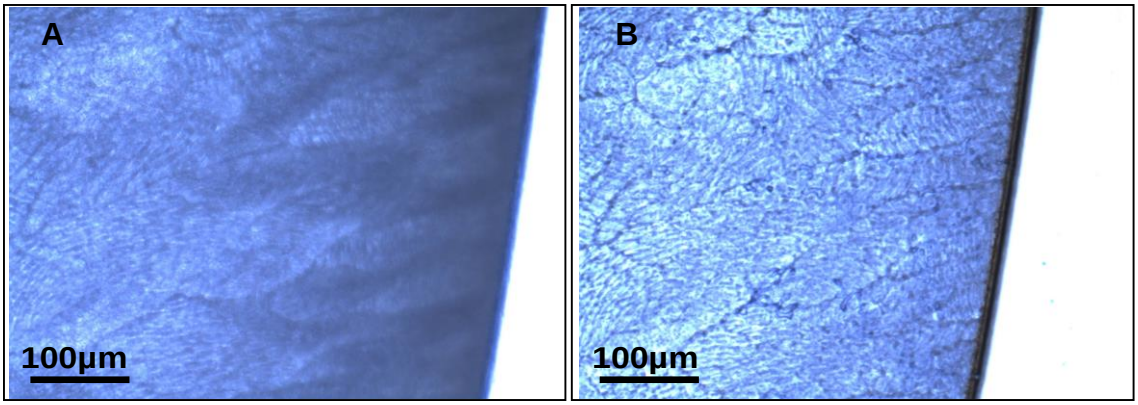

Figure 6.15: A. 10% Coffee frozen (with AgI) at 10 K.min^{-1} to -40˚C. **B.** 10% Coffee annealed at -10˚C and cooled at 10 K.min^{-1} to -40˚C (profile IV). Images are representative of at least four repeat runs.

Figs. 6.15 A & 6.15 B shows the change in the thickness of edge of the sample before and after the annealing process. This thickening of the edge, due to evaporative drying, increased the resistance of the edge layer which resulted in the slight increase in α values of annealed samples in the case of both AgI and non-AgI containing samples of 10% coffee shown in Fig. 6.16 A. Fig. 6.15 B shows the ice crystals in the frozen 10% coffee solution after annealing which were seen to be much larger and more evenly distributed than before annealing. This translated into much lower resistance of the dried layer, i.e., β values, as can be seen in Fig. 6.16 B which was due to larger ice crystals which resulted in fewer barriers to mass transfer facilitating easier and quicker removal of water from the sample.

Figs. 6.16 A and 6.16 B also show a comparison between AgI and non-AgI samples for annealed and non-annealed coffee samples and in the case of both α and β values AgI containing samples were found to have slightly lower resistances than samples freeze-dried without AgI.

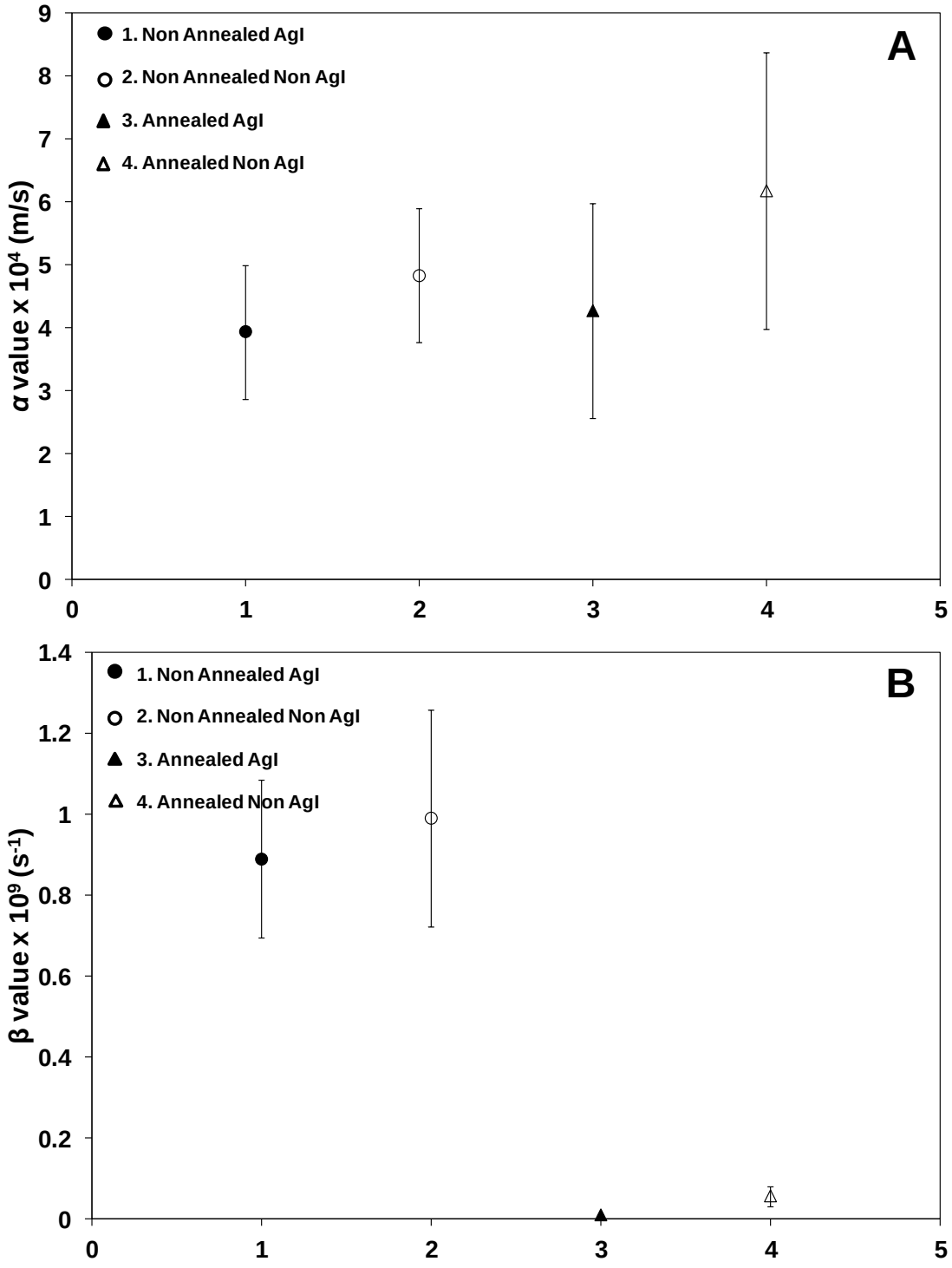

Figure 6.16: A. Alpha values of 10% coffee compared with non-annealed samples without AgI with annealing profile IV, freeze dried under FDM at -40˚C and 1 Pa. **B.** Beta values of 10% coffee compared with non-annealed samples without AgI with annealing profile IV, freeze dried under FDM at -40˚C and 1 Pa. Values are average of at least four repeat runs with standard deviation as error in each case.

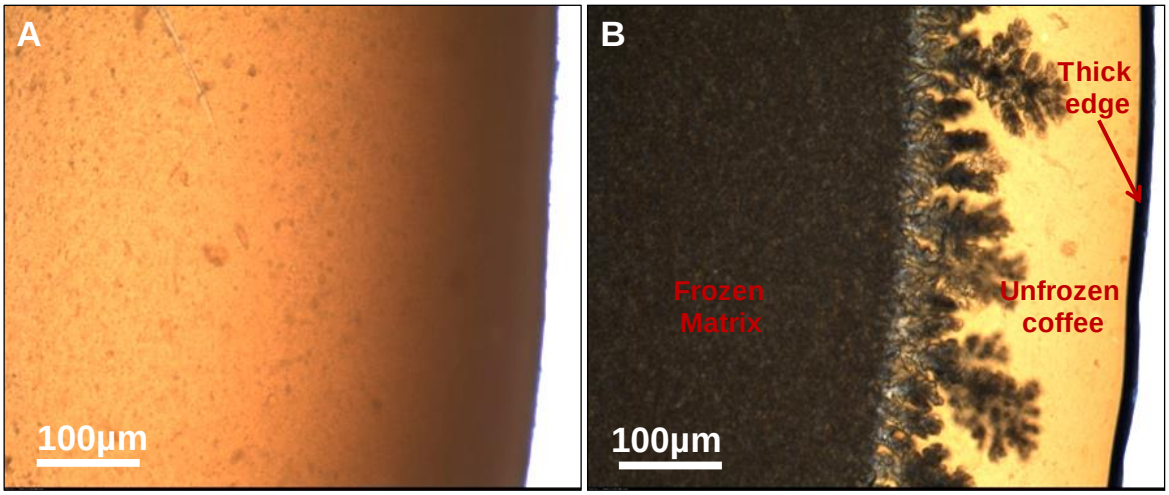

Figure 6.17: A. 50% Coffee frozen (with AgI) at 10 K.min^{-1} to -40˚C. **B.** 50% Coffee annealed at -10˚C and cooled at 10 K.min^{-1} to -40˚C (profile IV). Images are representative of at least four repeat runs.

In 50% coffee samples, during the heating and holding period at -10˚C, increase in ice crystal size was observed (Fig. 6.17 B). However, the solution was not found to re-freeze completely to the edge of the sample when cooled again to -40˚C. The dark region represents the recrystallized ice while the lighter region unfrozen concentrated coffee solution (it could be oil separation from the aqueous coffee solution). This caused an absence of sublimation as the frozen matrix was found to be surrounded by unfrozen concentrated and/or dried coffee (Fig. 6.17 B). It also displayed a thick edge formed due to the long duration of the annealing process though it was not a dry edge formed due to evaporation from the surface; instead it was found to be quite mobile due to the liquid nature of the adjacent unfrozen coffee layer. Thus, the results presented were only for 10% coffee in Fig. 6.16 as freeze-drying was difficult to achieve in high concentration coffee after annealing.

6.3.6 Collapse temperature

The effect of initial solid content of coffee solutions (2, 5, 10, 20, 30, 40 & 50%) on the collapse temperature was also investigated. The samples were freeze dried under FDM at -40˚C at 1 Pa vacuum pressure and collapsed by heating at 1 K.min^{-1}. The collapse temperature was determined by the point where the coffee sample starts to lose its structure due to viscous flow as the temperature is increased in Fig. 6.18. Fig. 6.18 shows the process of structural collapse as seen under FDM for 10% and 50% coffee freeze dried with AgI; the onset of collapse was measured by observing the

light band formation in FDM images obtained while heating the sample at a heating rate 1 K.min^{-1}.

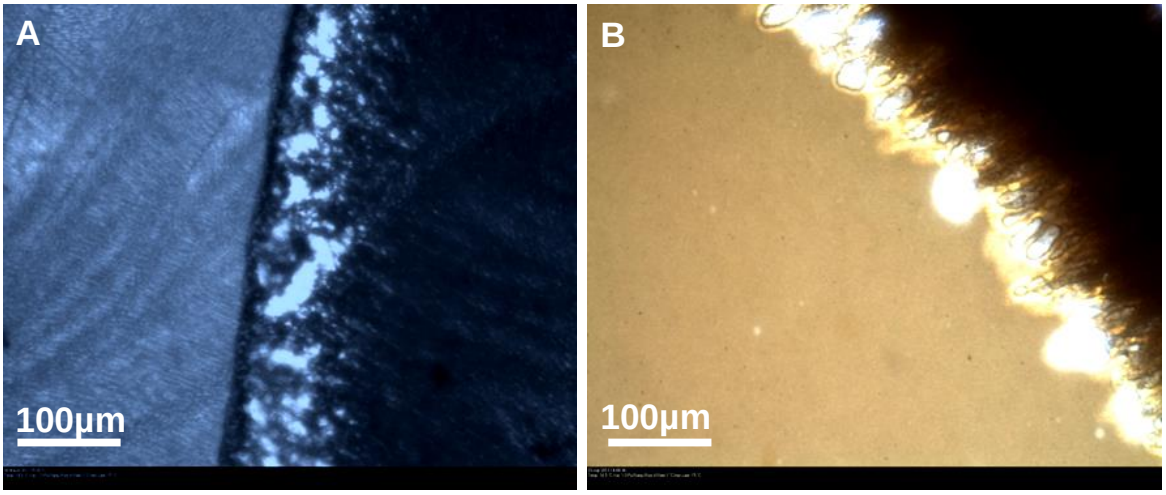

Figure 6.18: A. The process of collapse observed in 10% coffee freeze dried under FDM at -40˚C at 1 Pa vacuum pressure and collapsed by heating at 1 Kmin^{-1}. **B.** The process of collapse observed in 50% coffee freeze dried under FDM at -40˚C at 1 Pa vacuum pressure and collapsed by heating at 1 Kmin^{-1}. Images are representative of at least six repeat runs.

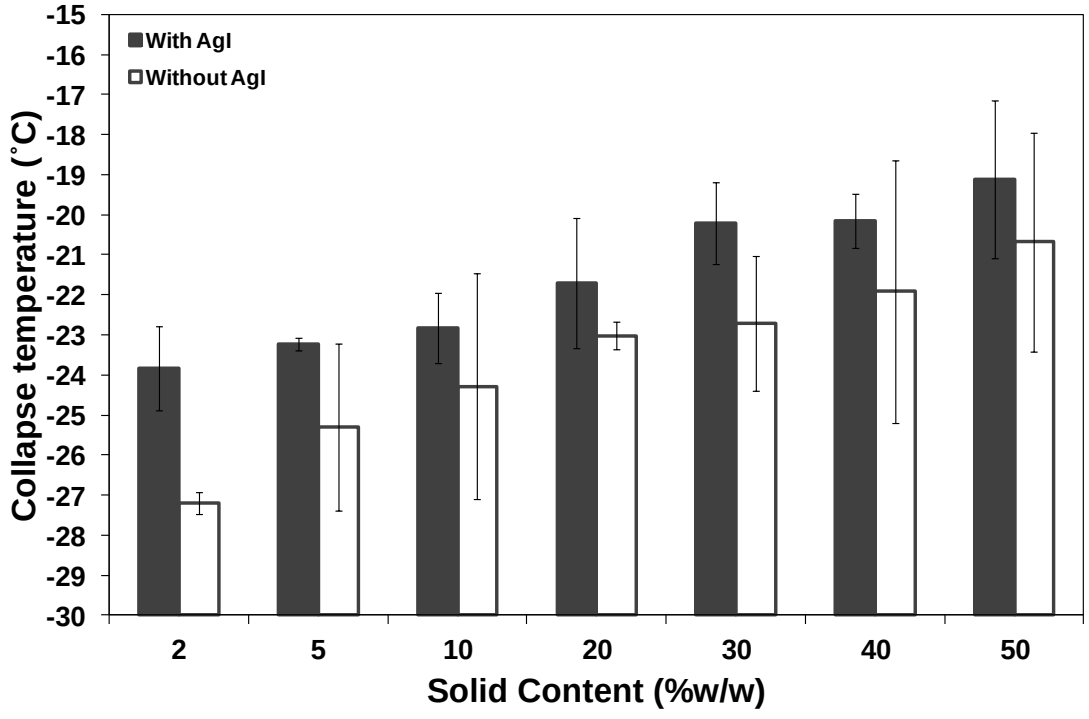

:

Figure 6.19: Effect of coffee solid content on the collapse temperature (T_c) observed in 2, 5, 10, 20, 30, 40 & 50% coffee with and without AgI freeze dried under FDM at -40˚C at 1 Pa vacuum pressure and collapsed by heating at 1 K.min^{-1}. Values are average of at least six repeat runs with standard deviation as error in each case.

For all the coffee samples, with and without AgI, the collapse temperatures showed an increasing trend with increasing solid content (Fig. 6.19). Higher initial coffee solid content samples were found to be more tolerant of higher temperatures than lower solid contents as discussed for lactose which showed similar trends in chapter 4. This increasing trend of collapse with increasing solid content is in agreement with values that have been shown for different materials such as PVP, Trehalose, previously by various researchers (Meister *et al.,* 2009 and Yang *et al.*, 2010).

A comparison of samples with and without AgI for all solid contents showed that AgI containing samples had higher collapse temperatures than samples without AgI. Thus, it reinforces the fact that the nucleation temperature does affect the collapse temperature by affecting the ice crystal size and pore-size distribution (Pikal & Shah, 1990 and Meister *et al.,* 2009).

Glass transition temperatures: Measurement of the onset glass transition temperature (T_g'), another measure of the critical formulation temperature, was carried out using DSC (Fig. 6.20) with the protocol described in Section 3.8.

The step change in heat flow, shown in Fig. 6.20, due to the change in heat capacity at the glass transition is rather significant in case of coffee samples compared to lactose samples in previous chapter 4 (see e.g. Fig. 4.19) compared to the overall melting thermogram obtained from DSC. The T_g' has been calculated as the onset of the glass transition phenomena in this study as shown in Fig. 6.21.

The onset glass transition temperatures of 10% and 50% coffee with and without AgI are summarized in Table 6.2. AgI containing samples were found to have slightly higher T_g' values (only 0.5˚C) compared to samples without AgI for 10% whereas for 50% coffee solutions with AgI, T_g' values are higher by 1.5˚C, although the error margin was also higher for 50% coffee.

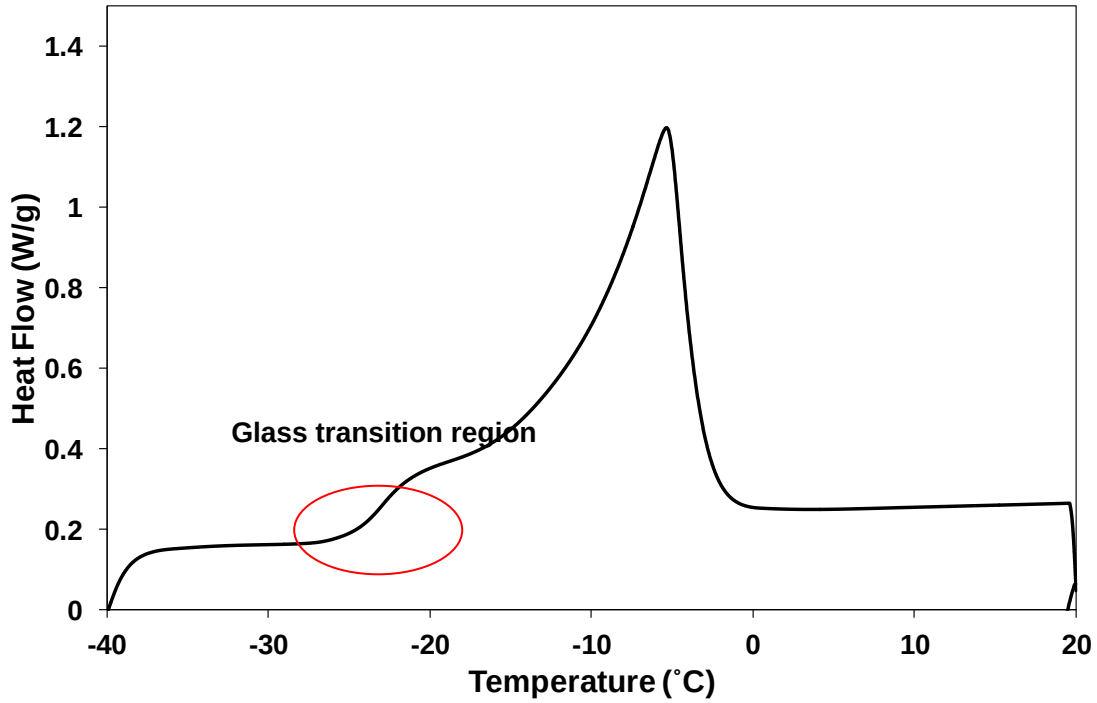

Figure 6.20: DSC thermogram of 10% coffee with AgI cooled at 10 K.min^{-1} and heated at 5 K.min^{-1}. Curve is representative of at least three repeat runs.

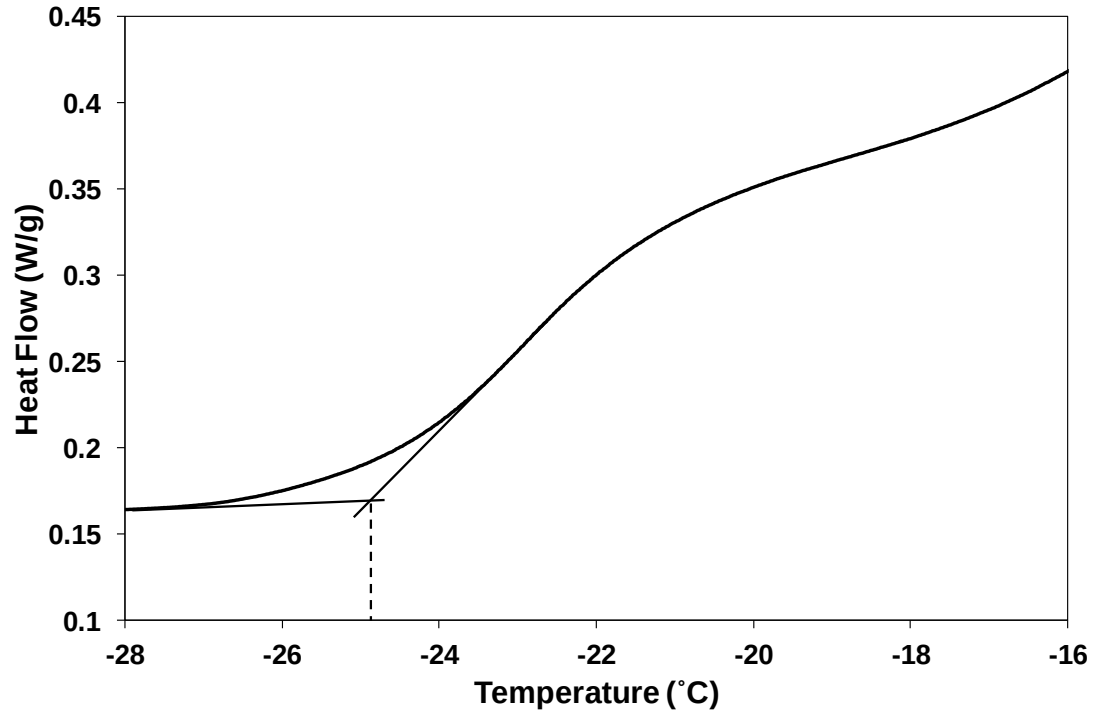

Figure 6.21: DSC thermogram of 10% coffee with AgI cooled at 10 K.min^{-1} and heated at 5 K.min^{-1} highlighting the glass transition temperature. Curves are representative of at least three repeat runs.

Table 6.2 Onset glass transition temperatures and collapse temperatures of 10% and 50% coffee determined using DSC with and without AgI calculated from average of at least three repeats.

Glass transition temperature (˚C)			
10% Coffee		50% Coffee	
With AgI	Without AgI	With AgI	Without AgI
-24.3±0.3	-24.6±0.1	-25.5±1.0	-27.2±1.3
Collapse temperature (˚C)			
10% Coffee		50% Coffee	
With AgI	Without AgI	With AgI	Without AgI
-22.8±0.9	-24.3±2.8	-19.1±2.0	-20.7±2.7

Comparing these T_g' values, from Table 6.2, to the collapse temperatures in Fig. 6.19, it is clear that for 10% coffee, the T_g' values were quite close to the collapse temperature. However, these values are lower by 3˚C for 50% coffee with and without AgI. This comparison of the temperatures is quite close to the trends suggested in the literature that collapse temperatures for aqueous solutions are generally 1-2˚C above the glass transition temperatures, while in some cases, it can increase with the increase in the complex nature of the sample in question (like 50% coffee), for example, in complex bacterium preservation media it can be as high as 10˚C above T_g' (Fonseca *et al.,* 2004 and Yang *et al.,* 2010).

6.3.7 Effect of aeration

50% coffee solutions were aerated with N_2O gas which introduced gas bubbles of an average diameter of 20-30μm into the sample (see Fig 6.22 B) and aerated samples were then freeze dried at -40˚C at 1 Pa (Fig. 6.22 C). Aeration was found to increase the nucleation temperature (from -28˚C to -20˚C) which suggests that bubbles may act as nucleation promoters. Fig 6.22 C shows a freeze drying front that has just passed through a bubble. The air bubbles were found to provide pathways for easier removal of water vapour resulting in faster drying. It can be seen that the bubble appears to present negligible resistance to mass transfer, as the front spreads out again evenly along the far side of the bubble boundary.

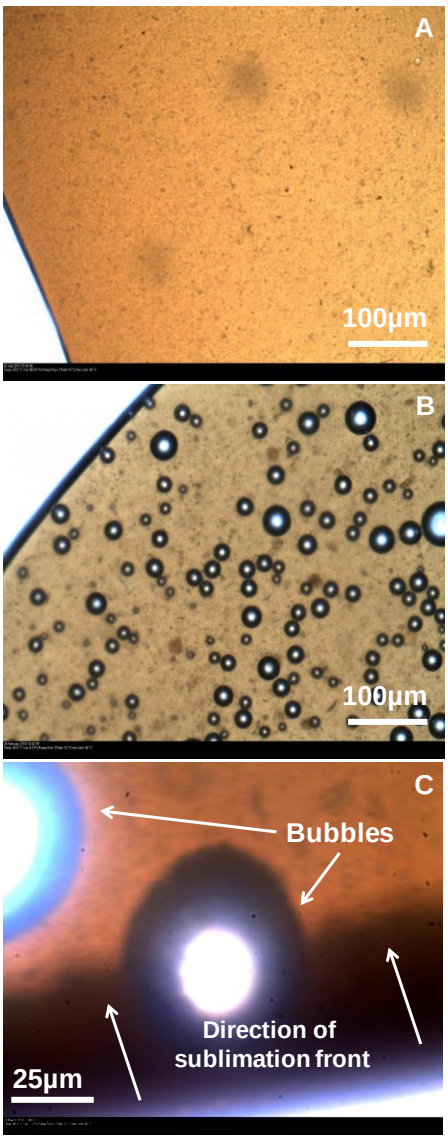

Figure 6.22: A. 50% coffee frozen without aeration. **B.** 50% coffee frozen with aeration. **C.** 50% coffee with aeration during freeze drying at -40˚C and 1 Pa. Images are representative of at least five repeat runs.

The frontal distance vs time plots of 11 lines of a single run of non-aerated and aerated 50% coffee samples are shown in Fig. 6.23. Aerated samples were found to dry faster with "jumps" in the plot wherever a bubble was encountered in the microstructure (Fig. 6.23 B). These jumps were not observed in plots of non-aerated samples (Fig. 6.23 A). Due to these jumps, accurate fitting of the model was difficult and hence α and β values are not presented for these experiments. However, it can be seen that the fronts have moved further in case of aerated samples than in the non-aerated samples by a factor of 3-4. This is a lot more than might be expected given the relatively lower number of bubbles observed at the sample edge.

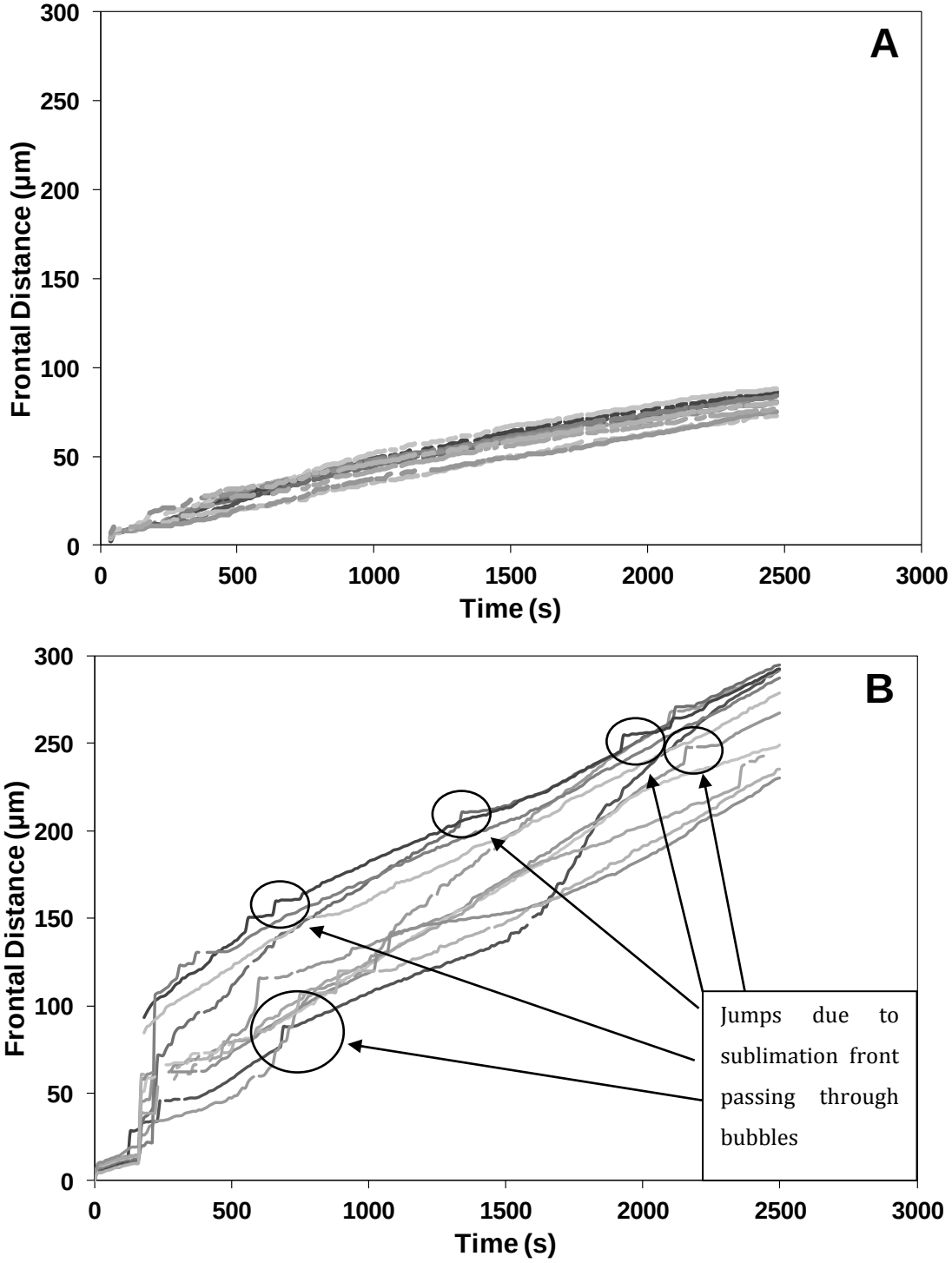

Figure 6.23: A. Frontal distance vs time plot of 50% coffee freeze dried at -40˚C at 1 Pa under FDM without aeration (the 11 lines obtained from MATLAB for one run). **B.** Frontal distance vs time plot of 50% coffee freeze dried at -40˚C at 1 Pa under FDM with aeration (the 11 lines obtained from MATLAB for one run). Curves representative of at least five repeat runs.

A lower concentration of coffee was not investigated, since, generally high initial concentrations are aerated and used in a conventional coffee freeze-drying system.

Moreover, the method of aeration employed with lower concentrations resulted in bubbles larger than the desired size range (>100 μm).

6.4 CONCLUSIONS

The purpose of this study was to achieve a better understanding of the various factors which affect the primary drying phase of freeze-drying of coffee solution using FDM. Microscope images were analysed using MATLAB to determine the distance travelled by the front with time.

Freeze drying microscopy was used to study the sublimation kinetics of coffee solutions of various concentrations. Poor reproducibility of nucleation temperatures and frontal velocities were observed between samples even under near-identical conditions. In response, silver iodide was added to induce ice nucleation at higher temperatures. This was achieved, but reproducibility did not significantly improve.

The effect of nucleation temperature on the structure of the frozen matrix and hence, on the freeze-drying process has been studied. It can be concluded that the size of ice crystals plays a significant role in determining sublimation front velocities. Although the use of AgI could not significantly improve reproducibility of results, it did influence the ice crystal structure and hence lowered the resistance of the dried layer to mass transfer showing that there was a clear link between increased freeze drying rates and larger crystal sizes.

A further understanding of the effect of solid content (5 to 40% w/w) and final temperature of drying (-30˚C, -40˚C & -50˚C) on the representative edge resistance (α) and the representative resistance of the dried region (β) were also investigated. The α values were found to reach a maximum at 40% coffee solid content followed by a slight decrease at higher solid contents while β values were found to increase with increasing solid content. The effect of increasing sample drying temperature from -50˚C to -30˚C showed the expected decrease in α and β values due to the increase in saturation vapour pressure of ice which are included within these parameters.

Furthermore, a study of the effect of annealing also shows that the process dramatically increase crystal sizes whilst simultaneously reducing bulk resistances to mass transfer.

Aeration of coffee solutions caused also sublimation rates to increase, and this was more than would be expected due to simple volume fraction considerations. The use of aeration is shown to be highly beneficial in improving freeze drying rates, and reinforces its use in the already established commercial coffee manufacture.

Although, the freeze-drying microscopy systems differs quite significantly from a conventional freeze drying set-up, the results discussed in this chapter do suggest that methods for increasing crystal sizes such as other forced nucleation techniques (as AgI is not consumable) and annealing could be considered for speeding up the sublimation step of the freeze drying process.

7

TRAY FREEZE-DRYING OF COFFEE

Freeze drying of coffee in trays and the effect of microstructure on the mass transfer of water vapour was investigated. The effects of cooling rate, solid content, annealing and aeration on the primary drying were also studied. Primary drying durations of these processes were compared to the drying times estimated from the equivalent freeze drying microscopy experiments.

7.1 Introduction

In food industry, freeze drying is a drying method which allows obtaining a higher quality product with better flavour, aroma and bioactivites compared to other drying methods such as spray drying, mainly due to the low operating temperatures of the process. As has been described repeatedly in previous chapters, freeze drying involves removal of a solvent from the frozen material by sublimation (primary drying), followed by desorption of the adsorbed solvent (secondary drying), generally under reduced pressure. The performance of the overall freeze drying process depends significantly on the freezing stage. The shapes, sizes and connectivity of the ice crystals formed directly influence the sublimation process and thus, the primary drying rates are quicker for samples which display large crystal sizes as it allows easier removal of water vapour (Boss *et al.,* 2004).

Apart from the pharmaceutical industry, freeze-drying is commonly used to produce high quality dried instant coffee. Freeze-dried coffee is preferred as it a better quality product than those obtained from spray drying, although the process is more energy intensive and expensive (Ratti, 2001 and Pardo *et al.,* 2002). The process of freeze-drying is important for the food industry, since the number of food products produced using this technique are on the rise. However, the main concern in using this method is reducing drying times, in turn reducing the energy consumption (and thus, the cost) whilst still maintaining the requisite residual moisture content and product quality (Ferguson *et al.,* 1993). In terms of energy consumption, the most significant step is primary drying, which accounts for nearly half of the total energy required by the process (Ratti, 2001).

Optimization of the primary drying stage has been widely discussed by various researchers in the scientific literature so as to minimize the overall drying time. It has been suggested previously that optimization can be achieved by using suitable monitoring and control system (Fissore & Barresi, 2011) and mathematical modelling. Mathematical modelling can be used to determine optimal operating conditions. Baressi *et al.,* (2013) have recently used freeze-drying of coffee extract in trays as a case study to develop a simple model to describe ice sublimation and dynamics of water vapour removal in the freeze dryer. Apart from this, Pardo *et al.,*

(2002) have also discussed the effects of freezing rates on ice crystal sizes in frozen coffee extract described using Neumann's model (see Section 2.5). Other researchers have also tried to understand and optimise the freeze drying processes using mathematical modelling based on effects of heater temperature, ambient moisture content and chamber pressure on the drying time (Ferguson *et al.,* 1993 and Boss *et al.,* 2004). However, there is a serious lack in the available literature on the use of freeze drying microscopy as a tool to understand and develop process parameters that directly affect the primary drying duration especially based on mass transfer of water vapour.

The objective of this chapter is to overcome this gap and focus on the freeze-drying of coffee in metal trays to improve to gain a deeper knowledge of the effect of mass transfer on the sublimation process. To achieve this, freeze -drying was performed on a coffee system with two different solid contents with and without the use of a nucleating agent (AgI). The effects of various cooling profiles, annealing and aeration on the process were investigated with primary focus on the effect of microstructure of the frozen material on the primary drying kinetics. The sublimation kinetics, especially the mass transfer phenomenon, were also studied with respect to primary drying times and compared to the data extrapolated from the freeze-drying microscopy of coffee.

7.2 Materials and methods

7.2.1 Materials

Nescafe coffee (Spray-dried) was purchased from the local supermarket and silver iodide was purchased from Fisher Scientific (Loughborough, UK) for the purpose of this research as described in Section 3.1.

7.2.2 Moisture content determination

Moisture content of the coffee bought was determined using the hot-air oven drying method as discussed in Section 3.3.2.

7.2.3 Sample preparation

Sample preparation of varying coffee solid contents was carried out as explained in Section 3.4.1.

7.2.4 Tray freeze drying

Conventional freeze drying of sample solutions was carried out in metal trays for coffee solutions in a VirTis AdVantage Plus Benchtop shelf based Freeze Dryer (SP Industries, Warminster, PA) as described in Section 3.7.

7.2.5 Field Emission Gun Scanning Electron Microscopy

FEGSEM was carried out on the freeze dried samples obtained from FDM as described in Section 3.7.

7.3 Results and discussion

Instant coffee is commonly produced all around the world by either spray drying or freeze drying of coffee extract. Hence, the kinetics of freeze drying of coffee is of interest to researchers and commercial food industries. However, very few researchers have focussed specifically on its freeze drying kinetics in trays as it is usually dried in such a way in an industrial set-up.

Aside from the use of trays over vials, the typical industrial coffee process differs in other ways from the pharma process: (i) the frozen contents of the trays are milled to produce frozen granules prior to freeze drying, (ii) heating is supplied during freeze drying from radiant heaters from above rather than by controlling shelf temperatures, (iii) coffee solutions are often aerated to produce a foamed structure prior to freezing to aid mass transfer during freeze drying.

Thus, this research project aims to improve the understanding of the basic aspects of the freeze drying kinetics of coffee (in trays) and gain knowledge on the effect of ice nucleation and ice crystal morphology on the primary drying rates.

Radiant heating was not possible with the VIRTIS freeze dryer used in Chapter 5 without extensive modification, and so the temperature controlled shelf method was used as with the lactose vials in the previous chapter. Shelf heating is not a suitable method for heating granular materials due to the poor thermal contact and so it was decided to investigate frozen slabs of coffee instead. Although this is different to the industrial process it would allow the freeze drying process to be studied in a reproducible manner. It was however possible to aerate the samples prior to freezing and this was done for some samples.

Freeze drying of coffee (initial solid contents – 10% and 50% w/w) was thus performed in circular metal trays (dia. 90 mm) with and without the use of silver iodide (AgI). Each run involved the use of 4 trays of coffee sample (90 ml – about 14 mm in depth) with three temperature measuring T-type thermocouples in every tray at three different depths (3 mm, 7 mm, 11 mm) from the top of the sample. Thermal grease was used to gain good thermal conductivity between the bottom of the trays and freeze dryer shelf.

Fig. 7.1 shows the temperature vs time plot for coffee freeze-drying in trays measured using the three thermocouples placed inside the tray. It also displays the measure of shelf temperature from a separate thermocouple attached to the freeze dryer shelf. The plots are in good correlation with those presented by various researchers and the calculation of endpoint of sublimation was in line with the method used in literature (Passot *et al.,* 2007 and Schneid & Gieseler, 2008).

The temperature measurement curves from the tray (Fig. 7.1) also show the increase in temperature at the three different sample depths with the curves achieving a constant when the samples reach end point of sublimation, as was determined in the case of lactose samples freeze-dried in vials. It was also observed that the sample undergoes sublimation consecutively at the three sample depths investigated with the top thermocouple measuring higher temperature first, followed by middle thermocouple and then lowest thermocouple. Thus, it proves that sublimation front moves through the sample from the surface towards the bottom of the sample and it takes longer for water vapour removal from bottom than from top of the sample.

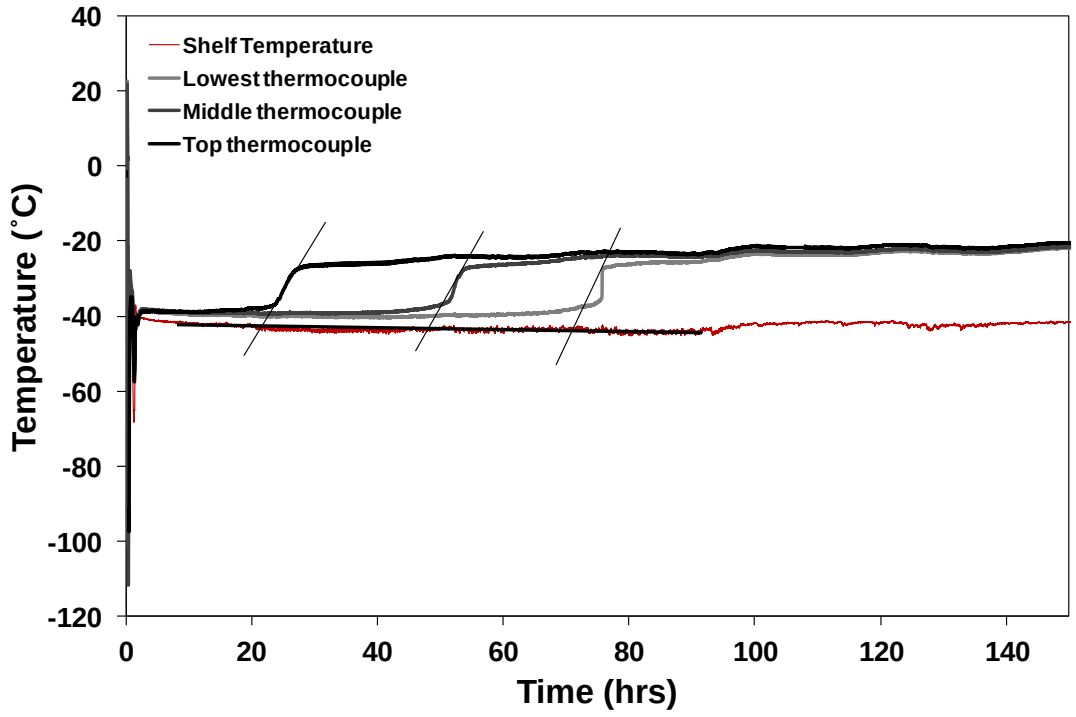

Figure 7.1: Tray freeze-drying data plot of 10% coffee freeze dried at -40˚C at 10 Pa indicating the shelf temperature and temperature change with time as the sublimation front moves through the tray passing the three thermocouples at different depths. Curves are representative of at least four repeat runs.

As has been discussed in detail in previous chapters, the rate of primary drying in a freeze drying process is primarily controlled by heat transfer and mass transfer processes. Both the heat and mass transfer resistances associated with these processes play equally important roles in governing the sublimation rate and thus the overall duration of freeze drying. However, this research focuses primarily on the mass transfer of water vapour that takes place within the frozen matrix in the tray during sublimation. It is acknowledged that the heat transfer also does affect this process, but it will not be discussed in detail in terms of this current research. The main reason for this is the inadequacy in our freeze dryer equipment to measure the various factors required to determine the heat transfer resistances during freeze drying especially pressure within the chamber.

7.3.1 Tray vs Tray Comparison

Fig. 7.2 shows a comparison between the temperature measurements of the three thermocouples of two different trays containing 10% coffee with AgI. The

reproducibility between the trays was observed and it was seen that the temperature curves in the two cases are slightly different. The temperatures in the Tray 2 increased quite steeply in comparison to Tray 1 where the temperatures were found to increase gradually. The reason for difference was not apparent, but could be due to differences in microstructure in the two trays. However, the end points of sublimation calculated from tangents on the two curves were quite close.

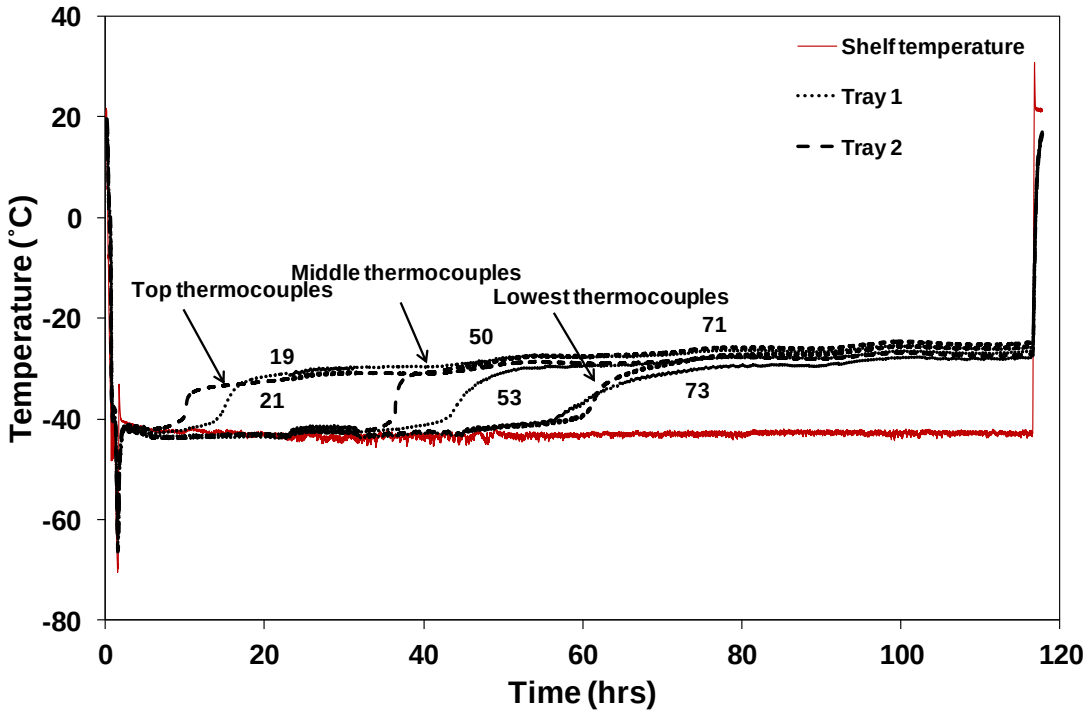

Figure 7.2: Tray freeze-drying data plot of 10% coffee without AgI freeze dried at -40˚C at 10 Pa displaying comparison of temperature (at three depths) vs time plot between two trays. Curves represent at least four repeat runs.

SEM microstructures of freeze-dried coffee from below the surface of samples from two different trays with 10% coffee with AgI are shown in Fig. 7.3. It is evident from the figure that the microstructure of the two trays freeze-dried under similar conditions is quite similar in size and shape of ice crystal voids. The internal structure of sample from Tray 1 however seems to be a little denser than in the case of Tray 2 where the sample looks more porous and open in structure. This could be the reason for the quicker increase in temperatures measured by thermocouples in Tray 2 seen in Fig. 7.2. Since the samples were frozen and freeze dried with AgI, they were seen to have some uniformity in structure, though it is not as significant as was the case of

lactose samples freeze dried in vials in the presence of AgI. This behaviour was also found to be consistent with that seen in coffee samples freeze dried with AgI under the freeze dried microscope as discussed in the previous chapter.

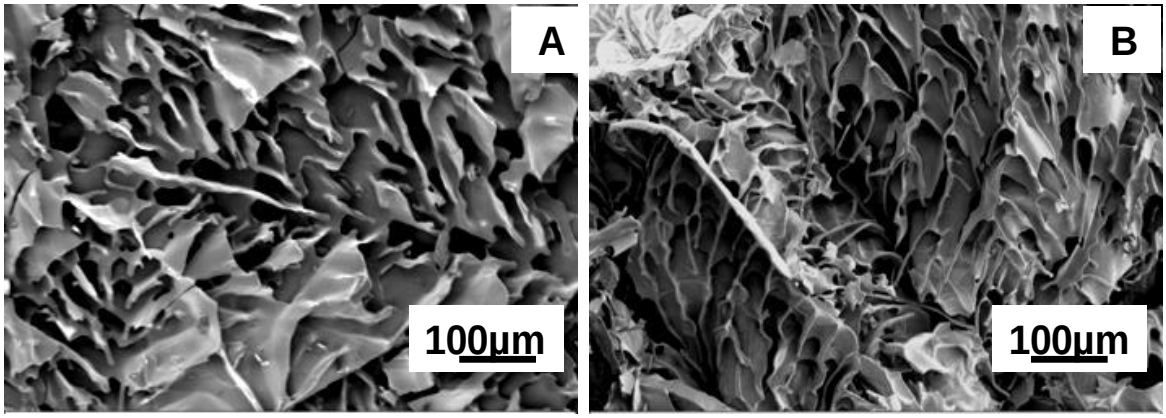

Figure 7.3: FEGSEM image of internal microstructure from top of the sample of 10% coffee freeze dried at -40˚C at 10 Pa with AgI in **A.** Tray 1 & **B.** Tray 2 (see Fig. 7.2). The previous cooling rate was 1 $K.min^{-1}$ in both cases. Images represent at least four repeat runs.

7.3.2 Effect of freezing profiles (10% Coffee)

The effects of freezing conditions (cooling rate, use of an annealing step, presence of AgI) are investigated for 10% w/w coffee samples in this section.

Slow cooling: Fig. 7.4 shows the internal microstructure of 10% coffee with and without AgI freeze dried in trays at a slow cooling rate (1 $K.min^{-1}$). The top two SEM images (Figs. 7.4 A & 7.4 B) are from the surface of the samples (without and with AgI). The AgI containing sample was seen to have delicate surfaces on top in comparison to samples without AgI which displayed a thicker surface. Also, the surface of samples with AgI seemed much more porous in comparison to non-AgI samples. The size of cracks on the surface seem larger in samples freeze-dried without AgI compared to AgI containing samples, however, a greater number of pores were found in samples with AgI. The cracks seen in lactose samples from vials (see Chapter 5) were not evident here.

Figs. 7.4 C & 7.4 D show the internal microstructure of cross-section of the sample from the top (just below the surface layer), while Figs. 7.4 E & 7.4 F display the vertical cross section and Figs. 7.4 G & 7.4 H show horizontal cross-sections of the

samples from the bottom of the trays. In terms of vertical cross section, the sample microstructures do not look significantly different; however, in case of internal ice crystal morphologies the samples are very variable in shape and size especially towards the top of the sample. Similar to lactose sample, the microstructure varies with the depth into the tray with larger ice crystal voids towards the top of the sample and smaller voids towards the bottom of the tray in both cases. Higher sub-cooling was experienced at the bottom of the sample, thus giving smaller crystals, and with larger ice crystals towards the top of the sample surface. Coffee samples freeze dried with AgI were found to have slightly larger ice crystal pores (left behind after drying) in comparison to non-AgI samples, especially towards the top of the sample.

There was less evidence of orientation and uniformity visible in the tray freeze dried samples, in terms of internal microstructure, than with lactose. This is thought to be due to the complex multi-component coffee system. It is possible that the metal tray having a better thermal conductivity than glass vials could influence freezing, however heat transfer through the base of the trays was seen to be good (small temperature differences) in either case. The metal would result in better heat transfer up the sides of the tray and so coffee near the tray sides is likely to freeze almost as quickly as the bottom layer. However, most samples were taken away from the tray sides. Therefore the lack of directionality seen in the SEMs is likely to be a material effect.

The above discussed microstructural features were used to understand its effect on primary drying rate and duration of freeze-drying of coffee with and without AgI with a slow cooling rate shown in Figs. 7.5 A, 7.5 B & Table 7.1. These figures display the experimental and estimated drying times determined from the freeze dryer and calculated from freeze drying microscope data respectively. The freeze-dryer primary drying times are calculated from the actual freeze drying temperature vs time plot (as shown in Fig. 7.1) while the estimated drying times are extrapolated from the a & b values (apparent edge resistance and resistance of dried layer) determined from the freeze drying microscope frontal distance vs time data.

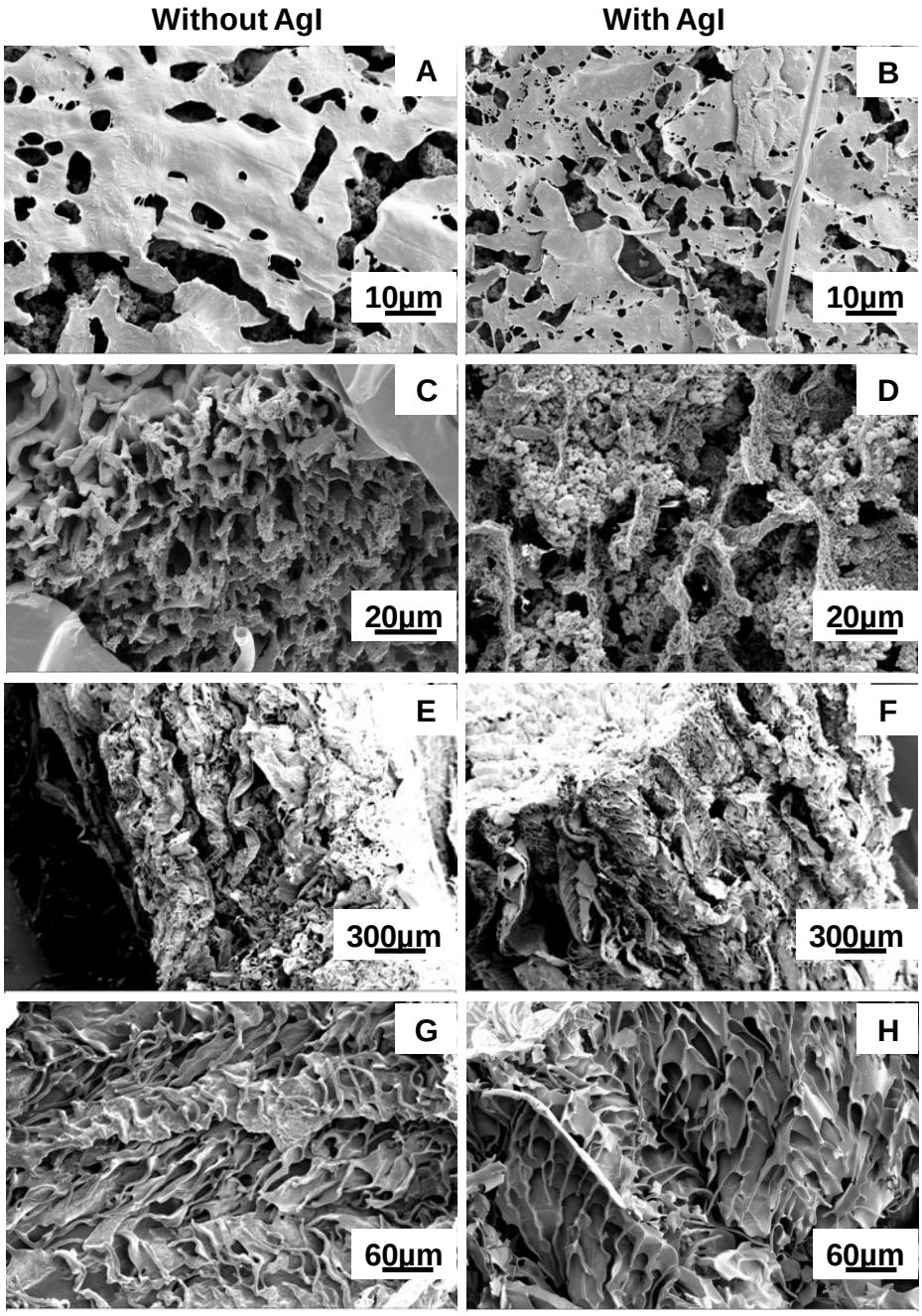

Figure 7.4: FEGSEM images of **10% coffee** frozen at a cooling rate of **1 K.min^{-1}** and freeze dried at -40˚C at 10 Pa without AgI (left) and with AgI (right). **A** & **B.** Surface microstructure. **C** & **D.** Comparison of cross-sectional internal microstructure of samples collected from the top layer. **E** & **F.** Vertical cross-sectional microstructure. **G** & **H.** Comparison of cross-sectional internal microstructure of samples collected near the bottom of the trays. Images represent at least four repeat runs in each case.

Table 7.1 Freeze drying times for 10% coffee with and without AgI for the different cooling rates obtained experimentally from freeze dryer (1 K.min^{-1} and liquid nitrogen quenching) and estimated from freeze drying microscopy (2 K.min^{-1}, 10 K.min^{-1} and 50 K.min^{-1}). Values represent average of at least four repeat runs with standard deviation as error for both estimated and experimental drying times.

Freeze drying time		Sample depth (mm) / Cooling rate (K.min^{-1})	3	7	11
Experimental (hrs)	Without AgI	1	13.0±3.3	43.1±15.0	65.5±0.3
		LN_2 quenching	37.6±2.2	54.9±10.0	124.7±32.4
	With AgI	1	12.1±4.7	36.7±6.0	59.5±2.2
		LN_2 quenching	40.8±15.3	56.5±7.4	91.1±13.6
Estimated (hrs)	Without AgI	2	21.9±20.5	111.9±108.5	271.4±265.9
		10	97.6±26.5	521.8±141.4	1282.2±347.4
		50	100.4±50.4	541.1±273.0	1332.5±673.4
	With AgI	2	12.1±6.4	59.7±33.5	143.2±81.8
		10	87.1±49.6	467.4±265.4	1149.5±652.3
		50	32.1±20.3	169.9±107.8	416.3±264.2

Primary drying times of AgI containing coffee samples were found to be slightly lower (i.e., faster) than those of non-AgI samples. This behaviour was attributed to slightly larger ice crystal size in AgI containing samples resulting in quicker and easier removal of ice in the form of water vapour. Experimental times were found to deviate from estimated drying times obtained from freeze drying microscopy. Sublimation was quicker in the actual freeze drying process, particularly so in samples cooled at 2 K.min^{-1} under the freeze drying microscope freeze dried without AgI.

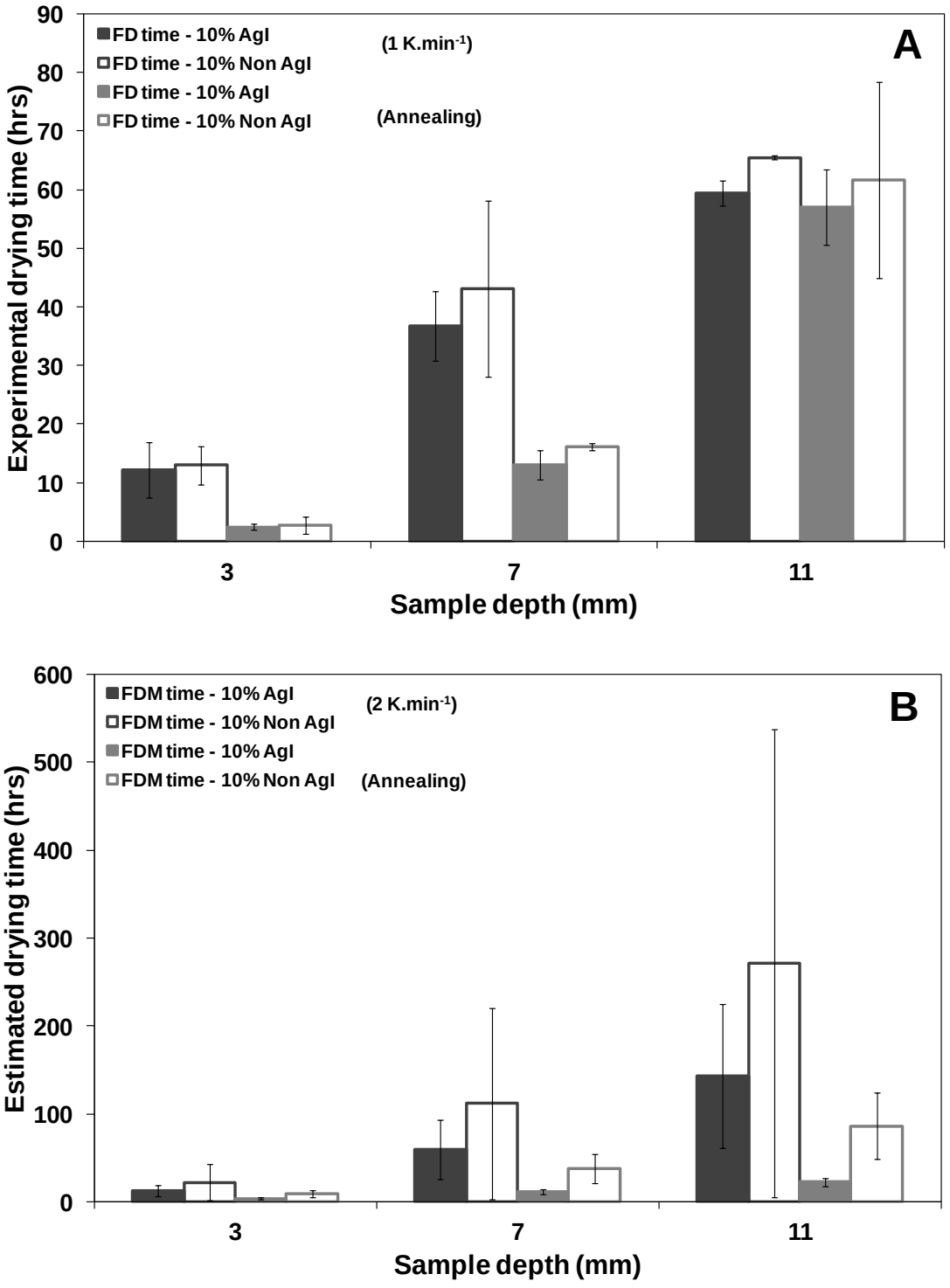

Figure 7.5: A. Experimental tray drying times for freeze drying of **10% coffee** at -40˚C and 10 Pa obtained that had either been slow cooled at a rate of **1 K.min^{-1}** or subjected to an additional **annealing** step, with or without AgI **B.** Drying times for the same distances estimated from *a* and *b* values from equivalent FDM data at -40˚C at 1 Pa for **10% coffee** (with or without AgI) frozen previously either at a cooling rate of **2 K.min^{-1},** or via an **annealing profile at -10˚C** and then frozen at a cooling rate of 1 K.min^{-1}. Values represent average of at least four repeat runs with standard deviation as error for both estimated and experimental drying times.

Annealing: as with lactose samples, coffee samples were also subjected to an annealing process. Fig. 7.6 shows the FEGSEM images of 10% coffee without and with AgI annealed at -10˚C for 2 hours in trays. Figs. 7.6 A & 7.6 B show the internal microstructure beneath surfaces and Figs. 7.6 C & 7.6 D show the vertical cross-sections of annealed sample without and with AgI after freeze drying. These also show magnified images of the edge of sample (at the top) and microstructure of the 'sheets' seen in the vertical cross section in both cases. Figs. 7.6 E & 7.6 F also show the magnified images of the internal morphology of observed in the vertical cross-section in Figs. 7.6 C & 7.6 D. Figs. 7.6 G & 7.6 H show the internal microstructure of the annealed samples without and with AgI at the bottom of the tray.

As is clear from Fig. 7.5, annealed samples seem to slightly take lesser time for sublimation in comparison to other slow cooling rate. It is obvious from Fig. 7.6 C & 7.6 D that surface layer becomes thicker with the longer duration of freezing process in an annealing experiment in comparison to the simple cooling treatment (Fig. 7.4 A & 7.4 B). However, the top surface was found to be quite porous and just beneath the surface many small ice crystal voids were observed (ice crystals forged through the thick top layer).

Both the vertical cross section and internal microstructure seem quite similar when compared between AgI and non-AgI samples. The use of AgI seems to have little or no effect on the ice crystal re-formation and hence the morphology is somewhat uniform in both samples. The ice crystal voids seem randomly formed thus showing to the fact that during annealing, the ice crystals are reformed from previously melted ice crystals. In comparison to Fig. 7.4, the size of the ice crystal voids is smaller in comparison at the top of the sample (Figs. 7.6 A & 7.6 B), though larger in number and larger in size at the bottom of the sample (Figs. 7.6 G & 7.6 H).

Estimated drying times of annealed 10% coffee sample from FDM (Table 7.2) show good prediction when compared with actual experimental drying times indicating that the microstructure in the two cases are similar. Standard deviation displayed in Table 7.2 for the estimated drying times were also extrapolated from the error calculated from FDM data.

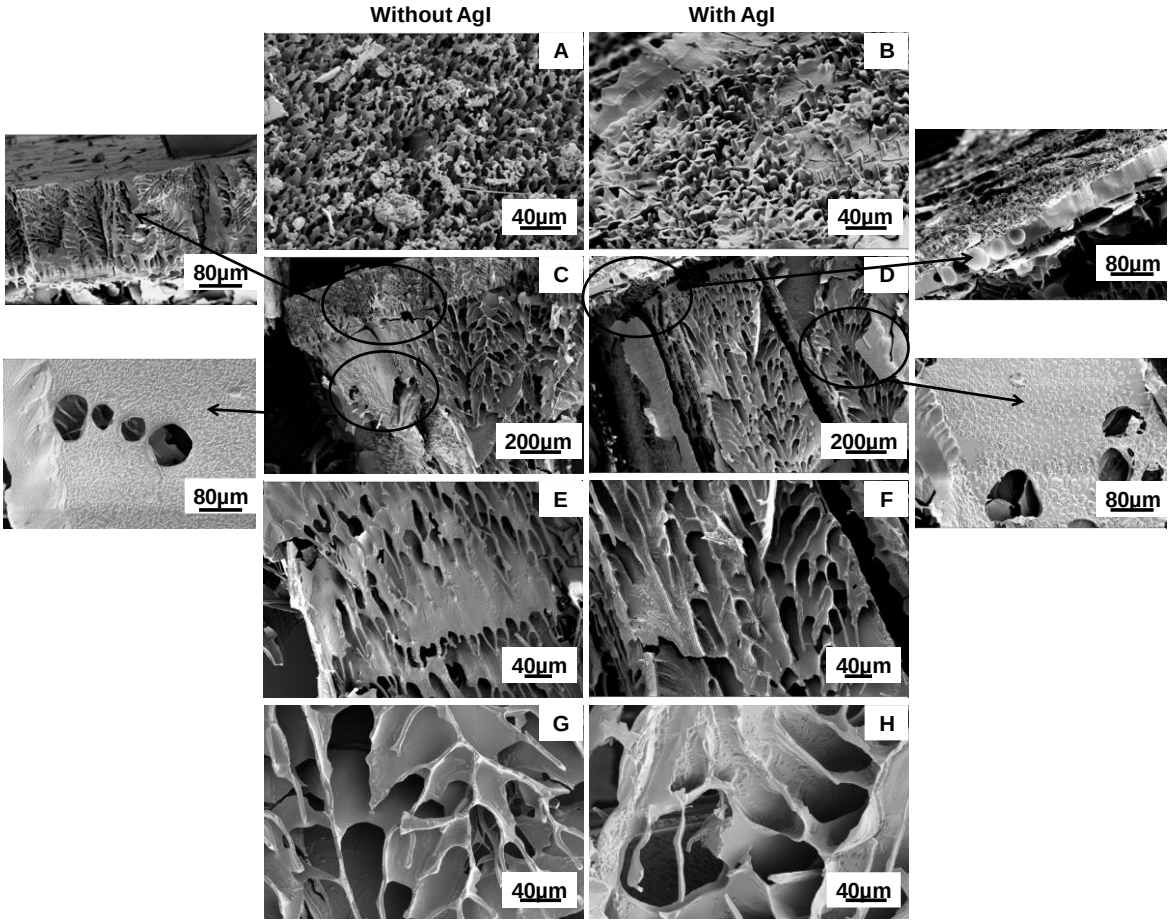

Figure 7.6: FEGSEM images of **10% coffee** frozen at a cooling rate of 1 K.min^{-1} and **annealed at -10˚C** and again cooled at 1 K.min^{-1} and freeze dried at -40˚C at 10 Pa without AgI (left) and with AgI (right). **A** & **B.** Surface microstructure. **C** & **D.** Edge layer microstructure of samples collected from the top layer. **E** & **F.** Vertical cross-sectional microstructure. **G** & **H.** Internal microstructure of samples collected from the bottom layer of the trays. Images represent at least four repeat runs in each case.

The estimated times of 10% coffee samples with and without AgI annealed under the microscope were found to be quite close to the experimental freeze drying times of the equivalent non-annealed samples although they were still slightly higher (Fig 7.5 A). The main reason was this behaviour was thought to be due to ice crystal size similarity between annealed samples of the microscope to the ones seen in Fig. 7.4 C & 7.4 D.

Table 7.2 Freeze drying times for 10% coffee with and without AgI for the different cooling rates obtained experimentally from freeze dryer (annealing at -10˚C) and estimated from freeze drying microscopy (annealing with profile IV). Values represent average of at least four repeat runs with standard deviation as error for both estimated and experimental drying times.

Freeze drying time	Cooling profile \ Sample depth (mm)		3	7	11
Experimental (hrs)	Annealing (at -10˚C)	Without AgI	2.7±1.5	16.1±0.5	61.7±16.8
		With AgI	2.4±0.5	13.1±2.6	57.0±6.5
Estimated (hrs)	Annealing (Profile IV on FDM)	Without AgI	9.2±3.8	38.1±16.5	85.9±37.9
		With AgI	3.63±1.1	11.3±2.8	22.3±4.7

Liquid nitrogen quenching: The effect of fast cooling rate on the ice crystal morphology and hence on the primary drying behaviour was also investigated. To achieve this, the 10% coffee solution containing trays were frozen using LN_2 quenching (dipping the trays into liquid nitrogen).

Fig. 7.7 shows the FEGSEM images of 10% coffee without and with AgI frozen by liquid nitrogen quenching and freeze dried on a pre-cooled shelf at -40˚C and 10 Pa pressure. Figs. 7.7 A & 7.7 B show the surface of the samples without and with AgI after freeze drying, frozen with a fast cooling rate respectively. The bigger cracks observed in the AgI containing samples were formed during the preparation process (collection of samples from trays for sputtering) for performing FEGSEM and not due to the freeze-drying process. In comparison to the other slow cooling rates the surface morphology of these samples is quite stable and the pores or cracks on the surface are not as large (in size and number) as in Fig. 7.4 A & 7.4 B (1 $K.min^{-1}$ cooling rate).

Figs. 7.7 C & 7.7 D show the microstructure just above the bottom layer of the samples while Figs. 7.7 E & 7.7 F display the vertical cross-sections and Figs. 7.7 G & 7.7 H show the internal morphology from the top of the sample. The microstructures of vertical and internal cross-section are different to each other and this shows clear evidence of directionality of crystallisation. The internal microstructure was also seen to vary throughout the tray, being smaller at the bottom and larger in size at the top.

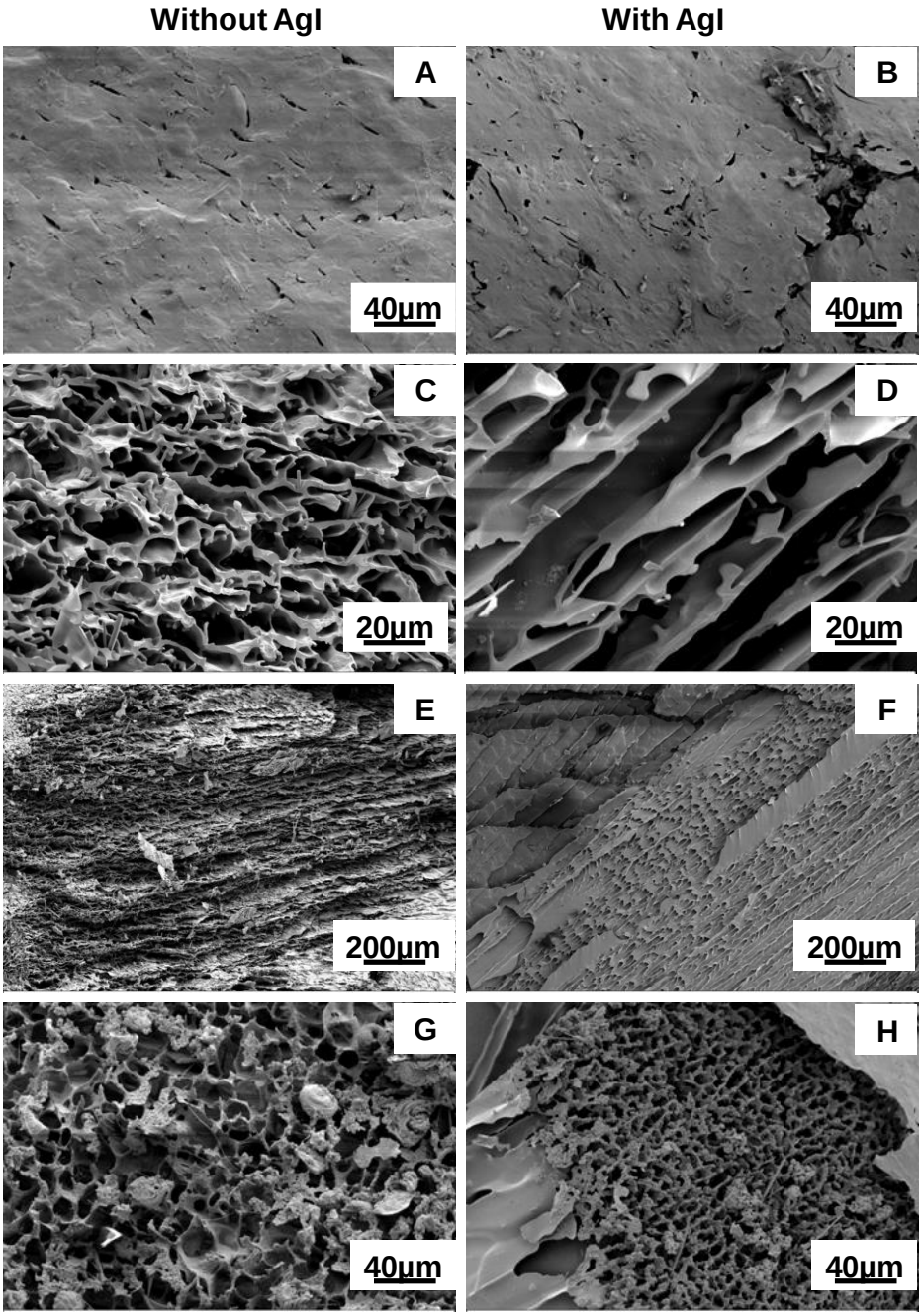

Figure 7.7: FEGSEM images of **10% coffee,** frozen by **liquid nitrogen quenching** and freeze dried at -40˚C at 10 Pa without AgI (left) and with AgI (right). **A** & **B.** Surface microstructure. **C** & **D.** Internal microstructure of samples collected from the top layer. **E** & **F.** Vertical cross-section microstructure observed under the surface layer. **G** & **H.** Cross-sectional microstructure of sample from the bottom layer. Images represent at least four repeat runs in each case.

The size of these voids was found to be smaller than the ice crystal sizes of the other slower cooling rates. The use of AgI did seem to affect the freezing process especially towards the top of the sample surface with larger ice crystal voids in size than

samples frozen without AgI. In both cases, the crystals at the bottom of the tray were observed to be random since the cooling rate was too fast, however, since significant temperature gradients would have developed during freezing, the ice crystals were seen to grow in a directional manner rather than from all sides of the vial as seen in case of lactose.

For LN_2 quenched samples, it was difficult to relate primary drying rates with structural morphology of samples. The AgI containing samples do not seem different from samples without AgI when comparing the primary drying times (see Fig. 7.8 and Table 7.1), it shows that the latter is at par with the former except near the bottom of the tray. The AgI containing sample was seen to dry faster only at this depth and it was difficult to pin point the exact reason for this behaviour. The plot in Fig. 7.8 A was also compared to the primary drying duration of Fig. 7.5 A and it shows that in both cases (AgI and non-AgI) the drying times are higher than the range (0-70 hrs) when compared to other slow cooling rates at all the sample depths investigated. This is an expected trend as the ice crystal void sizes are smaller in this case than those seen in other cooling rates at all sample depths.

Apart from comparison with drying times of other cooling rates, Figs. 7.8 A & 7.8 B also compare the primary drying times determined from the freeze dryer data and the drying times obtained from extrapolating from *a* and *b* values obtained from the freeze drying microscopy data for the cooling rates – 10 $K.min^{-1}$ and 50 $K.min^{-1}$. All the drying time predictions were much higher than the actual experimental drying times obtained from the freeze dryer data. This was not observed in the case of lactose. This must presumably due to different microstructures between the FDM and tray samples, with presumably greater directionality with the tray samples. There may also be cracking occurring with the coffee tray samples as the samples themselves are much larger and cracking may arise as a result of large thermally induced stresses building up.

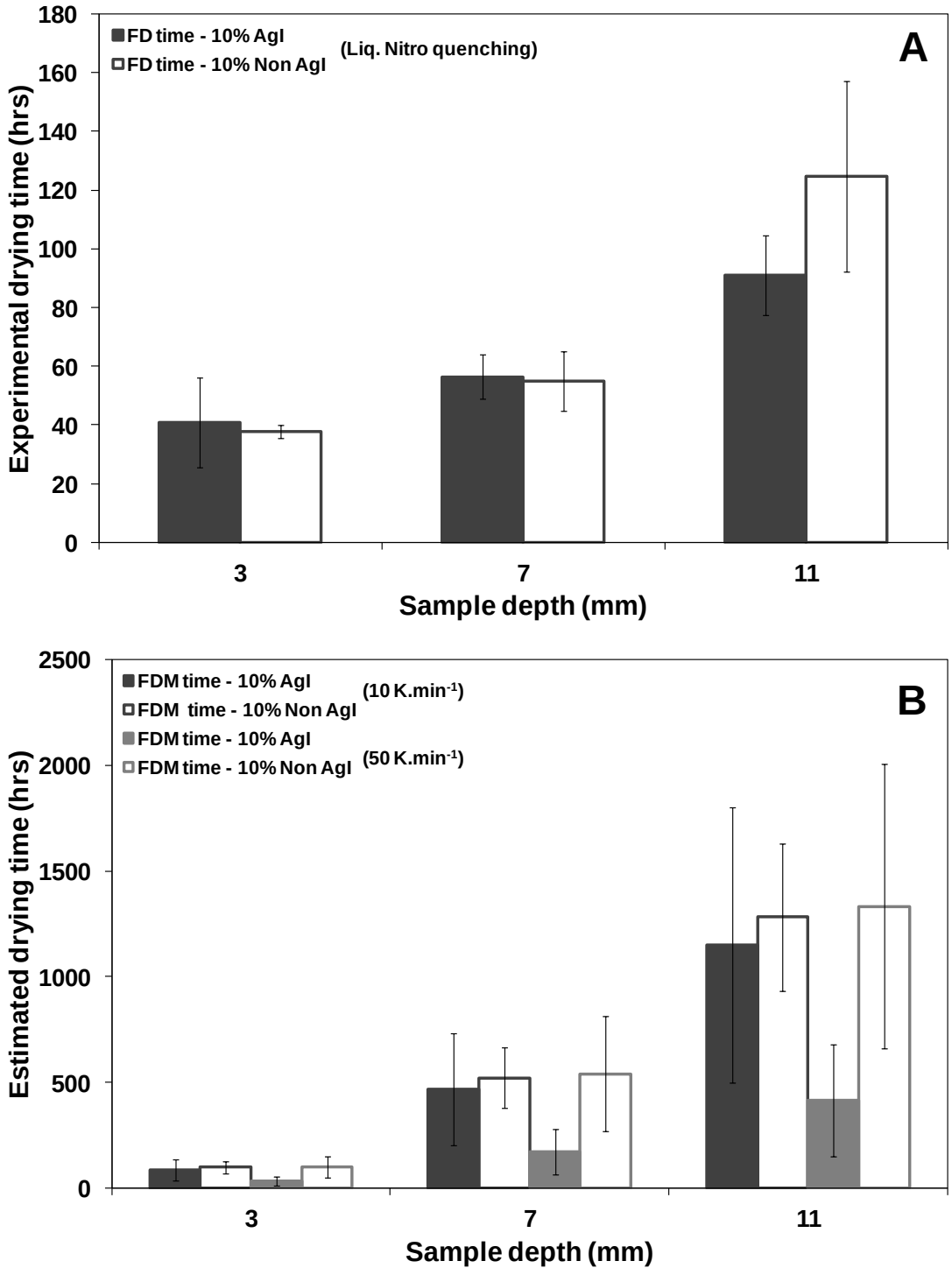

Figure 7.8: A. Experimental tray drying times at -40˚C and 10 Pa obtained for **10% coffee** that had previously been frozen using **liquid nitrogen quenching**, either with or without AgI **B.** Drying times for the same distances estimated from *a* and *b* values from equivalent FDM data at -40˚C at 1 Pa for **10% coffee** samples (with or without AgI) that had been previously frozen either at a cooling rate of **10 K.min^{-1}**, or **50 K.min^{-1}**. Values represent average of at least four repeat runs with standard deviation as error for both estimated and experimental drying times.

7.3.3 Effect of freezing profile (50% Coffee)

Slow cooling: The microstructure of 50% coffee solution, frozen in trays at 1 K.min^{-1} and freeze-dried at -40˚C and 10 Pa, is presented in Fig. 7.9. The surface morphology of 50% coffee freeze dried without and with AgI is displayed in Figs. 7.9 A & 7.9 B.

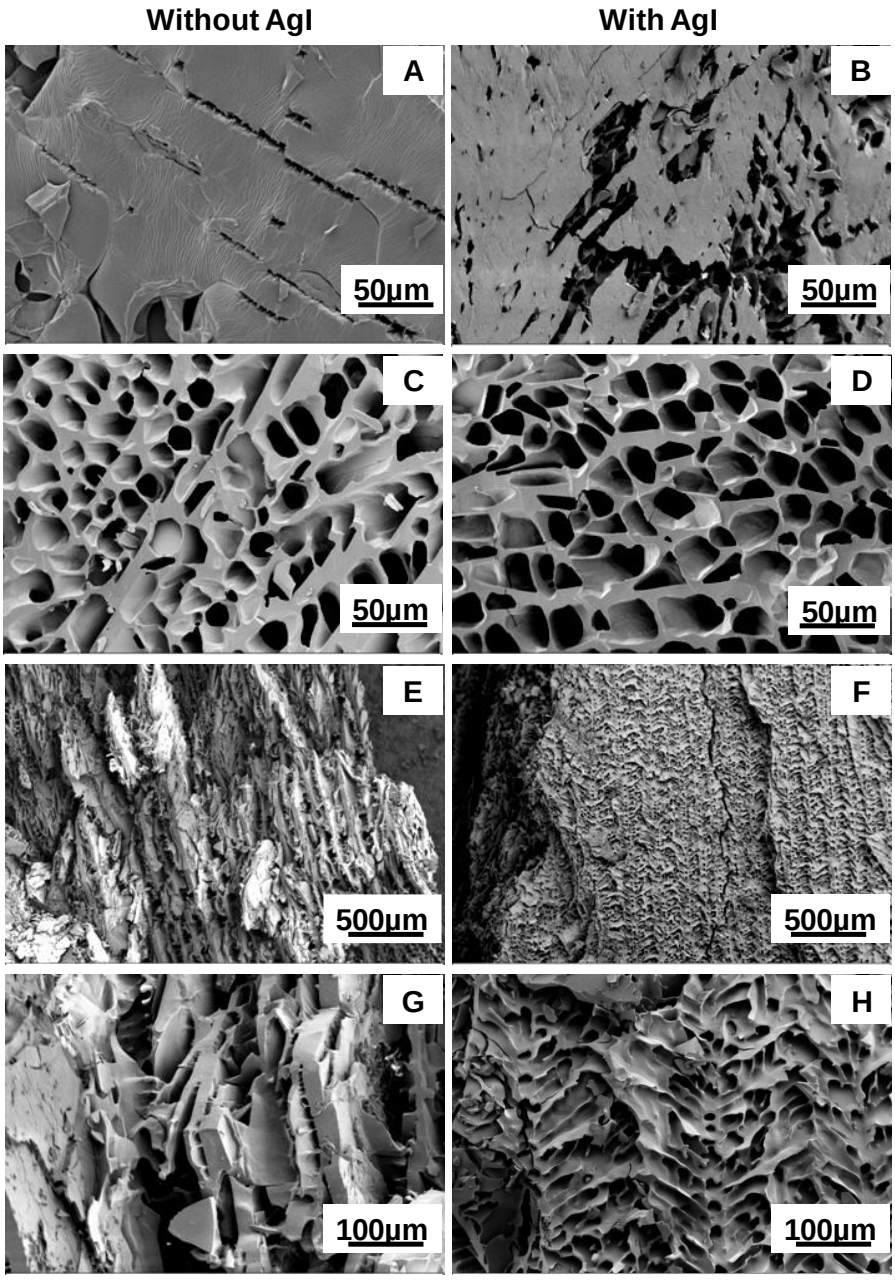

Figure 7.9: FEGSEM images of **50% coffee** frozen at a cooling rate of **1 K.min^{-1}** and freeze dried at -40˚C and 10 Pa with and without AgI. **A** & **B.** Surface microstructure. **C** & **D.** Cross-sectional internal microstructure of samples collected near the top layer of the samples. **E** & **F.** Vertical cross-sectional microstructure. **G** & **H.** Vertical cross-sectional microstructure (magnified).Images represent at least four repeat runs in each case.

Figs. 7.9 C, 7.9 D, 7.9 E & 7.9 F show the vertical cross-section of 50% coffee without and with AgI at different magnifications while Figs. 7.9 G & 7.9 H shows the internal structure from samples at the top beneath the surface layer. The surface layer of samples without AgI is observed to be thicker and with fewer pores or cracks on the surface than 50% coffee with AgI which looks much more fragile and porous at the surface. The vertical and horizontal cross sections of microstructure appear quite different (horizontal is honeycombed whereas vertical shows flat surfaces) which is evidence of directionality of crystallisation. AgI containing samples were found to have slightly more uniformity in structure compared to non-AgI samples which was quite random throughout the cross-section. However, the internal cross-section of 50% coffee with and without AgI at the top is quite random in both cases, though AgI containing sample has a slightly more open and porous structure than samples without AgI (seem denser with thicker coffee boundaries). As with 10% coffee samples the pore sizes are larger towards the top of the samples, but pore sizes are consistently lower for the 50% samples.

Table 7.3 Freeze drying times for 10% coffee with and without AgI for the different cooling rates obtained experimentally from freeze dryer (1 K.min^{-1}, annealed at -10˚C and LN_2 quenching) and estimated from freeze drying microscopy (2 K.min^{-1}, 10 K.min^{-1} and 50 K.min^{-1}). Values represent average of at least four repeat runs with standard deviation as error for both estimated and experimental drying times.

Freeze drying time		Sample depth (mm) / Cooling rate(K.min^{-1})	3	7	11
Experimental (hrs)	Without AgI	1	5.2±0.7	66.6±8.2	123.1±1.7
		Annealing at -10˚C	42.2±5.1	80.9±16.0	148.2±2.4
		LN_2 quenching	27.8±9.1	75.9±29.7	158.5±32.0
	With AgI	1	5.0±0.7	66.0±16.6	108.7±11.3
		Annealing at -10˚C	58.2±17.4	76.3±6.9	129.2±0.6
		LN_2 quenching	10.3±4.1	22.2±10.6	79.3±29.9
Estimated (hrs)	Without AgI	2	965.4±471.9	5221.0±2550.3	12869.0±6285.2
		10	888.9±356.4	4800.6±1928.7	11828.1±4754.9
		50	1309.7±335.0	7092.7±1804.6	17489.1±4443.2
	With AgI	2	85.1±48.3	454.3±259.4	1115.8±638.5
		10	440.9±171.2	2369.6±924.6	5830.9±2278.3
		50	249.8±145.2	1331.9±777.0	3270.1±1909.6

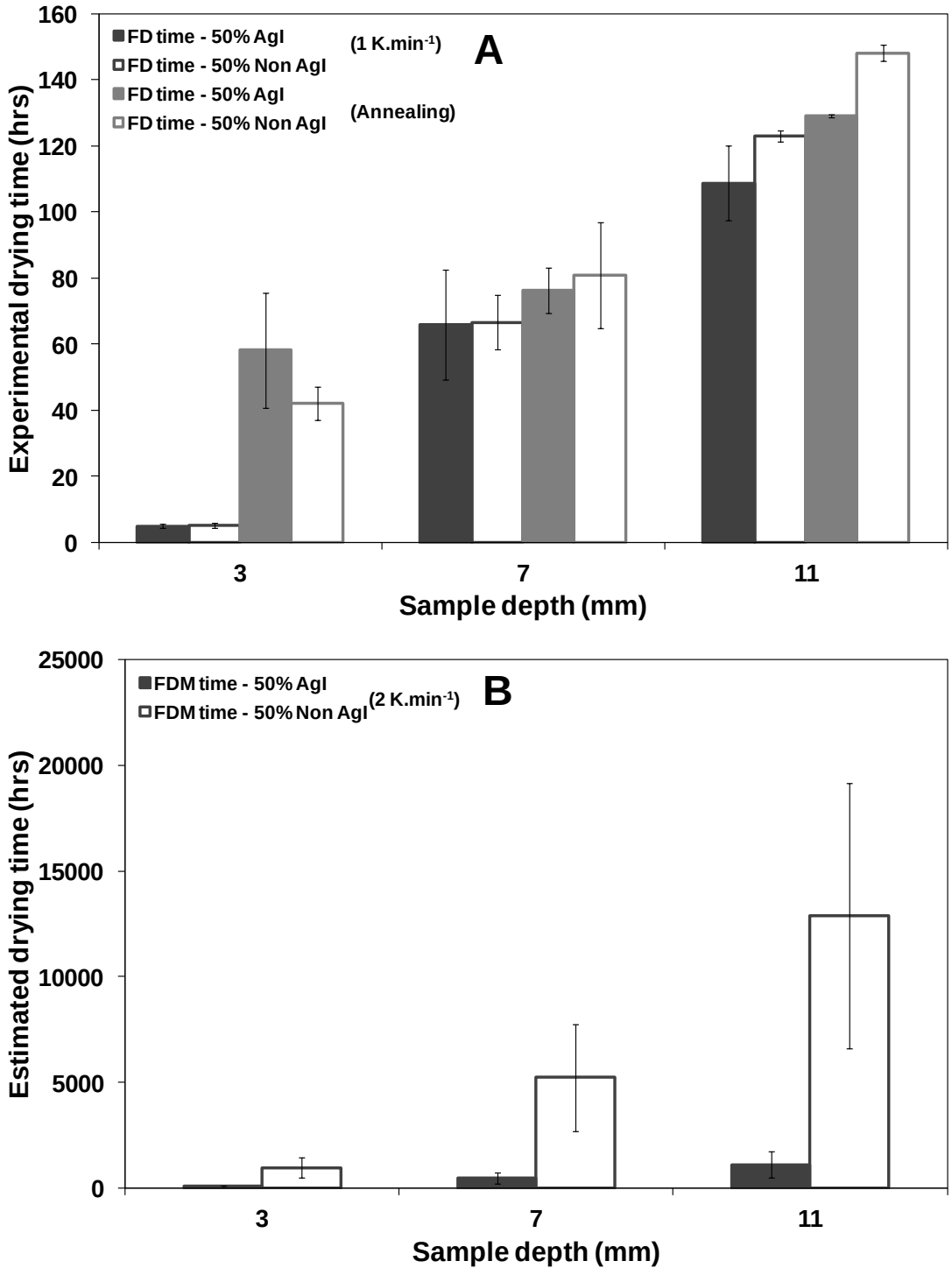

Figure 7.10: A. Experimental tray drying times at -40˚C and 10 Pa obtained for **50% coffee** that had been slow cooled at a rate of **1 K.min^{-1}**, either with or without AgI **B.** Drying times for the same distances estimated from *a* and *b* values from equivalent FDM data at -40˚C at 1 Pa for **50% coffee** samples (with or without AgI) frozen previously either at a cooling rate of **2 K.min^{-1}**. Values represent average of at least four repeat runs with standard deviation as error for both estimated and experimental drying times.

Figs. 7.10 A, 7.10 B and Table 7.3 displays the experimental and estimated drying times of 50% coffee freeze dried without and with AgI with slow cooling rates respectively. Experimental drying times were calculated from the freeze dryer temperature vs time plot while estimated drying times were calculated from *a* & *b* values obtained from FDM data for 50% coffee at the three different depths investigated. Experimental primary drying times of 50% coffee with and without AgI for cooling rate of 1 $K.min^{-1}$ did not display any significant difference between both cases except at 11 mm depth from the top (as was also seen in case of 10% coffee slow cooling). The reason for this difference at the bottom of the tray was not clear with respect to internal morphology as the microstructure was similar to the ice crystal voids seen at the top of the trays. However, comparison of estimated and experimental primary drying durations show a vast difference and again, this difference was thought to be due to microstructure.

Annealing: Along with this slow cooling rate (1 $K.min^{-1}$), the effects of annealing on the microstructure and thus on the primary drying duration on freeze drying of 50% coffee with and without AgI were also investigated. Figs. 7.11 A & 7.11 B show the surface of the freeze dried samples which display the magnified images of the pores on the surface of samples in both cases. Figs. 7.11 C & 7.11 D display the vertical cross-section of samples in both cases and magnified microstructure of the same while Figs. 7.11 E & 7.11 F show the internal morphology of 50% coffee samples without and with AgI from the middle of both trays. The comparison of horizontal and vertical cross sections clearly indicates a directionality of solidification in the vertical direction in this case also like lactose samples.

Figs. 7.11 G & 7.11 H display the bottom layer of the samples freeze-dried in trays. It is evident from all these images, the surface morphology, vertical microstructure and internal structures do not exhibit any difference with respect to presence or absence of AgI. The surface microstructures also display enhanced thickness and lack of porosity due to annealing process in comparison to surface observed in Figs. 7.9 A & 7.9 B. The pores or cracks observed were thought to be pores formed due to forced water vapour expulsion from the sample. The internal microstructure showed smaller ice crystal voids compared to the other slow cooling rate investigated.

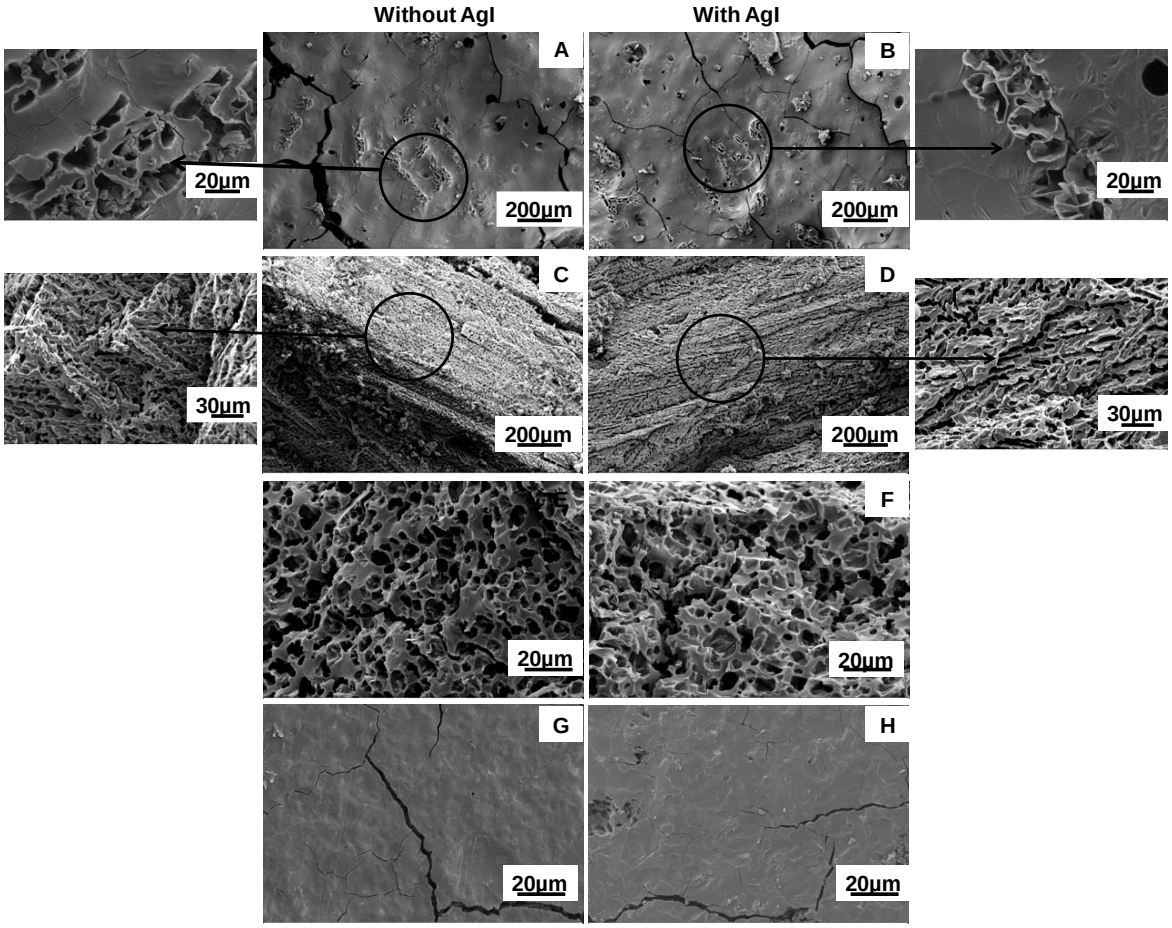

Figure 7.11: FEGSEM images of **50% coffee** frozen at a cooling rate of 1 K.min^{-1}, then **annealed at -10˚C** and again cooled at 1 K.min^{-1} before finally freeze dried at -40˚C at 10 Pa without (left) and with AgI (right). **A** & **B.** Surface microstructure. **C** & **D.** Vertical cross-sectional microstructure. **E** & **F.** Cross-sectional internal microstructure of samples collected near the bottom layer. **G** & **H.** Bottom layer microstructure. Images represent at least four repeat runs in each case.

The primary drying duration observed in Fig. 7.10 A and Table 7.3 shows the effect of these microstructural features caused due to annealing. Primary drying durations of annealed samples with and without AgI were found to be longer than those without annealing. The main reason for this difference was attributed to the thick surface morphology and smaller ice crystal sizes seen in annealed samples compared to the other cooling rate microstructure displayed in Fig. 7.9.

Comparisons with predicted drying times from FDM data are difficult because it was not possible to successfully freeze dry 50% annealed samples in the FDM (see Chapter 6). Annealing of 50% coffee with and without AgI under FDM did not achieve complete recrystallization of the samples after melting resulting in absence of a

sublimation front in the samples. Comparison of experimental primary drying durations and estimates from simple cooled FDM experiments (see Fig. 7.10 A & 7.10 B) display vast differences in the two, as was seen in previous cooling rates and the reasons were again attributed to microstructural differences (such as directional solidification).

Liquid nitrogen quenching: To investigate the effect of a faster cooling rate on the primary drying of 50% coffee solutions (with and without AgI) in trays were subjected to LN_2 quenching by dipping the trays in a container of liquid nitrogen. The samples were then transferred to a pre-cooled freeze dryer shelf (at -40˚C) and subjected to sublimation at 10 Pa vacuum pressure.

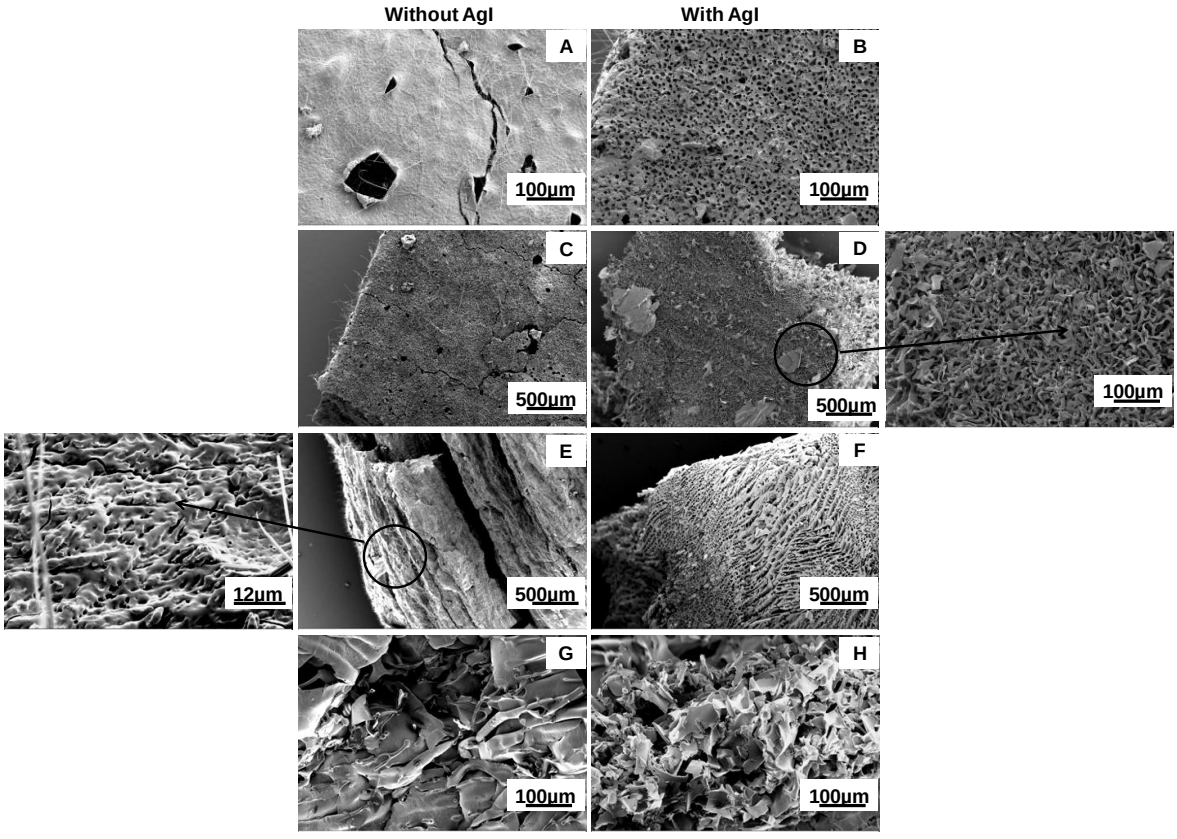

Figure 7.12: FEGSEM images of **50% coffee** frozen by **liquid nitrogen quenching** and freeze dried at -40˚C at 10 Pa without (left) and with AgI (right). **A** & **B.** Surface microstructure. **C** & **D.** Cross-sectional microstructure observed under the surface layer. **E** & **F.** Vertical cross-section microstructure under the surface layer. **G** & **H.** Internal microstructure of samples collected from the bottom layer of the samples. Images represent at least four repeat runs in each case.

Fig. 7.12 shows the FEGSEM images of coffee (with and without AgI) frozen by LN_2 quenching and freeze dried in trays. Fig. 7.12 A & 7.12 B shows the surface of 50% coffee (initial concentration) without and with AgI respectively. The surface of the AgI containing sample is quite porous in comparison to samples without AgI which seems to be a dense layer at the surface and lacks the pores or cracks clearly visible in Fig. 7.12 A.

The internal morphologies of the surface below the top layer of the samples without and with AgI are displayed in Figs. 7.11 C & 7.11 D. The vertical cross sections of the samples are shown in Figs. 7.11 E & 7.11 F while 7.11 G & 7.11 H show the internal microstructure of samples obtained from near bottom of the trays. Samples containing AgI were found to have much more uniform ice crystal void lattice especially visible in the vertical cross section while samples freeze dried without AgI were found to have random morphology throughout the trays. The vertical cross sections show much larger pores in this cross section which indicates some directionality of crystallisation. The top of the samples display similar microstructure with small ice crystal voids while at the bottom of the tray, the microstructure was so fragile and was found to lack ice crystal voids and seem concentrated with coffee material (in both cases).

When this microstructure is compared to that of 10% coffee (Fig. 7.4, 7.6 & 7.7), it is evident that due to higher initial concentration, the morphology of 50% coffee is denser and has smaller ice crystal voids. The effect of these microstructural features will be discussed with respect to primary drying times calculated from the freeze dryer.

Fig. 7.13 A and Table 7.3 also shows difference between primary drying times between 50% coffee with and without AgI. It again displays that AgI does affect the microstructure and also the surface morphology of the sample. AgI containing samples as shown and discussed above reveal larger ice crystal voids and much more open and porous structure thereby resulting in significant lower sublimation durations of AgI containing samples compared to samples without AgI.

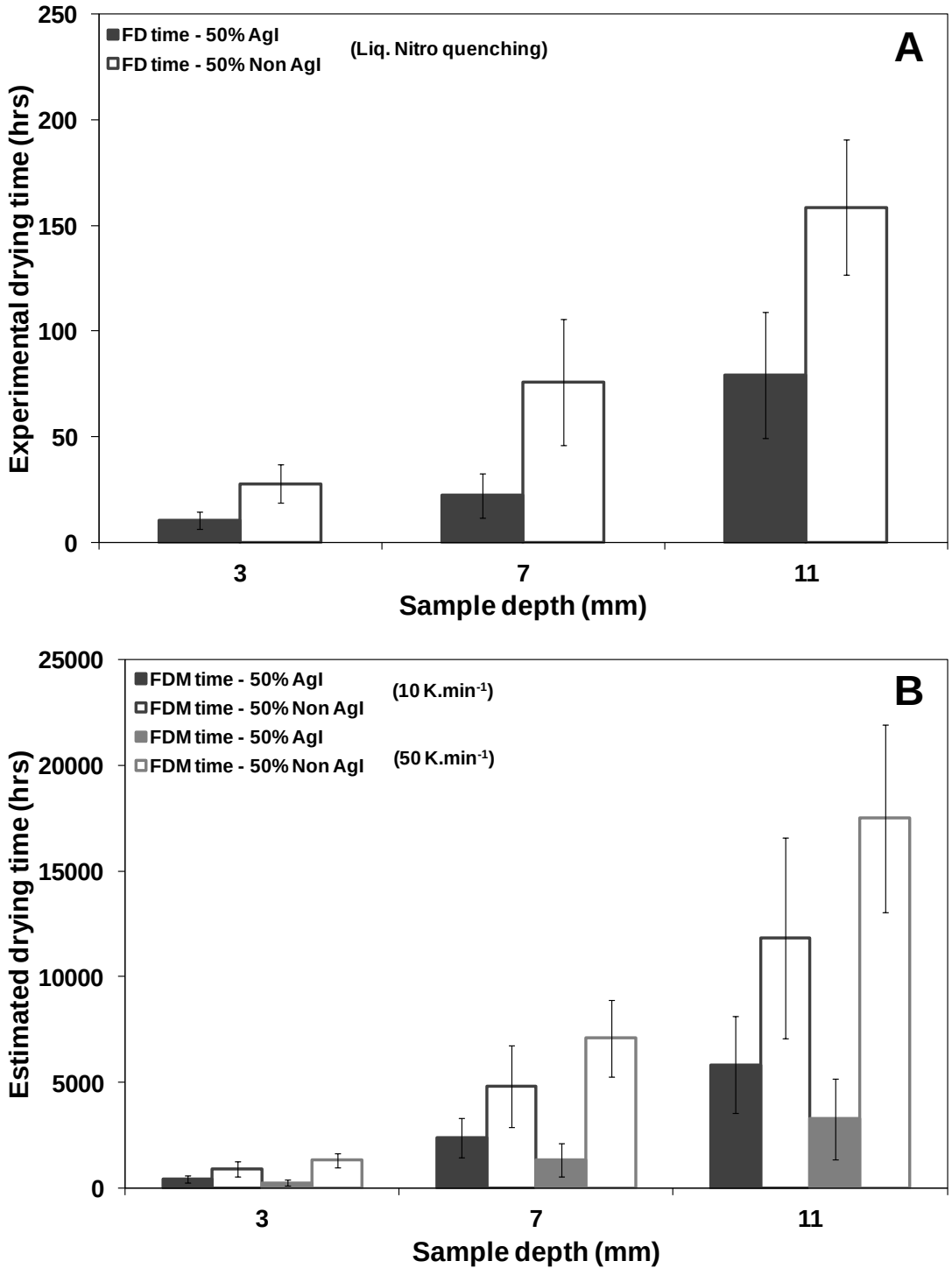

Figure 7.13: A. Experimental tray drying times at -40˚C and 10 Pa obtained for **50% coffee** that had previously been frozen using **liquid nitrogen quenching**, either with or without AgI **B.** Drying times for the same distances estimated from *a* and *b* values from equivalent FDM data at -40˚C at 1 Pa for **50% coffee** samples (with or without AgI) that had been previously frozen either at a cooling rate of **10 K.min^{-1}**, or **50 K.min^{-1}**. Values represent average of at least four repeat runs with standard deviation as error for both estimated and experimental drying times.

When the drying times of 50% coffee freeze dried with and without AgI subjected to a fast cooling rate (by LN_2 quenching), seen in Fig. 7.13 A & 7.13 B, it was observed that even in this case, the experimental and estimated drying times were significantly different as seen for the slow cooling rates. The experimental drying times were found to be much lower to the estimated times and the reason for this difference is again likely to be due to microstructural differences due to the larger volume of sample and predominantly directional solidification in the vertical direction (in which mass transfer occurs) in the tray drying experiments, but not in the FDM. The actual drying times compared for the slow and fast cooling rate does point out that slow cooling rate samples dry faster when compared to samples frozen with faster cooling rate. The reason for this behaviour was thought to be due the difference in morphology seen for the two cooling rates – larger crystal voids in slow cooling and smaller crystal voids in fast cooling.

Apart from comparison between the estimated and experimental drying times, freeze drying in trays was also studied based on the different cooling profiles used – slow cooling, fast cooling and annealing for both 10% and 50% Coffee at the three different sample depths -3 mm, 7 mm and 11 mm. Fig. 7.14 shows the drying time comparison of 10% and 50% coffee samples subjected to different cooling profiles with and without AgI.

In both cases, AgI containing samples displayed quicker freeze-drying than samples without AgI for all cooling rates and sample depths except 50% annealed coffee sample at 3mm depth. It further confirms the results observed in FDM that AgI facilitates quicker water vapour removal due to large ice crystals formed. The unusual result in the case of 50% annealed coffee was thought to be due to the high solid content in the solution and long duration of annealing process resulting in thicker edge irresepective of the presence of AgI.

In case of 10% coffee, effect of cooling rates – slow, fast cooling and annealing on sublimation duration at three sample depths was displayed in Fig. 7.14 A, 7.14 B & 7.14 C. The fast cooling rate investigated shows slower drying at all depths in comparison to both slow cooling and annealing rates. It was thought to be due to larger ice crystals formed in the latter case due to the long duration available for ice

crystals to grow in size and thus allowing faster water vapour removal. Annealing experiments displayed almost two times quicker drying than slow cooling rate investigated. This behaviour was consistent with the annealing experiments studied under FDM and also with those published in literature (Searles *et al.,* 2001; Abdelwahed *et al.,* 2006b and Arshad *et al.,* 2014). All the research published displays the enhanced sublimation rate of different annealed samples such as Hydroxyethyl starch, maltodextrin and freeze drying of nanocapsules.

In case of 50% coffee, the cooling rates did not display consistent pattern in the effect on sublimation duration. However, faster cooling did display faster sublimation especially in AgI containing samples compared to the other cooling rates investigated. Annealing did not seem to enhance sublimation rate and was an unusual behaviour since annealing is expected to increase the amount of ice crystals present in the sample and thus causing quicker water vapour removal. The main reason for this behaviour was thought to be due to the high solute concentration and thick surface microstructure displayed by annealed sample in comparison to other cooling rates investigated thus resulting in drying time to be slower in initiation and thus through the rest of the sample.

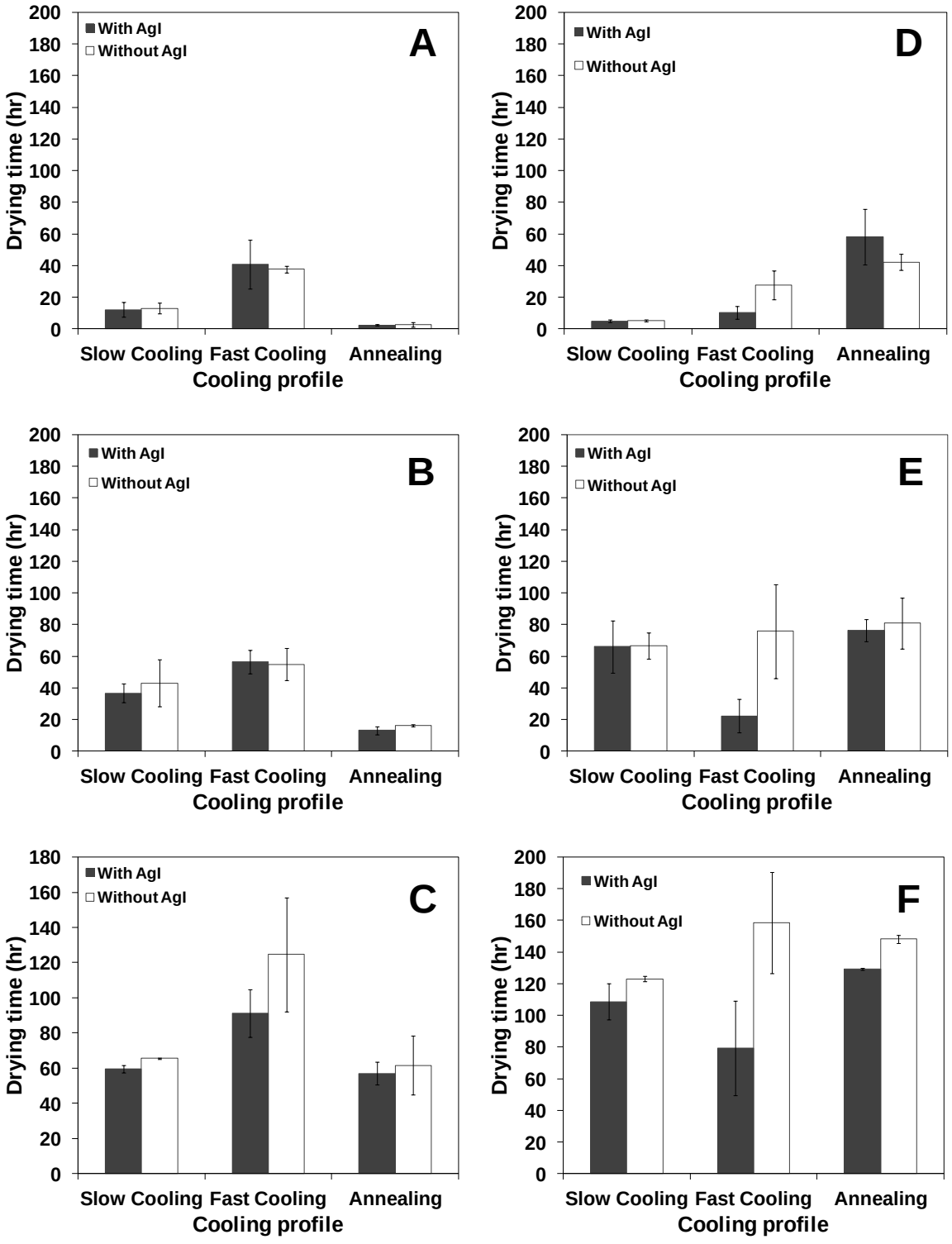

Figure 7.14: Effect of cooling profiles – slow, fast cooling and annealing on the drying times at different depth of the sample. **A. & D.** 3 mm. **B. & E.** 7mm. **C. & F.** 11mm for 10% Coffee and 50% Coffee respectively. Values represent average of at least four repeat runs with standard deviation as error for both estimated and experimental drying times.

7.3.4 Effect of cooling profile (50% coffee – aerated)

Freeze drying of coffee with aeration of the soluble coffee extract was also investigated. In the industrial freeze drying process for coffee, aeration is one of the key steps performed. The process of aeration improves the rehydration properties of the dried product considerably and also generates the 'frothy' characteristics of the final brewed product. By also increasing the porosity of the solid, it also improves the rate of freeze drying. In this instance, the effect of aeration on microstructure of the frozen material and hence on primary drying duration was studied.

50% coffee was aerated and two different cooling profiles –slow cooling (1 $K.min^{-1}$) and fast cooling (liquid nitrogen quenching) were investigated. Fig. 7.15 shows the microstructure of aerated 50% coffee without and with AgI frozen at -40˚C and freeze dried at 10 Pa. Figs. 7.15 A & 7.15 B display the surface morphology of the samples without and with AgI respectively. The surfaces in both cases are quite porous with water vapour expelled through the surface from pores where bubbles were present on the surface slightly bigger in samples without AgI. Figs. 7.15 C & 7.15 D show the internal microstructure of the sample near the top surface of the samples in both cases while Figs. 7.15 E & 7.15 F show the magnified images of the aerated bubbles and the internal microstructure between the bubbles. The bubbles were found to be of increased size (~about 300μm) than the size initially obtained from the aeration of samples (as seen under FDM ~30-40 μm) though slightly smaller in samples containing AgI. This increase in size was thought to be due to coalescing of bubbles due to the slow cooling rate as it allows the bubbles to join together and grow in size. There is also a possibility that pipetting solutions for the FDM experiments may have selected against the larger bubble sizes. Samples containing AgI are expected to freeze at a higher temperature due to the presence of nucleating agent thereby resulting in slightly smaller bubbles (due to lesser time for bubbles to grow in size). Figs. 7.15 G & 7.15 H display the internal microstructure near the bottom of the trays while Figs. 7.15 I & 7.15 J show the bottom surface of the sample in both cases. The ice crystal voids present near the bottom of the trays are devoid of any bubbles and only constitute the coffee and ice matrix. The reason for this behaviour is very likely to be due to the rise of bubbles to the top leaving the coffee solution at the bottom. The figures also display denser microstructure (more coffee around ice crystal voids)

in samples without AgI while samples with AgI seem to have a more porous morphology. However, the size of the voids in both cases is quite small compared to the microstructure of 50% coffee samples without aeration.

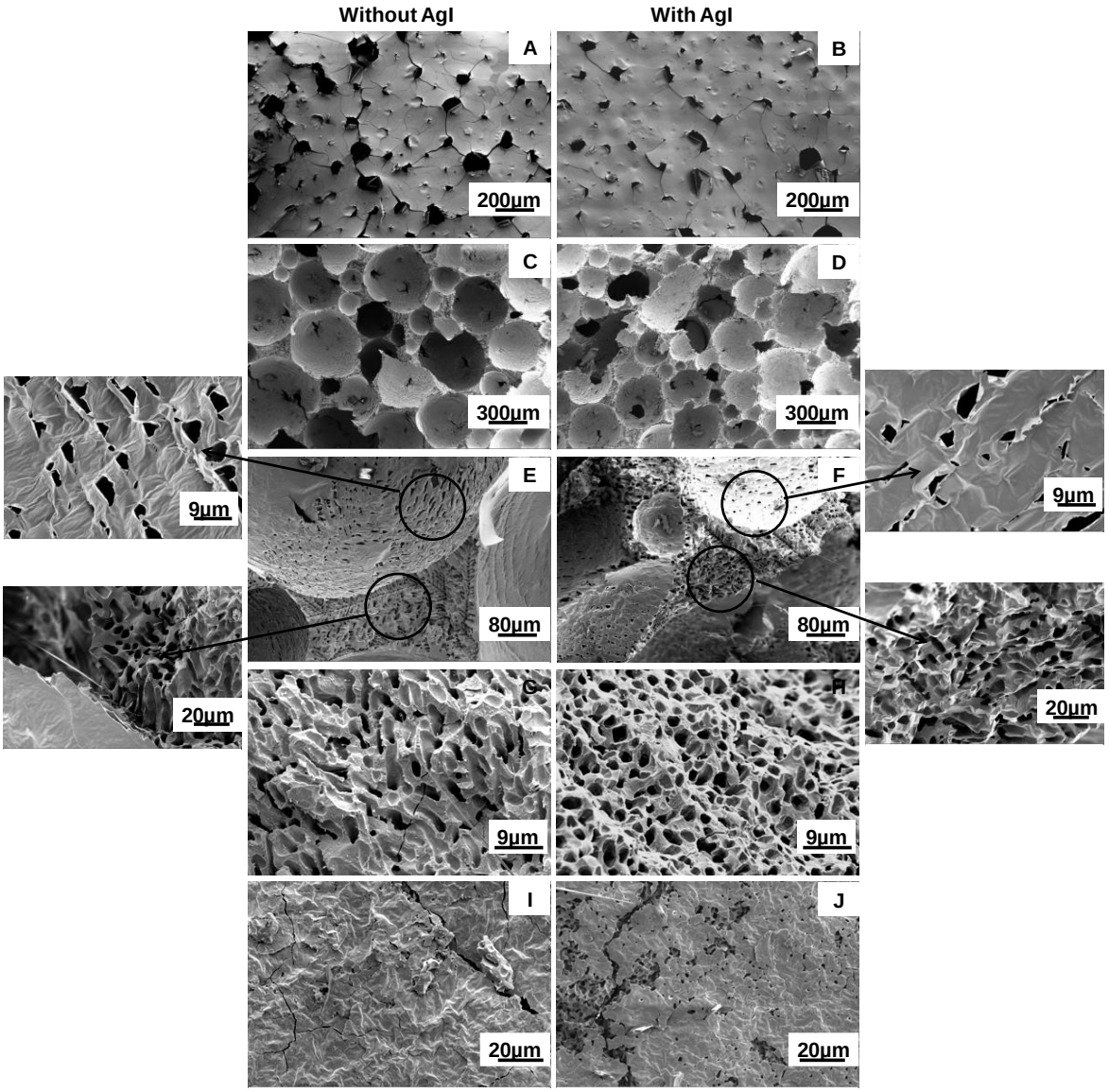

Figure 7.15: FEGSEM images of **50% aerated** coffee frozen at a cooling rate of **1 K.min^{-1}** and freeze dried at -40˚C at 10 Pa without AgI (left) and with AgI (right). **A** & **B.** Surface microstructure. **C** & **D.** Vertical cross-sectional microstructure. **E** & **F.** Cross-sectional internal microstructure between bubbles of samples collected from the top layer. **G** & **H.** Cross-sectional internal microstructure of samples collected near the bottom of the trays. **I** & **J.** Comparison of bottom layer microstructure. Images represent at least four repeat runs in each case.

Apart from using the slow cooling rate, the effect of fast cooling on microstructure and the primary drying rates was also investigated using liquid nitrogen quenching of

50% aerated coffee extract trays. Figs. 7.16 A & 7.16 B display the surface microstructure of the samples without and with AgI respectively. The surfaces look similar and the surface pores are quite similar size and number in both cases. The pores look smaller than those observed for the slow cooling rate displayed in Fig. 7.15 A & 7.15 B as expected since the quicker cooling rate results in similar frozen matrix in both cases.

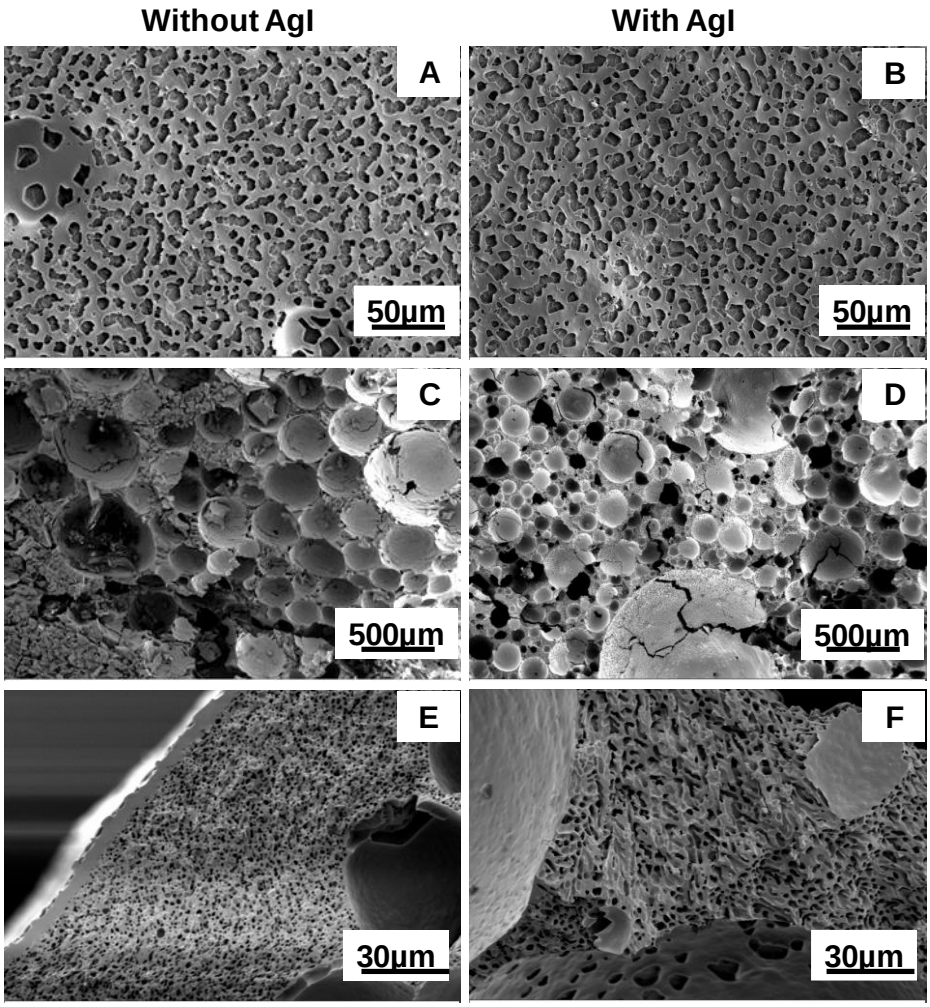

Figure 7.16: FEGSEM images of **50% aerated** coffee frozen by **liquid nitrogen quenching** and freeze dried at -40°C at 10 Pa without AgI (left) and with AgI (right). **A** & **B.** Surface microstructure. **C** & **D.** Cross-sectional microstructure. **E** & **F.** Internal microstructure of samples collected from the bottom layer. Images represent at least four repeat runs in each case.

Figs. 7.16 C & 7.16 D display the internal morphology of both cases beneath the top surface of the samples. The sizes of the bubbles look slightly smaller in comparison with slow cooling rate freeze dried samples (Figs. 7.15 C & 7.15 D) while AgI

containing samples displaying smaller bubble sizes than samples without AgI. Figs. 7.16 E & 7.16 F show the internal microstructure between bubbles especially depicted from bottom of the tray and was found to be same throughout the tray. This behaviour was attributed to the fast cooling rate applied and hence the ice crystal size was found to be uniform throughout the depth of the sample.

Based on the microstructural features described above for both cooling rates, primary drying durations of both cases were analysed. Primary drying times of all the aerated samples are presented in Table 7.4. Aerated samples exhibit drastic difference in primary drying duration when compared to other non-aerated samples for both cooling profiles investigated. All the aerated samples with and without AgI display significantly lower times for sublimation (compared with Figs. 7.10 & 7.13) as was an expected trend due to the presence of bubbles in the sample facilitating easier removal of water vapour. The bubble surfaces were also found to have pores (see Fig. 7.15 E) in them which helped in the quicker escape of water vapour from the samples.

Table 7.4 Experimental primary drying times at three different depths determined for 50% aerated coffee with and without at the two different cooling profiles. Values represent average of at least four repeat runs with standard deviation as error in both cases.

Cooling rate	Sample depth (mm)	Experimental primary drying duration (hrs)	
		Without AgI	With AgI
Slow cooling (1 $K.min^{-1}$)	3	4.0 ± 1.0	1.3 ± 0.7
	7	8.5 ± 5.3	8.0 ± 2.1
	11	19.7 ± 8.0	15.7 ± 3.0
Fast cooling (LN_2 quenching)	3	4.6 ± 1.3	2.1 ± 0.7
	7	9.2 ± 4.7	8.6 ± 2.3
	11	21.1 ± 7.5	16.8 ± 3.0

Aerated coffee samples also displayed differences in primary drying times with respect to cooling rates applied to the samples. Slow cooling rates were found to have a slightly quicker primary drying duration than samples cooled by liquid nitrogen quenching for samples both with and without AgI. This behaviour was an anticipated one, as samples with slower cooling rates displayed larger bubble sizes and also faintly bigger ice crystal sizes facilitating quicker water vapour removal from the sample.

Primary drying times of 50% aerated coffee samples were also compared relating to the presence or absence of AgI. It is evident from Table 7.4 that AgI containing samples were seen to dry faster initially (3 mm depth) and towards the end of the drying process (11 mm depth), while in the middle of the samples the difference was not pronounced for both cooling rates considered. The microstructure of the sample seems to play an important part in explaining this behaviour. Although the surface microstructure in both cases does not seem to help in understanding this behaviour (as pores in both cases look quite similar), however, samples with AgI have smaller sized bubbles but larger in number thereby assisting in removal of a greater amount of water vapour from the samples. Also, towards the bottom of the tray, samples with AgI display a more porous microstructure with slightly larger ice crystal size compared to samples without AgI.

The experimental primary drying times were not compared with the estimated drying times from FDM as it was difficult to determine *a* & *b* values from the data plot of 50% aerated coffee samples obtained from FDM due to the presence of various jumps in the curve and thus, it was not possible to extrapolate the estimated times for the three depths investigated in this study.

7.4 Conclusions

Freeze drying of coffee in trays with two different initial solid contents (10% and 50% w/w) with and without the presence of AgI was achieved successfully. The effect of different cooling rates, annealing and aeration on the freezing phase and thus on ice crystal morphology was investigated. The ice crystal void microstructure after freeze drying was analysed using scanning electron microscopy images and its effect on the primary drying kinetics of coffee was also described in details in this chapter. A comparison was also be made with the kinetics of lactose freeze drying in vials presented in Chapter 6.

Metal trays with coffee solutions for both solid contents and with and without nucleating agent and/or aeration were subjected to three different cooling profiles – slow cooling (1 $K.min^{-1}$), fast cooling (LN_2 quenching) and annealing (except aerated

sample). The average primary drying times were calculated for minimum four trays once it was seem that there was quite good reproducibility between the temperature measurement of different trays.

Cooling rates were found to significantly affect the ice crystal morphology of 10% coffee and 50% coffee. In the slow cooling rate investigated, the samples dried in the trays displayed different morphologies within the tray. The samples were found to show signs of directional solidification with freezing from bottom towards the top of the sample. The microstructure of coffee sample was similar to those discussed previously for freeze-dried coffee by Khwanpruk, (2009). The author investigated a 20% w/w initial solid content of coffee solution and freeze-dried the same, resulting in the random ice crystal void morphology (as seen in this research as well) due to the lack of any ice nucleating agent in the research. It also displays the thick edge in the freeze-dried sample formed similar to the one seen in Fig. 7.6 C. The ice crystal voids were seen to grow from smaller size to larger size towards the top of the sample though this behaviour was not as prominent as in case of lactose freeze dried in vials in the previous chapter. Also, the effect of AgI on the freezing of the sample was not as pronounced as was observed in lactose samples and seem to be in correlation with the behaviour seen in coffee freeze-dried under FDM with AgI. Faster cooling rate resulted in different surface morphologies and smaller ice crystal voids than the slower rates investigated as the crystals could not grow due to the fast cooling rate throughout the sample. Fast frozen samples were found to have a fragile flaky structure (see Fig. 7.12) which is similar to the microstructure previously displayed in research published by Ishwarya & Anandharamakrishnan, (2015). Samples frozen with different freezing rates display different ice crystal sizes, slow cooling rate resulted in larger ice crystals and vice versa. This behaviour confirms the previous results published by Pardo *et al.,* (2002), displaying the effect of freezing rate on ice crystal size of coffee extracts. Annealing of samples resulted in larger ice crystals in 10% coffee however, in 50% coffee it resulted in thicker surfaces while samples with slow and fast cooling showed thinner surface layer. The ice crystal voids were seen to penetrate through the surface layer only in the slow and faster cooling rates.

Average primary drying times obtained from the freeze dryer data was compared with the drying times obtained from the extrapolation of *a* and *b* values from FDM (based on mass transfer) for both solid contents and cooling profiles. It was observed that for 10% and 50% coffee frozen with all three cooling rates investigated, displayed extreme differences between the predicted and experimental drying times including the annealing process. The much shorter experimental drying times is presumed to be due to directional solidification (in the same direction as the subsequent mass transfer) occurring in the trays, which did not occur in the FDM experiments. The presence of cracks in the tray dried coffee samples could also provide a route for mass transfer.

The exception to these results was the estimated drying times of 10% coffee samples with and without AgI annealed under the freeze drying microscope, which were found to be quite close to the experimental freeze drying times of coffee freeze-dried in trays (though they were still slightly higher) due to ice crystal size similarity between annealed samples of the microscope to the freeze dried ones. The difference in samples with and without AgI was quite similar to the cases seen in lactose freeze drying in vials with AgI containing samples drying faster than non-AgI samples. Also, annealing different results for the two solid contents investigated. Annealed 10% coffee samples were seen to dry faster than non-annealed samples while annealed 50% coffee samples dried slower than the non-annealed 50% coffee. The main reason for this difference was thought to be the microstructural difference between the samples, especially the surface morphology and internal ice crystal structure. 10% coffee samples with annealing achieved larger ice crystal sizes causing easier water vapour removal, however, annealed 50% coffee displayed thicker surface morphology thereby resisting the escape of water vapour and thus, increasing primary drying duration.

Apart from the different cooling rates, the effect of process of aeration of coffee extract on the primary drying kinetics was also investigated in this study. Coffee extract with initial concentration of 50% was aerated using a cream whipper and it was freeze dried with and without AgI using the two different cooling profiles investigated for other coffee samples – slow cooling and fast cooling. The microstructure of aerated coffee was found to be similar to that of commercially

available freeze dried coffee with size of bubbles around the same size as displayed in this study (see MacLeod *et al.,* 2006). It was concluded that aeration of the sample drastically reduces the primary drying times as expected as the bubbles provide easy pathways for water vapour removal from the frozen matrix.

The main conclusions that were drawn from this research were that cooling rate, annealing, aeration and solid content play an important role in governing the ice crystal morphology and thus directly influences primary drying phase of the freeze-drying process. Cooling rate results in governing the surface layer and ice crystal morphology which in turn causes faster or slower drying rates. Slower cooling rates and annealing process result in faster primary drying of samples due to larger ice crystal size and thus quicker removal of water vapour while faster cooling rate take slightly longer durations due to smaller ice crystal size. As the solid content increases the rate of primary drying reduces with higher solid content samples drying slower than low solid concentrations (same as was observed in FDM). However, the predicted drying times from FDM were quite different when compared to actual drying times. Aeration of the sample also has a major effect on the primary drying kinetics (reduces the drying time considerably) and might be employed in real systems to reduce the duration of a freeze drying process thereby reducing the overall cost of the method.

8

CONCLUSIONS

This chapter provides an overview of the conclusions that can be drawn from the results of the work presented in this thesis. Some aspects of the works that require further development and improvement, which may form the basis for future investigations, are proposed.

8.1 General Conclusions

The purpose of this study was to use FDM to gain a better insight into the various factors such as initial solid content (lactose - 5, 10, 20, 30 & 40% w/w and coffee - 2, 5, 10, 20, 30, 40 & 50% w/w), freezing rate (2, 10 & 50 $K.min^{-1}$), annealing, aeration (50% coffee) and lyophilisation temperature (-30, -40 & -50˚C) that affect the primary drying phase of the freeze-drying process. A model lactose system and a complex coffee system were used for this purpose and the information obtained from FDM was compared to the actual freeze drying of lactose (10 & 40% w/w) and coffee (10 & 50% w/w) in a lab-scale freeze-dryer in vials and trays respectively.

In initial FDM experiments, poor reproducibility of nucleation temperatures and frontal velocities even under near-identical conditions led to the use of silver iodide to induce ice nucleation which was found to bring a consistent pattern to nucleation temperatures especially for lactose samples. The addition of a nucleation agent resulted in crystal sizes large enough to be observed for dilute (≤10% solids) lactose systems. The ice crystal size and orientation (prominent in case of lactose) were found to directly influence the frontal velocity. Ice crystals parallel to the direction of sublimation and the larger ice crystals in AgI containing samples were found to have a faster front velocity. Although the use of AgI could not significantly improve reproducibility of results in the case of coffee samples, it did influence the ice crystal structure and hence demonstrated a clear link between increased freeze drying rates and larger crystal sizes.

Apart from effect of microstructure, the FDM experiments were also used to develop a quadratic mass transfer model and to determine the effect of product resistance ("edge" resistance - α and "bulk" resistance - β) & on the sublimation kinetics of the samples. The presence of an edge resistance has long been hypothesised in the literature before but is clearly observable in FDM experiments. The edge resistance could be attributed to a solid layer of material with no ice crystals at the surface of the sample. In some cases (mainly more dilute samples) the surface resistance could be equivalent to a 3mm depth of the porous material which is quite small and may not be too effective in conventional freeze drying experiments. Based on the data obtained from the fitting of the twin-resistance model, the amount of dried solid produced with time was calculated and while in the case of low bulk resistances, the higher solid

contents seemed to produce higher amount of dry solid but when experiments were performed over longer time-scale, the effect of bulk resistance was evident from the curvature on the frontal distance versus time plot and it displayed that indeed lower solid contents will lead to production of higher amount of dried solid within the same time-frame. The edge resistance α was found to increase initially with solid content reaching a maximum at 20% lactose and 40% coffee followed by a decrease at higher solid contents(30 & 40% for lactose and 50% for coffee) while β values were found to increase with increasing solid content in both cases.

Cooling rates were mainly found to affect the edge resistance α and this may be due to different levels of surface drying when the samples are being cooled for different lengths of time. It could also arise from different amounts of freeze concentrated liquid being "squeezed" out to the surface when crystallised at different rates. Primary drying rates also increased with increasing temperature approximately in line with the saturated vapour pressure of ice which is widely believed to constitute the main driving force for mass transfer. Hence, the effect of increasing sample drying temperature from -50˚C to -30˚C showed the expected decrease in product resistance α and β values due to the increase in SVP of ice which is included within these parameters.

Furthermore, a study of annealing process during freezing of samples (10% lactose and coffee) also shows that the process dramatically increases ice crystal sizes whilst simultaneously reducing bulk resistances to mass transfer. 40% lactose was seen to result in crystallization of lactose from the freeze-concentrated matrix (which was later confirmed in actual freeze-drying experiments) and hence, sublimation kinetics was not investigated in great detail.

The effect of aeration was also studied under FDM in case of 50% coffee as it is a common technique used in the coffee industry to enhance product rehydration properties. The aeration of coffee extracts prior to freeze drying resulted in increase of sublimation rate, and this increase was more than anticipated due to lesser concentration of bubbles at the sample edge being investigated. It, thus, reinforces its use in the already established commercial coffee manufacture.

The information on ice crystal morphology and sublimation kinetics of samples obtained from freeze-drying microscopy were further used to understand and

correlate the primary drying behaviour of lactose (10% and 40% w/w) and coffee (10% and 50% w/w) with and without AgI freeze-dried in a conventional lab-scale freeze dryer in glass vials and metal trays respectively. The effect of different cooling rates - slow cooling ($1K.min^{-1}$), fast cooling (liquid nitrogen quenching) and annealing (except aerated 50% coffee samples), on the ice crystal morphology and thus on the mass transfer phenomenon of primary drying phase were also investigated. The ice crystal void microstructure after freeze drying was analysed using scanning electron microscopy. The average primary drying times were calculated for minimum five vials and four trays. It was seen that there was quite good reproducibility between the temperature measurements between the different vials and different trays. In case of lactose samples, the vials were kept away from the walls of the freeze drying chamber (to avoid radiation effects).

In the slow cooling rate investigated the samples were found to show signs of directional solidification with freezing from bottom towards the top of the sample. The ice crystal voids were seen to grow from smaller size to larger size towards the top of the sample though this behaviour was much more prominent in the case of lactose samples. Also, the effect of AgI on the freezing of the coffee sample was not as pronounced as was observed in lactose samples and seem to correlate with the behaviour seen in coffee freeze-dried under FDM with AgI. However, faster cooling rate displayed different surface morphologies and smaller ice crystal voids throughout the vials or trays as a consequence of a faster rate of nucleation and lesser time available for crystal growth. Annealing of samples resulted in larger ice crystals in 10% lactose and coffee however, in 50% coffee it resulted in thicker surfaces while un-annealed samples showed thinner surface layer which were easily penetrated by ice crystal growing from beneath the surface.

Conventional freeze drying is governed by two most important phenomena – heat transfer and mass transfer. The focus of the current research was mainly on the effect of cooling rates and initial solid contents on the mass transfer phenomenon in the primary drying phase of the process. In FDM, the samples are almost isothermal as heat is transferred uniformly to the sample from the silver temperature controlled block. In both tray and vial drying, the temperature associated with the sublimation front could be taken to be close to that of the shelf temperature (difference in temperature being about ±3˚C) due to the high thermal conductivity of the icy phase

which lies between the two. Average primary drying times obtained from the freeze dryer data was compared with the drying times obtained from FDM. It was observed that for 10% lactose and 10% coffee annealed samples the predicted and experimental drying times were quite close in all the cooling rates investigated including the annealing process. The similarity between the samples was thought to be due to ice crystal size similarity between samples of the microscope to the freeze dried ones. Apart from this, all other solid contents analysed, displayed very extreme difference between the predicted and experimental drying times including the annealing process. In case of lactose, slow cooling rates resulted in crystallization of lactose out of initial solution, thus, causing faster drying times. However, even with fast cooling rates, freezing of lactose was achieved without any solute crystallization and in this case also, primary drying times were faster in comparison to predicted FDM drying times. Annealed samples were seen to dry faster than non-annealed samples as expected due to larger microstructure and easier water vapour removal while annealed 50% coffee samples dried slower than the non-annealed 50% coffee. The main reason for this difference was thought to be the variation in surface morphology of the samples with 50% annealed coffee displaying thicker surface microstructure thereby resisting the escape of water vapour. The deviation between predicted and actual sublimation times was largely attributed to directional solidification occurring in vial and tray samples which was not reflected in FDM samples. The directionality of ice crystals aligns the channels so that mass transfer can take place easily through the sample, thereby speeding up mass transfer in the actual freeze-drying setup. It is also possible that cracks forming in the larger vial and tray samples provide an additional route for mass transfer.

Apart from different cooling rates, the effect of aeration of coffee extract on the primary drying kinetics was also investigated. 50% aerated coffee extract was freeze dried using two different cooling profiles – slow cooling and fast cooling. It was concluded that aeration of the sample drastically reduces the primary drying times as expected as the bubbles provide easy pathways for water vapour removal from the frozen matrix and reaffirms the results obtained from FDM that bubbles (irrespective of their concentration) do result in faster drying of the samples

The main conclusions that were drawn from this research were that ice crystal morphology, cooling rate and solid content play an important role in governing the

primary drying phase of the freeze-drying process. Cooling rate results in governing the surface layer and ice crystal morphology which in turn causes faster or slower drying rates. Slower cooling rates and annealing process result in larger ice crystals which increase the rate of water vapour removal from the sample while faster cooling results in comparatively smaller crystals and thus slightly longer durations of drying. Higher solid content samples were found to dry slower than low solid concentrations which displayed larger ice crystals and thus easier removal of water from the sample (same as seen in FDM). However, the predicted drying times from FDM were quite different when compared to actual drying times from freeze dryer. This is due to the different microstructures produced in the two cases. Aeration of the sample also has a major effect on the primary drying kinetics significantly reducing drying time and might be employed in real systems to reduce the duration of a freeze drying process thereby reducing the overall cost of the method.

Although, freeze-drying microscopy is significantly different from an actual freeze drying set-up, the results obtained from FDM suggest that methods for increasing crystal sizes such as forced nucleation techniques and annealing can help in increasing the sublimation rate during the freeze drying process. Silver iodide was only used in this research as a convenient way to provide some degree of control over nucleation but it is acknowledged that it would not be possible to use it in a real system of food or pharmaceutical industry applications as it would be viewed as a contaminant. However, it does show that controlling nucleation (which can be achieved via a variety of means such as ice fog technique) may result in better optimization of such systems. Overall, it can be concluded that the FDM can be a useful and valuable tool to study the kinetics of freeze drying process *in-situ*. In a real vial or tray freeze drying system, since ice crystal morphologies generally are affected by directional solidification and the sublimation kinetics are highly dependent on microstructure, for FDM to be of most use will require similar microstructures to be generated on the microscope slide.

8.2 Future work

The findings of this project were utilized to suggest avenues of future work in this research field as follows:-

- ✓ Freeze drying microscopy was used to explore varied combinations of operating parameters on freeze drying of samples except pressure. 1 Pa of vacuum pressure was used for all the experiments and it would be useful to study the effects of different values of vacuum pressure on sublimation kinetics of samples.
- ✓ Another aspect that can be investigated under the freeze drying microscope is the behaviour of products which have organic solvents instead of aqueous solution as base and the behaviour of such solvents under low temperature and pressure conditions.
- ✓ Freeze drying microscopy can also be used to understand the freeze-drying kinetics of a multiple component system consisting of different materials such as sugars, proteins, drug compound) generally found in pharmaceutical excipients. The drying kinetics studied in the freeze dryer were focussed on only one temperature of drying and thus can be expanded to study the effects of changing temperatures of drying on sublimation kinetics of samples freeze-dried in a conventional set-up.
- ✓ Methods could be investigated to generate directional (oriented) microstructures in FDM experiments for all sample types, so as to better replicate the kinetics found in real vial and tray systems. The kinetic parameters obtained can then be used in modelling real freeze drying processes.
- ✓ The model used in this study has scope for improvement. It can be improved upon by incorporating other factors which may play an important role in the primary drying process. These factors may include increase in ice crystal size with increase in volume and operating conditions in a real freeze-drying system, effects of heat transfer (if any), terms to include effects of water vapour diffusion through the frozen matrix.

REFERENCES

1. Abdelwahed, W., Degobert, G., Stainmesse, S. and Fessi, H., 2006a. Freeze-drying of nanoparticles: Formulation, process and storage considerations. *Advanced Drug Delivery Reviews*, 58, 1688–1713.
2. Abdelwahed, W., Degobert, G., and Fessi, H., 2006b. Freeze-drying of nanoparticles: Impact of annealing on the drying process. *International Journal of Pharmaceutics,* **324**, 74–82.
3. Abu Baker, M. R., 2010. Process analytical technology based approaches for the monitoring and control of size and polymorphic form in pharmaceutical crystallisation processes. *PhD thesis*, Loughborough University, UK.
4. Acharya, T., 2008. Freezing processes in cell suspensions evaluated using cryomicroscopy. *MSc., thesis*. Louisiana State University, Louisiana, United States of America.
5. Adams, G. D. J. and Ramsay, J. R., 1996. Optimizing the lyophilization cycle and the consequences of collapse on the pharmaceutical acceptability of *erwinia* L-Asparaginase. *Journal of Pharmaceutical Sciences,* **85**, 12, 1301–1305.
6. Aguilera, J. M., 2003. Why food microstructure? *Journal of Food Engineering,* **67**, 3–11.
7. Aguilera, J. M., 2003. Drying and dried products under the microscope. *Food Science and Technology International,* 9, 137-143.
8. Arshad, M.S. Smith, G., Polygalov, E. and Ermolina, I., 2014. Through-vial impedance spectroscopy of critical events during the freezing stage of the lyophilization cycle: The example of the impact of sucrose on the crystallization of mannitol. *Euroupean Journal of Pharmaceutics and Biopharmaceutics*, **87**, 3, 598-605.
9. Baressi, A. A., Pisano, R., Fissore, D., Rasetto, V., Velardi, S. A., Vallan, A., Parvis, M. and Galan, M., 2009. Monitoring of the primary drying of a lyophilization process in vials. Chemical Engineering and Processing, **48**, 408–423.
10. Bogdani, E., Daoussi, R., Vessot, S., Jose, J. and Andrieu, J., 2011. Implementation and validation of the thermogravimetric method for the determination of equilibrium vapor pressure and sublimation enthalpies of

frozen organic formulations used in drug freeze-drying process. *Chemical Engineering Research and Design*, **89**, 2606–2612.

11. Borgognoni, C. F., Bevilacqua, J. S. and Pitomboi, R. N. M., 2012. Freeze-drying microscopy in mathematical modeling of a biomaterial freeze-drying. Brazilian Journal of Pharmaceutical Sciences, **48**, 2, 203-209.

12. Boss, E. A., Filho, R. M., & de Toledo, E. C. V., 2004. Freeze-drying process: real time model and optimization. *Chemical Engineering and Processing*, **43**, 1475–1485.

13. Brezova, V., Šlebodová, A. and Staško, A., 2009. Coffee as a source of antioxidants: An EPR study. *Food Chemistry*, **114**, 3, 859–868.

14. Brulls, M. and Rasmuson, A., 2002. Heat transfer in vial lyophilisation, *International Journal of Pharmaceutics,* **246**, 1-16.
15. Brulls, M., Folestad, S., Sparén, A. and Rasmuson, A., 2002. In-situ near-infrared spectroscopy monitoring of the lyophilization process. *Pharmaceutical Research,* **20**, 3, 494-499.
16. Cannon, A. J. and Trappler, E. H., 2000. The influence of lyophilization on the polymorphic behavior of mannitol. *Journal of Pharmaceutical Science & Technology,* **54**, 1, 13-22.
17. Carullo A. and Vallan A., 2012. Measurement uncertainty issues in freeze-drying processes. *Measurement*, **45**, 7, 1706-1712
18. Chang, B. S. & Patro, S. Y., 2004. Freeze-drying process development for protein pharmaceuticals. In: *Lyophilization of biopharmaceuticals*, Eds. - Costantino, H. R. and Pikal, M. J., VA: AAPS Press, Arlington, 113-138.
19. Chen, C., 2003. Evaluation of Air Oven Moisture Content Determination Methods for Rough Rice. *Biosystems Engineering*, **86**, 4, 447–457.
20. Chen, R., Slater, N. K. H., Gatlin, L. A., Kramer, T. and Shalaev, E. Y., 2008. Comparative rates of freeze-drying for lactose and sucrose solutions as measured by photographic recording, product temperature, and heat flux transducer. *Pharmaceutical Development and Technology,* **13**, 5, 367–374.
21. Clausse, D., Bouabdillah, D., Cochet, N., Luquet, M. P. and Pulvin, S., 1991. Ice crystallization induced by silver iodide and bacteria in microsize droplets dispersed within emulsions. *Pure and Applied Chemistry*, **63**, 1491-1494.

22. Claussen, I. C., Strømmen, I., Egelandsdal, B. and Strætkvern, K. O., 2007. Effects of Drying Methods on Functionality of a Native Potato Protein Concentrate. *Drying Technology*, **25**, 6, 1091-1098.
23. Cochet, N. and Widehem, P., 2000. Ice crystallization by *Pseudomonas syringae*. *Applied Microbiology and Biotechnology*, **54**, 153-161.
24. Cook, K. L. K. and Hartel, R.W., 2011. Effect of freezing temperature and warming rate on dendrite break-up when freezing ice cream mix. *International Dairy Journal*, **21**, 447-453.
25. Corrêa, P. C., Goneli, A. L. D., Júnior, P. C. A., de Oliveira, G. H. H. and Valente, D. S. M. 2010. Moisture sorption isotherms and isosteric heat of sorption of coffee in different processing levels. *International Journal of Food Science and Technology*, **45**, 2016–2022.
26. Craig, D. Q. M., Royall, P. G., Kett, V. L. and Hopton, M. L., 1999. The relevance of the amorphous state to pharmaceutical dosage forms: glassy drugs and freeze dried systems. *International Journal of Pharmaceutics*, **179**, 179–207.
27. Crewe, A. V., Eggenberger, D. N., Wall, J. and Welter, L. M., 1968. Electron Gun Using a Field Emission Source. *Review of Scientific Instruments,* **39**, 576-583.
28. Cui, J. X., Lib, C., L., Deng, Y., Wang, Y. L. and Wang, W., 2006. Freeze-drying of liposomes using tertiary butyl alcohol/water cosolvent systems. *International Journal of Pharmaceutics,* **312**, 1–2, 131–136.
29. De Beer, T. R. M., Vercruysse, P., Burggraeve, A., Quinten, T., Ouyang, J., Zhang, X., Vervaet, C., Remon, J. P. and Baeyens, W. R. G., 2009a. In-line and real-time process monitoring of a freeze drying process using Raman and NIR spectroscopy as complementary process analytical technology (PAT) tools. *Journal of Pharmaceutical Sciences*, **98**, 9, 3430-3446.
30. De Beer, T. R. M., Wiggenhorn, M., Veillon, R., Debacq, C., Mayeresse, Y., Moreau, B., Burggraeve, A., Quinten, T., Friess, W., Winter, G., Vervaet, C. Remon, J. P. and Baeyens, W. R. G., 2009b. Importance of Using Complementary Process Analyzers for the Process Monitoring, Analysis and Understanding of Freeze Drying. *Analytical Chemistry,* **81**, 7639–7649.

31. Dincer, T. D., Parkinson, G. M., Rohl, A. L. and Ogden, M. I., 1999. Crystallization of α-lactose monohydrate from dimethyl sulfoxide (DMSO) solutions: influence of β-lactose. *Journal of crystal growth*, **205**, 3, 368-374.
32. Edwards, G. R. and Evans, L. F., 1960. Ice nucleation by silver iodide: I. Freezing vs sublimation. *Journal of Meteorology*, **17**, 627-634.
33. Edwards, G. R. and Evans, L. F., 1960. Ice nucleation by silver iodide: II. Collision efficiency in natural clouds**.** *Journal of Meteorology*, **18,** 760–765.
34. Edwards, G. R., Evans, L. F. and La Mer, V. K., 1962. Ice nucleation by monodisperse silver iodide particles. *Journal of Colloid Science*, **17**, 749-758.
35. Elia, A. M. and Barresi, A. A., 1998. Intensification of transfer fluxes and control of product properties in freeze-drying. *Chemical Engineering and Processing,* **37**, 347–358.
36. Ergun, R., Lietha, R. and Hartel, R. W., 2010. Moisture and shelf life in sugar confections. *Critical Reviews in Food Science and Nutrition*, **50**, 162–192.
37. Evans, J., Adler, J., Mitchell, J., Blanshard, J. and Rodger, G., 1996. Use of confocal laser scanning microscope in conjunction with a conduction heat transfer stage in order to observe dynamically the freeze–thaw cycle in an autofluorescent substance and to measure ice crystal size in situ. *Cryobiology,* **33**, 1, 27–33.
38. Ferguson, W. J., Lewis, R.W. and Tömösy, L., 1993. A finite element analysis of freeze-drying of a coffee sample. *Computer Methods in Applied Mechanics and Engineering*, **108**, 341-352.
39. Fissore, D., Pisano, R. and Barresi A. A., 2011. Monitoring of the secondary drying in freeze-drying of pharmaceuticals. *Journal of Pharmaceutical Sciences*, **100**, 2, 732-742.
40. Fissore, D., Pisano, R. and Barresi, A. A., 2011a. Advanced approach to build the design space for the primary drying of a pharmaceutical freeze-drying process. *Journal of pharmaceutical sciences*, **100**, 11, 4922-4933.
41. Fissore, D., Pisano, R., Barresi, A. A., 2014. Applying Quality-by-Design to develop a coffee freeze-drying process, *Journal of Food Engineering*, **123,** 179-187.

42. Flink, J. M. and Hansen, F. G., 1978. Two simple freeze drying microscope stages, *Review of Scientific Instruments,* **49**, 269-271.
43. Fonseca, F., Passot, S., Cunin, O. and Marin, M., 2004. Collapse temperature of freeze-dried Lactobacillus bulgaricus suspensions and protective media. *Biotechnology progress*, **20**, 1, 229-238.
44. Foster, K. D., Bronlund J. E. and Pasterson, A. H. J., 2006. Glass transition related cohesion of amorphous sugar powders. *Journal of Food Engineering*, **77**, 997-1006.
45. Franks, F., 1998. Freeze-drying of bioproducts: putting principles into practice. *European Journal of Pharmaceutics and Biopharmaceutics,* **45**, 221–229.
46. Franks, F., 2007. *Freeze Drying of pharmaceuticals and biopharmaceuticals – Principles and practice.* RSC Publishing, London, UK.Freedman, J., Whittam. J. and Rosano, H., 1972. Temperature gradient freeze-drying microscope stage. *Journal of Food Sciences*, **37**, 492-493.
47. Frost-Meyer, N. J. and Logomarsino, J. V., 2012. Impact of coffee components on inflammatory markers: A review. Journal of Functional Foods, 4, 4, 819–830.
48. Fureby, A. M., Malmsten, M., and Bergenståhl, B., 1999. Surface characterisation of freeze-dried protein/carbohydrate mixtures. *International Journal of Pharmaceutics*, **191**, 2, 103–114.
49. Gan, K. H., Bruttini, R., Crosser O. K. and Liapis A. I., 2005. Freeze-drying of pharmaceuticals in vials on trays: effects of drying chamber wall temperature and tray side on lyophilization performance. *International Journal of Heat and Mass Transfer,* **48**, 1675–1687.
50. Ganguly, A., Alexeenko, A. A., Schultz, S. G., Kim, S. G., 2013. Freeze-drying simulation framework coupling product attributes and equipment capability: Toward accelerating process by equipment modifications. *European Journal of Pharmaceutics and Biopharmaceutics*, **85**, 2, 223-235.
51. Garnier, S., Petit, S. and Coquerel, G., 2002. Influence of supersaturation and structurally related additives on the crystal growth of α-lactose monohydrate. *Journal of Crystal Growth*, **234**, 2002, 207–219.

52. Garside, J., 1987. General principles of crystallization. In: *Food structure and behaviour,* Eds. – Blanshard, J. M. V. and Lillford, P., Harcourt Brace Jovanovich Publishers, London, UK, 35-50.
53. Garside, J., Mersmann, A. and Nyvlt, J., 2002. In: *Measurement of crystal growth and nucleation rates*, Published by Institution of chemical engineering, Rugby, UK.
54. Gearing, J., Malik, K. P. and Matejtschuk, P., 2010. Use of dynamic mechanical analysis (DMA) to determine critical transition temperatures in frozen biomaterials intended for lyophilisation. *Cryobiology*, **61**, 1, 27-32.
55. Giordano, A., Barresi, A. A., & Fissore, D., 2011. On the use of mathematical models to build the design space for the primary drying phase of a pharmaceutical lyophilization process. *Journal of Pharmaceutical Sciences*, **100**, 311-324.
56. Gieseler, H., 2004. Product Morphology and Drying Behaviour delineated by a new Freeze-Drying Microbalance. *PhD thesis*, University of Erlangan, Germany.
57. Gieseler, H., Kessler, W. J., Finson, M., Davis, S. J., Mulhall, P. A., Bons, V., Debo, D. J., and Pikal, M. J. 2007. Evaluation of Tunable Diode Laser Absorption Spectroscopy for in-process water vapor mass flux measurement during freeze drying. *Journal of Pharmaceutical Sciences*, **96**, 1776-1793.
58. Gieseler, H. and Lee, G., 2008. Effect of freeze-dryer design on drying rate of an amorphous protein-formulation determined with a gravimetric technique. *Pharmaceutical Development and Technology,* **13**, 463–472.
59. Giulietti, M., Seckler, M. M., Derenzo, S., Ré, M.I. and Cekinski, E., 2001. Industrial crystallization and precipitation from solutions: state of the technique. *Brazillian Journal of Chemical Engineering*, **18**, 4, 423-440.
60. Grabe, D. F. 1989. Report of the seed moisture committee. *Seed Science & Technology,* **7**, (Supplement 1), 87-93.
61. Gutiérrez, L. F., Hamoudi, S. and Belkacemi, K., 2012. Lactobionic acid: A high value-added lactose derivative for food and pharmaceutical applications *International Dairy Journal*, **26**, 103-111.

62. Hartel, R. W., Ergun, R. and Vogel, S., 2011. Phase/State transitions of confectionery sweeteners: Thermodynamic and kinetic aspects. *Comprehensive reviews in Food Science and Food Safety*, **10**, 1, 17-32.
63. Hindmarsh, J. P., Russell, A. B. and Chen, X. D., 2007. Fundamentals of the spray freezing of foods—microstructure of frozen droplets. *Journal of Food Engineering*, **78**, 136–150.
64. Hottot, A., Vessot, S., & Andrieu, J., 2005. Determination of mass and heat transfer parameters during freeze-drying cycles of pharmaceutical products. *PDA Journal of Pharmaceutical Science and Technology*, **59**, 138-153.
65. Hsu, J. W. P., Lee, M. and Deaver, B. S., 1995. A non-optical tip–sample distance control method for near-field scanning optical microscopy using impedance changes in an electromechanical system. *Review of Scientific Instruments*, **66,** 5, 3177 – 3181.
66. Huang, M. and Zhang, M., 2013. Tea and coffee powders. *Handbook of Food Powders - Processes and Properties.* Eds. Bhandari, B., Bansal, N., Zhang, M. & Schuck, P. Woodhead Publishing Series in Food Science, Technology and Nutrition, Pages 513–531.
67. Ishwarya, S. P. and Anandharamakrishnan, C., 2015. Spray-Freeze-Drying approach for soluble coffee processing and its effect on quality characteristics. *Journal of Food Engineering*, **149**, 171–180.
68. Islam, M. I. U. and Langrish, T. A. G., 2010. An investigation into lactose crystallization under high temperature conditions during spray drying. *Food Research International*, **43**, 46–56.
69. Izutsu, K., Fujii, K., Katori, C., Yomota, C., Kawanishi, T., Yoshihashi, Y., Yonemochi, E. and Terada K., 2010. Effects of solute miscibility on the micro- and macroscopic structural integrity of freeze-dried solids. *Journal of Pharmaceutical Sciences*, **99**, 11, 4710-4719.
70. Johnson, J. M. and Conforti, F. D., 2003. *Lactose. Encyclopedia of Food Sciences and Nutrition*, academic press, Oxford, *3472*-3476.
71. Karimi, F., 2010. Properties of the drying of agricultural products in microwave vacuum: A review article. *Journal of Agricultural Technology,* **6**, 2, 269-287.

72. Kasper, J. C. and Friess, W., 2011. The freezing step in lyophilisation: Physico-chemical fundamentals, freezing methods and consequences on process performance and quality attributes of biopharmaceuticals. *European Journal of Pharmaceutics and Biopharmaceutics*, **78**, 2, 248-263.
73. Kasper, J. C., Pikal, M. J. and Friess, W., 2013. Investigations on polyplex stability during the freezing step of lyophilization using controlled ice nucleation—the importance of residence time in the low-viscosity fluid state. *Journal of pharmaceutical sciences*, **102**, 3, 929-946.
74. Kedward, C. J., MacNaughtan, W., Blanshard, J. M. V. and Mitchell, J. R., 1998. Crystallization kinetics of lactose and sucrose based on isothermal differential scanning calorimetry. *Journal of food science*, **63**, 2, 192-197.
75. Kedward, C. J., MacNaughtan, W. and Mitchell, J. R., 2000. Isothermal and non-isothermal crystallization in amorphous sucrose and lactose at low moisture contents. *Carbohydrate research*, 329, 2, 423-430.
76. Khwanpruk, 2009. Volatile Retention in the Formation and Dehydration of Food Powders. *PhD thesis*, Loughborough University, UK.
77. Kiani, H. and Sun, D. W., 2011. Water crystallization and its importance to freezing of foods: A review. *Trends in Food Science & Technology*, **22**, 407-426.
78. Kochs, M., Schwindke, P. and Koerber, C., 1989. A microscope stage for the dynamic observation of freezing and freeze-drying in solutions and cell-suspensions. *Cryoletters*, **10**, 401-.
79. Kochs, M., Köber, C. H., Heschel, I and Nunner, B., 1993. The influence of the freezing process on vapour transport during sublimation in vacuum freeze-drying of macroscopic samples. *International Journal of Heat & Mass Transfer*, **36**, 7, 1727-1738.
80. Konstantinidis, A. K., Kuu, W., Otten, L., Nail, S. L., Sever, R. R., 2011. Controlled nucleation in freeze drying: Effects on pore size in the dried product layer, mass transfer resistance and primary drying rate. *Journal of Pharmaceutical Sciences*, **100**, 3453-3470.
81. Krokida, M. K., Karathanos, V. T. and Maroulis, Z. B., 1998. Effect of Freeze-drying Conditions on Shrinkage and Porosity of Dehydrated Agricultural Products. *Journal of Fodd Engineering,* **35**, 369-380.

82. Kuu, W. Y., Nail, S. L., & Sacha, G., 2009. Rapid determination of vial heat transfer parameters using tunable diode laser absorption spectroscopy (TDLAS) in response to step-changes in pressure set-point during freeze-drying. *Journal of Pharmaceutical Sciences*, **98**, 1136-1154.
83. Lewicki, P. P., 2006. Design of hot air drying for better foods. *Trends in Food Science & Technology,* **17**, 153–163.
84. Liu, J., 2006. Physical Characterization of Pharmaceutical Formulations in Frozen and Freeze-Dried Solid States: Techniques and Applications in Freeze-Drying Development. *Pharmaceutical Development and Technology,* **11**, 1, 3-28.
85. Lombrana, J. I. and Villarán, M. C., 1996. Drying rate and shrinkage effect interaction during freeze-drying in an adsorbent medium. *Journal of Chemical Engineering of Japan*, **29**, 2, 242-250.
86. López-Galilea, I., Androit, I., de Peña, M. P., Cid, C. and Guichard, E., How Does Roasting Process Influence the Retention of Coffee Aroma Compounds by Lyophilized Coffee Extract?. *Journal Food Science S: Sensory and Food Quality,* **73**, 3, S165-171.
87. Lu, X. and Pikal, M. J., 2004. Freeze-drying of mannitol-trehalose-sodium chloride-based formulations: the impact of annealing on dry layer resistance to mass transfer and cake structure. *Pharmaceutical Development & Technology*, **9**, 1, 85-95.
88. MacKenzie, A. P., 1964. Apparatus for microscopic observations during freeze-drying (AFBR freeze-drying microscope model 2). *Biodynamica*, **9**, 213-222.
89. MacLeod C. S., McKittrick J. A., Hindmarsh J. P., Johns M. L. and Wilson, D. I. 2006. Fundamentals of spray freezing of instant coffee. *Journal of Food Engineering,* **74**, 451–461.
90. Mascarenhas, W. J., Akayavby, H. U. and Pikal M. J., 1997. A computational model for finite element analysis of the freeze-drying process. *Computer Methods in Applied Mechanics and Engineering*, **148**, 105-124.
91. Mateus, M. L., Rouvet, M., Gumy, J. C. and Liardon, R., 2007. Interactions of water with roasted and ground coffee in the wetting process investigated

by a combination of physical determinations. *Journal of Agricultural and Food Chemistry,* **55**, 2979-2984.

92. McDonald, E. J. and Turcotte, A. L., 1948. Density and Refractive Indices of Lactose Solutions. *Journal of Research of the National Bureau of Standards,* **41**, 63-68.
93. McLeod, J., 2007. Nucleation and growth of alpha lactose monohydrate, *PhD Thesis*, Massey University, New Zealand.
94. McLeod, J., Paterson, A. H. J., Jones, J. R. and Bronlund, J. E., 2011. Primary nucleation of alpha-lactose monohydrate: The effect of supersaturation and temperature. *International Dairy Journal*, **21**, 455-461.
95. Meister, E. and Gieseler, H., 2008. Freeze-dry microscopy of protein/sugar mixtures: drying behaviour, interpretation of collapse temperatures and a comparison to corresponding glass transition data. *Journal of pharmaceutical sciences*, **98,** 9, 3072-3087.
96. Meister, E., 2009. Methodology, data interpretation and practical transfer of freeze-dry microscopy. *PhD thesis*, University of Erlangen, Germany.
97. Meister, E., Šašić, S. and Gieseler, H. 2009. Freeze-dry microscopy: Impact of nucleation temperature and excipient concentration on collapse temperature data. *PharmSciTech*, **10**, 2, 582-588.
98. Miyata, K. and Kanno, H. 2005. Supercooling behavior of aqueous solutions of alcohols and saccharides. *Journal of Molecular Liquids,* **119,** 189–193.
99. Mullin, J. W., 2001. *Crystallization*, Published by Butterworth- Heinemann, Oxford, USA.
100. Muzzio, C. R. and Dini, N. G., 2011. Simulation of freezing step in vial lyophilization using finite element method. *Computers and Chemical Engineering*, **35**, 2274– 2283.
101. Myerson, A. S., 2002. In: *Handbook of industrial crystallization*, published by Butterworth-Heinemann, Woburn, USA.
102. Nakagawa, K., Hottot, A., Vessot, S., Andrieu, J., 2006. Influence of controlled nucleation by ultrasounds on ice morphology of frozen formulations for pharmaceutical proteins freeze-drying. *Chemical Engineering and Processing: Process Intensification,* **45**, 9, 783–791.

103. Nakagawa, K., Hottot, A., Vessot, S. and Julien Andrieu, J., 2007. Modeling of freezing step during freeze-drying of drugs in vials. *American Institute of Chemical Engineers Journal,* **53,** 5, 1362–1372.
104. Nakagawa, K., Murakami, W., Andrieu, J. and Vessot, S., 2009. Freezing step controls the mannitol phase composition heterogeneity. *Chemical Engineering Research and Design,* **87**, 8, 1017–1027.
105. Nail, S. L., Her, L. M., Proffitt, C. P. B. and Nail, L. L., 1994. An improved microscope stage for direct observation of freezing and freeze drying. *Pharmaceutical research*, **11**, 8, 1098-1100.
106. Nam, J. H., and Song, C. S., 2007. Numerical Simulation of Conjugate Heat and Mass Transfer during Multi- Dimensional Freeze Drying of Slab-Shaped Food Products. *International Journal of Heat and Mass Transfer*, **50**, 4891-4900.
107. Nasirpour, A., Landillon, V., Cuq, B., Scher, J., Banon, S. and Desobry, S., 2007**.** Lactose Crystallization Delay in Model Infant Foods made with Lactose, *β*-Lactoglobulin, and Starch *Journal of Dairy Science*, **90**, 8, 3620–3626.
108. Navaratne, S. B. 2013. Selection of polymer based packing material in packing of hygroscopic food products for long period of storage. *European International Journal of Science and Technology*, **2**, 7, 1-6.
109. Nehrke, G., 2007. Calcite precipitation from aqueous solution: transformation from vaterite and role of solution stoichiometry. PhD thesis, Utrecht University, Netherlands.
110. Oetjen, G. W. and Haseley, P., 2004. *Freeze-Drying*, Wiley-VHC, Weinheim, Germany.
111. Omar, A. M. E. and Roos, Y. H., 2007. Water sorption and time-dependent crystallization behaviour of freeze-dried lactose–salt mixtures. *LWT – Food Science and Technology*, **40**, 520-528.
112. Pardo, J. M., Suess, F. and Niranjan, K., 2002. An investigation into the relationship between freezing rate and mean ice crystal size for coffee extracts. *Trans IChemE*, **80**, 176-182.

113. Pardo, J. M. and Niranjan, K. 2011. Freezing. *Food Processing Handbook*, Second Edition, eds. Brennan J. G. and Grandison A. S., Wiley-VCH, Weinheim, Germany.
114. Passot, S., Fonseca, F., Barbouche, N. and Marin, M., 2007. Effect of Product Temperature During Primary Drying on the Long-Term Stability of Lyophilized Proteins. *Pharmaceutical Development and Technology,* **12**, 543–553.
115. Patapoff, T. W. and Overcashier, D. E., 2002. The Importance of Freezing on lyophilization cycle development. *BioPharm International*, **15**, 3, 16-22.
116. Patel, S. M., Bhugra, C., Pikal, M. J., 2009. Reduced pressure ice fog technique for controlled ice nucleation during freeze-drying. AAPS PharmSciTech, 10, 1406-1411.
117. Patel, S. M. and Pikal, M. J., 2011. Emerging Freeze-Drying Process Development and Scale-up Issues. *AAPS PharmSciTech*, **12**, 1, 372-378.
118. Patil, V. V. , Dandekar, P. P. , Patravale, V. B. and Thorat, B. N. 2010. Freeze drying: potential for powdered nanoparticulate product. *Drying Technology*, **28**, 624-635.
119. Petzold, G. and Aguilera, J. M., 2009. Ice morphology: Fundamentals and technological applications in foods. Food Biophysics, 4, 378-396.
120. Pikal, M. J., Shah, S., Senior, D. and Lang, J. E., 1983. Physical chemistry of freeze-drying: measurement of sublimation rates for frozen aqueous solutions by a microbalance technique. *Journal of Pharmaceutical Sciences,* **72**, 635–650.
121. Pikal, M. J., Roy, M. L. and Shah, S., 1984. Mass and heat transfer in vial freeze-drying of pharmaceuticals: role of the vial. *Journal of Pharmaceutical Sciences*, **73**, 1224-1237.
122. Pikal, M. J. and Shah, S., 1990. The collapse temperature in freeze drying: Dependance on measurement methodology and rate of water removal from the glassy phase. *International Journal of Pharmceutics*, **62**, 2-3,165-186.
123. Pisano, R., Fissore, D. and Barresi, A. A., 2011. Heat transfer in freeze-drying apparatus. *Developments in Heat Transfer,* Ed. Bernardes, M. A. S., InTech, 91-114.

124. Pisano, R., Fissore, D. and Barresi, A. A., 2011. Freeze-Drying Cycle Optimization Using Model Predictive Control Techniques. *Industrial & Engineering Chemistry Research,* **50**, 7363–7379.
125. Pisano, R., Fissore, D., Barresi, A. A., Brayard, P., Chouvenc, P. and Woinet, B., 2013. Quality by design: optimization of a freeze-drying cycle via design space in case of heterogeneous drying behaviour and influence of the freezing protocol. *Pharmaceutical development and technology,* **18**, 1, 280-295.
126. Qin F. G. F., Zhao, J. C., Russell, A. B., Chen, X. D., Chen, J. J. and Robertson, L., 2003. Simulation and experiment of the unsteady heat transport in the onset time of nucleation and crystallization of ice from the sub-cooled solution. *International Journal of Heat and Mass Transfer*, **46**, 3221–3231.
127. Quast, D. G. and Karel, M., 1968. Dry layer permeability and freeze-drying rates in concentrated fluid systems. *Journal of Food Science,* 33, 171-175.
128. Ratti, C., 2001. Hot air and freeze-drying of high-value foods: A review. *Journal of Food Engineering*, **49**, 311–319.
129. Rene, F., Wolff, E. and Rodolphe, F., 1993. Vacuum freeze-drying of a liquid in a vial: determination of heat and mass-transfer coefficients and optimisation of operating pressure. *Chemical Engineering and Processing*, **32**, 4, 245-251.
130. Rey, L., Pirie, N. W., Whitman, W. E. and Kurti, N., 1975. Freezing and freeze-drying. *Proceedings of the Royal Society B,* **191,** 9-19.
131. Reyes, A., Vega, R., Bustos, R. and Araneda, C., 2008. Effect of processing conditions on drying kinetics and particle microstructure of carrot. *Drying Technology*, **26**, 1272–1285.
132. Rivera, W., Velascoa, X., Gálveza, C., Rincóna, C., Rosales, A. and Pedro Arango, P., 2011. Effect of the roasting process on glass transition and phase transition of Colombian Arabic coffee beans. *Procedia Food Science,* **1**, 385 – 390.
133. Roelfsema, W. A., Kuster, B. F. M., Heslinga, M. C., Pluim, H. and Verhage, M., 2010. Lactose and Derivatives. In: *Ulmann's encyclopedia of Industrial Chemistry,* 7th edn. Wiley & Sons, New York, NY.

134. Roos, Y. H. and Karel, M., 1992. Crystallization of amorphous lactose. *Journal of Food Science*, **57**, 3, 775–777.
135. Roos, Y. H., 1997. Frozen phase transitions in relation to freeze-drying. *Journal of Thermal Analysis*, **48**, 535-544.
136. Roos, Y. H., 2002. Importance of glass transition and water activity to spray drying and stability of dairy powders. *Lait*, **82**, 475-484.
137. Roos, Y. H., 2009. Solid and Liquid states of Lactose. In: *Advanced Dairy Chemistry, Volume 3: Lactose, Water, Salts and Minor Constituents*, Eds. – McSweeney, P. L. H. and Fox, P. F., 17-33.
138. Rosenthal, M., and Rall, W. F., 1984. Digital temperature controller for low-temperature light microscopy. *Medical & Biological Engineering & Computing*, **22**, 471-474.
139. Roth, C., Winter, G. and Lee, G., 2001. Continuous measurement of drying rate of crystalline and amorphous systems during freeze-drying using an *In –Situ* microbalance technique. *Journal of pharmaceutical sciences*, **90**, 9, 1345-1355.
140. Roy, M. L. and Pikal, M. J., 1989. Process control in freeze-drying: determination of the endpoint of sublimation drying by an electronic moisture sensor. *Journal of Parenteral Science and Technology*, **43**, 2, 60-66.
141. Rückold, S., Grobecker, K. H. and Isengard, H. D., 2000. Determination of the contents of water and moisture in milk powder. *Fresenius Journal of Analytical Chemistry*, **368**, 522–527.
142. Sablani, S. S., Syamaladevi, R. M. and Swanson, B. G., 2010. A review of methods, data and applications of state diagrams of food systems. *Food Engineering Reviews*, **2**, 168–203.
143. Sacha, G. A. and Nail, S. L. 2008. Thermal analysis of frozen solutions: Multiple glass transitions in amorphous systems. *Journal of Pharmaceutical Sciences*, **98**, 9, 3397-3405.
144. Sadikoglu, H., Ozdemir, M. and Seker, M., 2006. Freeze-Drying of Pharmaceutical Products: Research and Development Needs, *Drying Technology*, **24**, 7, 849 — 861.

145. Sagara, Y. and Ichiba, J., 1994. Measurement of transport properties for the dried layer of coffee solution undergoing freeze-drying. *Drying technology,* **12,** 5, 1081-1103.
146. Sagara, Y., 2001. Advances in Transport Phenomena during Freeze-Drying of Food Materials: Fundamentals and Applications. *Food Science and Technology Research,* **7,** 3, 183–190.
147. Sagara, Y., Kaminishi, K., Goto, E., Watanabe, T., Imayoshi, Y. and Iwabuchi, H., 2005. Characteristic Evaluation for Volatile Components of Soluble Coffee Depending on Freeze-Drying Conditions. *Drying Technology*, **23,** 2185–2196.
148. Sane, S. U. and Hsu, C. C., 2010. Considerations for Successful Lyophilization Process Scale-Up, Technology Transfer, and Routine Production. *Formulation and Process Development Strategies for Manufacturing Biopharmaceuticals*, Eds. Jameel, F. and Hershenson S., John Wiley & Sons, Inc.
149. Santivarangkna, C., Kulozik, U. and Foerst, P., 2007. Alternative drying processes for the industrial preservation of lactic acid starter cultures. *Biotechnology Progress*, **23**, 302-315.
150. Sawyer, L. C., Grubb, D. T. and Meyers, G. F., 2008. *Polymer microscopy.* Third edition. Springer Science+Business Media, New York, United States of America.
151. Schneid, S. C. and Gieseler, H., 2008. Evaluation of a New Wireless Temperature Remote Interrogation System (TEMPRIS) to Measure Product Temperature During Freeze Drying. *AAPS PharmSciTech*, **9**, 3, 729-739.
152. Schneid, S. C., Gieseler, H., Kessler, W. J., Luthra, S. A. and Pikal, M. J., 2011. Optimization of the secondary drying step in freeze drying using TDLAS Technology. *PharmSciTech,* **12**, 1, 379-387.
153. Schoen, M. P., Braxton, B. K., Gatlin, L. A., Jefferis III, R. P., 1995. A simulation model for the primary drying phase of the freeze-drying cycle. *International Journal of Pharmaceutics,* **114**, 159-170.
154. Schuck, P. and Dolivet, A., 2002. Lactose crystallization: Determination of α-lactose monohydrate in spray dried dairy products, *Lait- Dairy Science and Technology,* **82**, 4, 401–414.

155. Searles, J. A., Carpenter, J. F. and Randolph, T. W., 2001. The ice nucleation temperature determines the primary drying rate of lyophilisation for samples frozen on a temperature-controlled shelf. *Journal of Pharmaceutical Sciences*, **90**, 860-871.
156. Searles, J. A., 2004. Freezing and annealing phenomena in Lyophilization. In: *Freeze drying/Lyophilization of pharmaceutical and biological products*, Eds. – Rey, L. and May, J. C., Marcel Dekker Inc., New York, **137,** 109-146.
157. Segura, L. A. And Oyarzún, C. A., 2012. Experimental evidence of mass transfer mechanisms during freeze-drying in a capillary porous medium. *International journal of refrigeration*, **35**, 2102-2109.
158. Sheehan, P. and Liapis, A. I., 1998. Modeling of the primary and secondary drying stages of the freeze-drying of pharmaceutical product in vials: numerical results obtained from the solution of a dynamic and spatially multi-dimensional lyophilisation model for different operational policies. *Biotechnology & Bioengineering*, **60,** 712-728.
159. Smith, G., Arshad, M.S., Polygalov, E. and Ermolina, I., 2013. An application for impedance spectroscopy in the characterisation of the glass transition during the lyophilization cycle: The example of a 10% w/v maltodextrin solution. *European Journal of Pharmaceutics and Biopharmaceutics*, **86,** 3, 1130-1140.
160. Smith, G.; Arshad, Muhammad Sohail; Polygalov, E., Ermolina, I. (2014). Through-Vial Impedance Spectroscopy of the Mechanisms of Annealing in the Freeze-Drying of Maltodextrin: The Impact of Annealing Hold Time and Temperature on the Primary Drying Rate. *Journal of Pharmaceutical Sciences*, **103**, 6, 1799-1810.
161. Song, C. S., Nam, J. H., Kim, C. J. and Ro, S. T., 2005. Temperature distribution in a vial during freeze-drying of skim milk. *Journal of Food Engineering,* **67**, 467–475.
162. Stapley, A. G. F., 2008. Freeze drying. In: *Frozen food science and technology*, Ed. – Evans. J. A., Blackwell publishing, Oxford, UK, 248-275.
163. Steckel, H. and Bolzen, N., 2004. Alternative sugars as potential carriers for dry powder inhalations. *International Journal of Pharmaceutics,* **270**, 297–306.

164. Tang, X. and Pikal, M. J., 2004. Design of Freeze-Drying Processes for Pharmaceuticals: Practical Advice. *Pharmaceutical Research,* **21**, 2, 191-200.
165. Tang, X., Nail, S. L. and Pikal, M. J., 2005. Freeze-Drying Process Design by Manometric Temperature Measurement: Design of a Smart Freeze-Dryer *Pharmaceutical Research,* **22**, 4, 685-700.
166. Tavcar, E., Turk, E. and Kreft, S., 2012. Simple modification of Karl-Fischer titration method for determination of water content in coloured samples. *Journal of Analytical Methods in Chemistry*, **2012**, 1-6.
167. Tsourouflis, S. P. C., 1975. Collapse temperature of freeze-dried carbohydrate solutions: effects of composition and moisture content. *PhD thesis*, Aristotelian University, Greece.
168. Ubbink, J., Burbidge, A. and Mezzenga, R., 2008. Food structure and functionality: a soft matter perspective. *Soft Matter*, **4**, 1569–1581.
169. Varshosaz, J., Eskandari, S. and Tabbakhian, M., 2012. Freeze-drying of nanostructure lipid carriers by different carbohydrate polymers used as cryoprotectants. *Carbohydrate Polymers*, **88**, 1157–1163.
170. Awotwe-Otoo, D. A. and Khan, M.A., 2015. Lyophilization of Biologics: An FDA Perspective. In:*Lyophilized Biologics and Vaccines: Modality-Based Approaches,* Eds. Varshney, D. and Singh, M., 341-360.
171. Vessot, S. and Andrieu, J., 2012. A Review on Freeze Drying of Drugs with tert-Butanol (TBA) + Water Systems: Characteristics, Advantages, Drawbacks. *Drying Technology: An International Journal*, **30**, 4, 377-385.
172. Voda, A., Homan, N., Witek, M., Duijster, A., Dalen, G. V., Sman, R. V. D., Nijsse, J., Vliet, L. V., As, H. V. and Duynhoven, J. V., 2012. The impact of freeze-drying on microstructure and rehydration properties of carrot. *Food Research International,* **49**, 2, 687–693.
173. Vollenbroek, J., Hebbink, G. A., Ziffels, S. and Steckel, H., 2010. Determination of low levels of amorphous content in inhalation grade lactose by moisture sorption isotherms. *International Journal of Pharmaceutics*, **395**, 1-2, 62-70.

174. G. Vuataz, G., Meunier, V. and Andrieux, J. C., 2010. TG–DTA approach for designing reference methods for moisture content determination in food powders. *Food Chemistry,* **122**, 2, 436–442.
175. Wang, W., 2000. Lyophilization and development of solid protein pharmaceuticals. *International Journal of Pharmaceutics*, **203**, 1–2, 1–60.
176. Wei, W., Mo, C. and Guohua, C., 2012. Issues in freeze drying of aqueous solutions. *Chinese Journal of Chemical Engineering,* **20**, 3, 551-559.
177. Widehem, P. and Cochet, N., 2003. *Pseudomonas syringae* as an ice nucleator - application to freeze-concentration. *Process Biochemistry*, **39**, 405-410.
178. Whittier, 1933. Freezing points and osmotic pressures of lactose solutions. *Journal of Physical Chemistry*, **37,** 7, 847–849.
179. Widehem, P. and Cochet, N., 2003. *Pseudomonas syringae* as an ice nucleator – application to freeze-concentration. *Process Biochemistry*, **39**, 405-410.
180. Woinet, B., Andrieu, J. and Laurent, M., 1998a. Experimental and theoretical study of model food freezing. Part I. Heat transfer modelling. *Journal of Food Engineering*, **35**, 381-393.
181. Woinet, B., Andrieu, J., Laurent, M. and Min, S. J., 1998b. Experimental and theoretical study of model food freezing. Part II. Characterization and modelling of the ice crystal size. *Journal of Food Engineering*, **35**, 395-407.
182. Wolff, E., Gibert, H. and Rodolphe, F., 1989. Vacuum freeze drying kinetics and modelling of a liquid in a vial. *Chemical Engineering and Processing*, **25**, 3, 153-158.
183. Xiao, X., Tao, L. R. and Hua, T. C., 2007. Micro-computed tomography observation of sublimation interface and image analysis on sublimation process during freeze-drying, *Cryo Letters*, **28**, 4, 253-260.
184. Yang, G., Gilstrap, K., Zhang, A., Xu, L. X. and He, X., 2010. Collapse temperature of solutions important for lyopreservation of living cells at ambient temperature. *Biotechnology and Bioengineering,* **106**, 2, 247-259.
185. Yeom, G. S. and Song, C. S., 2010. Experimental and Numerical Investigation of the Characteristics of Spray-Freeze Drying for Various Parameters:

Effects of Product Height, Heating Plate Temperature, and Wall Temperature. *Drying Technology*, **28**, 2, 165-179.

186. Zhai, S., Sanches, R. and Slater, N. K. H., 2003. Measurement of lyophilisation primary drying rates by freeze-drying microscopy. *Chemical engineering science*, **58,** 11, 2313-2323.
187. Zhai, S., Hansen, R. K., Taylor, R., Skepper, N. J., Sanches, R. and Slater, N. K. H., 2004. Effect of freezing rates and excipients on the infectivity of a live viral vaccine during lyophilization. *Biotechnology Progress*, **20**, 1113–1120.
188. Zhai, S., Su, H., Taylor, R. and Slater, N. K. H., 2005. Pure ice sublimation within vials in a laboratory lyophiliser; comparison of theory with experiment. *Chemical Engineering Science*, **60**, 1167 – 1176.

Appendix A: Freeze drying microscope stage temperature calibration

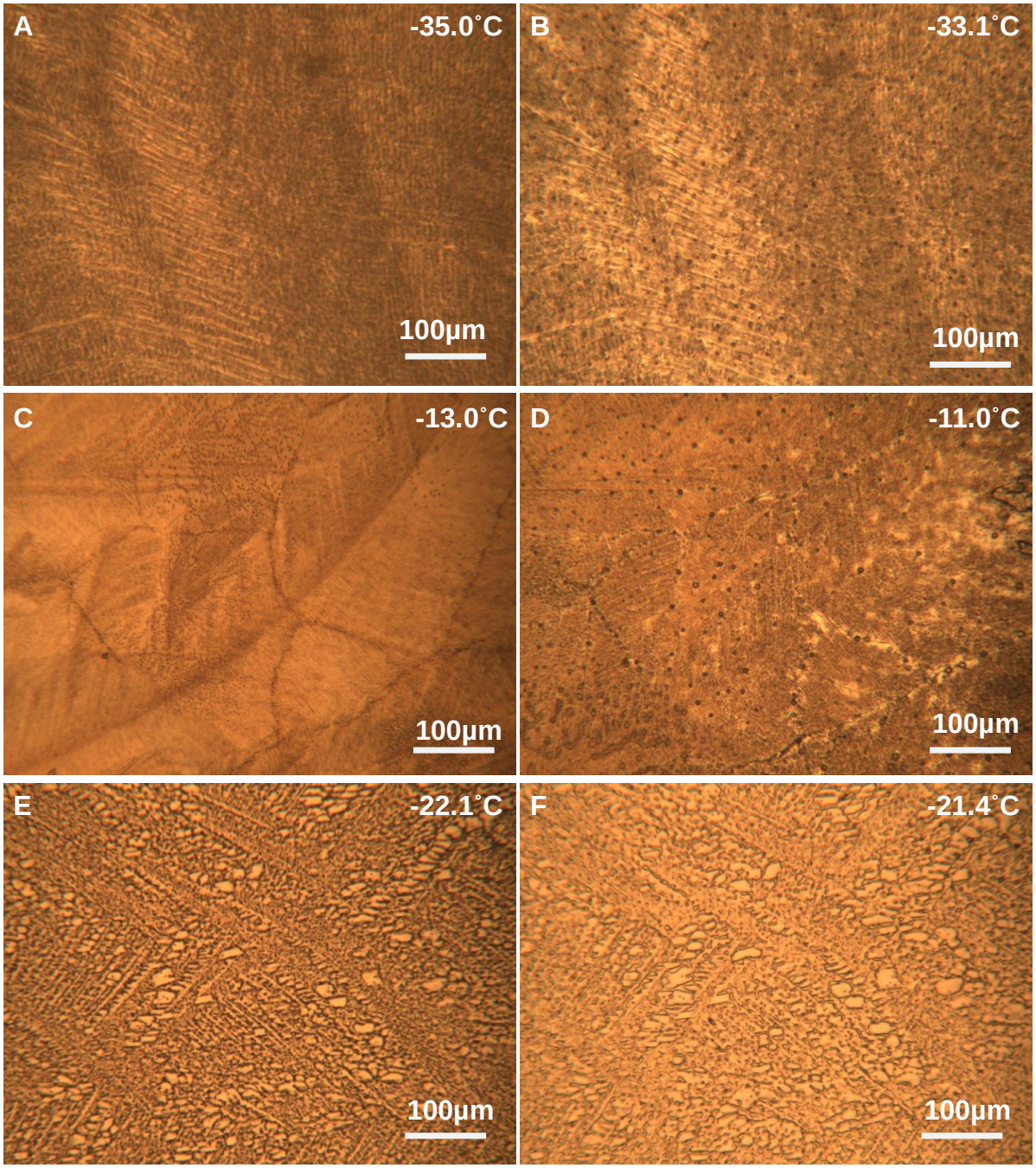

Figure A.1: Freeze drying microscope stage temperature calibration. **A.** Frozen microstructure of 10% w/w $MgCl_2$-ice eutectic mixture. **B.** Melting of salt crystals of $MgCl_2$ from the eutectic mixture. **C.** Frozen microstructure of 10% w/w KCl-ice eutectic mixture. **D.** Melting of salt crystals of KCl from the eutectic mixture. **E.** Frozen microstructure of 10% w/w NaCl-ice eutectic mixture. **F.** Melting of salt crystals of NaCl from the eutectic mixture.

Appendix B: Sample preparation for FEGSEM

Figure B.1: Nitrogen purged glove bag used for storage of samples after freeze drying to prepare samples for FEGSEM to avoid contact with air.

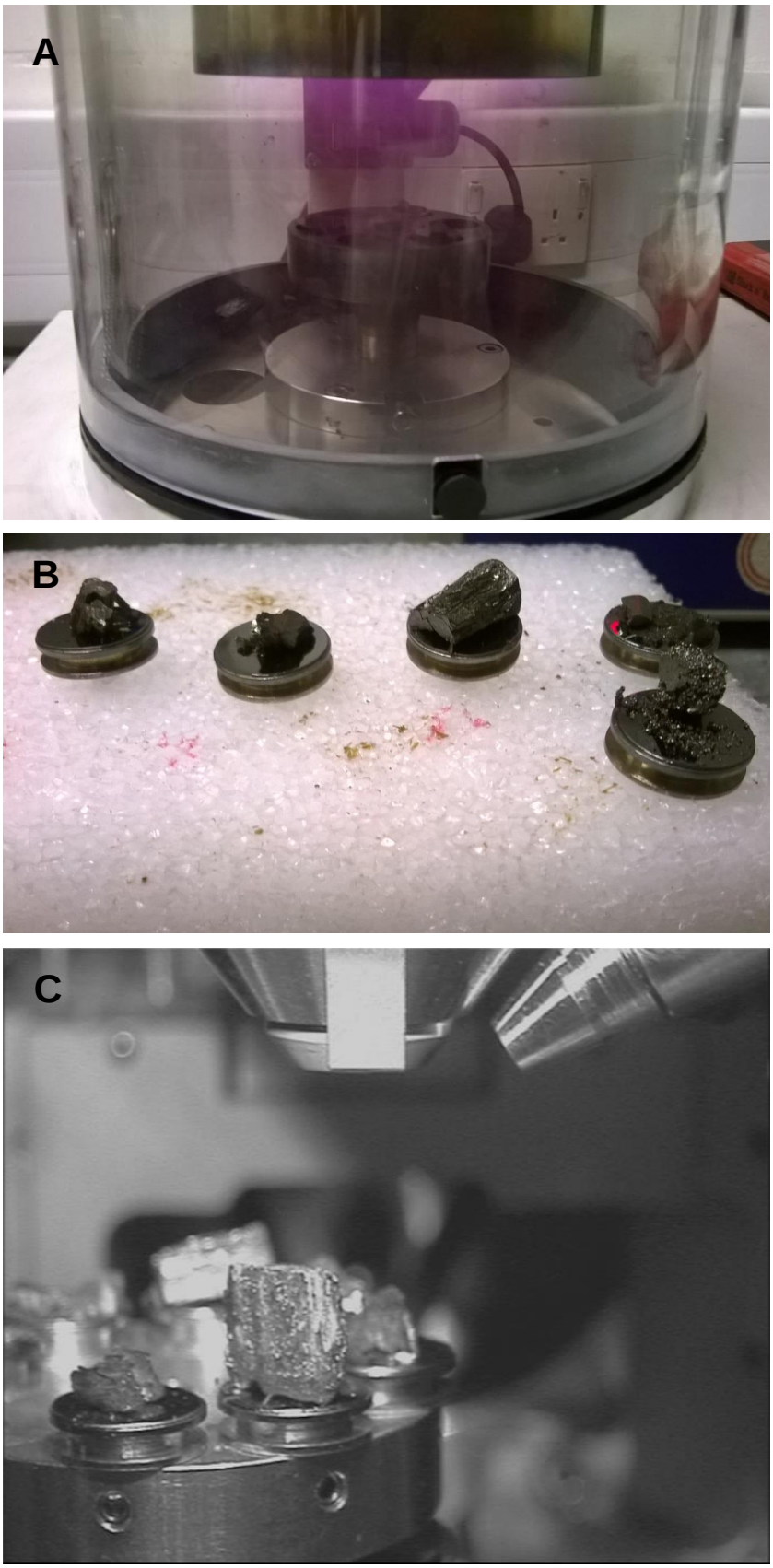

Figure B.2: A. Gold sputtering of freeze dried coffee samples prior to FEGSEM. **B.** Gold-coated tray freeze dried coffee samples. **C.** Coated freeze dried coffee samples on the microscope stage inside the FEGSEM.

Appendix C: Example of 40% lactose freeze-dried without AgI using different cooling profiles.

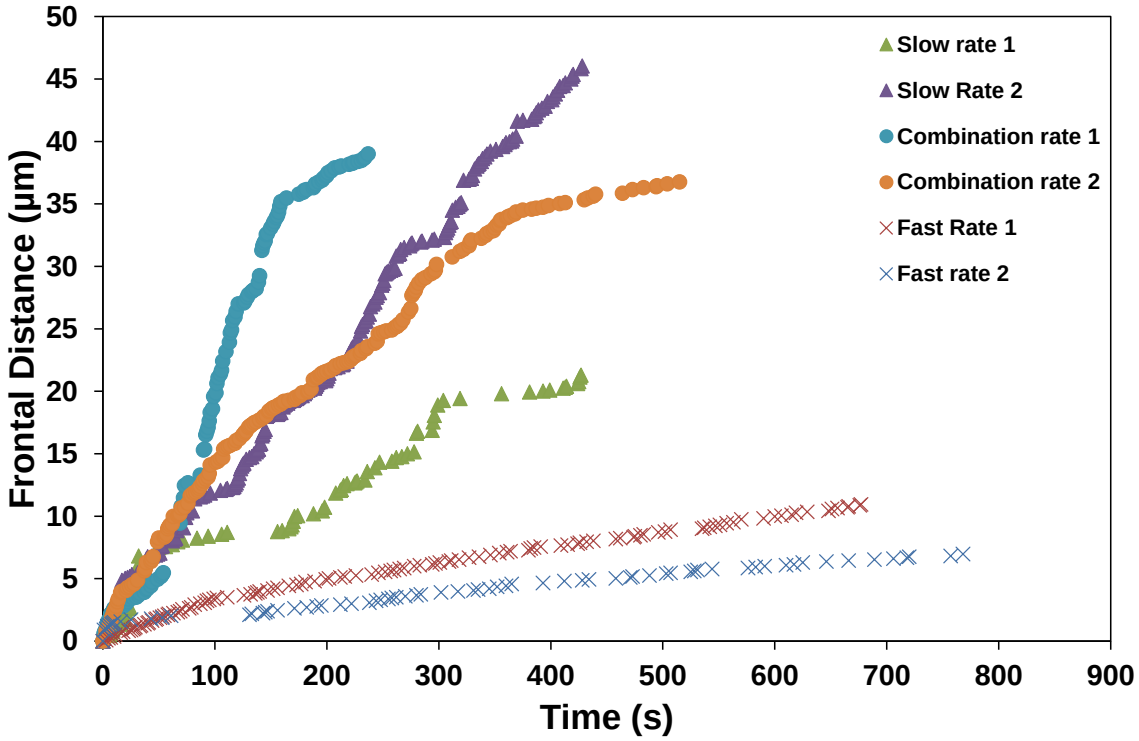

Figure C.1: Frontal distance vs time plots of two repeat runs of freeze-drying of 40% lactose without AgI with three different cooling profiles investigated . Slow rate - 1K.min^{-1}, Fast rate – 50K.min^{-1} and combination rate - 10K.min^{-1} to -10°C followed by 1K.min^{-1} to -40°C.

Appendix D: Example of calculations of edge resistance, α and resistance of dried layer, β for lactose and coffee.

Table D.1 Numerical details of all the parameters required for the calculation of edge resistance, α and resistance of dried layer, β for lactose.

Pressure	Moisture Content		Frozen solid density ρ (kg.m^{-3})	Solid content (%w/w)	a x 10^{6}(s.m^{-1})		b x 10^{12}(s.m^{-2})		$\alpha=a\Delta P/[\rho(M_i-M_f)]$ x 10^{4}		$\beta=b\Delta P/[\rho(M_i-M_f)]$ x 10^{9}	
	M_i	M_f			Parallel orientation	Perpendicular orientation	Parallel orientation	Perpendicular orientation	Parallel orientation	Perpendicular orientation	Parallel orientation	Perpendicular orientation
P_{sat} = 12.8 Pa	19	0.25	50.34	0.05	1.40	2.89	0.0013	0.0061	1.75	3.61	0.0164	0.0763
	9	0.25	102.88	0.10	1.68	3.82	0.0015	0.0069	2.21	5.01	0.0191	0.0902
P = 1 Pa	4	0.25	214.58	0.20	3.75		0.0196		5.51		0.2875	
	2.33	0.25	331.02	0.30	2.12		0.0495		3.64		0.8483	
	1.5	0.25	465.28	0.40	2.46		0.1706		5.00		3.4618	

Table D.2 Numerical details of all the parameters required for the calculation of edge resistance, α and resistance of dried layer, β for coffee.

Pressure	Moisture Content		Frozen solid density ρ (kg.m^{-3})	Solid content (%w/w)	a x 10^{6}(s.m^{-1})	b x 10^{12}(s.m^{-2})	$\alpha=a\Delta P/[\rho(M_i-M_f)]$ x 10^{4}	$\beta=b\Delta P/[\rho(M_i-M_f)]$ x 10^{9}
	M_i	M_f						
P_{sat} = 12.8 Pa	49	0.25	19.87	0.02	1.26306	0.0074309	1.538627	0.090521
	19	0.25	50.31	0.05	2.343052	0.01195229	2.930949	0.149512
	9	0.25	103.01	0.10	3.27308	0.04575875	4.285003	0.599058
	4	0.25	213.72	0.20	3.250806	0.07239994	4.786264	1.065967
P = 1 Pa	2.33	0.25	332.04	0.30	6.09798	0.17905401	10.41872	3.059231
	1.5	0.25	453.03	0.40	15.06703	0.27748325	31.39588	5.782049
	1	0.25	581.75	0.50	6.068012	0.39930818	16.41084	10.79922

Appendix E: Effect of heating or cooling rate on Collapse temperature

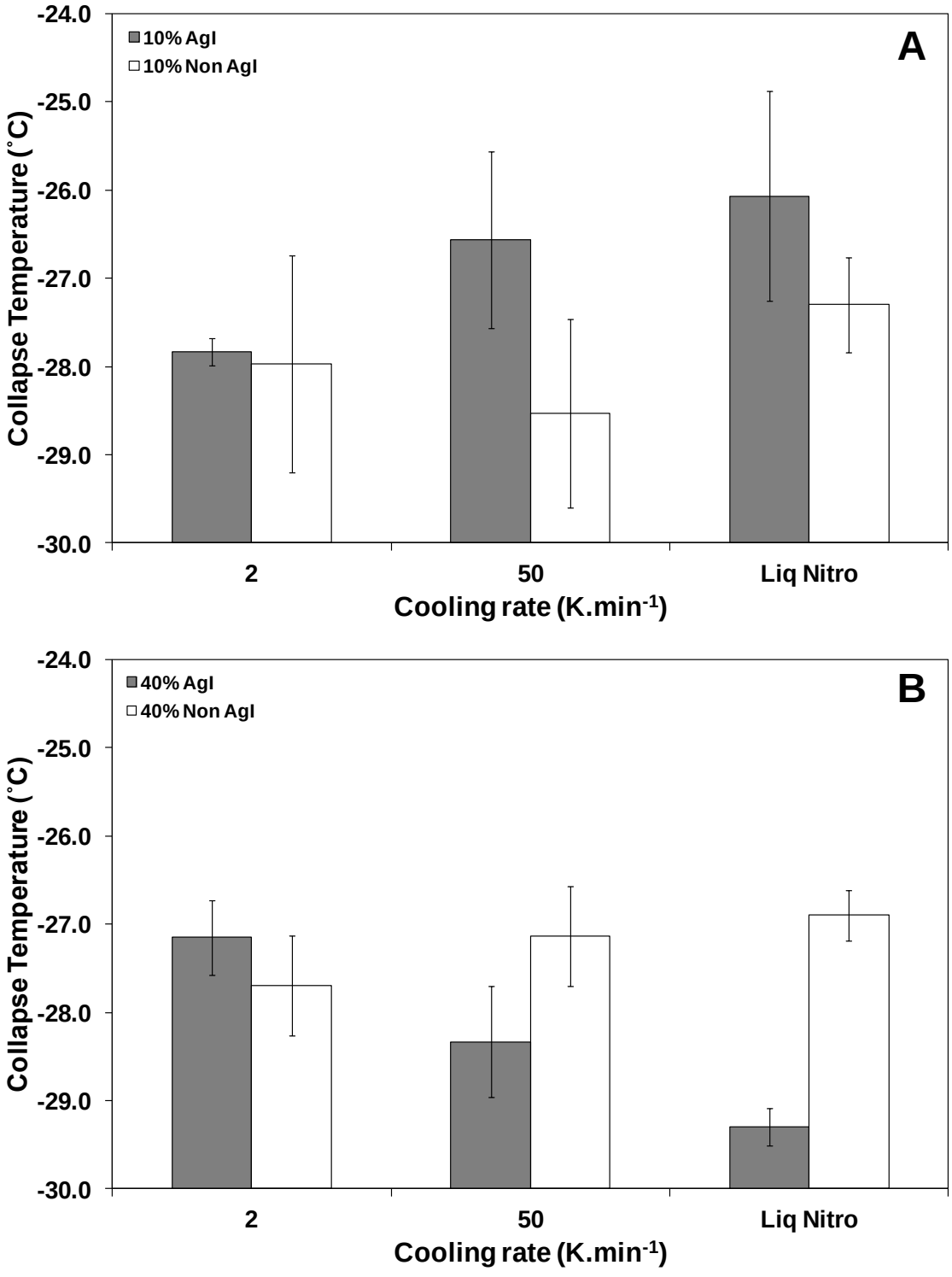

Figure E.1: Effect of cooling rates on collapse temperature. **A.** 10% with and without AgI, freeze dried at 1 Pa and heated at 1 K.min^{-1} **B.** 40% with and without AgI, freeze dried at 1 Pa and heated at 1 K.min^{-1}.

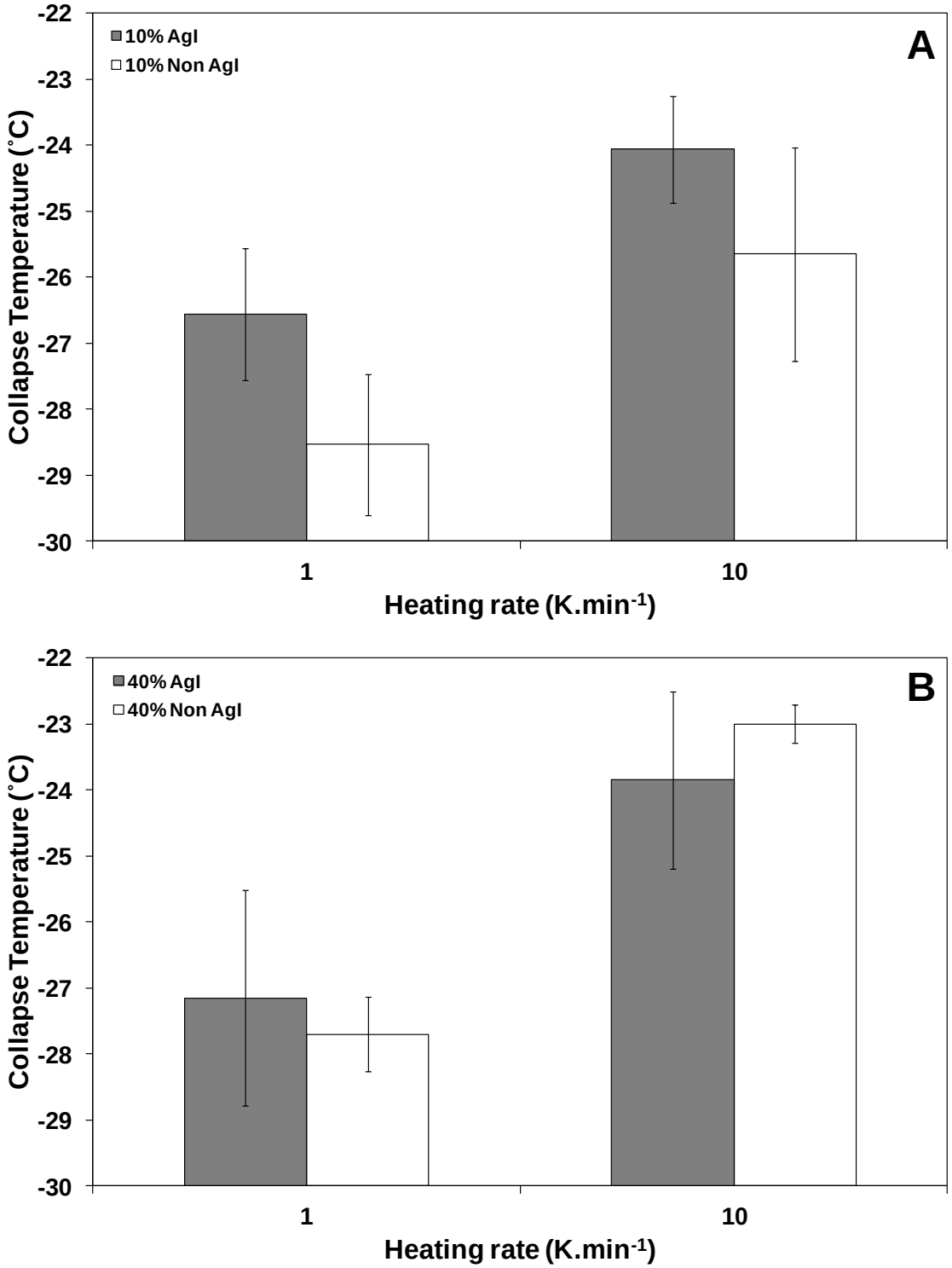

Figure E.2: Effect of heating rates on collapse temperature. **A.** 10% with and without AgI with a cooling rate of 50 K.min^{-1}. **B.** 40% with and without AgI with a cooling rate of 50 K.min^{-1}.

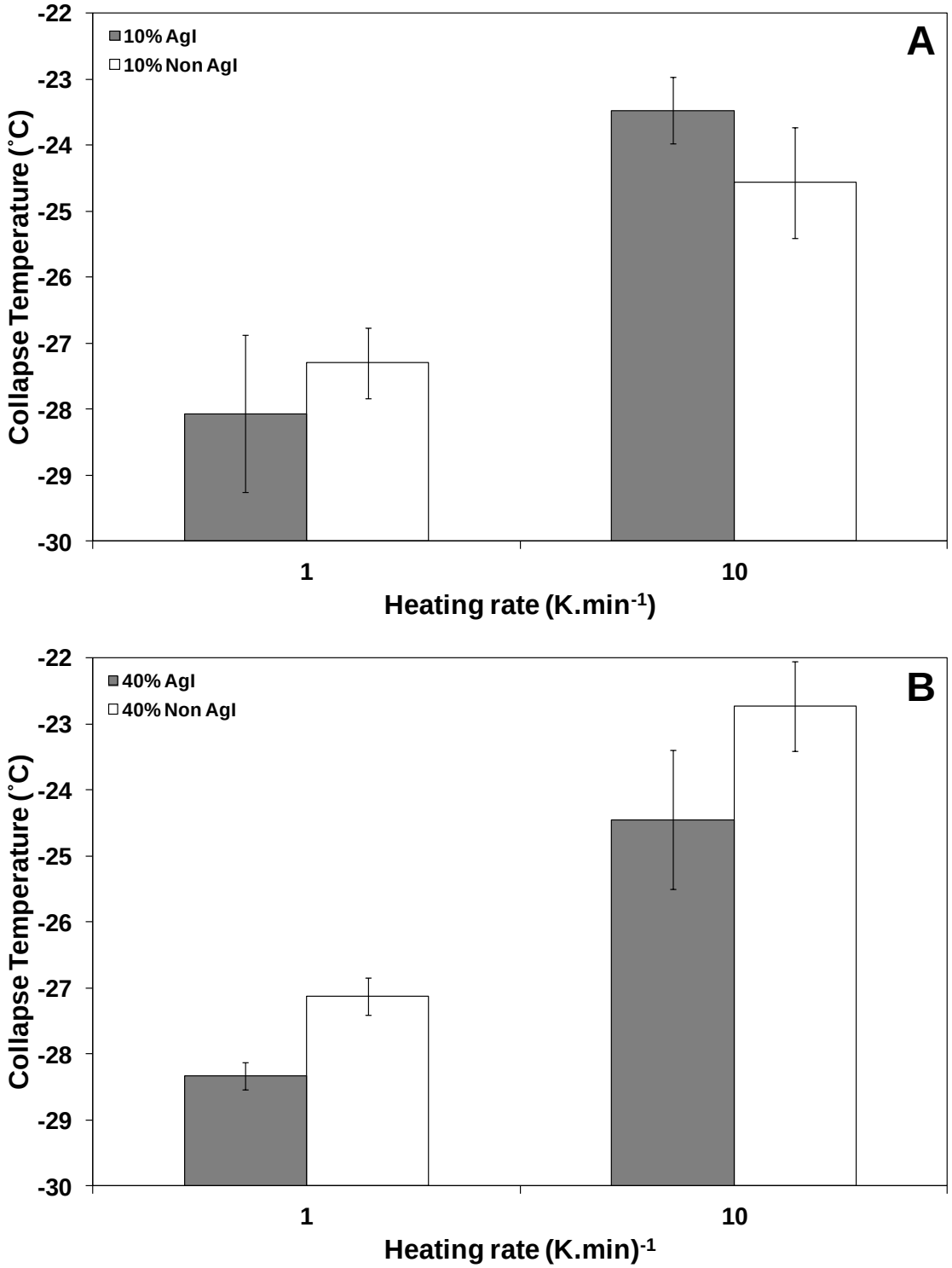

Figure E.3: Effect of heating rates on collapse temperature. **A.** 10% with and without AgI with a cooling by quenching with liquid nitrogen. **B.** 40% with and without AgI with a cooling by quenching with liquid nitrogen.

PERSONAL PROFILE

Purnima Raman

Route de La Croix-Blanche 44
1066, Epalinges, Switzerland
E-Mail: P.Raman@lboro.co.uk
Nationality: Indian

EDUCATION

MSc in Applied Biomolecular Technology (72 %, Distinction)
University Of Nottingham, Nottingham, UK
2008-2009

Thesis:
Carrageenan-Protein Interactions in Pet-food products - Possible alternatives *(Sponsored by Mars, Verden, Germany)*

B. Tech Biotechnology (CGPA-9.035/10, First Class)
SRM University, Chennai, India
2004-2008

Dissertation:
Isolation and Characterization of Heparin and Heparin-like glycosaminoglycans from *Cynoglossus semifasciatus* and *Conus betulinus*.

PUBLICATIONS AND PRESENTATIONS

Journal Publications:
P. Raman, C. D. Rielly, A. G. F. Stapley, Freeze-drying microscopy as a tool to study the kinetics of sublimation process in a model lactose system, 2015 (*plan to submit to Chemical Engineering Science Journal*)

Oral Presentations:
1. *19th International Drying Symposium, August 24-27th, 2014, Lyon, France*
   Studying lyophilisation kinetics using Freeze Drying Microscopy
2. *EuroDrying, October 2-4th, 2013 Paris, France*
   Keynote lecture - Freeze-drying microscopy as a tool to study the kinetics of sublimation in a model lactose system

Poster Presentations:
1. *19th International Drying Symposium, August 24-27th, 2014, Lyon, France*
   Freeze Drying Microscopy to study the kinetics of sublimation of coffee solutions
2. *Research That Matters, March 7th, 2013, Loughborough University, Loughborough, UK*
   Optimisation of the Freeze Drying Process for the Food and Pharmaceutical Industry

3. *'Leishmania' in Genomera 2006 – 'Recent trends in Biotechnology', Periyar Maniammai College of Technology for Women, Tanjore, India.*

ACADEMIC EXPERIENCE

Food Engineering Lab assistantship, Chemical Engineering Department, Loughborough University (2012-2014)

ACADEMIC ACHIEVEMENTS

- `Highly Commended´ for poster presentation in Loughborough University Research Conference (2013)
- PhD project funding from Department of Chemical Engineering, Loughborough University (2010-2014)
- Awarded Developing Solutions Scholarship (2008) from, International Office, University of Nottingham, UK
- Awarded 1st Position for being an outstanding student in my secondary school examinations (2000-2002)

Freeze drying microscopy as a tool to study the kinetics of sublimation in a model lactose system

P. Raman, C.D. Rielly, A.G.F. Stapley*,
Department of Chemical Engineering, Loughborough University, UK.

*Author to whom all correspondence should be addressed: electronic mail: A.G.F.Stapley@Lboro.ac.uk.

Keywords

Lyophilisation, microstructure, frontal velocity, image analysis.

Abstract

Freeze drying is a commonly-used technique in the pharmaceutical and food industries to preserve labile products. Many different instruments have been developed over the years to study and improve freeze drying processes; a recent one being freeze drying microscopy (FDM). This has mainly been used as a tool to study collapse temperatures, but the purpose of this study was to use FDM to gain a better insight into the factors which affect the kinetics of sublimation processes, which may help in optimising real systems.

In this study, 2 µL of various concentrations of lactose solution was initially frozen (typically at -40°C) in a Linkam FDCS freeze drying microscope stage followed by sublimation by applying a vacuum of 1 Pa. Images showing the movement of the sublimation front were captured at regular intervals. An example is shown in Fig 1A, where the freeze-dried region can be seen as distinctly darker than the undried (frozen) region. The movement of the front through the images was tracked using an image analysis program written in MATLAB, which identifies the dried region using an intensity threshold. Analyses were typically performed along 11 lines parallel to the direction of movement of the front (see Figure 1B, where the positions of the fronts from previous images are shown as red dots). The front progress along a single line can then be extracted and an example is shown in Fig 1C.

Initial experiments under nominally identical conditions showed poor reproducibility between samples with as much as a factor of two difference in measured frontal velocities. In response, silver iodide was added to induce ice nucleation at higher temperatures in the samples. This produced much larger crystal sizes and enabled the microstructure to be clearly visible (see Fig 2B c.f. Fig 2A). The observed crystal structures showed distinct directionality which was confirmed by SEM (Fig 2C). Furthermore, the measured frontal velocities correlated well with the observed directionality, with faster velocities observed when ice crystals were oriented "parallel" to the direction of movement of the front, as opposed to "perpendicular". These different structures present different resistances for mass transfer and can explain the previous reproducibility issues.

The effect of ice nucleation temperature, freezing rate, ice crystal size and orientation, initial solid content and final temperature of drying on the sublimation front velocity were then investigated. The frontal data were fitted to a twin resistance model, comprising a fixed surface resistance plus a resistance that increased with depth into the sample. The surface resistance controls the initial front velocity, which then slows as the front penetrates the sample. The initial front velocity was found to decrease with lactose solid content between 5, 10 and 20% w/w, but this then increased again at higher solid contents (30 and 40% w/w). Increasing the freeze drying temperature from -50°C to -30°C led to an increase in the sublimation front velocity in line with the increase in svp of ice at these temperatures.

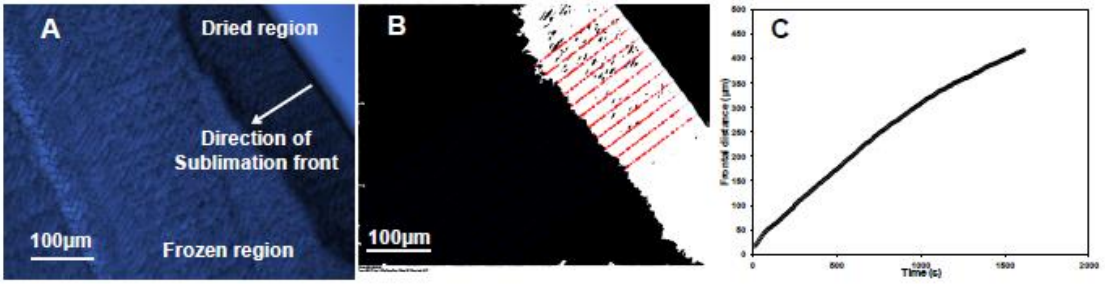

Fig. 1 - (A) Microscope image showing sublimation front, (B) MATLAB analysis, (C) frontal distance vs time.

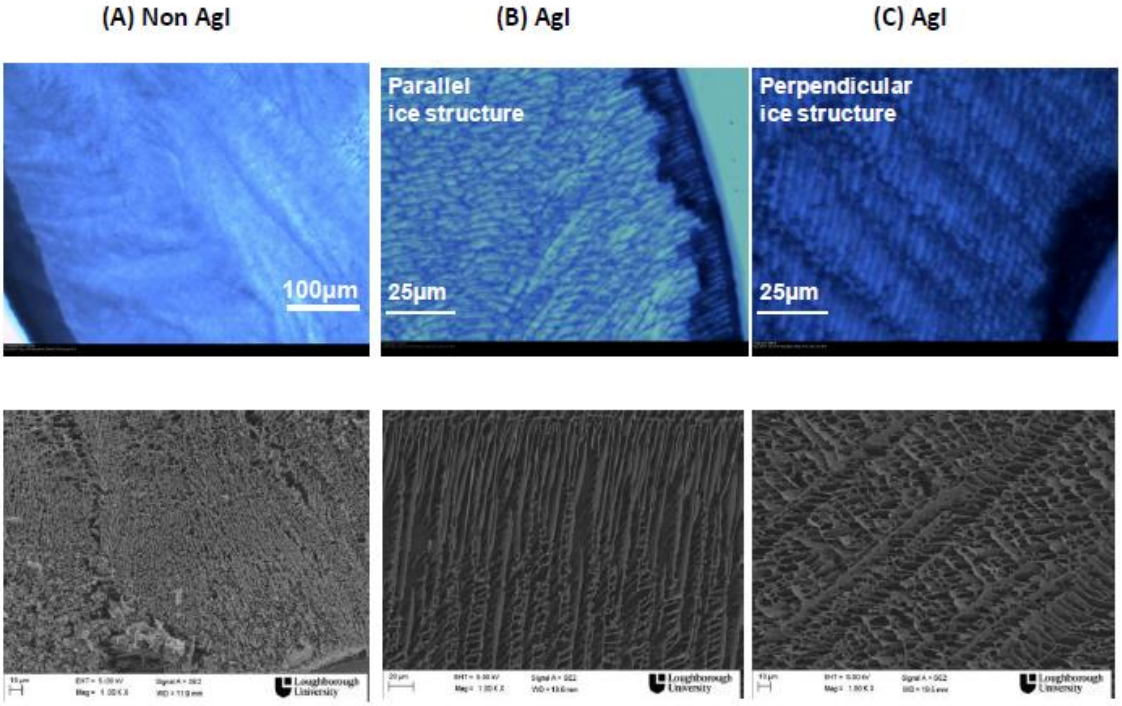

Fig. 2 - Microscope images during freeze drying (above) and SEM images of dried samples (below) from lactose solutions (10%) frozen either without AgI (A), or with AgI (B and C).

EFCE Working Party on Drying

CENTRALE PARIS

AgroParisTech

FCBA INSTITUT TECHNOLOGIQUE

AFSIA

Freeze drying microscopy to study the kinetics of sublimation of coffee solutions

Purnima Raman, Chris D. Rielly, Andrew G. F. Stapley
Department of Chemical Engineering, Loughborough University, UK, LE11 3TU
Email : P.Raman@lboro.ac.uk

Loughborough University

Objectives

- The main aim of this study was to use freeze drying microscopy to study the kinetics of freeze drying of coffee solutions.
- Aeration is a process commonly used in the coffee industry and the effects of aeration on the freeze drying kinetics of coffee were also investigated.
- The effects of nucleation temperature, temperatures of drying and annealing on sublimation kinetics were also investigated.

Freeze drying microscopy

Freeze drying microscopy (FDM) can provide fundamental information in order to optimise the process in a real system.

What can be determined?

- Sublimation front velocity (related directly to sublimation rate)
- Collapse temperature
- Optimum freezing profile
- Optimum drying temperature

Sublimation front velocity

- In-house programme was developed using MATLAB image analysis software to automatically track the sublimation front.
- Uses a sequence of binary images to track the width of the dark freeze drying band and marks the points on the moving front on the images.
- Outputs sublimation front distance with time and a & b values – representative edge resistance and resistance of dried layer respectively.

(A) Sublimation front movement (Lactose) (B) Matlab Analysis (C)Frontal distance vs time

Coffee system

Effect of ice crystal size and orientation

Coffee solutions of various solid content were frozen and freeze dried with and without nucleating agent (AgI).

Nucleating agent had a pronounced effect on nucleation temperature, ice crystal structure and orientation.

- Nucleation temperature decreases with increasing solid content.

Microscopic images of frozen coffee solution (10%)

Non-AgI AgI

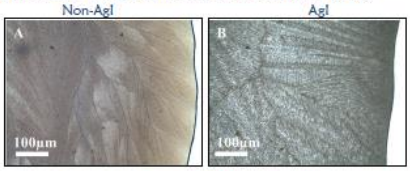

FEGSEM images of 10% (A&B) & 50% (C&D) coffee freeze dried in FDM

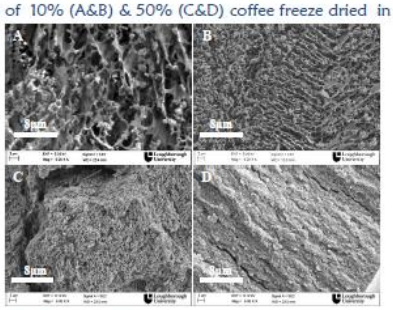

Effect of solid content

Edge resistance (a) initially increased with increasing solid content but decreased with further increase in solid content (50%) while the resistance of the dried layer (b) increased continuously with increasing solid content. It might be attributed to a decrease in the amount of water in 40 & 50% Coffee.

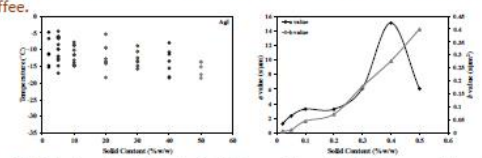

(A) Nucleation temperature (with AgI) vs. solid content (B) a& b vs. solid content

Effect of drying temperature

Three different temperatures of drying were investigated (-30, -40 & -50°C).

Both *a* and *b* values decreased with increasing temperature. This is mainly due to the variation with temperature of the saturated vapour pressure (SVP) of ice, which both the *a* and *b* values incorporate.

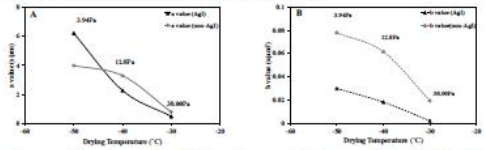

(A) a value vs. drying temperature (B) b value vs. drying temperature of 10% coffee

Annealing

Annealing involved freezing the sample to -40°C, heating to -10°C, holding for ~60 minutes to allow melting and recrystallization and then cooling the sample to -40°C.

Ice crystals in frozen coffee solution after annealing was seen to be much larger and more evenly distributed than before annealing.

This translated into much lower bulk resistance (*b*) values when the samples were freeze dried at 1 Pa.

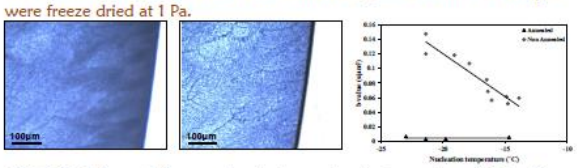

10% Coffee before and after annealing, b value vs nulceation temperature of 10% coffee with annealing

Aeration

50% coffee solutions were "aerated" with N_2O gas and freeze dried.

Aerated samples were found to dry faster with "jumps" in the front distance vs time plot wherever a bubble was encountered in the microstructure .

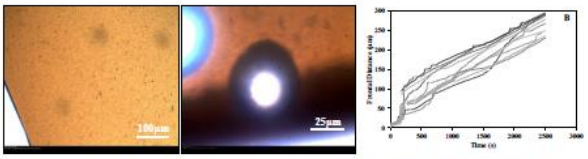

Non-aerated and aerated 50% coffee (B) frontal distance vs time plot of aerated 50% coffee freeze dried under FDM

Conclusions

FDM provides information regarding optimum solid content, drying temperature and freezing profile which can be used for formulation & cycle development of a real freeze drying system.

Acknowledgement: Financial support from the Department of Chemical Engineering, Loughborough University

19th International Drying Symposium (IDS 2014)
Lyon, France, August 24-27, 2014

FREEZE DRYING MICROSCOPY AS A TOOL TO STUDY THE SUBLIMATION KINETICS OF A FREEZE DRYING PROCESS

P. Raman, C.D. Rielly, A.G.F. Stapley*

Department of Chemical Engineering, Loughborough University, Loughborough, Leicestershire, LE11 3TU, UK.

**Corresponding author: Tel.:+44-1509-222525, E-mail: A.G.F.Stapley@lboro.ac.uk*

Abstract: An automated image analysis method was developed in MATLAB to extract frontal movement data from Freeze Drying Microscope (FDM) images to gain a better insight into the sublimation kinetics of freeze drying systems. A twin resistance mass transfer model was proposed, to describe the sublimation kinetics of lactose and coffee samples, namely a fixed edge resistance and a resistance of the dried layer which increased with front depth. Freeze drying rates were strongly dependent upon sample microstructure and initial solids content and were approximately proportional to the saturated vapour pressure of water, confirming the long-held belief that water vapour pressure is the main driving force for mass transfer in freeze drying systems.

Keywords: Frontal velocity, lyophilisation, sublimation kinetics modelling, silver iodide

INTRODUCTION

Freeze-drying is a drying method used in the pharmaceutical and food industries to stabilise and preserve the quality of temperature-sensitive products. Pharmaceutical applications include the freeze-drying of living cells, enzymes and biological media using various excipients and protecting agents or as nasal drug carriers. In the food industry, freeze-drying is applied to the manufacture of products such as coffee, milk powder and infant formula [1-6]. The process involves first freezing the product, followed by sublimation and secondary drying [7].

Many different methods and devices have been developed over the past few years to study and improve freezing and freeze-drying processes [8,9]. One such development is the Freeze-Drying Microscope (FDM) stage. This allows the direct visualisation of the sublimation front, as the dried region appears much darker than undried icy material. This is due to greater light scattering in the dried region than the icy region. Light is able to transmit through the icy region with minimal scatter as the two phases (ice and the freeze concentrated matrix) have similar refractive indices. However, when the ice sublimes to leave voids, the differences in refractive index between the air pores and the solid matrix causes significant scatter. The stark contrast in brightness of the two regions means that the position of the freeze drying front is easy to elucidate.

The most common use of FDM currently is to determine the collapse temperature (T_c) of a product to be freeze-dried [10-14]. The collapse temperature is defined as the temperature where loss of structure (or shrinkage) of the product occurs. It is of great importance as it defines the highest temperature that the product can be exposed to during primary drying without adversely affecting rehydration properties.

The collapse temperature can be found using FDM by gradually increasing the temperature as the sample is freeze dried. The loss of structure that occurs on collapse results in a clear transmission of light and so corresponds to a transition from a dark to a light band at the first point of collapse. The temperature at which this first occurs recorded as the collapse temperature.

However, very few researchers have focussed on using FDM to determine frontal velocity or to link it to sublimation rate; potentially this information could be used to better understand the freeze drying process and improve its efficiency, thereby decreasing its overall cost. Zhai *et al.*, 2003[11] have been among the few researchers who have tried to measure the primary drying rates using FDM; they characterised the drying rate by determining an effective diffusion coefficient, D_{eff} and suggested that sublimation rate increase near the collapse temperature was due to increase in channelling of water vapour through the dried layers. They also showed that the sublimation times calculated using these D_{eff} values were in practical agreement with the sublimation times in a conventional laboratory freeze-dryer [11].

The purpose of the current study was to use FDM to obtain fundamental information on sublimation kinetics as well as collapse temperature which may help to better understand real systems.

MATERIALS AND METHODS

Materials

α-lactose monohydrate, silver iodide (AgI) purchased from Fisher Scientific (Loughborough, UK). Lactose was stored in an air-tight bottle to prevent any moisture absorption.

Determination of moisture content

A *Karl Fischer titration* was used to determine the moisture content of the as received α-lactose monohydrate [15]. The moisture content of the α-lactose monohydrate was determined on a wet basis to be 5.8 ± 0.3%.

Sample preparation

Different solid concentrations of α-lactose monohydrate (5 to 40%) were prepared, taking into account the initial moisture content of the lactose powder.

Freeze-drying microscopy

Experiments were performed on a Linkam FDCS196 variable temperature control stage with an Olympus BX43 microscope connected to a QImaging Retiga 2000R digital camera. The stage was sealed so that vacuum could be drawn using a vacuum pump. The pressure was measured using a Pirani gauge over a range of 1 Pa to 100 000 Pa. Liquid nitrogen was used as the coolant and was passed through a silver block upon which the slides were mounted to gain good thermal control throughout the sample. The stage pressure, temperature and image capture were controlled using Linksys 32 software.

2 µL of sample solution was prepared and loaded onto the microscope stage. The sample solution was frozen by cooling at a constant rate to a set drying temperature followed by a reduction of the vacuum pressure to 1 Pa to initiate freeze drying. This resulted in the sublimation of ice into water vapour from the sample and movement of the sublimation front was generally observed for about 1000s. For some experiments, a miniscule amount of AgI was placed on the bottom glass slide before loading of the sample. The purpose of the AgI (which is a nucleating agent for ice) was to induce nucleation at a higher temperature in the samples. Three different drying temperatures (-30, -40 and -50°C) were also investigated.

To study the ice crystal structures using scanning electron microscope, 10% and 40% (w/w) lactose solutions were also freeze-dried under the microscope overnight (with and without AgI) in order to obtain dried samples without any structural collapse.

Image analysis of the sublimation front movement

The camera software captured images from the microscope at a rate of 1 per 10 seconds. These images were analysed using an in-house image analysis program developed in MATLAB. The images obtained were first calibrated and then thresholded to a set value in the program to produce a binary image, with the sublimation front seen as a white band on a black background (Fig. 1).

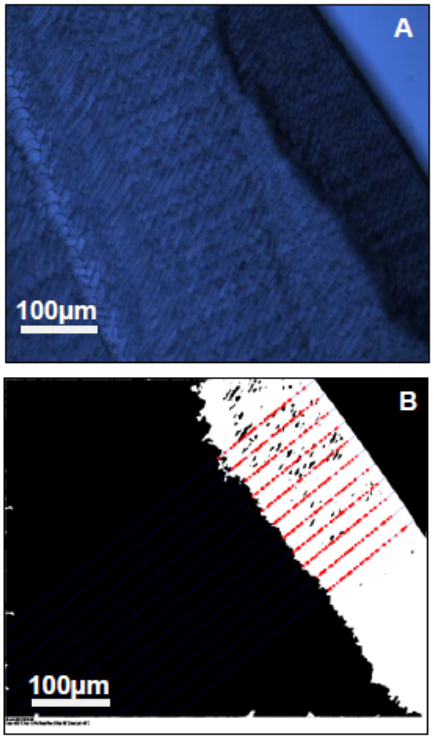

Fig. 1. A. Sublimation front movement of 10% lactose, frozen and freeze dried at a vacuum pressure of 1 Pa. B. Binary image of (A) showing multiple line analysis obtained from image analysis program.

The threshold values were only sensitive to the solids content of the sample and were not required to be changed for repeat runs of a single solid content. The user would then define a line parallel to the freeze drying front by fixing two pixel points on the sample edge on the first image. Multiple lines perpendicular to the sublimation front would be constructed by the program at set intervals. The movement of the sublimation front was then tracked along each line (as the transition from white to black pixels) on each successive image (Fig. 1A and 1B). These pixel points were recorded and converted to frontal distance (µm). The average frontal position across all lines was then plotted against time (s), but checks were made to ensure that the measured frontal positions were reasonably consistent across the width of the front.

Parameterised Modelling to describe the sublimation front movement

A simple mass transfer model was developed to fit to the sublimation front movement data. As the sample was very thinly spread between two impermeable glass slides in good thermal contact with a temperature-controlled microscope stage. Hence, the sample was considered to be isothermal and heat transfer was not considered to limit the speed of the sublimation front. Fig. 2 shows the components of the model.

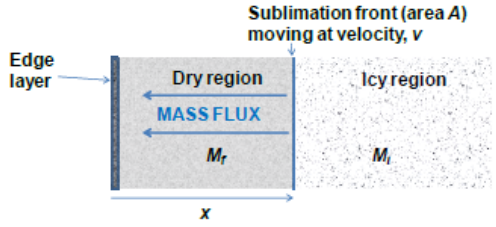

Fig. 2. A model of the sublimation front movement defining the direction of mass flux, edge of the sample and dried region.

The primary drying rate was controlled by mass transfer from the sublimation front where the water vapour flows through the dried region and then through the edge layer of the sample, both of which provide a resistance to mass transfer. It was assumed that water vapour was the only gas in the vapour phase around the sample with all the other gases being withdrawn by the vacuum pump. The pump applies a pressure P at the edge of the sample whereas at the sublimation front the pressure is equal to the saturated vapour pressure of ice P_{sat} at the specific temperature. The frozen matrix was initially at a uniform moisture content of M_i (dry basis), solid frozen density (dry basis) of ρ and dried by sublimation to a final moisture content of M_f (dry basis). The water content of edge layer of the sample was assumed to be negligible.

The frontal data obtained were fitted to the model based on two resistance terms – a constant edge layer resistance (α) and resistance of the internal dried region (β) that increases proportionally with distance (x) of sublimation front to the edge of the sample.
The mass flux of water vapour perpendicular to the drying front (driving force/resistance) is thus given by,

$$\text{Mass flux} = \frac{P_{sat} - P}{\alpha + \beta x} \quad (1)$$

The mass flux can also be related to the movement of the sublimation front as follows. If the velocity (v) is:

$$v = \frac{dx}{dt} \quad (2)$$

Then the amount of dry solid swept out per unit time

$$= \frac{\rho A dx}{dt} \quad (3)$$

Moisture removed per unit time

$$= \frac{\rho(M_i - M_f) A dx}{dt} \quad (4)$$

Hence, Mass flux

$$= \frac{\rho(M_i - M_f) dx}{dt} \quad (5)$$

Combining equation 1 and equation 5,

$$\frac{\rho(M_i - M_f) dx}{dt} = \frac{P_{sat} - P}{\alpha + \beta x} = \frac{\Delta P}{\alpha + \beta x} \quad (6)$$

This can be more simply expressed as velocity of the front,

$$v = \frac{dx}{dt} = \frac{1}{a + bx} \quad (7)$$

Where,

$$a = \frac{\alpha\rho(M_i - M_f)}{\Delta P} \text{ and } b = \frac{\beta\rho(M_i - M_f)}{\Delta P} \quad (8)$$

Integrating equation 7 gives:

$$t = ax + \frac{bx^2}{2} \quad (9)$$

Data were fitting to the above equation using least squares regression in order to obtain the representative edge 'resistance' (a) and 'resistance per unit depth' from the dried region (b). The parameter b is associated with the reduction in drying rate as time proceeds. In some situations it was necessary to study sublimation for a longer duration (1 hour) in order to gain a better estimate of this value. The representative surface or edge resistance (a) determines the initial frontal velocity.

Field Emission Gun Scanning Electron Microscopy

To study the ice crystal structure of the freeze-dried samples, a Leo 1530VP high resolution field emission gun scanning electron microscope (FEGSEM) was used at a range of magnifications. Initially, a thin layer of Au coating was sputtered onto the samples via an EMITECH SC7640 Au/Pd sputter coater for about 90s. The imaging of the internal structures was achieved using secondary electrons released from the top surfaces of the samples, which were generated by an incident electron beam with 5 kV accelerating voltage within a working distance of ~20 mm.

Conventional freeze drying

Conventional freeze drying of 10% lactose solutions in glass vials was carried out in a VirTis AdVantage Plus Benchtop shelf based Freeze Dryer (SP Industries, Warminster, PA). The vials were filled with about 4 mL of lactose solution to ~14 mm height in the vial and thermocouples were placed at three different depths inside the sample: 3, 7 and 11 mm. An additional thermocouple was attached to the surface of the shelf to measure the shelf temperature. The vials were kept in good thermal contact with the shelf using thermal grease. The samples in the vials were cooled to a temperature of about -40˚C at 1 K/min and then freeze dried at 10 Pa. The samples were freeze dried until the temperatures of the thermocouples had risen to a steady value above the shelf temperature. The dried samples were also prepared for scanning electron microscopy. The temperature data were recorded onto a computer using the Labview-Signal express program.

RESULTS AND DISCUSSION

An example image taken during freeze drying of a 10% lactose solution is depicted in Fig. 3. This clearly shows the dried and icy regions. The microscope is able to show the presence of a microstructure, however the microstructure is very fine and it is difficult to observe microstructural features.

Frontal distances are plotted against time in Fig. 4 for three repeat runs. The data represent the average displacement along 11 analysis lines. The data were also fitted to the model described in previous section and were found to fit the experimental data quite well.

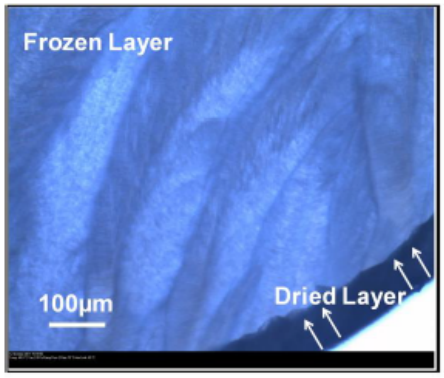

Fig. 3. Frozen layer, dried layer and direction of sublimation in 10% lactose solution frozen at -40˚C and freeze dried at 1 Pa under FDM

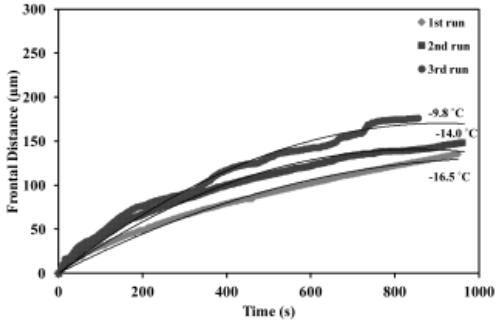

Fig. 4. Frontal distance vs time plot for 10% lactose freeze dried under FDM displaying repeat runs under near-identical conditions.

However, the frontal distance versus time plot did not show reproducibility when compared between repeat runs in near-identical experimental conditions.

One possibility for the variation was that there were significant differences in nucleation temperature between runs. Freezing typically took place extremely rapidly during cooling, so much so that when acquiring images at 1 second time intervals it was rarely able to see freezing in progress. However, the temperature at which freezing/nucleation took place showed large variations.

To test this, different cooling rates were explored during the freezing step – slow (1 K/min), fast (50 K/min), very fast (130 K/min), to try to achieve more consistent results. However, results were still inconsistent. Another method tried was to scratch the slides using a metal file in order to create sites for forced nucleation to occur, but this method also did not yet again result in reproducible nucleation temperatures and frontal velocities.

Experiments with silver iodide

One method that did overcome the problem of reproducibility was to place a small amount of silver iodide (AgI) on the bottom glass slide before adding the sample solution. β-AgI has been reported to have a hexagonal crystal structure similar to that of ice and is quite stable at low temperatures; hence it is able to act as a seed for ice crystal formation. This has found applications in cloud seeding and snow making. AgI was found to bring much better reproducibility to the nucleation temperature as shown in Fig. 5, which showed a decrease with increasing solids content, mirroring the trend in melting point depression.

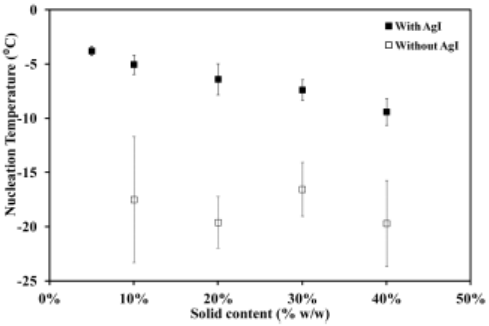

Fig. 5. Nucleation temperatures of lactose solutions with and without AgI (5-40% w/w). Error bars show standard deviations from at least 5 repeats.

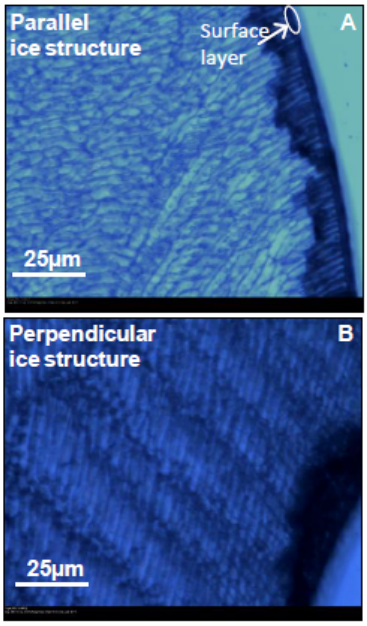

Fig. 6. A and B show "parallel" and "perpendicular" ice crystal orientations observed in 100X magnification respectively in 10% lactose solution in the early stages of freeze drying.

The increase in nucleation temperature by the addition of AgI also resulted in much larger crystals and these were large enough to be visible and distinct under the microscope. The crystals were generally long and thin and could have any orientation. Fig. 6A and Fig. 6B show two different orientations: parallel and perpendicular to the direction of movement of the front respectively. These crystal orientations were visible only in the case of 5% and 10% (w/w) lactose solutions. Fig. 6A also clearly shows the presence of a surface layer which was purely freeze concentrated material that had not contained ice crystals. This shows visual evidence of the surface resistance component of the mass transfer model.

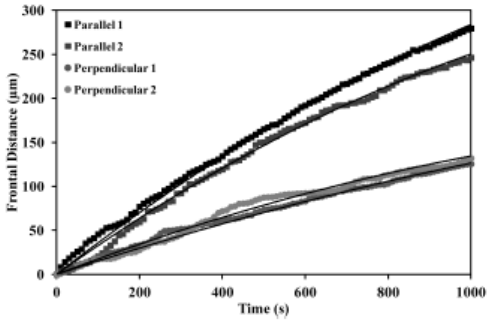

Fig. 7. Difference between frontal distance with time of parallel and perpendicular crystal orientation of 5% w/w Lactose sample with AgI freeze dried under FDM.

The crystal orientations were also found to directly influence in the frontal velocity of the sample. Frontal velocities were seen to be faster in the parallel orientation than in the perpendicular orientation (Fig. 7), by approximately a factor of two. This demonstrates that the orientation of the microstructure has a direct effect on frontal velocities and also possibly explains the lack of reproducibility in the earlier samples without AgI as these are also likely to have had differences in microstructure orientation.

Scanning electron microscopy

To further examine the microstructures, samples that had been fully dried were taken for examination by Scanning Electron Microscopy (SEM). Fig. 8 shows SEM images obtained at two different magnifications 1KX and 5KX from 10% and 40% lactose solutions (w/w) both with and without AgI.

The use of AgI was found to affect the size and order of ice crystal formation significantly as the absence of AgI resulted in much finer and more randomly shaped crystals in 10% lactose (Fig. 8A, B, C and D), although some directionality in the structure was still evident. This gives some weight to the hypothesis that differences in crystal orientation were responsible for the lack of reproducibility in the non AgI samples. The directionality was also observed in freeze dried samples obtained from 40% lactose, although the size of ice crystal was much smaller due to the presence of higher amounts of lactose in the sample (Fig. 8E, F, G and H). This further proves the effect of concentration on the freezing point depression and, in turn, on the nucleation temperature which results in smaller ice crystals and no specific orientation of the crystals. The cracks observed in Fig. 8E and Fig. 8G were thought to be due to the removal of unfrozen water which takes place during secondary drying of samples under FDM.

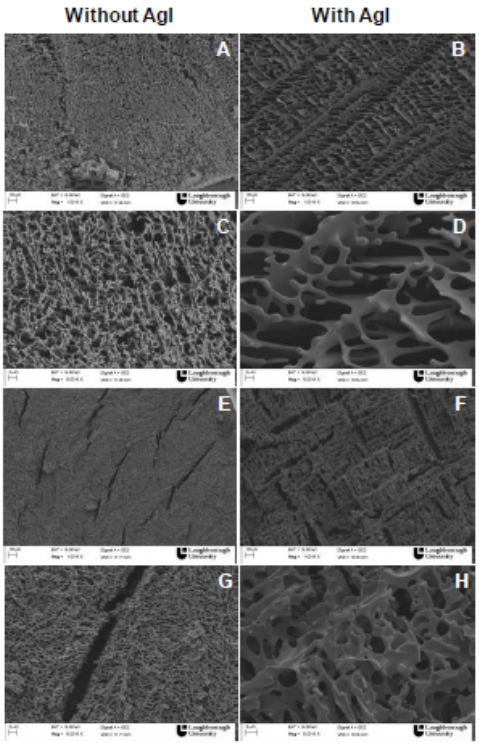

Fig. 8. FEGSEM images. A and C. 10% lactose freeze dried without AgI (1KX and 5KX). B and D. With AgI (1KX and 5KX). E and G. 40% lactose freeze dried without AgI (1KX and 5KX). F and H. With AgI (1KX and 5KX).

Variation of kinetics with initial solids content

The data obtained from all the various experiments was fitted to the twin-resistance model described in the previous section and the representative edge resistance '*a*' and dried layer resistance '*b*' were obtained for all the runs. The results for freeze drying at -40°C for various lactose concentrations after cooling at 10K/min are shown in Fig. 9 and Fig. 10.

The surface resistance term (Fig. 9) is inversely related to the initial speed of the sublimation front. It can be seen that there is a finite resistance for pure water which can be attributed to mass transfer resistances in the FDM equipment. Additional resistances can be attributed to the surface layer of the sample itself. It can be seen that with low concentrations of lactose a higher surface resistance was present in samples where the crystal orientations were perpendicular to the direction of frontal movement. In the case of parallel orientation some crystals are able to penetrate into this layer and thus reduce the effective resistance of the surface. For concentrations above 20% the microstructure is indistinct but 20% shows the highest surface resistance and this then drops as the concentration increases.

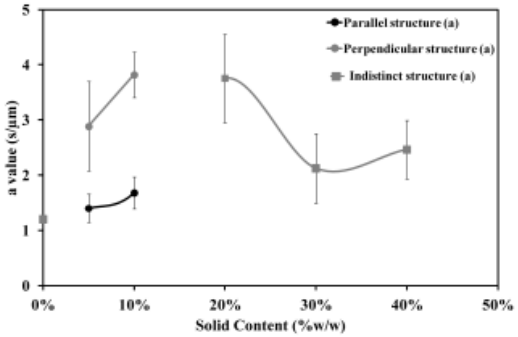

Fig. 9. Variation of surface resistance term (a) with solids content for lactose solutions when freeze drying at -40°C.

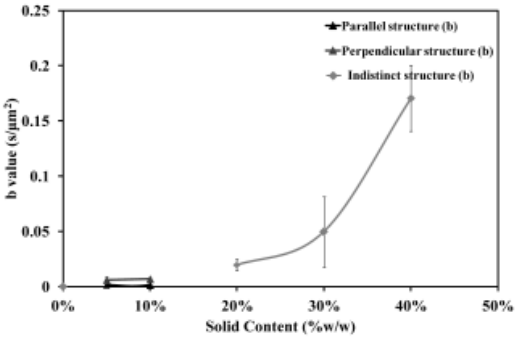

Fig. 10. Variation of resistance per unit depth term (b) with solids content for lactose solutions when freeze drying at -40°C.

The resistance per unit depth (Fig. 10) is a strong increasing function of solids content as the amount of solid material that water needs to pass through increases. There is a lower resistance to mass transfer when the crystals are oriented parallel to the direction of front movement than when the orientation is perpendicular. This is due the increase in the number of barriers that need to be crossed in order to move a unit distance through the material.

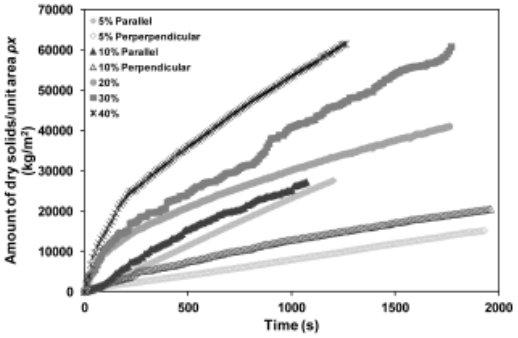

Fig. 11. Amount of dried solid produced with time for the different initial solid contents of lactose (5-40% w/w) freeze dried under FDM.

However, when the amount of dried matter produced is plotted against time (Fig. 11) it can be seen that even though the higher solids content samples have a higher resistance, they yield a greater "production rate" as less water is required to sublime per unit mass of solid.

Variation of initial front velocity with temperature

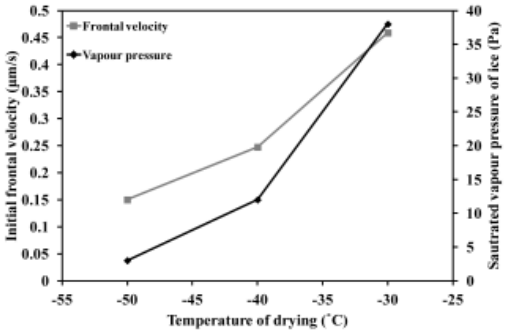

Fig. 12. Variation of initial front velocity with freeze drying temperature for 40% lactose solutions and comparison with saturated vapour pressure.

Three different final freeze drying temperatures were investigated (-30°C, -40°C and -50°C) for 40% (w/w) lactose solutions. The initial front velocities (Fig. 12) are a strong increasing function of temperature and showed a similar variation with temperature to the saturated vapour pressure of water, confirming that water vapour pressure difference is the main driving force for mass transfer in freeze drying systems.

Shelf freeze drying of lactose

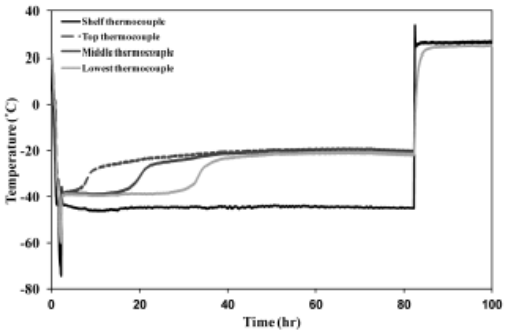

Fig. 13. Temperature vs time profile of vial freeze drying of 10% lactose dried in a shelf freeze dryer.

Fig. 13 shows the temperature vs time data obtained for freeze drying of 10% lactose in a glass vial. After freezing has occurred during the first hour of operation, the three thermocouples all remain constant at approximately -40°C which is very close to the shelf temperature. The temperatures then rise once the sublimation front has passed each thermocouple, starting with the highest placed thermocouple. This thus gives a good indication of

Table 1 shows the sublimation time predicted from the model and the comparison to the actual freeze drying time (hrs) for vial freeze drying of lactose samples

Solid Content (%w/w)		Sample Depth (mm)	Experimental FD time (hrs)	Predicted FD Time (hrs)
10	‖	11mm	41.9	29.7
		7mm	31.7	13.2
		3mm	20.7	3.23
	⊥	11mm	41.9	127
		7mm	31.7	54.2
		3mm	20.7	11.8
40		11mm	187	2870
		7mm	131	1170
		3mm	78.9	215

the time taken for the sublimation front to reach each thermocouple position. This can be compared to predictions from microscopy data.

Table 1 shows the comparison of times for the sublimation front to reach each depth between the measured (vial) data and those predicted from the FDM model for 10% and 40% lactose samples. In case of 10% lactose, freeze drying times were predicted based on the two different types of ice crystal orientations – parallel (‖) and perpendicular (⊥). In the case of 10% lactose the actual values were in between the two models (which might be regarded as two extremes), however in the case of 40% lactose the FDM model severely underpredicted the freeze drying times observed in the vials. This is mainly a consequence of the high values of b used in the FDM model. The faster times observed with the vials (particularly at greater depths) may be due to the formation of cracks in the vial samples which may effectively reduce the mass transfer resistance in the samples.

CONCLUSIONS

Freeze drying microscopy is a very useful tool for studying and optimising the process of lyophilisation. FDM is functional way for visualising the process of sublimation as it occurs and the effect of microstructure on the front movement velocity can be easily observed. The images obtained from FDM were analysed successfully using MATLAB and practical information can be obtained from fitting the data to the twin resistance model proposed, which comprised a surface resistance term and a resistance that increased with the depth into the sample. A non-porous layer could be seen at the surface of many

samples, which is seen as the origin of the surface resistance.

The orientation and size of ice crystals were found to have a direct influence on the sublimation velocity, after they had sublimed to leave behind pores. Pores oriented parallel to the direction of the frontal movement were able to provide a much lower resistance to mass transfer within the material but also reduced the surface resistance as they were better able to penetrate the surface layer. Sublimation rates were also seen to increase with temperature approximately in line with the variation of saturated vapour pressure.

NOMENCLATURE

A Area	m^2
t time	s
x frontal distance	µm
v frontal velocity	μms^{-1}
M moisture content	
P Pressure applied for sublimation	Pa
a Representative edge resistance	$s\mu m^{-1}$
b Representative resistance of dried layer	$s\mu m^{-2}$
Greek letters	
ρ dry solid density	$kg.m^{-3}$
α Actual edge resistance	ms^{-1}
β Actual resistance of dried layer	s^{-1}
Subscript	
Sat saturated vapour pressure of ice	Pa
i initial moisture content of frozen solid	
f final moisture content of dry solid	

REFERENCES

1. Pardo, J. M.; Suess, F.; Niranjan, K.. An investigation into the relationship between freezing rate and mean ice crystal size for coffee extracts. Food and Bioproducts Processing **2002**, 80, 176-182.

2. Fonseca, F.; Passot, S.; Cunin, O.; Marin, M. Collapse temperature of freeze-dried *Lactobacillus bulgaricus* suspensions and protective media. Biotechnology Progress **2004**, 20, 229-238.

3. Thomas, M. E. C.; Scher, T. J.; Desorby, S. Lactose/β-Lactoglobulin interaction during storage of model whey powders. Journal of Dairy Science **2004**, 87, 1158-1166.

4. Nasirpour, A.; Landillon, V.; Cuq, B.; Scher, J.; Banon, S.; Desorby, S. Lactose crystallization delay in model infant foods made with lactose, β-Lactoglobulin and starch. Journal of Dairy Science **2007**, 90, 3620-3626.

5. Chow, K. T.; Zhu, K.; Tan, R. B. H.; Heng, P. W. S. Investigation of electrostatic behaviour of a lactose carrier for dry powder inhalers. Pharmaceutical research **2008**, 25, 2822-2834.

6. Yang, G.; Gilstrap, K.; Zhang, A.; Xu, L. X.; He, X. Collapse temperature of solutions important for lyopreservation of living cells at ambient temperature. Biotechnology and Bioengineering **2010**, 106, 247-259.

7. G-W.Oetjen. Freeze Drying, Wiley-VCH; Weinheim, Germany, 1999.

8. Rosenthal, M.; Rall, W. F. Digital temperature controller for low-temperature light microscopy. Medical & Biological Engineering & Computing **1984**, 22, 471-474.

9. Nail, S. L.; Her, L-M; Proffitt, P. B.; Nail, L. L. An improved microscope stage for direct observation of freezing and freeze drying. Pharmaceutical research **1994**, 11, 1098-1100.

10. Adams, G. D. J.; Ramsay, J. R. Optimizing the lyophilization cycle and the consequences of collapse on the pharmaceutical acceptability of *Erwinia* L-Asparaginase. Journal of Pharmaceutical Sciences **1996**, 85, 1301-1305.

11. Zhai, S.; Taylor, R.; Sanches, R.; Slater, N. K. H. Measurement of lyophilisation primary drying rates by freeze-drying microscopy. Chemical Engineering Science **2003**, 58, 2313-2323.

12. Meister, E.; Sasic, S; Gieseler, H. Freeze-Dry Microscopy: Impact of nucleation temperature and excipient concentration on collapse temperature data. AAPS: PharmSciTech **2009**, 10, 582-588.

13. Meister, E.; Gieseler, H. Freeze-Dry microscopy of protein/sugar mixtures: Drying behaviour, interpretation of collapse temperature and a comparison to corresponding glass transition data. Journal of Pharmaceutical Sciences **2009**, 98, 3072-2087.

14. Yang, G.; Gilstrap, K.; Zhang, A.; Xu, L. X.; He, X. Collapse temperature of solutions important for lyopreservation of living cells at ambient temperature. Biotechnology and Bioengineering **2010**, 106, 247-259.

15. Schuck, P.; Dolivet, A. Lactose crystallization: determination of α-lactose monohydrate in spray dried dairy products. Lait: EDP Sciences **2002**, 82, 413-421.

19th International Drying Symposium (IDS 2014)
Lyon, France, August 24-27, 2014

FREEZE DRYING MICROSCOPY TO STUDY THE KINETICS OF SUBLIMATION IN A MODEL LACTOSE SYSTEM

P. Raman, C.D. Rielly, A.G.F. Stapley*

Department of Chemical Engineering, Loughborough University, Loughborough, Leicestershire, LE11 3TU, UK.

**Corresponding author: Tel.:+44-1509-222525, E-mail: A.G.F.Stapley@lboro.ac.uk*

Abstract: Freeze drying microscopy was used to study the effect of different freezing conditions on the subsequent sublimation kinetics of aqueous lactose solutions. Initial experiments showed poor reproducibility of frontal velocities between samples under nominally identical conditions. Consistent nucleation was achieved using silver iodide as a nucleation promoter. Ice crystal orientation had a clear influence on sublimation velocities - faster in "parallel" orientation to the direction of front movement than "perpendicular". Faster freezing produced lower resistances relating to a surface layer, but with little change in bulk resistance; whilst annealing produced dramatic changes in bulk resistance but not surface resistance.

Keywords: Induced nucleation, frontal velocity, silver iodide, lyophilisation

INTRODUCTION

Freeze-drying is a commonly used technique in the pharmaceutical industry to preserve labile drug compounds, organisms and proteins. These applications include living cells, biological media and nasal drug carriers [1,2]. The process consists of three main steps - freezing of the desired product solution, followed by sublimation and secondary drying [3]. Sublimation is the primary drying stage of the process, where removal of ice as water vapour takes place. Secondary drying follows where the initially dried product is further subjected to higher temperatures to remove any adsorbed water remaining in the sample. The only major disadvantages of the freeze-drying method are that it is a time and energy consuming process [4].

Freezing and sublimation steps have been reported to indirectly and directly influence the process cycle duration [5]. Improvements to the freezing process are often focussed on reducing refrigeration costs. However, the freezing step also determines the internal structure of the frozen material; in particular the rate of freezing influences the size of dendritic and cellular ice crystals. A highly porous structure with reduced diffusional resistance will improve mass and heat transfer during sublimation thereby reducing the primary drying cycle duration and improving the overall process efficiency.

Many different tools and techniques have been developed to improve and increase the rate of the sublimation process. One such method is Freeze Drying Microscopy (FDM) [6,7]. Although the most common use of FDM currently is to determine the collapse temperature of a product which is to be freeze-dried it also allows visualisation of the process of sublimation in the form of a dark band moving along the frozen matrix since the dried material prevents the light to penetrate [8].

Very few researchers have focussed on using FDM to determine frontal velocities or to measure sublimation rates. Potentially this information can be used to better understand the freeze drying process and improve its efficiency, thereby decreasing its overall cost. Zhai *et al.*, 2003[9] were among the few researchers who have tried to measure primary drying rates using FDM.

The purpose of this study was to examine the effect of prior freezing conditions on the freeze drying kinetics of lactose solutions. This includes the addition of a nucleating agent (silver iodide) to induce and control nucleation at higher temperatures, employing different cooling rates during freezing, and assessing the effect of annealing (freezing, and then warming to -10°C before cooling again). The insights gained from being able to visualise the freeze drying process can help in the understanding of conventional freeze drying systems.

MATERIALS AND METHODS

Materials

α-lactose monohydrate and silver iodide (AgI) were purchased from Fisher Scientific (Loughborough, UK).

Determination of Moisture Content

Karl Fischer titration was used to determine the moisture content of the as received α-lactose monohydrate [10]. The moisture content of the α-lactose monohydrate was determined on a wet basis to be 5.8 ± 0.3%.

Sample preparation

Different solid concentrations of α-lactose monohydrate (5 to 40%) were prepared, taking into account the initial moisture content of the as received lactose powder.

Freeze-drying microscopy

Experiments were performed on a Linkam FDCS196 temperature control stage with an Olympus BX43 microscope connected to a QImaging Retiga 2000R digital camera. The stage was sealed so that vacuum could be drawn using a vacuum pump. The pressure was measured using a Pirani gauge over a range of 1 Pa to 100 000 Pa. Liquid nitrogen was used as the coolant and was passed through a silver block upon which the glass slides were mounted to gain good thermal control throughout the sample. The stage pressure, temperature and image capture were controlled using Linksys 32 software.

A sample volume of 2 µL of lactose (mass percentages - 5, 10, 20, 30 and 40%) was prepared and loaded on to the microscope stage for the frontal velocity determination. The sample solution was frozen to -40°C followed by a reduction of the vacuum pressure to 1 Pa (below the equilibrium vapour pressure of ice at -40°C of 12.8 Pa). The movement of the sublimation front was generally observed for about 1000 s. For some experiments, a miniscule amount of AgI was placed on the bottom glass slide before loading of the sample. The purpose of the AgI was to induce nucleation at a higher temperature in the samples. Different cooling profiles (2, 10 and 50 K/min) were also considered in experiments containing AgI.

For annealing studies, 10% lactose solution was placed on to the slides and was frozen to -40°C at 10 K/min followed by heating to -10°C at 2 K/min where it was held for 60 minutes. This was followed by cooling the sample again at 2 K/min to -40°C and reduction of vacuum pressure to 1 Pa which resulted in sublimation in the sample.

Determination of collapse temperatures

To measure the collapse temperature, the sample solution was cooled at 10 K/min to -40°C and a vacuum pressure of 1 Pa was applied. Once the vacuum pressure had reached 1 Pa, the sample was heated at a rate of 1 K/min until structural collapse was observed.

Image analysis of the sublimation front movement

The camera software captured images from the microscope at a rate of 1 per 10 seconds. These images were analysed using an in-house image analysis program developed on MATLAB. The pixel points of front movement were recorded and converted to frontal distance (µm) which was then plotted as a function of time (s). The frontal data obtained were fitted to a simple twin resistance model based on two resistance terms – a constant edge layer resistance (α) and a resistance of the internal dried region (β) that increases proportionally with the distance of the sublimation front from the edge of the sample. Data fitting was incorporated into MATLAB program based on the model, in order to obtain the representative edge resistance (a) and resistance from the dried region (b). The model and data fitting has been described in detail in another paper submitted to this conference [11].

RESULTS AND DISCUSSION

Experiments with uncontrolled nucleation

Fig. 1 inset shows the microstructure of a 10% (w/w) lactose solution without AgI undergoing sublimation under FDM The ice crystals formed were very small, and were not clearly visible in structure, size or orientation even under high magnification. The ice structure was only visible in the frozen matrix by means colour variation, and individual crystals could not be observed.

The frontal velocities of uncontrolled nucleation experiments were found to vary over a range of values (Fig. 1). This behaviour may be attributed to the varying nucleation temperatures, degree of sub-cooling and varied ice crystal formation between the repeat runs as the nucleation temperatures for these runs were found to vary between -9.8°C to -17.3°C.

Ice nucleation in a freeze-drying process is a very random process, with the range of sub-cooling depending on process and product parameters. The degree of sub-cooling increases as the temperature decreases which is said to have a significant effect on the ice crystal formation[12] by affecting the nucleation rate. The delay in the point of nucleation results in rapid nucleation which results in a larger number of small crystals which are not able to grow in size while higher point of nucleation gives a small number of crystals which grow to larger crystal sizes.

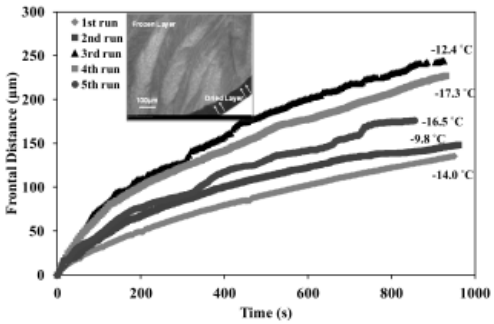

Fig. 1 Frontal distance vs time of 10% (w/w) lactose frozen at -40°C at a cooling rate of 10 K/min and freeze dried at vacuum pressure of 1Pa without AgI. Inset - Sublimation front of 10% (w/w) Lactose.

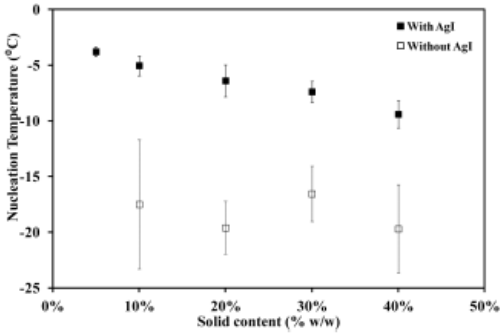

Fig. 2 Nucleation temperatures of lactose solutions with AgI and without AgI (5-40% w/w). Error bars represent deviation in measured nucleation temperature data of at least 5 repeat runs.

Hence, the nucleation temperature has a very strong effect on the overall freeze drying cycle by affecting the rate of ice sublimation [13]. The sublimation rate is found to be slower in samples where nucleation temperature is lower due to smaller ice crystals [6]. It has been widely reported in literature that the freezing profile and the nucleation temperature have a direct effect on the sublimation rate in a freeze drying process [13,14].

In order to overcome this inconsistency in reproducibility of the nucleation temperature, various methods were investigated. Different cooling profiles were explored – fast (50 K/min), very fast (130 K/min), slow (1 K/min), and combination rate (10 K/min to -10°C followed by 1 K/min to -40°C) to achieve more consistent nucleation behaviour. The varying cooling rates were applied in order to control the rate of sub-cooling and in turn control the nucleation temperature - slow rate (1 K/min) to allow the crystals to nucleate and grow at the same rate and/or the fast rate (50 K/min) to cause smaller ice crystals in all the repeat runs. However, yet again the methods did not result in reproducible nucleation temperatures and frontal velocities. This behaviour may be due to presence of minute non-uniformities on the glass slides used which provide sites for ice crystals to nucleate at different points.

Experiments with controlled nucleation

In order to improve experimental reproducibility, the use of silver iodide (AgI) was tried as an ice nucleating agent. β-AgI has been reported to have a hexagonal crystal structure similar to that of ice and is quite stable at low temperatures; hence it is able to act as a seed and can cause ice crystal formation [13,15,16,17].

The use of AgI was found to both increase the nucleation temperature and improve the reproducibility (Fig. 2).

This pattern of decreasing nucleation temperature with solid content was presumed to be brought about by the freezing point depression caused due to the increase of lactose solid content. All solutions exhibit freezing point depression with increasing solid content and nucleation takes place just below the freezing point temperature thus reached. Previous studies [18] have reported a freezing point depression of about 2°C in lactose solutions for 40% (w/w) lactose which was found to be quite similar to the nucleation temperature data with AgI (Fig. 2).

In comparison to experiments with uncontrolled nucleation, the addition of AgI also reduced the relative rate of nucleation compared to growth during solidification, which increased the mean crystal size such that individual ice crystals were now visible. Long thin ice crystal structures with distinct directionality were observed when compared to non-AgI frozen samples. Various different orientations, particularly parallel and perpendicular, were observed.

Fig. 3A and Fig. 3B show "parallel" and "perpendicular" ice crystal orientations observed in the frozen samples respectively. These orientations were defined as the orientation of the ice crystals with respect to the direction of the sublimation front movement.

These crystal orientations were visible only in the case of 5% and 10% lactose solutions. As the concentration increased the crystal sizes and orientations became less distinct. This effect may be attributed to the fact that the amount of sub-cooling on nucleation increases with increasing lactose solid content.

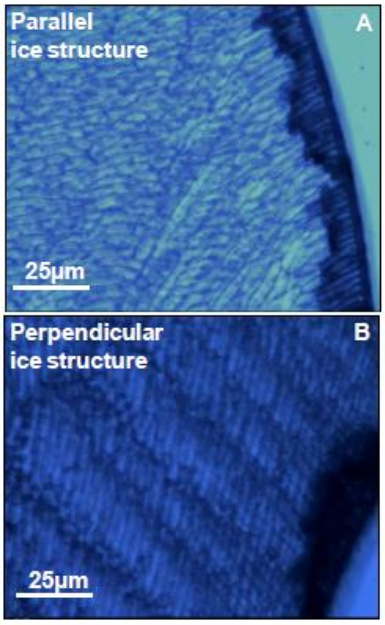

Fig. 3 A and B show the parallel and perpendicular ice crystal orientations observed at 100X magnification respectively in 10% lactose solutions in the early stages of freeze drying.

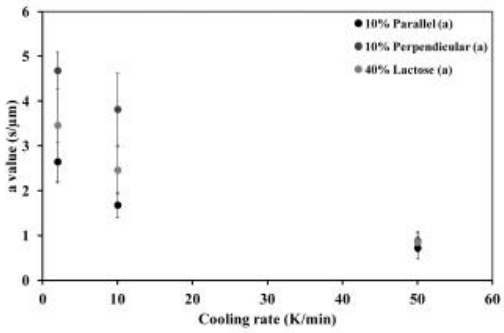

Fig. 4 Variation in edge resistance (*a*) of 10% and 40% (w/w) lactose solutions after freezing at different cooling rates.

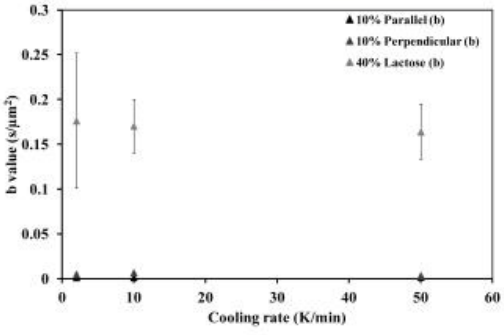

Fig. 5 Variation in resistance of dried layer (*b*) of 10% and 40% (w/w) lactose solutions after freezing at different cooling rates.

Effect of cooling rate

Three different cooling rates (2 K/min, 10 K/min and 50 K/min) were investigated for AgI doped samples in order to study their effect on the freezing and in turn on the sublimation process. Figs. 4 and 5 shows the effect of the cooling profiles on *a* and *b* values respectively for 10% and 40% (w/w) lactose solution. *a* values were found to decrease with decreasing cooling rate of the both solid contents of lactose samples. This could be ascribed to the increase in dried edge thickness and resistance when the cooling rate is low as it takes longer to reach the final temperature of drying.

The thick edge formation was partly ascribed to evaporative drying when the sample reaches the final drying temperature (-40˚C) just before the start of sublimation. While the *b* values were found to be quite low and quite similar for parallel and perpendicular orientations of 10% lactose, higher concentration of lactose (40%) showed higher b values as was expected due to higher resistance of the dried region of lactose.

Effect of annealing

Fig. 6 shows the difference in microstructure caused by annealing. Annealing involves freezing of sample (to -40˚C) followed by heating the sample to a higher temperature (-10˚C) where it is held for a defined duration (~60 minutes) to allow partial melting of the sample and finally cooling of the sample (to -40˚C).

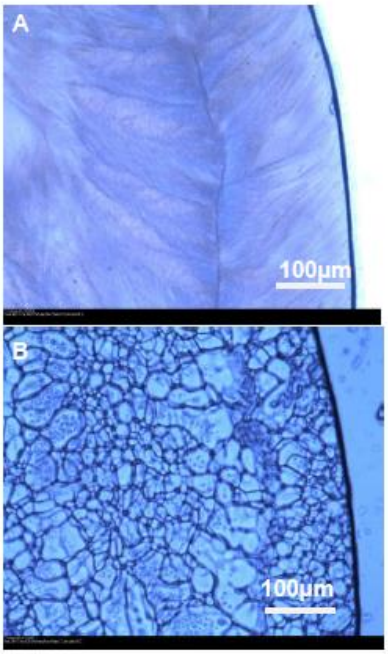

Fig. 6 A.10% Lactose frozen at 10 K/min. B. Annealed at -10˚C and cooled to -40˚C.

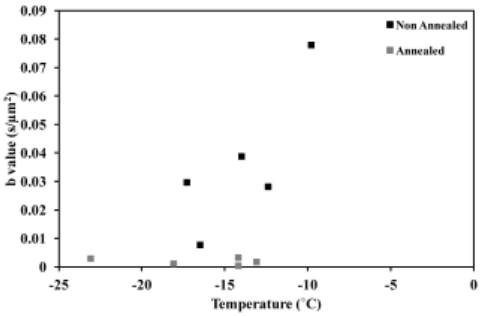

Fig. 7 *b* values of annealed and non-annealed 10% lactose samples (non AgI) freeze dried at -40°C under FDM. The x axis values represent the original nucleation temperature.

It is clear from the microstructure that the process of annealing dramatically increases the size of the ice crystals formed and the effect of these large ice crystals was evident in the increased frontal velocity thus observed.

Though *a* values of the samples were found to be similar in annealed and non-annealed samples. These were not too varied since the surface layer thickness was not too different before and after annealing. However, b values showed significant differences (see Fig. 7) which are clearly due to the difference in the internal ice crystal structure. Annealed samples had large ice crystals which resulted in fewer barriers to mass transfer and thus easier removal of water vapour from the sample.

Collapse temperatures

Apart from studying microstructure and sublimation kinetics, the freeze drying microscope was also used to study the effect of solid content on the collapse temperature of the lactose solutions. The collapse temperature is where the frozen lactose sample starts to lose its structure due to viscous flow arising from an increase in temperature. The collapsed region is apparent as light is able to pass through the sample relatively unscattered as a result of the loss of porous structure.

Fig. 8 (inset) shows the process of structural collapse as seen under FDM. The onset of collapse was measured by observing the temperature at which a light band was first visible in the FDM images while heating the sample. Collapse temperatures were found to show an increasing trend with increasing solid content (Fig. 9). This is presumably because the more dilute samples reach a higher solids concentration in the freeze concentrated matrix on crystallisation. Similar collapse temperatures were recorded for both AgI and non-AgI samples, indicating that the nucleation temperature does not significantly affect the collapse temperature.

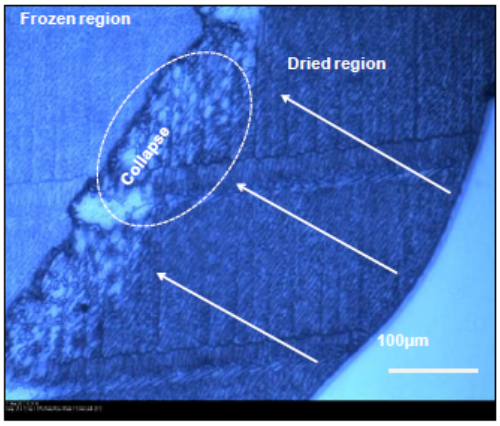

Fig. 8 Structural collapse observed in 10% w/w lactose sample with AgI. frozen at 10 K/min to -40°C, freeze dried at 1 Pa and heated at 1 K/min.

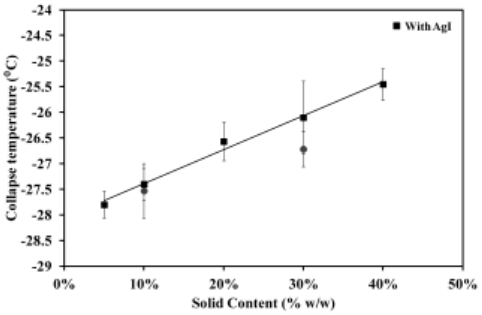

Fig. 9 Collapse temperature vs solid content of lactose with and without AgI frozen at 10 K/min to -40°C, freeze dried at 1 Pa and heated at 1 K/min.

Experiments with non-AgI samples with solid contents 10% and 30% solid content were also conducted for comparison. 10% lactose solutions were found to have almost similar collapse temperature both with and without AgI. The 30% lactose solutions showed a little variation however the difference was within ±1°C between AgI and non-AgI samples (Fig. 9).

CONCLUSIONS

The purpose of this study was to use FDM to gain a better insight into how variations in the prior freezing process affect sublimation rates during freeze drying of lactose solutions. Microscope images were analysed using MATLAB to determine the distance travelled by the front with time.

The effect of adding a nucleating agent, different cooling rates during freezing (2 K/min, 10 K/min and 50 K/min) and the addition of an annealing step were investigated. It was found that addition of AgI as a nucleating agent raised nucleation temperatures and made them more reproducible. It was also possible to

discern individual crystals for dilute solutions and this showed that the orientation of crystals formed during freezing had an effect on both the surface layer and bulk resistances to mass transfer. The effect of increasing cooling rate was to reduce the surface resistance but bulk resistance values were not significantly affected by cooling rate. Annealing resulted in dramatically larger crystal sizes and reduced the bulk resistances to mass transfer (b values) but did not significantly affect surface resistances (a values).

The collapse temperature of lactose solutions was found to be an increasing function of initial solids content, and appeared unaffected by the addition of AgI to raise nucleation temperatures.

ACKNOWLEDGEMENT

The authors would like to thank the Department of Chemical Engineering, Loughborough University, UK for funding this work.

REFERENCES

1. Pardo, J. M.; Suess, F.; Niranjan, K.. An investigation into the relationship between freezing rate and mean ice crystal size for coffee extracts. Food and Bioproducts Processing 2002, 80, 176-182.
2. Fonseca, F.; Passot, S.; Cunin, O.; Marin, M. Collapse temperature of freeze-dried *Lactobacillus bulgaricus* suspensions and protective media. Biotechnology Progress 2004, 20, 229-238.
3. G-W. Oetjen. Freeze Drying, Wiley-VCH; Weinheim, Germany, **1999**.
4. Tang, X.; Pikal, M. J. Design of freeze drying processes for pharmaceuticals: Practical advice. Pharmaceutical Research **2004**, 21, 191-200.
5. Meister, E.; Sasic, S; Gieseler, H. Freeze-Dry Microscopy: Impact of nucleation temperature and excipient concentration on collapse temperature data. AAPS: PharmSciTech **2009**, 10, 582-588.
6. Rosenthal, M.; Rall, W. F. Digital temperature controller for low-temperature light microscopy. Medical & Biological Engineering & Computing **1984**, 22, 471-474.
7. Nail, S. L.; Her, L-M; Proffitt, P. B.; Nail, L. L. An improved microscope stage for direct observation of freezing and freeze drying. Pharmaceutical research **1994**, 11, 1098-1100.
8. Pikal, M. J.; Shah, S. The collapse temperature in freeze drying: Dependence on measurement methodology and rate of water removal from the glassy phase. International journal of pharmaceutics **1990**, 62, 165-186.
9. Zhai, S.; Taylor, R.; Sanches, R.; Slater, N. K. H. Measurement of lyophilisation primary drying rates by freeze-drying microscopy. Chemical Engineering Science **2003**, 58, 2313-2323.
10. Schuck, P.; Dolivet, A. Lactose crystallization: determination of α-lactose monohydrate in spray dried dairy products. Lait: EDP Sciences **2002**, 82, 413-421.
11. Raman, P., Rielly, C.D., A.G.F. Stapley. Freeze Drying Microscopy as a Tool to Study the Sublimation Kinetics of a Freeze Drying Process. Submitted to 19th International Drying Symposium, Lyon, France, August 24-27, 2014.
12. Franks, F. Freeze drying of pharmaceuticals and biopharmaceuticals- Principles and practice.RSC Publishing, Cambridge, UK, **2007**.
13. Searles, J. A.; Carpenter, J. F.; Randolph, T. W. The ice nucleation temperature determines the primary drying rate of lyophilisation for samples frozen on a temperature-controlled shelf. Journal of Pharmaceutical Sciences **2001**, 90, 860-871.
14. Patel, S. M.; Bhugra, C.; Pikal, M. J. Reduced pressure ice fog technique for controlled ice nucleation during freeze-drying. AAPS PharmSciTech **2009**, 10, 1406-1411.
15. Edwards, G. R.; Evans, L. F.; La Mer, V. K. Ice nucleation by monodisperse silver iodide particles. Journal of Colloid Science **1962**, 17, 749-758.
16. Clausse, D.; Bouabdillah, D.; Cochet, N.; Luquet, M. P.; Pulvin, S. Ice crystallization induced by silver iodide and bacteria in microsize droplets dispersed within emulsions. Pure and Applied Chemistry **1991**, 63, 1491-1494.
17. Petzold, G.; Aguilera, J. M. Ice morphology: Fundamentals and technological applications in foods. Food Biophysics **2009**, 4, 378-396.
18. Whittier, E. O., 1933. Freezing Points and Osmotic Pressures of Lactose Solutions. Journal of Physical Chemistry, *37*, 847–849.

Freeze drying microscopy as a tool to study the sublimation process

Purnima Raman, Chris D. Rielly, Andrew G. F. Stapley
Department of Chemical Engineering, Loughborough University, UK, LE11 3TU
Email : P.Raman@lboro.ac.uk

Loughborough University

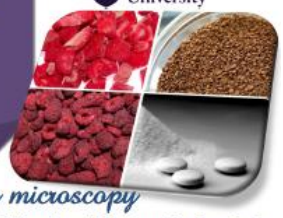

What is freeze drying ?

Freeze drying (via sublimation) is an effective way of drying materials without harming them.

During freeze drying, the product temperature is maintained high enough for faster drying but should be below the point of collapse of product structure (Collapse temperature).

Applications include - Instant coffee, dried fruits in breakfast cereals or snacks, culinary herbs, in pharmaceutical formulations and even "astronaut foods".

Process Overview

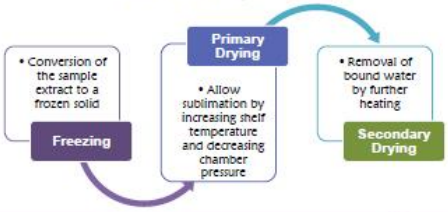

Freeze drying microscopy

Freeze drying microscopy (FDM) can provide fundamental information in order to optimise the process in a real system.

What can be determined?

- Sublimation front velocity (related directly to sublimation rate)
- Collapse temperature
- Optimum freezing profile
- Optimum drying temperature

Freeze drying microscopy system

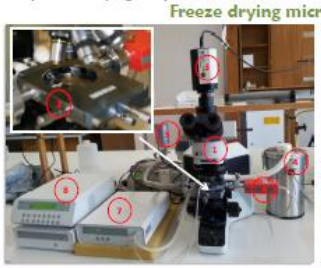

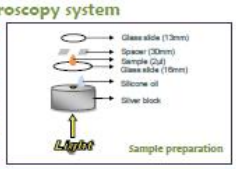

1. An Olympus BX42 microscope.
2. A Linkam FDCS196 freeze drying stage.
3. A Retiga 2000R digital camera.
4. Liquid nitrogen carrier.
5. A Vacuum pump.
6. A Pirani gauge
7. Liquid nitrogen pump
8. Temperature controller

Model lactose system

Determination of sublimation front velocity

- In-house programme was developed using MATLAB image analysis software to automatically track the sublimation front.
- Uses a sequence of binary images to track the width of the dark freeze drying band.
- Marks the points on the moving front on the images.
- Outputs sublimation front distance with time.

(A) Sublimation front movement (Lactose) (B) Matlab Analysis (C)Frontal distance vs time

Effect of ice crystal size and orientation

Lactose solutions of various solid content were frozen and freeze dried with and without nucleating agent (**AgI**).

Nucleating agent had a pronounced effect on nucleation temperature, ice crystal structure and orientation.

- Nucleation temperature decreases with increasing solid content.
- Two different ice crystal orientations were classified with respect to sublimation front movement as – parallel and perpendicular.

Microscopic images of frozen lactose solution (10%)

Non-AgI AgI AgI

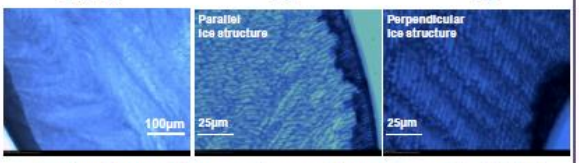

Scanning Electron Microscope images of lactose freeze dried in FDM

Non-AgI AgI AgI

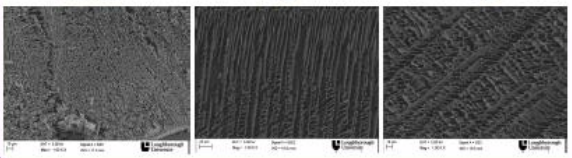

Collapse temperature

- Collapse temperature increases with increasing solid content (5 to 40%).

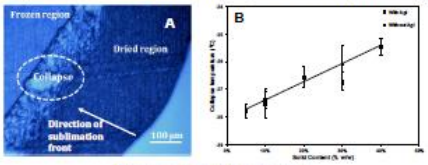

Effect of solid content

- Front velocity initially decreased with increasing solid content but increased with further increase in solid content (40%). It might be attributed to a decrease in the amount of water in 30 & 40% Lactose.

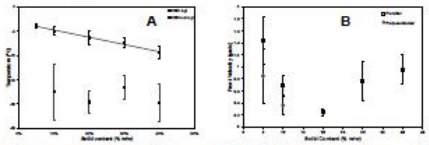

(A) Nucleation temperature vs. solid content (B) Initial frontal velocity vs. solid content

Effect of drying temperature

- Drying temperature is maintained at least 5°C below collapse temperature.
- Three different temperatures of drying were investigated (-30, -40 & -50 ° C).
- Frontal velocity decreases with decrease in drying temperature and depends directly on the equilibrium vapour pressure of ice.

Effect of cooling rate

- Three cooling rates to achieve freezing were investigated (2, 10 & 50 K/min).
- Frontal velocity increases with increase in rate of cooling since it directly influences degree of supercooling and hence the size of ice crystal formation.

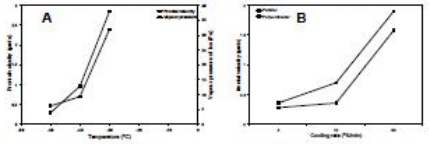

(A)Initial frontal velocity vs. drying temperature (B) Initial frontal velocity vs. cooling rate

Conclusions

FDM provides information regarding optimum solid content, drying temperature, freezing profile and collapse temperature which can be used for formulation & cycle development of a real freeze drying system.

Acknowledgement : Financial support from the Department of Chemical Engineering, Loughborough University